PNWD-3387
WTP-RPT-103, Rev 0

Comparison Testing of Multiple Resorcinol-Formaldehyde Resins for the River Protection Project—Waste Treatment Plant

S. K. Fiskum
B. S. Augspurger
K. P. Brooks
W. C Buchmiller
R. L. Russell
M. J. Schweiger
L. A. Snow
M. J. Steele
K. K. Thomas
D. E. Wallace
N. H. Wong
J. D. Yeager
D. L. Blanchard, Jr.

January 2004

Prepared for Bechtel National, Inc.
under Contract No. 24590-101-TSA-W000-00004

LEGAL NOTICE

This report was prepared by Battelle Pacific Northwest Division (Battelle) as an account of sponsored research activities. Neither Client nor Battelle nor any person acting on behalf of either:

MAKES ANY WARRANTY OR REPRESENTATION, EXPRESS OR IMPLIED, with respect to the accuracy, completeness, or usefulness of the information contained in this report, or that the use of any information, apparatus, process, or composition disclosed in this report may not infringe privately owned rights; or

Assumes any liabilities with respect to the use of, or for damages resulting from the use of, any information, apparatus, process, or composition disclosed in this report.

References herein to any specific commercial product, process, or service by trade name, trademark, manufacturer, or otherwise, does not necessarily constitute or imply its endorsement, recommendation, or favoring by Battelle. The views and opinions of authors expressed herein do not necessarily state or reflect those of Battelle.

Comparison Testing of Multiple Resorcinol-Formaldehyde Resins for the River Protection Project—Waste Treatment Plant

S. K. Fiskum
B. S. Augspurger
K. P. Brooks
W. C Buchmiller
R. L. Russell
M. J. Schweiger
L. A. Snow
M. J. Steele
K. K. Thomas
D. E. Wallace
N. H. Wong
J. D. Yeager
D. L. Blanchard, Jr.

January 2004

Prepared for Bechtel National, Inc.
under Contract No. 24590-101-TSA-W000-00004

COMPLETENESS OF TESTING

This report describes the results of work and testing specified by Test Specification 24590- PTF-TSP-RT-02-016, Rev. 0 and Test Plan TP-RPP-WTP-210, Rev. 0. The work and any associated testing followed the quality assurance requirements outlined in the Test Specification/Plan. The descriptions provided in this test report are an accurate account of both the conduct of the work and the data collected. Test plan results are reported. Also reported are any unusual or anomalous occurrences that are different from expected results. The test results and this report have been reviewed and verified.

Approved:

Paul Beeman S. GHB 11/14/04

Gordon H. Beeman, Manager — Date
WTP R&T Support Project

Contents

Figures

Tables

This page intentionally left blank

Terms and Abbreviations

AP-101	AP-101 tank waste simulant diluted to 5 M Na
ASO	Analytical Support Operations
AZ-102	AZ-102 tank waste simulant concentrated to 5 M Na
ASR	analytical services request
ASTM	American Society for Testing and Materials
AV	apparatus volume
BNI	Bechtel National, Inc.
BS	blank spike
BV	bed volume
CSTR	continuously stirred tank reactor
DAS	Data Acquisition System
DF	decontamination factor
DI	deionized (water)
DOE	U.S. Department of Energy
EQL	estimated quantitation limit
F	furnace (method)
FMI	Fluid Metering, Inc., Syosset, NY
GEA	gamma energy analysis
HP	hot persulfate (method)
IBC	IBC Advanced Technologies, Inc., American Fork, Utah
IC	ion chromatography
ICP-AES	inductively coupled plasma-atomic emission spectrometry
ICP-MS	inductively coupled plasma-mass spectrometry
IDL	instrument detection limit
J	data flag indicating estimated value
LAW	low-activity waste
LCS	laboratory control sample
L/D	length to diameter (ratio)
MDL	method detection limit
MRQ	minimum reportable quantity

MS	matrix spike
M&TE	measuring and test equipment
NA	not applicable
NCAW	neutralized current acid waste
ND	not detected
NIST	National Institute of Standards and Technology
NM	not measured
NR	not required
PB	preparation blank
PNWD	Battelle—Pacific Northwest Division
PSD	particle-size distribution
QA	quality assurance
QC	quality control
QAPjP	Quality Assurance Project Plan
RF	resorcinol-formaldehyde
RPD	relative percent difference
RPP-WTP	River Protection Project-Waste Treatment Plant
RPL	Radiochemical Processing Laboratory (PNWD facility)
SRTC	Savannah River Technology Center
TIC	total inorganic carbon
TOC	total organic carbon
WTPSP	Waste Treatment Plant Support Project

Terms of Measurement

ΔP	pressure drop
μ	solution viscosity
μCi	microcuries
μg	micrograms
ρ	density, g/mL
cp	centipoise
C/C_o	analyte concentration in column effluent divided by analyte concentration in feed, dimensionless
F-factor	ratio of dry resin mass to wet resin mass, dimensionless
g	gram
h	hour
K	column permeability, m^2
mL	milliliter
psi	pounds per square inch
q	superficial liquid velocity, m/s
s	second

This page intentionally left blank

Testing Summary

The U.S. Department of Energy (DOE) is responsible for the disposition of millions of gallons of high-level radioactive wastes stored at the Hanford site in Washington State. The waste is to be vitrified following specific pretreatment processing, separating the waste into a relatively small-volume high-activity waste fraction and a large-volume low-activity waste (LAW) fraction. To allow for contact handling of the immobilized LAW and land disposal, cesium-137 will need to be removed from the tank waste. Ion exchange is the baseline method for removing ^{137}Cs from Hanford high-level tank waste in the River Protection Project-Waste Treatment Plant (RPP-WTP). The current pretreatment flowsheet includes the use of Cs-selective, elutable, organic ion exchange material, SuperLig® 644 (SL-644), for Cs removal from the aqueous-tank-waste fraction. This material has been developed and supplied solely by IBC Advanced Technologies, Inc., American Fork, UT. To provide an alternative to this sole-source resin supply, the DOE Office of River Protection directed Bechtel National Incorporated (BNI) to initiate the process of selecting and testing an alternative ion exchange resin for Cs removal in the RPP-WTP. Resorcinol-Formaldehyde (RF) resin was selected as the most viable alternative.[(a)]

Battelle—Pacific Northwest Division (PNWD) was contracted to evaluate different RF resins, provide data supporting WTP's selection of one type of RF resin for further developmental work, and set preliminary RF resin purchase specifications. Work was conducted under contract number 24590-101-TSA-W000-00004. Appendix C of the *Research and Technology Plan*[(b)] defines the initial evaluation of RF resins under Technical Scoping Statement A-222.

Objectives

The primary test objective was to provide data supporting WTP's selection of one type of RF resin for further development work. This objective was implemented through sub-objectives, including:

- determination of bulk properties, such as shrink-swell characteristics, particle-size distribution (PSD), morphology, and bed density
- determination of batch-distribution coefficients as a function of Cs concentration and resin type
- determination of multi-cycle Cs load and elution behavior as a function of resin type
- determination of multi-cycle bed permeability or parameters affecting permeability for RF types.

Secondary objectives were to compare RF Cs load and elution performance data to SL-644 performance data and develop a preliminary RF purchase specification.[(c)] These test objectives are further discussed in Table S.1.

(a) R Peterson, H Babad, L Bray, J Carlson, F Dunn, A Pajunen, I Papp, and J Watson. 2002. *WTP Pretreatment Alternative Resin Selection,* 24590-PTF-RPT-RT-02-001, Rev. 0, Bechtel National, Inc., Richland, WA.

(b) S Barnes, R Roosa, and R Peterson. 2003. *Research and Technology Plan,* 24590-WTP-PL-RT-01-002, Rev. 2, Bechtel National, Inc., Richland, WA.

(c) The preliminary purchase specification will be addressed in a separate document.

Table S.1. Test Objectives

Test Objective	Objective Met?	Discussion
Provide data supporting WTP's selection of one type of RF resin for further development work.	Yes	This test objective was met by fulfilling the next five sub-objectives. PNWD tested several RF resin types (different morphologies, compositions, and manufacturers).
Determine bulk properties.	Yes	Bulk-property testing included determination of particle morphology using micrographs, particle-size distributions as Na-form resin and H-form resin, settled resin bed density, and shrink-swell behavior. These properties are summarized in Figure S.1, Table S.3, and Section 3.0. Skeletal densities and bed porosities were measured for one ground-gel RF, one spherical RF, and SL-644. The skeletal density results appeared to be biased low.
Determine batch-distribution coefficients as a function of Cs concentration and resin type.	Yes	Batch-distribution measurements were conducted in duplicate at five different Cs concentrations ranging from 4E-4 M Cs to 3E+2 M Cs in the AZ-102 simulant for all (nine) RF resin samples. Results are summarized in Figures S.2, S.3, and Section 4.0. Cs capacities were estimated from the isotherms and are summarized in Table S.4 and Section 4.0.
Determine multi-cycle Cs load and elution behavior as a function of resin type.	Yes	Multi-cycle load and elution testing was conducted on five different RF resins. Three load and elute cycles were conducted followed by a load cycle mimicking polishing column conditions. One resin test was halted early because of poor performance. Test results are summarized in Table S.5 and Section 5.0.
Determine multi-cycle bed permeability or parameters affecting permeability for RF types.	Yes	Hydraulic properties were tested for one spherical RF resin, one ground-gel RF resin, and SL-644. Resin-bed permeability, expansion pressures, particle-size decrease, compressibility, and angle of internal friction were measured for each resin. Results are summarized in Table S.6 and Section 6.0.
Compare RF performance data to SL-644 performance data.	Yes	Resin comparison was limited to column load and elution performance and hydraulic properties testing. Two different SL-644 resin batches were column tested in parallel with RF; however, because of experimental difficulties, only 1.5 process cycles were conducted. The SL-644 column-performance results are presented in Table S.5 and Section 5.0. Hydraulic-properties testing results are presented in Table S.6 and Section 6.0.
Develop a preliminary purchase specification.	Yes	This was prepared and delivered under separate cover to the BNI R&T Lead for the current task.

Test Exceptions

Specific test details were modified in Test Exceptions 24590-WTP-TEF-RT-03-022, 24590-WTP-TEF-RT-03-031, and 24590-WTP-TEF-RT-03-074. Table S.2 summarizes the test exceptions to the test plan and provides a discussion of the impacts on the tests.

Table S.2. Test Exceptions

Test Exception ID	Test Exceptions	Discussion
24590-WTP-TEF-RT-03-022	Decrease the sample size of the batch-contact test resin from 0.5 g to 0.2 g and maintain the phase ratio of 100:1 solution volume to resin mass.	Previous testing with SL-644 demonstrated that the larger sample size was not required to obtain high precision with the batch-contact testing. The reduced sample size, and thus reduced contact solution volume, allowed more batch contacts to be conducted in parallel. This helped meet the requirements of testing where 180 batch-contact samples were performed within the project time and budget constraints.
24590-WTP-TEF-RT-03-031	Change each reference to the concentration of 0.25 M NaOH RF regeneration solution in this test plan to the concentration of 1 M NaOH or a concentration of NaOH approved by the R&T Lead for this test.	Initial RF column tests resulted in some bubble formation in the bed after loading AZ-102 simulant and AP-101 simulant. Therefore, the change was implemented. However, much testing had already been conducted, such as pre-conditioning and bulk-property testing. Therefore, the change only affected follow-on column processing for evaluating load and elution behavior and hydraulic properties testing.
	Change the Test Specification Table 3 Cs MRQ from 5.0E-4 μg/mL to 5.0 E-1 μg/mL.	There was no impact to the testing as a result of this change. The Test Specification Table 3 analysis criterion was relevant to the Cs eluate. The corrected concentration was provided in the initial, approved, version of the Test Plan. The eluate Cs concentration is expected to be at least a factor of 100 above the revised detection limit.
24590-WTP-TEF-RT-03-074	Added a new Step (6c) to Section 7.3 to allow for the use of load cells on the bottom and side of the column for indication-only pressure measurements.	Load cells were not specified in the plan for permeability testing but were found in other testing to be a useful diagnostic tool. BNI requested that indication-only load cells be added to the permeability test columns.
	Modified Step 8, Section 7.3 so the elution will be at 6 BV/h instead of 1 to 2 BV/h.	Elution condition during permeability testing was specified at 1 to 2 BV/h. However, the rate of elution had no effect on test results, and by increasing the rate of elution, the speed of completion of testing could be improved.
	Modified Section 7.3, Step 13 so only a portion of the resin is converted to hydrogen form. PNWD was instructed to convert a fraction of the resin back into the hydrogen form by soaking it in 0.5 M HNO_3 for 2 hours, then DI water for 2 hours.	The plan indicated all the resin would be converted to the hydrogen form for particle-size analysis, but only a small fraction of the resin needed to be converted to complete the particle-size analysis.

Table S.2 (Contd)

Test Exception ID	Test Exceptions	Discussion
24590-WTP-TEF-RT-03-074	Replaced X-100 with S-3000 in Step 14 of Section 7.3.	A Microtrac X-100 was specified in Step 14 Section 7.3, but the high side of the particle-size range was beyond the indication range of the Microtrac X-100. A Microtrac S-3000 was available that could better read this higher product size distribution.
	Deleted Step 16 (measurement of angle of incline), Section 7.3. Renumbered Step 17 to Step 16, and added final part f to Step 16 (as renumbered) Section 7.3. Step 16 now reads as follows: 16. PNWD will measure resin bed compressibility in AP-101 simulant over the pressure ranges anticipated in plant operations, using resin obtained from the permeability tests. a. Na-form resin will then be rinsed with DI water and transferred quantitatively into a column and AP-101 simulant suspending solution. b. The resin bed dimensions will be determined based on material availability and with the WTP R&T Lead's approval. The compression configuration will allow the resin bed to be saturated, but allow liquid to escape during compression. c. Before measuring compressibility, the resin bed will be preconditioned by vibration. d. The resin bed height will be measured with varying pressures placed on the resin bed. e. The resin bed compaction (height) will be measured over the range of compression expected due to flow and resin bed expansion. The range of compression measurements will be developed with assistance from the WTP R&T Lead. f. Using load cells, the force on the bottom and side of the ion exchange column will be recorded for each force on the resin bed. These measurements will be for indication only. The results will be used to determine the angle of internal friction.	BNI authorized the substitution of "compressibility" testing for "angle-of-incline" testing. The angle-of-incline testing was originally planned to allow the prediction of the relative horizontal to vertical pressures. Once load cells were added to the columns, the need to measure the angle of incline was eliminated. Resin compressibility was of greater interest.
	Deleted part (a), Step 16 (as renumbered), Section 7.3. (See revision above.)	Because only a small fraction of resin was removed in Step 13 of Section 7.3 for PSD testing, the remainder of the resin was still in Na-form. No conversion to Na-form was required.

Table S.2 (Contd)

Test Exception ID	Test Exceptions	Discussion
24590-WTP-TEF-RT-03-074	Reference of applying pressure until hysterisis is obtained was replaced with vibration in Part c (as relabeled) Step 16 (as renumbered) Section 7.3.	BNI provided authorization to prepare resin for compressibility testing by vibrating the resin bed. The vibration is expected to pack the bed sufficiently before the testing.
	Replaced term "masses" with "pressures" in Part d (as re-labeled), Step 16 (as renumbered), Section 7.3.	BNI authorized replacement of "masses" with "pressures" Part d, Step 16, Section 7.3. The effect on resin packing is the same.
	Edited Section 7.5.2 Step 7 to read, "PNWD will composite selected column eluate sample(s) and analyze for ^{137}Cs."	Not all eluates were of interest for further testing based on poor column load and elution performance. BNI directed the compositing of only one Cs eluate from the entire process testing defined in Section 7.5.
	Edited Section 9.0 Reporting to indicate that the preliminary purchase specification will be prepared as a separate document.	BNI agreed to receive the preliminary purchase specification as a separate document. The preliminary purchase specification is considered to be a "living" document, undergoing changes as additional information is learned. It did not make sense to bury it in the report where changes/updates to the specification, and thus report, would become unwieldy. This approach avoids built-in obsolescence of the report as the purchase specification changes.

Results and Performance Against Success Criteria

The RPP-WTP project would consider this test successful when data are collected supporting WTP's selection of an RF type most likely to meet plant requirements (for further development work). Data supporting this determination includes multi-cycle loading and elution results, batch-distribution results, physical-property testing, and hydraulic-property testing. Results from this testing are summarized herein.

Ground-gel RF resins and spherical RF resins were tested. Representative micrographs of these resin types are given in Figure S.1 along with a micrograph of SL-644 (a ground-gel type of resin) for comparison. Morphological distinctions between the ground-gel RF resin and the SL-644 resin were minimal, where each resin consists of irregular, angular edges and smooth surfaces. The spherical resin products, in contrast, were uniformly spherical.

(a)

(b)

(c)

Figure S.1. Micrographs of Ground Gel (a) and Spherical (b) RF resins and SL-644 Resin (c)

The results of the physical-property testing are summarized in Table S.3. All spherical resin forms had tight PSDs; the granular materials exhibited significantly broader PSD distributions.

Table S.3. Physical-Property-Testing Summary

Resin ID	Shape	PSD Range H-Form, μm[(a)]	PSD Range Na-Form, μm[(a)]	Dry-Bed Density, H-Form g/mL	Expansion Factor H-Form to Na-form
1	Granular	600 – 870	630 – 900	0.41	1.38
3	Spherical	450 – 522	500 – 620	0.41	1.51
4	Spherical	480 – 510	510 – 660	0.41	1.67
6	Spherical	440 – 515	510 – 640	0.41	1.54
7	Spherical	430 – 500	500 – 620	0.41	1.74
8	Granular	550 – 780	550 – 770	0.47	1.62
9	Granular	640 – 890	670 – 930	0.50	1.65
10	Granular	530 – 810	610 – 870	0.45	2.22
11	Granular	520 – 794	640 – 890	0.49	2.22
(a) Range incorporates the 10% to 90% volume fraction.					

The bed porosity was measured for Resin #3 and #9 and averaged 0.38 (dimensionless) for both resins. The skeletal density was measured on both resins; Resin #3 averaged 1.41 ± 10% g/mL, and Resin #9 resulted in a single useable value of 1.42 g/mL.

The batch-distribution contacts were confirmed to reach equilibrium for all resins tested within a 24-h contact time. The batch-equilibrium values as a function of Cs concentration are summarized in Figures S.2 and S.3. Resins #1, #3, and #8 had higher K_ds at the higher Cs concentrations. Resins #1, #8, #10, and #11 had higher K_ds at the extremely low Cs concentrations.

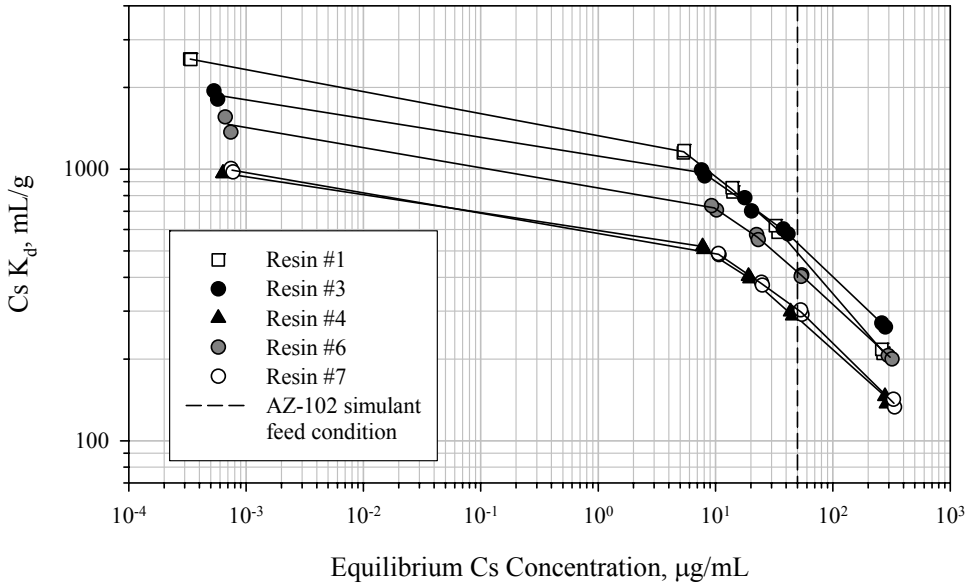

Figure S.2. Batch-Contact Equilibrium Values for Resins #1, #3, #4, #6, and #7 (H-form mass basis)

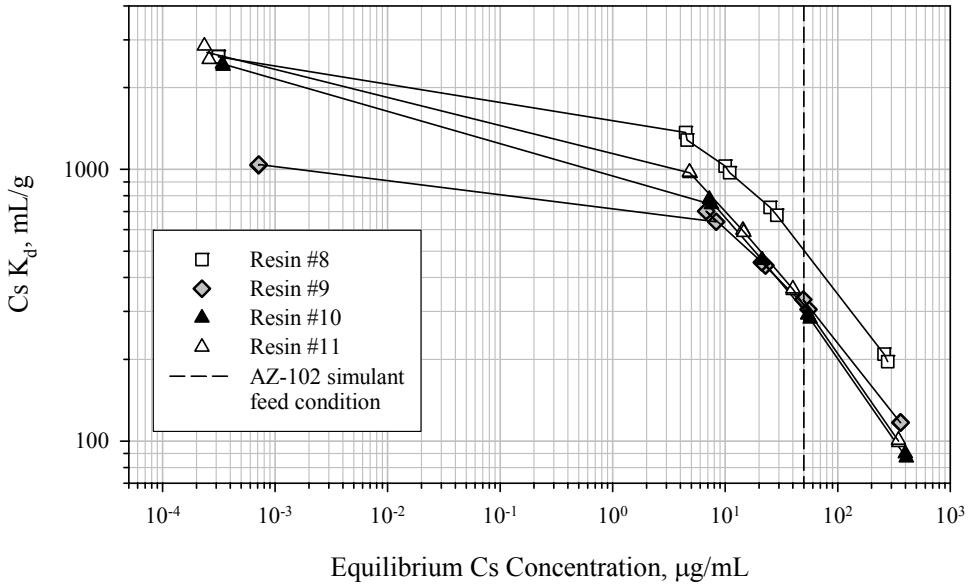

Figure S.3. Batch-Equilibrium Results for Resins #8, #9, #10, and #11 (H-form mass basis)

Isotherms were generated from the batch-contact data. Clear plateaus for each resin were not established. However, capacities could be estimated from the highest Cs concentration tested. Resin #3 had the highest measured capacity at 0.54 mmoles Cs/g resin. A summary of the estimated capacities is provided in Table S.4.

Table S.4. Estimated Cs Capacities for RF Resins

	Cs Capacity			Cs Capacity	
Resin ID	mg Cs / g resin[(a)]	mmoles Cs / g resin[(a)]	Resin ID	mg Cs / g resin[(a)]	mmoles Cs / g resin[(a)]
1	56	0.42	8	54	0.41
3	72	0.54	9	42	0.32
4	40	0.30	10	36	0.27
6	62	0.47	11	35	0.26
7	45	0.34			
(a) Based on dry H-form resin.					

The column testing for Cs load and elution profiles are summarized in Table S.5. The start of Cs breakthrough (where % C/C_o >4E-3) and interpolated 50% Cs breakthrough are provided in units of BV. SuperLig® 644 results are provided for comparison. Resin #1 load behavior was poor, and its test was ended early. The Resin #3 initial Cs breakthrough was similar to that of SL-644 from production-batch C-01-11-05-02-35-60, wet-sieved 20- to 30-mesh fraction. However, Resin #3 reached 50% C/C_o sooner than the SL-644. Resin #9 performed nearly as well as the SL-644 from production-batch C-01-05-28-02-35-60 with the AZ-102 simulant matrix. Resin #9 resulted in early Cs breakthrough with the AP-101 simulant, a high K concentration matrix. The early Cs breakthrough was largely attributed to the competing ion effect with K. Also, the AP-101 simulant was loaded at twice the flowrate of the AZ-102 simulant, and the increased flowrate may have contributed to the early and slow Cs breakthrough.

Table S.5. Cs Load and Elution Summary

Resin ID (Type)	Simulant Feed	Cs Breakthrough		Cs Bleed	Cs Elution		
		Onset, BV	50% C/C_o, BV	% C/C_o (Cycle #)	Peak C/C_o	1% C/C_o, BV	0.1% C/C_o, BV
1 (ground gel)	AZ-102	20	50	NA[a]	32	12	15
3 (spherical)	AZ-102	80	143	≤ 2E-3 (4)	118	15	18
6 (spherical)	AZ-102	45	85	2.3E-3 (4)	42.6	13	17
9 upflow elution (ground gel)	AZ-102	130	180–190	< 1E-2 (2)	52.9[b]	22–25	>35
9 (ground gel)	AZ-102	130	170–185	< 4E-3 (4)	150	15	23
9 (ground gel)	AP-101	25	205	1.4E-2 (4)	66.2[b]	17	>34[c]
11 (ground gel)	AZ-102	70	110	3.4E-3 (4)	68.8	16	32
12 (SL-644)[d]	AZ-102	180	240	< 3E-2 (2)	90.6	15[f]	25
SL-644[e] (20-30 mesh)	AZ-102	80	190	≤ 3E-3 (2)	133	12	17

(a) NA = not applicable, early breakthrough precluded calculation.
(b) Elution peak displayed broadening.
(c) The third process cycle manifested 0.1% C/C_o at 24 BVs.
(d) SL-644 production batch C-01-05-28-02-35-60, ground gel.
(e) SL-644 production batch C-01-11-05-02-35-60, ground gel.
(f) The BV is probably biased high.

The Cs bleed measured in the fourth process load cycle (second cycle where only two cycles were conducted) is also shown in Table S.5. The greatest Cs bleed was associated with the high K waste processing. Resins #6 and #11 resulted in detectable Cs-bleed concentrations. All other tests, Resins #9, #3, and SL-644, resulted in no detectable Cs bleed. In all cases, the bleed did not cause failure to meet the RPP-WTP design-basis Cs-decontamination requirement.

The Cs-elution parameters, also summarized in Table S.5, include the peak C/C_o concentration and the BVs required to reach 1% C/C_o. All resins eluted well with peak maxima at 4 to 6 BVs of processed eluant. Except for Resins #1 (with low Cs loading) and #6, downflow elution of the RF resins required ≥25% more BVs to reach 1% C/C_o than with the 20- to 30-mesh SL-644. Resin #1 (with low Cs loading) and spherical Resins #3 and #6 downflow elution volumes were equivalent to the 20- to 30-mesh SL-644 elution volume required to reach 0.1% C/C_o. The ground-gel RF resins generally required ≥35% more BVs to reach 0.1% C/C_o. Upflow elution resulted in predictable elution-peak broadening and required large process volumes to reduce the effluent Cs concentration to 1% C/C_o. The AP-101 simulant processing also exhibited elution-peak broadening.

Table S.6 summarizes the resin hydraulic properties testing results from Resins #3, #9, and SL-644.

The spherical RF Resin #3 had the highest permeability of the resins tested (Resin #9 and SL-644). In spite of the fact that the permeability dropped over multiple cycles, there was much less particle breakage of Resin #3 than seen with the other resins, and the permeability remained higher than the other resins after four cycles. The Resin #3 had higher compressive strength, which would result in less decrease in the void fraction as the differential pressure increases across the resin bed. However, it did build up higher pressures on the bottom and side walls than the other resins tested. This may be caused

by the low resin compressibility that prevents the resin from absorbing the increased pressure build-up due to resin expansion, or the high angle of internal friction that prevents the resin from dispersing the pressure throughout the resin bed.

Table S.6. Summary of Properties Evaluated in Hydraulic Testing

Property	Units	Resin #3	Resin #9	Resin #12
Permeability[(a)]	m^2	1.92×10^{-10}	1.05×10^{-10}	6.83×10^{-11}
Expansion Pressure[(b)]	psi	35.3	22.9	20.6
Particle Size Decrease[(c)]	μm	7	154	164
Compression[(d)]	percent	1	3	15
Angle of Internal Friction[(e)]	degrees	47	47	52

(a) Average permeability in Cycle #4 for 1600 mL/min of NaOH and the column L/D = 2.7.
(b) Highest sidewall pressure exerted in Cycle #2 for 1600 mL/min and the column L/D = 2.7.
(c) Change in volume-based mean particle size from pre-testing to post testing based on column L/D = 2.7.
(d) Relative height decrease at 20 psi for the last cycle.
(e) Angle taken at 20 psi for the last cycle.

The granular SL-644 (Resin #12) had the lowest permeability of the three resins tested and compressed significantly more than the other resins. This will result in higher column pressure drops than would be seen with the other resins. Microscopy and PSD measurements indicated significant particle breakage with SL-644, which probably contributed to the observed permeability and compressibility results. In spite of these disadvantages, the build-up in resin-to-wall pressure during regeneration for SL-644 was less than that seen with Resin #9 and #3, possibly due to its higher compressibility and the breakage of the resin. Furthermore, SL-644 did not show a significant decrease in permeability for each subsequent cycle, indicating that the resin damage and resultant lower permeability may have occurred in the initial cycle and did not worsen with subsequent cycles. This effect may also have been a result of removing and re-adding the resin bed when a pressure sensor failed. Resin #12 also had a higher angle of internal friction than the other materials, although not significantly.

The granular RF Resin #9 was similar to Resin #3 in terms of compressibility, but in most other respects was more similar to SL-644, Resin #12. Resin #9 had similar, but higher permeability and lower angle of internal friction than Resin #12 and a similar but slightly higher expansion pressure than Resin #12. Both Resin #12 and Resin #9 had significant changes in particle size during cycling.

Quality Requirements

PNWD implemented the RPP-WTP quality requirements by performing work in accordance with the quality assurance project plan (QAPjP) approved by the RPP-WTP Quality Assurance (QA) organization. This work was conducted to the quality requirements of NQA-1-1989, Basic and Supplements, and NQA-2a-1990, Part 2.7, as instituted through PNWD's *Waste Treatment Plant Support Project Quality Assurance Requirements and Description* (WTPSP) Manual and to the approved Test Plan, TP-RPP-WTP-210, Rev. 0.

PNWD addressed verification activities by conducting an "independent technical review" of the final data report in accordance with Procedure QA-RPP-WTP-604. This review verified that the reported results were traceable, that inferences and conclusions were soundly based, and that the reported work satisfied the Test Plan objectives.

R&T Test Conditions

This report summarizes the testing of nine available RF resins, including ground-gel and spherical resins. Resins were assigned a random number identification to shield the manufacturer's identity.[(a)] All resins were subsampled, and suitable volumes were pretreated before testing. Pretreatment included washing resin in 0.5 M HNO_3, then converting it to the Na-form and then back to the H-form, and then repeating the conversions to Na-form and H-form once more. The pretreated resins were dried in the H-form under N_2 until a free-flowing form was obtained.

Resin physical properties were tested. The morphology was evaluated using optical microscopy. The shrink-swell behavior was measured in conjunction with resin-bed densities that were based on H-form resin mass and settled-resin-bed volumes in deionized water, 0.5 M HNO_3, 0.25 M NaOH, and AP-101 simulant. The H-form and Na-form PSDs were measured using a Micro TRAC S3000 Particle Size Analyzer. Selected ground-gel and spherical resins were tested for bed porosity and skeletal density.

Batch-distribution tests were conducted in duplicate with each resin in contact with AZ-102 simulant at four initial spiked Cs concentrations. A ^{137}Cs tracer was added to each stock contact solution, which allowed for rapid determination of Cs uptake by gamma energy analysis (GEA). The solution-volume-to-resin mass ratio ranged from 100 mL/g to 180 mL/g. The higher ratios were associated with the spherical resin that contained more water than anticipated (dry mass to wet mass ratios of 0.51). Samples were agitated on a reciprocal shaker for up to 96 hours.

Cesium ion exchange load and elution behaviors were tested on three ground-gel RF resins, two spherical RF resins, and two SL-644 resins using multiple process-cycle tests in a single-column format. Resin bed volumes (BVs) were nominally 20-mL in a 2-cm ID glass column with a nominal length-to-diameter ratio of 3 when the resin was in the Na-form. The AZ-102 simulant containing 50 μg/mL Cs was primarily used for column testing. One multi-cycle column test was conducted with AP-101 simulant at 6 μg/mL Cs. All feeds were spiked with ^{137}Cs or ^{134}Cs tracers to allow for rapid determination of Cs concentration by GEA. Load and elution processing was conducted according to nominal plant design and throughput. The AZ-102 simulant was loaded at 1.5 BV/h, and the AP-101 simulant was loaded at 3.0 BV/h; elution was conducted at 2 BV/h for the first 6 BVs and then at 1.4 BV/h for the duration. After elution and water rinse, the column assemblies (resin bed plus glassware) were counted directly by GEA to evaluate residual Cs content. The column processing was repeated a total of four times, with the fourth-cycle processing conducted using polishing column conditions (e.g., 0.032 μg/mL Cs in AZ-102 simulant at nominally half the flowrate). The SL-644 was tested in only one and one-half cycles; one test was halted early because the column was inadvertently run dry, and the other test was started halfway through the second four-week processing phase and was ended with the other column tests.

(a) A cross-reference of resin identification number with supplier and manufacturing conditions will be supplied to BNI in a separate confidential letter.

The hydraulic properties of permeability, compressibility, and angle of internal friction were measured for Resins #3 (spherical), #9 (ground gel), and #12 (SL-644). Permeability testing was performed in 5-cm-diameter beds at length-to-diameter (L/D) ratios of both 1.6 and 2.7. The resins were exposed to four load/elute/regenerate cycles. During the AP-101 simulant load and the 1 M NaOH regeneration cycles, flowrates were increased to produce similar pressure drops to those expected in a full-scale column. The resin-bed height, differential pressure, and flowrate were measured to calculate resin-bed permeability. Additionally, load cells were placed on the bottom and side inside the columns to measure the force generated due to resin expansion. These same columns were also used for the resin-compressibility study. The column pressure on the top of the resin bed was cycled between 0 and 20 psi under stagnant flow conditions. The resin-bed height and side and bottom forces were measured to determine bed compression as a function of exerted force and to estimate the resin angle of internal friction.

All test conditions delineated by the Test Plan and Test Exceptions were met except as delineated in Table S.7.

Table S.7. Test-Condition Deviation

R&T Test Condition	Discussion
AZ-102 and AP-101 simulants analytes are to agree with target composition within ±15%.	The AP-101 simulant chloride concentration was 18% high. The AZ-102 simulant free-hydroxide concentration was 38% low. No simulant composition adjustment was made because it would have caused a negative impact on other analytes. BNI approved the use of the simulants as prepared.
One test with RF resin (#9) was to be conducted with downflow loading, feed displacement, and rinse, and upflow elution, rinse, and regeneration.	The first test cycle was conducted as indicated except that downflow regeneration was applied. The fourth load cycle was accidentally loaded upflow instead of downflow.
One SL-644 test is to be conducted in parallel with RF load and elution testing.	The SL-644 test failed during the second cycle because the feed line was accidentally dislodged to a position above the feed fluid. This error made room in the test matrix for another SL-644 test, this time with a larger particle-size diameter of 20- to 30-mesh expanded in the wet sodium form.

Simulant Use

The use of simulants for this testing provided an adequate basis for resin comparisons. The use of actual tank waste was not warranted for preliminary resin property testing and down-selection. The AZ-102 simulant matched the actual waste well with respect to chemical and physical properties. The AP-101 simulant selected to test hydraulic properties matched the actual tank waste well with respect to chemical, rheological, and physical properties.

Discrepancies and Follow-on Tests

The RF skeletal-density determination resulted in large spreads between duplicate results and possible low bias. The methodology for determining the skeletal density needs to be further refined for application to RF resin.

The λ_{50} values calculated from the equilibrium batch-contact K_d values and bed densities were not good indicators of the measured BV at 50% Cs breakthrough. The source of the discrepancies is not currently understood.

1.0 Introduction

The U.S. Department of Energy (DOE) is responsible for the disposition of millions of gallons of high-level radioactive wastes stored at the Hanford site in Richland, Washington. The waste is to be vitrified following specific pretreatment processing, separating the waste into a relatively small-volume high-activity waste fraction and a large-volume low-activity waste (LAW) fraction. To allow for contact handling of the immobilized LAW and land disposal, ^{137}Cs will need to be removed from the tank waste. Ion exchange is the baseline method for removing ^{137}Cs from Hanford high-level tank waste in the River Protection Project-Waste Treatment Plant (RPP-WTP). The current pretreatment flowsheet includes the use of cesium-selective, elutable, organic ion exchange material, SuperLig® 644 (SL-644), for Cs removal from the aqueous-tank-waste fraction. This material has been developed and supplied solely by IBC Advanced Technologies, Inc., American Fork, UT. To provide an alternative to this sole-source resin supply, the DOE Office of River Protection directed Bechtel National Incorporated (BNI) to initiate the process for selecting and testing an alternative ion exchange resin for Cs removal in the RPP-WTP. Resorcinol-Formaldehyde (RF) resin was selected as the most viable alternative for use in Cs removal.[(a)]

The RF resin has been extensively tested in both batch-contact studies and load and elute column studies using various tank-waste simulants demonstrating successful Cs decontamination [1-6]. However, these initial tests indicated that the Cs elution from RF resin with 0.4 M HNO_3 may not be efficient; the elution profiles resulted in plateaus near a maximum value where 1% C/Co may or not be reached [4, 6]. The slow elution was thought to be associated with channeling in the resin bed caused from shrinkage on conversion from Na-form to H-form. Additional side-by-side comparisons of RF with SL-644 load and elute behaviors were needed to better compare and evaluate load and elute behaviors.

Previous testing with SL-644 has shown that high column fluid pressure drops and wall pressures were experienced during the regeneration step after multiple operating cycles.[(b)] Several reasons for the observed elevated pressures are being considered, including 1) fines that plug the column generated from osmotic shock resulting from cycling the resin between acid and base form, 2) high particle breakage and fines generated from wall and internal friction upon resin expansion during regeneration, and 3) bed compaction from compressive force due to flow-pressure drop, resulting in even higher pressure drops. Previous results also indicated that the column height-to-diameter ratio may be important. Thus, initial testing was needed to include parameters that would examine the hydraulic issues associated with the RF resin processing and how they compare to those associated with SL-644 processing.

Battelle—Pacific Northwest Division (PNWD) was contracted to evaluate different RF resins, provide data supporting WTP's selection of one type of RF resin for further developmental work, and set preliminary RF resin purchase specifications. Work was conducted under contract number 24590-101-

(a) R Peterson, H Babad, L Bray, J Carlson, F Dunn, A Pajunen, I Papp, and J Watson. 2002. *WTP Pretreatment Alternative Resin Selection,* 24590-PTF-RPT-RT-02-001, Rev. 0, Bechtel National, Inc., Richland, WA.

(b) PS Sundar. December 4, 2002. "Pressure Drop Excursion in Ion Exchange Columns using SuperLig 644 Resins for Cesium Removal." Memorandum to Todd Wright and Roger Roosa.

TSA-W000-00004. Appendix C of the *Research and Technology Plan*[(a)] defines the initial evaluation of RF resins under Technical Scoping Statement A-222.

An exhaustive search for RF resin suppliers was conducted by BNI, Savannah River Technology Center (SRTC), and PNWD. Samples of freshly prepared RF resins were purchased from each identified supplier. The RF resins obtained represent a variety of manufacturing processes. To protect the identity of each supplier, neither supplier identification nor production details are discussed herein.[(b)]

The objectives of this work were to:

- provide data supporting WTP's selection of one type of RF resin for further development work by determining
  - bulk properties, including particle-size distribution (PSD), morphology, shrink-swell behavior, and bed density
  - batch-distribution coefficients as a function of Cs concentration and resin type
  - multi-cycle Cs load and elution behavior as a function of resin type
  - multi-cycle bed hydraulic behavior or parameters affecting hydraulic behavior for RF resin types.
- compare RF load and elute and hydraulic performance data to SL-644 performance data
- develop a preliminary RF purchase specification.[(c)]

All work was conducted according to Test Specification 24590-PTF-TSP-RT-02-016, Rev. 0,[(d)] Test Plan TP-RPP-WTP-210, Rev. 0,[(e)] and Test Exceptions 24590-WTP-TEF-RT-03-022, 24590-WTP-TEF-RT-03-031, and 24590-WTP-TEF-RT-03-074.

(a) S Barnes, R Roosa, and R Peterson. April 2003. Research and Technology Plan. 24590-WTP-PL-RT-01-002, Rev. 2, Bechtel National, Inc., Richland, WA.

(b) A crosswalk of resin identification number and supplier identification with known production information will be supplied to BNI under a separate, confidential letter.

(c) The preliminary purchase specification will be delivered to BNI in a separate document.

(d) MR Thorson. January 2003. Develop Requirements for Resorcinol Formaldehyde Alternate Resin. River Protection Project-Waste Treatment Plant, Bechtel National Inc., Richland, WA.

(e) SK Fiskum. April 2003. Initial RF Testing: Cs Load and Elution and Permeability Testing. Rev. 0. Battelle—Pacific Northwest Division. Richland, WA.

2.0 Experimental

The following sections describe the experimental approach and details used for RF resin handling, testing, data reporting, and analysis. All raw data generated in support of this testing are maintained in the project files at PNWD under Project 42365 records, inventory, and disposition system.

2.1 Simulant Preparation

Noah Technologies (San Antonio, TX) was contracted to prepare 130 L of AP-101 simulant without Cs according to the simulant recipe reported by Russell et al. [7]. After allowing the simulant to sit for 24 hours, it was filtered through a 0.5-μm pore size glass fiber filter. A 10-L aliquot was removed, and a pro-rated amount of $CsNO_3$ was added to the remaining 120 L to a final Cs concentration of 6 μg/mL, as established in the AP-101 simulant recipe. Noah Technologies was also contracted to prepare 130 L of AZ-102 simulant without Cs according to the simulant recipe reported by Hassan and Nash [8]. Solids were allowed to form for 24 hours before filtering through a glass-fiber filter with a pore size of 0.5 μm. After removing a 20-L aliquot, a pro-rated amount of $CsNO_3$ was added to the remaining 110 L simulant to a final Cs concentration of 50 μg/mL, as established in the AZ-102 simulant recipe. The AP-101 and AZ-102 simulant recipes are provided in Appendix E.

After arrival at PNWD, subsamples of each simulant were removed, filtered, and analyzed for density. All density determinations were performed in duplicate by measuring the net simulant mass in 25-mL Class A volumetric flasks. Additional subsamples were submitted to the Analytical Support Operations (ASO) under Analytical Services Request (ASR) 6769 for determination of free hydroxide, metals by inductively coupled plasma-atomic emission spectrometry (ICP-AES), total inorganic carbon (TIC or carbonate), Cs by inductively coupled plasma-mass spectrometry (ICP-MS), and anions by ion chromatography (IC). The ASO was responsible for assuring that the appropriate batch and analytical quality control (QC) samples were analyzed as well as providing any additional processing to the sub-samples that might be required.

The hydroxide, anions, and TIC were determined directly on the simulants. Hydroxide was determined using potentiometric titration with standardized HCl according to procedure RPG-CMC-228, *Determination of Hydroxyl (OH^-) and Alkalinity of Aqueous Solutions, Leachates, and Supernates and Operation of Brinkman 636 Auto-Titrator*. The free hydroxide was defined as the first inflection point on the titration curve. Anions were determined using a Dionix 4500 IC system equipped with a pulsed electrochemical detector according to procedure PNL-ALO-212, *Determination of Inorganic Anions by Ion Chromatography*. The TIC was determined by using silver-catalyzed hot persulfate (HP) oxidation according to procedure PNL-ALO-381, *Direct Determination of TC, TOC, and TIC in Radioactive Sludges and Liquids by Hot Persulfate Method*.

Simulant aliquots (nominally 1.0 mL) were acid-digested in duplicate according to procedure PNL-ALO-128, *HNO_3-HCl Acid Extraction of Liquids for Metals Analysis Using a Dry-Block Heater*. The acid-digested solutions were brought to a nominal 25-mL volume; absolute volumes were determined based on final solution weights and densities. Along with the sample and duplicate, the ASO processed a digestion preparation blank (PB), two blank spikes (BSs) (one for ICP-AES and one for ICP-MS), and

two matrix spikes (MSs) (one for ICP-AES and one for ICP-MS). Aliquots of the BS, MS, and PB, along with aliquots of the duplicate samples, were delivered to the ICP-AES and ICP-MS analytical workstations for analyses. The ICP-AES analysis was conducted according to procedure PNNL-ALO-211, *Determination of Elements by Inductively Coupled Argon Plasma Atomic Emission Spectrometry (ICPAES)*. The ICP-MS analysis was conducted according to procedure 329-OP-SC01, Rev. 0, *Inductively-Coupled Plasma Mass Spectrometry (ICP/MS) Analysis*.

The simulant analytical results are summarized in Table 2.1. All analytes measured were in good agreement with the target compositions (meeting the ±15% allowable tolerance), with two exceptions. The hydroxide in the AZ-102 simulant was 38% low. Adjusting the hydroxide concentration would have increased one or more cation concentrations (e.g., Na) significantly. The chloride concentration in the AP-101 simulant was 18% high, slightly exceeding the acceptance criterion (±15%). The chloride uncertainty at ±15% overlapped into the acceptable target range. The only recourse to correct the chloride concentration was to further dilute the simulant, thus affecting all other components. It was decided, in conjunction with the technical contact at BNI, to proceed with testing of both simulants with no matrix modification.

The simulant Cs concentration was modified for the fourth-cycle simulant feed of the ion exchange breakthrough and elution testing. In these cases, a simulant aliquot prepared by Noah Technologies that contained no added Cs was spiked with a 50 μg/mL stable Cs stock standard to a final Cs concentration of 2.40E-7 M (0.032 μg/mL) in the AZ-102 simulant and 1.06E-7 M (0.0141 μg/mL) in the AP-101 simulant.

2.2 RF Resin Receipt and Initial Handling

Each RF resin was assigned a unique identification number (#1 through #11) upon arrival at PNWD.[(a)] SL-644 from IBC production batch C-01-05-28-02-35-60 (also known as the first 25-gal production batch) was identified as Resin #12. The cross-reference to the identification number and actual resin supplier and manufacturing process is provided in a confidential letter to BNI.

Each RF resin was split and subsampled with the aid of an open-pan riffle sampler (Model H-3980, Humboldt Manufacturing, Co., Norridge, IL). Appropriately sized resin aliquots were taken to support follow-on testing. At least 10-mL of each as-received resin were reserved as sample archives in glass vials with a N_2 cover gas. The remainder of the resins (if any) were transferred to glass bottles and stored under N_2 cover gas.

(a) Resin receipt and bulk property testing were conducted according to, and documented in, Test Instruction TI-RPP-WTP-251, *Bulk Characterization of the RF Resin*, R Russell, May 2003. Resin skeletal density and bed porosity were conducted according to Test Instruction TI-RPP-WTP-310, *H-form Particle Density Determination*, R Russell, September 2003.

Table 2.1. AZ-102 and AP-101 Simulant Compositions

Analyte	Prep Blank, µg/mL	AZ-102 Simulant						AP-101 Simulant					
		Sample, µg/mL	Duplicate, µg/ mL	Average, µg/mL	Average M	Target M	% of Target	Sample, µg/mL	Duplicate, µg/ mL	Average, µg/mL	Average M	Target M	% of Target
Cs		49.7	47.7	48.7	3.66E-4	3.80E-4	96	5.99	6.02	6.01	4.52E-5	4.51E-5	100
Al	<11	1,350	1,370	1,360	5.04E-2	5.02E-2	100	6,820	6,880	6,850	2.54E-1	2.59E-1	98
Cr	<1.5	1,440	1,460	1,450	2.79E-2	2.67E-2	104	159	160	160	3.07E-3	2.92E-3	105
K	<250	5,700	5,740	5,720	1.46E-1	1.46E-1	100	27,700	27,900	27,800	7.11E-1	7.10E-1	100
Na	<22	118,000	121,000	119,500	5.20E+0	5.00E+0	104	122,000	124,000	123,000	5.35E+0	5.00E+0	107
P	[1.3]	323	322	323	1.04E-2	9.69E-3	107	407	413	410	1.32E-2	1.24E-2	107
Cl^-	NR	40 J[(a)]	NR	40 J(a)	1.13E-3 J[(a)]	0.00E+0	NA	1,700	1,730	1,715	4.84E-2	4.09E-2	118
NO_2^-	NR	54,600	NR	54,600	1.19E+0	1.19E+0	100	34,100	34,100	34,100	7.41E-1	7.07E-1	105
NO_3^-	NR	30,400	NR	30,400	4.90E-1	4.93E-1	99	103,000	103,000	103,000	1.66E+0	1.68E+0	99
PO_4^{3-}	NR	945	NR	945	9.95E-3	9.69E-3	103	1,130	1,150	1,140	1.20E-2	1.24E-2	97
SO_4^{2-}	NR	30,000	NR	30,000	3.12E-1	3.01E-1	104	4,050	3,770	3,910	4.07E-2	3.73E-2	109
OH^-	0	3,620	3,460	3,540	2.08E-1	3.34E-1	62	32,900	32,800	32,850	1.93E+0	1.94E+0	100
C as CO_3^{2-}	NR	10,900	10900	10,900	9.08E-1	8.76E-1	104	5,400	NR	5,400	4.50E-1	4.46E-1	101
Analyte	**Temp., ºC**	**g/mL**	**g/mL**	**Average, g/mL**		**Target g/mL**	**% of Target**	**g/mL**	**g/mL**	**Average, g/mL**		**Target g/mL**	**% of Target**
Density	23	1.2317	1.2346	1.233		1.237	99.7	1.2529	1.2546	1.254		1.26	99.5

(a) The chloride result for AZ-102 simulant is J-flagged because the analyte concentration was less than the estimated quantitation limit (EQL).

Notes: NR = not required (direct analysis does not require a preparation blank; IC batch precision was measured with AP-101 simulant duplicates; carbonate precision was measured with AZ-102 simulant duplicates)

NA = not applicable

The overall uncertainty for these analytes of interest is ±15%.

Bracketed results indicate that the analyte concentration uncertainty exceeded ±15%. Less-than (<) results indicate that the analyte concentrations were below the instrument detection limit (IDL); the dilution-corrected IDLs are given.

The total organic carbon (TOC) was also determined opportunistically. The AZ-102 simulant TOC was determined to be 11.2 mg C per mL, and the AP-101 simulant TOC was determined to be 1 mg C per mL.

ASR = 6769

Duplicate F-factor samples were taken to determine water content in the manufacturer-supplied resin form. Samples were nominally 0.5 g and were dried under vacuum at 50ºC to constant mass (where mass change was less than 0.01 g in a 12-h period). The F-factor was calculated according to Equation 2.1.

$$F = \frac{M_d}{M} \tag{2.1}$$

where F is the F-factor, M_d is the dry resin mass, and M is the starting resin mass.

A nominal 30- to 50-g sample split was processed for particle-size evaluation using American Society for Testing and Materials (ASTM) E-11 specification, 3-in. dry sieves with stainless steel cloth (Gilson, Lewis Center, OH; mesh sizes: 25, 30, 35, 40, 45, 50, and 60). The samples were hand-shaken until mass changes between shaking events on each sieve were minimal. Once mass was nearly constant for a given shaking interval, the shaking was stopped. The resin mass fraction on each sieve was calculated.

The as-received resin dry, bulk density was calculated from the net resin mass and settled resin volume in a 50-mL graduated cylinder (ID equal to 2 cm). The graduated cylinder was tapped and vibrated until a constant resin volume was obtained. The resin weight was corrected for water content and the dry, bulk density (δ_B) was calculated according to Equation 2.2.

$$\delta_B = \frac{m * F}{V} \tag{2.2}$$

where m was the measured net resin mass in the graduated cylinder, and V was the settled-resin volume.

Resins #2 and #5 were considered duplicates of one another since they were made by the same manufacturer under the same process conditions but several months apart. These two resins were therefore combined after dry-sieving was complete. The combined resins were re-identified as #9, and Resin #2 and #5 were eliminated from further testing.

2.3 Pretreatment

All resins were pretreated by cycling several times from the H-form to Na-form. Each resin was converted to the H-form by contacting it with 0.5 M HNO_3 in a 3 to 1 ratio of liquid-to-resin volume for 1 hour with occasional gentle swirling. The acid was then decanted, and the resin was rinsed with deionized (DI) water in a 3 to 1 ratio of liquid-to-resin volume for 10 minutes with gentle swirling. This DI water rinse was repeated until the solution pH was >4 or a minimum of three times. The resin was then contacted with 0.25 M NaOH in a 3-to-1 ratio of liquid-to-resin volume for 2 hours with occasional gentle swirling. The basic solution was then decanted, and the resin was rinsed with DI water in a 3-to-1 ratio of liquid-to-resin volume for 10 minutes with gentle swirling. This DI water rinse was repeated until the solution pH was <10 or a minimum of three times. These steps were then repeated. All resins were then converted back to H-form by repeating the acid contact and DI water rinse. The resins were then dried under flowing N_2 and/or under vacuum (25 mm Hg) at ambient temperature until they were free-flowing and had a nearly constant mass. Vacuum was typically used for extended unattended operations.

After drying, the resin sample materials were split for further testing as shown in Figure 2.1. Resins were selected in consultation with BNI for additional studies. The additional studies included skeletal density determination, breakthrough and elution testing, and hydraulic testing.

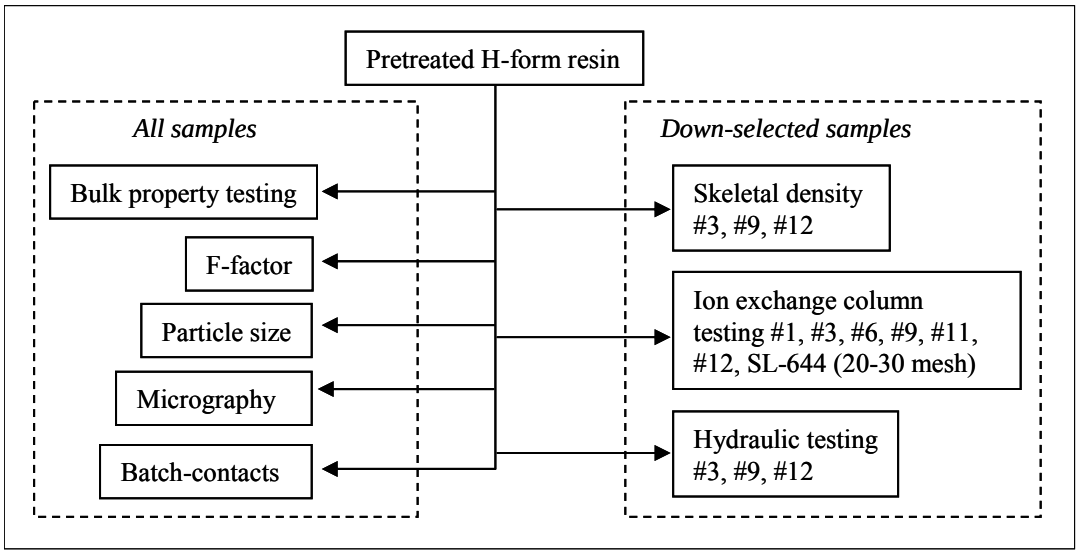

Figure 2.1. Pretreated Resin Processing

2.4 F-Factor Analysis

Duplicate F-factor samples were taken to determine water content in the pretreated resins. Aliquots of ~0.5 g were dried under vacuum at ambient temperature until a constant mass was obtained. The temperature was increased to 50°C, and the samples were dried under vacuum to constant mass. The temperature was increased to 85°C, and the samples were dried under vacuum again to constant mass. Observations were made at each weighing interval to qualitatively assess whether the resin was damaged by the heating process. The F-factor for each resin was calculated using Equation 2.1 for each drying temperature.

2.5 Bulk-Property Testing

The measured resin bulk properties included parameters of resin-bed density, shrink-swell characteristics, and swollen-resin density, and on selected resins, bed porosity and skeletal density. Resins were tested in duplicate in both the H-form and Na-form. In all cases, the mass was based on the dried H-form mass where the F-factor applied was relative to the 50ºC vacuum-dried mass (see Section 2.4). A flowchart for testing sequences is provided in Figure 2.2.

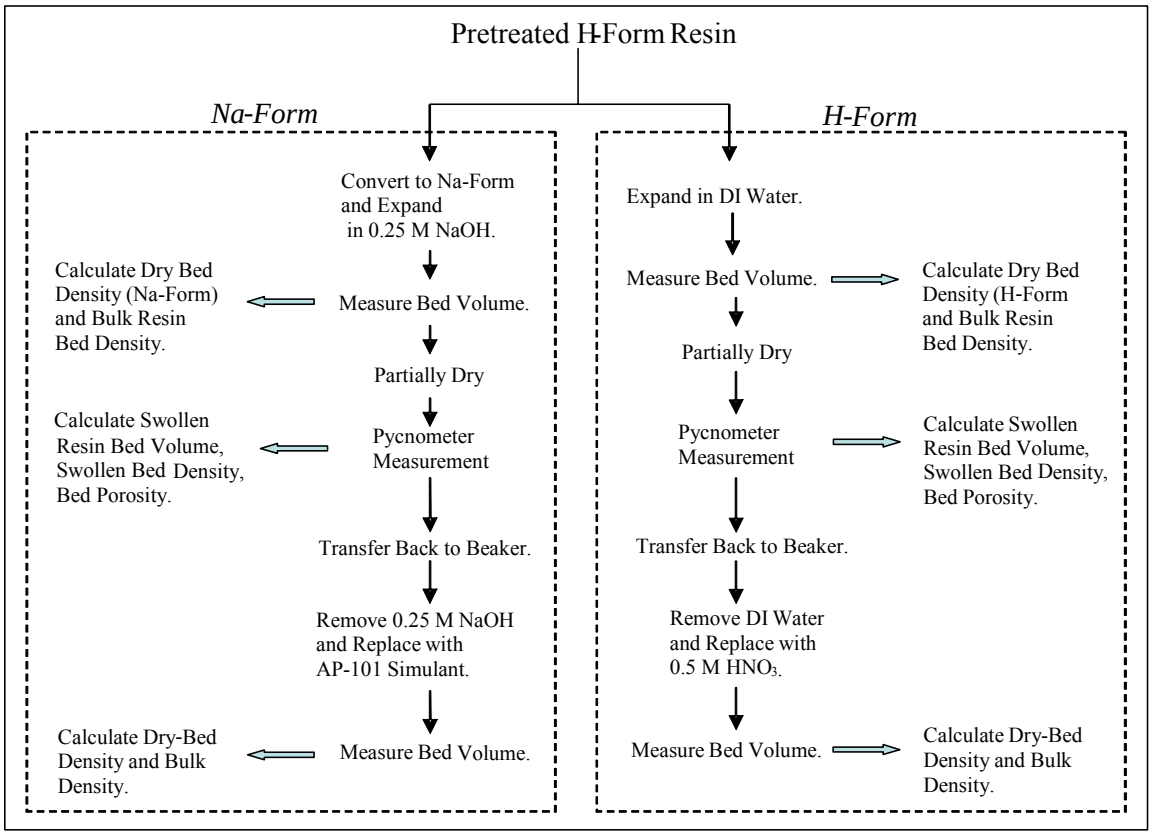

Figure 2.2. Flowchart for Bulk-Property Measurements

Four separate samples of each resin ranging from 3 g to 8 g were weighed to the nearest 0.001 g. Two subsamples for H-form testing were soaked in DI water for 1 hour to fully hydrate the resin. Two subsamples selected for Na-form testing were converted to the Na-form by contacting for 2 hours with a 3:1 volume ratio (liquid to solid) of 1 M NaOH, washing three times with DI water, and then mixing with 50-mL 0.25 M NaOH.

Shrink-Swell Characteristics and Dry-Bed Density. The resin shrink-swell characteristics and dry-bed density were measured on both resin forms. The resin slurries were transferred into 50-mL graduated cylinders (ID equal to 2 cm). The resins were allowed to settle in the graduated cylinders for 2 hours. The graduated cylinders were tapped and vibrated until constant volumes were obtained. The shrink-swell characteristic was determined from the settled resin bed volume (BV). The dry-bed density was calculated according to Equation 2.3:

$$\delta_{DRB} = \frac{M * F}{BV_s} \tag{2.3}$$

where δ_{DRB} = dry-bed density of resin
M = mass of pretreated resin measured in the H-form
F = F-factor of pretreated resin (50ºC)
BV_s = settled volume of wet resin.

Bulk Wet-Slurry Density. The bulk, wet slurry densities of the resins were also measured at this time. The gross slurry mass and the supernatant volume above the settled resin bed were measured in the graduated cylinder. The mass associated with the expanded resin-bed volume could then be calculated. The bulk, wet density was then calculated according to Equation 2.4:

$$\rho_w = \frac{M_T - M_H}{BV_s} \tag{2.4}$$

where ρ_w = bulk, wet slurry density (wet resin plus interstitial fluid density)
M_T = total mass (resin mass plus interstitial fluid mass plus solution mass above resin)
M_H = mass of solution head above resin = observed supernatant volume multiplied by supernatant density
BV_s = settled volume of wet resin.

Swollen-Resin Density. The resin was then filtered to remove interstitial fluids, and the swollen-resin density was measured using a calibrated 25-mL KIMAX® pycnometer. A portion of the filtered resin was placed in the calibrated pycnometer, weighed, filled with degassed DI water, and weighed again. The H-form resin was weighed in the H-form; the Na-form resin was weighed in the Na-form. The temperature of the resin/water mixture was also measured to the nearest 0.1°C. The swollen-resin volume was calculated according to Equation 2.5:

$$V_R = V_T - \left(\frac{m_w}{\delta_w} \right) \tag{2.5}$$

where V_R = swollen-resin volume
V_T = volume in flask (resin plus water)
m_w = mass of water in flask
δ_w = density of water in flask (temperature corrected).

The swollen-resin density was then determined by dividing the swollen resin mass by the swollen-resin volume.

The resin was then removed from the pycnometer, combined with the remaining resin, and placed in a beaker. The DI water was decanted from the resin. To the H-form resin samples, aliquots of 0.5 M HNO_3 were added and allowed to equilibrate for 1 hour. To the Na-form samples, aliquots of AP-101 simulant were added and allowed to equilibrate for 1 hour. The resin dry-bed density was then measured as described above.

Resin-Bed Porosity. The bed porosity was determined according to Equation 2.6 for Resins #3 (spherical), #9 (ground gel), and #12 (SL-644) from the settled-bed volume and the swollen-resin volume (V_R):

$$\varepsilon_B = \frac{BV_s - V_R}{BV_s} \tag{2.6}$$

where ε_B is the bed porosity (mL interstitial solution/mL BV), BV_s is the settled-bed volume (resin with interstitial fluid), and V_R is the swollen-resin volume.

Skeletal Density. The H-form skeletal density was measured on Resins #3, #9, and #12 by placing approximately 1.0 g of dried, free-flowing resin in a 25-mL pycnometer, weighing, filling the pycnometer with degassed DI water, and weighing again. All masses were measured to the nearest 0.0001 g. The temperature of the resin/water mixture was measured to the nearest 0.1°C. The resin was removed from the pycnometer using DI water to transfer, and was collected on a tared, glass-fiber, filter paper. The resin was dried to constant mass at 50ºC under vacuum. The H-form skeletal density was then calculated according to Equation 2.7.

$$\delta = \frac{m}{\left(V_p - \frac{m_w}{\delta_w}\right)} \tag{2.7}$$

where δ = H-form skeletal density
m = H-form resin mass (removed from pycnometer and dried at 50ºC under vacuum)
V_p = pycnometer volume
m_w = mass of water in pycnometer
δ_w = density of water in pycnometer.

Skeletal density determined by helium pycnometry would probably differ slightly from the value determined by this method (DI water pycnometry).

2.6 Expanded Particle-Size Distribution

The PSD was measured on each of the pretreated resins in both the H-form and the Na-form. This analysis was performed according to procedure TPR-RPP-WTP-222, Rev. 1, *S3000 Microtrac Particle Size Analyzer*, using a Micro TRAC S3000 Particle Size Analyzer. National Institute of Standards and Technology (NIST) traceable 100-μm and 500-μm standards were used before and after the PSD measurements to assure the accuracy of the results. The dispersion liquid for both the H-form and the Na-form resins was DI water. This particle-size analyzer was only capable of measuring particle sizes up to a maximum of 1410 μm.

2.7 Optical Microscopy

Optical micrographs of the dried, pretreated resins were taken at 10×, 25×, and 70× magnification to characterize particle shape and morphology. A pretreated resin sample was randomly distributed in a plastic Petri dish that was then placed on a white background. Several observations were made of the resin before the micrographs were taken to help assure that the photographed regions were representative of the overall resin. Because the spherical resin rolled so easily, it is possible that the observed

morphology was slightly biased; broken pieces would probably land face-down, obscuring the broken nature of the particle.

2.8 Batch-Contact Testing

Batch-distribution contact testing is a rapid method for determining relative performance of various ion exchange materials in a given matrix. All pretreated resins were batch-contact tested with the AZ-102 simulant matrix at five different Cs concentrations.[(a)]

Batch-contact stock solutions of AZ-102 simulant (spiked stock solutions 1 through 5) were prepared at five Cs concentrations. Aliquots of the 50 µg/mL Cs AZ-102 simulant were spiked with additional Cs from $CsNO_3$ spiking solutions at 1.05E-03 M (Spike 1) and 0.53 M (Spikes 2, 3, and 4). An aliquot of AZ-102 simulant with no added Cs was spiked with 1.05E-03 M $CsNO_3$ (Spike 5). The calculated initial Cs concentrations in the batch-contact stock solutions are shown in Table 2.2. A ^{137}Cs tracer was added to each stock solution to facilitate tracking of Cs-exchange behavior using gamma-energy analysis.

Table 2.2. Initial Cs Concentrations Used for the Batch-Distribution Tests

Solution	Cs Concentration mg/L	Cs Concentration Molarity
AZ-102 Cs Spike 5	6.55E-03	4.93E-08
AZ-102 Cs Spike 1	49.9	4.48E-04
AZ-102 Cs Spike 2	96.6	7.27E-04
AZ-102 Cs Spike 3	178	1.34E-03
AZ-102 Cs Spike 4	681	5.12E-03

The batch-distribution tests were performed in duplicate on each pretreated resin at each Cs concentration. Nominally 0.2 g of pretreated H-form resin was contacted with 20 mL of simulant in a 35-mL glass vial. The resin mass was determined to an accuracy of 0.0002 g. The simulant volume was transferred by pipet; the actual contact volume was determined by mass difference and solution density. The targeted phase ratio (liquid volume to exchanger mass) was 100 mL/g. The obtained ratio varied between 97 mL/g and 180 mL/g because the residual water contents in several resins were higher than anticipated. Sample-specific volumes and resin masses are given in Appendix B. The headspace above the simulant was purged with nitrogen gas just before capping. Resins 1, 8, 9, 10, and 11 began out-gassing (effervescing) upon contact with the simulant.[(b)] The amount of gas produced by Resins 1, 8, and 9 was minimal, while Resins 10 and 11 produced the largest amount.

Vials were placed lengthwise in an Eberback Corp. (Ann Arber, Mich.) reciprocal shaker set to 2.1 cycles per second. Rigorous mixing was observed for all samples. The resin materials were contacted for nominally 96 hours. The temperature was not controlled, but was generally between 22 and 29ºC during the contact period, as determined by a Fisher Thermo-Hygrometer (used for indication only). After contact, the samples were filtered through 0.45-µm nylon-membrane syringe filters.

(a) The batch-distribution testing, including AZ-102 Cs-spiked stock-solution preparation, was conducted according to Test Instruction TI-RPP-WTP-249, *Batch Contact Testing of Several Resins with AZ-102 Simulant for Resin Validation*, L Snow, May 2003.

(b) The out-gassing may be attributable to neutralization of the carbonate with the H^+ ions in H-form resin.

Equilibrium conditions were evaluated as a function of contact time for each resin. Replicate samples from each resin were prepared as described above with the Spike 4 contact solution. Duplicate samples were removed at 24-, 48-, and 72-h contact times. All remaining samples were removed after the 96-h contact time.

All solutions were analyzed by gamma-energy analysis (GEA) to determine the ^{137}Cs concentration. The ^{137}Cs tracer concentrations in the un-contacted simulant samples were used to define the initial Cs concentrations (C_o). Final (equilibrium) Cs concentrations (C_{eq}) were calculated relative to the ^{137}Cs tracer recovered in the contacted samples (C_1) according to Equation 2.8:

$$Cs_{Eq} = Cs_0 * \left(\frac{C_1}{C_0} \right) \tag{2.8}$$

where Cs_{Eq} = equilibrium Cs concentration in solution (μg/mL or M)
Cs_0 = initial Cs concentration in solution (μg/mL or M)
C_1 = equilibrium ^{137}Cs concentration in solution (cpm/mL)
C_0 = initial ^{137}Cs concentration in solution (cpm/mL).

The equilibrium Cs concentrations in the resins (Cs_R in units of mg Cs per g of dry resin mass) were calculated according to Equation 2.9:

$$Cs_R = \frac{\mathrm{Cs}_0 * V * \left(1 - \frac{C_1}{C_0} \right)}{M * F * 1000} \tag{2.9}$$

where Cs_R = equilibrium Cs concentration in the resin (mg Cs / g resin)
Cs_0 = initial Cs concentration in solution (μg/mL)
V = volume of the liquid sample (mL)
C_1 = final count rate of ^{137}Cs tracer in solution
C_0 = initial count rate of ^{137}Cs tracer in solution
M = mass of H-form ion exchanger (g)
F = F-factor
1000 = conversion factor to convert μg to mg.

The Cs batch-distribution coefficient (K_d) values were determined according to the standard formula shown in Equation 2.10.

$$K_d = \frac{(C_0 - C_1)}{C_1} * \frac{V}{M * F} \tag{2.10}$$

where K_d = batch-distribution coefficient (mL/g)
C_0 = initial ^{137}Cs concentration (cpm/mL)
C_1 = final (equilibrium) ^{137}Cs concentration (cpm/mL)
V = volume of the liquid sample (mL)
M = mass of pretreated H-form ion exchanger (g)
F = mass of the dried resin divided by the mass of the as-received resin.

Errors were kept small because Cs tracer was used; samples with low Cs concentrations were counted longer to reduce counting error. Sample count errors were less than 3% (1-σ) and were generally around 1% (1-σ).

To compare batch-contact results with previously reported data, the mass increase of H-form resin to Na-form resin (I_{Na}-factor) will need to be incorporated in Equation 2.9. This will effectively increase the resin contact mass and thus decrease the observed K_d. Determination of the I_{Na}-factor was beyond the current testing scope.

2.9 Ion Exchange Process Testing

Four different ion exchange tests were run simultaneously using four different single-column assemblies.[(a)] Conducting four tests in parallel reduced overall operating cost per test and speeded the required data-collection process. Figure 2.3 shows a schematic of a typical ion exchange column assembly. A system consisted of one glass column containing ion exchange resin, a small metering pump, three valves, a pressure gauge, and a pressure-relief valve. Valves 1 and 3 were two-way valves that could be turned to the flow position or no-flow position; Valve 2 was a three-way valve that could be turned to the column-flow position or an exhaust position to expel trapped air or fluids from the column input line. Valve 1 was placed at the outlet of the pump and was used to isolate the column from the pump. Valve 3 was primarily used to obtain samples and isolate the system during brief storage periods.

Columns were prepared at the Kontes Custom Glass Shop (Vineland, NJ). Each column was 10-cm tall with an inside diameter of 2.0 cm (corresponding to a resin volume of 3.1 mL/cm) and a 2.8-mm wall thickness. The glass was safety coated with polyvinyl chloride. Stainless steel, 200-mesh screens, provided by SRTC, supported the resin beds. The screens were stabilized with snug-fitting O-rings. The cavity below the screen support was filled with 3-mm-diameter glass beads, reducing the fluid-filled volume from 11 mL to 6 mL. The height of the resin bed (and thus shrinkage and swelling) was measured with a millimeter-scale ruler (the associated measurement error was estimated to be ±2 mm). The fluid level above the column was maintained at nominally the 9.5-mL height. Depending on whether the resin was expanded (nominally 6 cm tall) or contracted (nominally 4 cm tall), fluid volume above the resin bed varied from nominally 9 mL to 17 mL.

(a) The ion exchange column testing was conducted according to TI-RPP-WTP-248, *Column Ion Exchange Testing of Resorcinol Formaldehyde Resins*, SK Fiskum, May 2003.

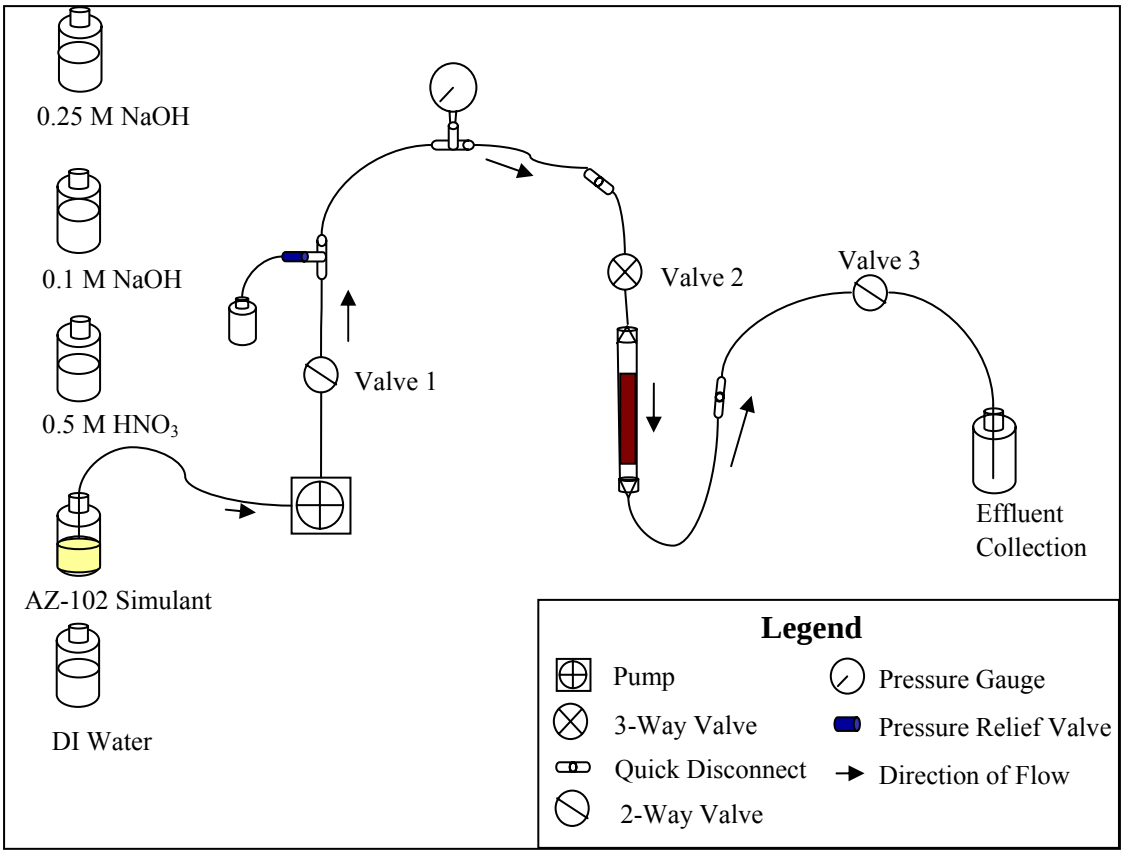

Figure 2.3. Ion Exchange Column Processing System

The connecting tubing was $^{1}/_{8}$-in. OD and $^{1}/_{16}$-in. ID and was made of Teflon. The end fittings were standard Kontes Chromaflex column end fittings with Teflon ferrules. The inlet sample line ended at the column fitting. The column assembly contained an in-line Swagelok Poppet pressure relief check valve with a 10 psi trigger (Solon, OH) and a 15-psi pressure gauge (McDaniel Controls Model #SA, Luling, LA). Valved quick-disconnects (Cole Parmer, Vernon Hills, IL) were installed in-line to allow for ease of column removal and switching. Fluid Metering, Incorporated (FMI) QVG50 pumps (Syosset, NY) equipped with a ceramic and Kynar® coated low-flow piston pump heads were used to introduce all fluids. The flowrate was controlled with a remotely-operated FMI stroke-rate controller. The pump was set up to deliver flowrates from 0.3- to 1.1-mL/min. The volume actually pumped was determined using the mass of the fluid collected divided by the fluid density. The holdup volume of the entire ion exchange system was the summed volume of all fluid-filled parts and ranged from 47 mL to 50 mL, depending on the resin-bed volume and solution-head volume.

The RF resin performance was tested in a side-by-side comparison with SL-644. Two different batches of SL-644 were tested. One was from the 95-L (25-gal) production batch, ID C-01-05-28-02-35-60. The other resin was provided by SRTC from the 946-L (250-gal) production batch ID, C-01-11-05-02-35-60. Personnel at SRTC first performed a wet-sieve screen of an aliquot of 946-L (250-gal) production-batch material and isolated the 20- to 30-mesh PSD fraction.[(a)] A subsample was forwarded to PNWD for testing. Both SL-644 resins were pretreated in a manner consistent with

(a) Product specification provided in e-mail message from C. Nash to S. Fiskum on July 16, 2003.

previous testing [9]. Each resin was provided from the vendor in the Na-form as a slurry. An aliquot was removed and rinsed with DI water and then contacted with a nominal three-fold volume of 0.5 M HNO_3 and allowed to soak for 1 hour. The acid was decanted and the contact repeated twice more with fresh acid. The resin was then rinsed with DI water until the pH was >5 as determined from short-range pH paper. The resin was then dried under a flow of N_2 gas until it was free-flowing. The pre-conditioned SL-644 resin was reddish brown with shiny surfaces.

Processing was conducted in two phases where four columns were operated at one time. Because of an early failure, a ninth column system could also be incorporated. The column tests were numbered as Columns 1 through 9. The mass basis of resin in the columns was the pretreated H-form resin. A quantity of pretreated H-form resin was weighed along with duplicate F-factor samples to correct for water content. The F-factor samples were dried at 50ºC under vacuum to constant mass. The F-factor was calculated according to Equation 2.1. The actual H-form resin mass, on a dry-weight basis, loaded in the columns was calculated according to Equation 2.11.

$$M_d = M_p * F \tag{2.11}$$

where M_d is the dry resin mass in the resin bed, M_p is the pretreated resin mass, and F is the water-loss factor dried at 50ºC. The Na mass basis was not calculated as part of this scope of work.

The resin identifications and corresponding column identifications along with the calculated dry-resin masses loaded into each test column are given in Table 2.3. The experimental F-factors are also provided from which the dry-resin masses were calculated. The duplicate F-factor values resulted in excellent precision as demonstrated by the low relative percent difference (RPD) between the duplicates.

Table 2.3. Column Cross-Reference to Resin ID and H-Form Resin Masses

Column ID	Resin ID #	Dry Mass Added (H-form), g	F-Factor	Duplicate F-Factor	RPD
1	12[(a)]	4.070	0.7872	0.7881	0.11
2	9	5.780	0.7027	0.7019	0.11
3	9	5.761	0.7027	0.7019	0.11
4	9	5.765	0.7027	0.7019	0.11
5	11	4.423	0.9063	0.9083	0.22
6	1	6.388	0.7417	0.7427	0.13
7	3	4.989	0.5722	0.5735	0.23
8	6	5.108	0.5759	0.5780	0.36
9	SL-644[(b)]	4.649	0.9619	0.9590	0.30

(a) SL-644 from 95 L (25-gal) production batch, IBC Batch ID C-01-05-28-02-35-60.
(b) SL-644 from 946 L (250-gal) production batch, IBC Batch ID C-01-11-05-02-35-60, 20 to 30 mesh fraction.
RPD = relative percent difference

Before process testing, the weighed aliquot of pre-treated H-form resin was soaked in a 10:1 ratio of 1 M NaOH volume-to-resin mass in a beaker to allow for free resin expansion. Gas evolution or effervescence occurred with SL-644 and Resin #11 when soaked in the caustic solution. The 1 M NaOH was replenished for #11 after 1.5 hours of soak time because effervescence was so pronounced. Effervescence in #11 ceased during the next 20-min interval, then 20 mL 2 M NaOH were added to #11. No additional effervescence was observed. After resins were soaked for 2 hours in the caustic medium, the NaOH was decanted, and the resin was slurried with an equivalent volume of DI water. The resin slurry was then transferred to the column. The resin bed was rinsed with DI water and cycled to the H-form and back to the Na-form; all processing was conducted downflow. Initial RF conditioning with Resin #9 mimicked that of the SL-644 conditioning where the Na-form resin was regenerated using 0.25 M NaOH. Gas formation was subsequently observed in the RF resin beds during simulant processing of Resin #9. Incomplete conversion of the resin to the Na-form was suspected to contribute to the bubble formation. A more concentrated NaOH regenerant solution (1 M) was tested on another preparation of Resin #9 in a column format. Bubble production was greatly diminished so 1 M NaOH regenerant solution was used on all subsequent RF tests. No evidence of bubble formation was observed during all subsequent tests.

Processing was generally performed downflow at ambient temperature. Columns 2 and 5 were exceptions where upflow elution, DI water rinse, and regeneration were tested. Specific processing details and experimental conditions are provided in Table 2.4 through Table 2.12. In all cases, one BV is defined as the BV loaded in the column as the Na-form resin. The volume differences from the load condition to the first regeneration condition for the columns were less than 12%, except for Column 1 where the difference was the greatest at +18%. The BV is an arbitrary value; all resin beds expanded and contracted significantly as a function of feed matrix. The fluid above the resin bed generally remained at a constant mark on the column.[(a)] Thus, the mixing volume above the resin bed increased from a nominal 9-mL volume to a nominal 15-mL volume (downflow processing) as the resin bed shrank.

The feed simulant was filtered through a 0.45-μm-pore-size nylon filter before use to assure that solids were not present. A suitable amount of simulant, typically 4-L per column test, was prepared by spiking with a radioactive Cs tracer. The first two cycles of Columns 1 through 4 used nominally 0.013 μCi/mL ^{134}Cs tracer. Activity concentrations were increased in subsequent cycles to nominally 0.075 μCi/mL ^{137}Cs tracer.

Samples were collected periodically during the simulant feed and elution steps to evaluate Cs breakthrough and elution behavior. Otherwise, each feed matrix (regeneration, feed displacement, DI water rinses) was collected separately as a composite effluent. Feed samples were collected two to three times per day. For the first two cycles of Columns 1 through 4, a 5-mL sample volume was collected. Subsequent tests used a 15-mL sample collection to enhance detection limits. Eluate samples were collected in nominal 1- to 2-BV increments. The Cs load and elute behavior was monitored from the Cs-tracer behavior using gamma spectrometry.

After process cycles 1 through 3, the ion exchange column assembly was disconnected at the quick disconnects and removed from the fume-hood containment. The column assembly was mounted in front of a side-looking GEA detector and counted. Care was taken to position the resin bed itself in front of the

(a) During upflow elution, the fluid above the resin bed increased as the void volume was filled.

detector face. The column assembly in the counting chamber included the ion exchange resin, the interstitial fluid, glassware, and the fluid-head and tail-mixing areas. Thus, Cs tracer in any of the non-resin areas could shine into the detector and bias the measurement. An approximate geometry correction was applied, although the exact geometry presented to the detector was neither calibrated nor was the Cs location on the system known. The calibration accuracy was checked by recounting one column system at a greater distance from the detector (minimizing geometry effects). Both calculated activities agreed well, lending support to the application of the geometry correction factor. A conservative uncertainty of a factor of two was applied to the column Cs-tracer measurements.

Table 2.4. Experimental Conditions for Column 1 Test, SL-644, Resin #12

Process step	Solution	Total Volume			Flowrate		Time	T, °C
		BV[(1)]	AV[(2)]	mL	BV/h	mL/min	h	
In-Situ Preconditioning (5/21/03)								
Water rinse	DI water	11.8	3.85	192	3.68	1.00	3.20	NR
Acid wash	0.5 M HNO_3	6.61	2.16	108	3.30	0.899	2.00	NR
Water rinse	DI water	10.0	3.27	163	3.73	1.01	2.70	NR
Cycle 1(Start 5/27/03)								
Regeneration	0.25 M NaOH	6.08	1.99	99.3	2.79	0.756	2.18	23
Loading column	AZ-102 Simulant	250.4	NA	4090	1.53	0.416	162.1	22-24
Feed displacement	0.1 M NaOH	3.62	1.18	59.1	2.86	0.778	1.27	NR
Rinse	DI water	3.54	1.16	57.8	2.87	0.781	1.23	22
Elution	0.5 M HNO_3	8.02	2.62	131	2.31	0.628	3.5	23
Elution	0.5 M HNO_3	30.6	9.98	500.6	1.41	0.384	21.7	21-23
Rinse	DI water	3.01	0.98	49.0	1.26	0.344	2.38	NR
Cycle 2 (Start 6/5/03)								
Regeneration	0.25 M NaOH	6.25	2.04	102	2.78	0.756	2.25	21
Loading column	AZ-102 Simulant	174	NA	2842	1.51	0.411	119.2	22-24
Feed displacement	0.1 M NaOH	4.21	1.38	68.8	2.78	0.756	1.52	23
Rinse	DI water	3.96	1.29	64.7	2.80	0.761	1.42	23
Elution	0.5 M HNO_3	7.13	2.32	116	2.45	0.668	2.92	24
Elution	0.5 M HNO_3	12.2	4.00	200	1.49	0.405	8.25	21-24
Rinse	DI water	4.14	1.35	67.7	1.44	0.393	2.87	NR

(1) BV = bed volume (16.3 mL in the Na-form volume as loaded in the column; the volume expanded to 19.2 mL in the 0.25 M NaOH first regeneration condition, 18% volume increase).
(2) AV = apparatus volume (50 mL).
NA = not applicable
NR = not recorded

Table 2.5. Experimental Conditions for Column 2 Test, Resin #9

Process step	Solution	Total Volume			Flowrate		Time	T, ºC
		BV[1]	AV[2]	mL	BV/h	mL/min	h	
In-situ Preconditioning (5/21/03)								
Water rinse	DI water	11.2	3.89	194	3.42	0.986	3.28	NR
Acid wash	0.5 M HNO_3	6.71	2.32	116	3.25	0.937	2.07	NR
Water rinse	DI water	9.23	3.19	160	3.26	0.940	2.83	NR
Cycle 1 (Start 5/27/03)								
Regeneration	0.25 M NaOH	6.15	2.13	106	3.16	0.910	1.95	23
Loading column	AZ-102 Simulant	205	NA	3550	1.50	0.431	142.6	22-24
Feed displacement	0.1 M NaOH	3.31	1.15	57.3	3.05	0.881	1.08	NR
Rinse	DI water	3.51	1.22	60.8	3.19	0.921	1.10	22
Elution (upflow)	0.5 M HNO_3	6.29	2.18	109	2.05	0.591	3.47	23-25
Elution (upflow)	0.5 M HNO_3	28.3	9.80	490	1.31	0.379	21.7	21-23
Rinse (upflow)	DI water	3.03	1.05	52.4	1.27	0.366	2.38	NR
Cycle 2(Start 6/5/03)								
Regeneration	1.0 M NaOH	6.21	2.15	107	3.05	0.881	2.03	21
Loading column	AZ-102 Simulant	194	NA	3349	1.53	0.442	125.4	22-24
Feed displacement	0.1 M NaOH	4.09	1.41	70.7	3.18	0.918	1.28	23
Rinse	DI water	3.95	1.37	68.4	3.16	0.912	1.25	23
Elution (upflow)	0.5 M HNO_3	5.46	1.89	94.5	2.02	0.584	2.92	24
Elution (upflow)	0.5 M HNO_3	9.81	3.39	170	1.32	0.380	7.46	21-24
Rinse (upflow)	DI water	4.27	1.48	73.8	1.27	0.365	3.37	21
Cycle 3 (Start 6/13/03)								
Regeneration (upflow)	1.0 M NaOH	7.12	2.46	123	2.99	0.861	2.38	23
Loading column	AZ-102 Simulant	185	NA	3193	1.53	0.440	121.1	20-24
Feed displacement	0.1 M NaOH	4.08	1.41	70.6	4.08	0.872	1.35	23
Rinse	DI water	3.76	1.30	65.1	3.18	0.917	1.18	23
Elution (upflow)	0.5 M HNO_3	5.56	1.92	96.2	1.98	0.571	3.11	23
Elution (upflow)	0.5 M HNO_3	18.9	6.55	328	1.37	0.395	13.8	20-23
Rinse (upflow)	DI water	3.43	1.19	59.3	1.35	0.390	2.53	20
Cycle 4 (Start 6/20/03)								
Regeneration (upflow)	1.0 M NaOH	6.92	2.39	120	3.19	0.920	2.17	21
Loading column (upflow)[3]	AZ-102 Simulant (2.40 E-7 M Cs)	85.4	NA	1478	0.743	0.214	116.1	20-24

(1) BV = bed volume (17.3 mL in Na form as loaded in column)
(2) AV = apparatus volume (50 mL)
(3) Loading was intended to be downflow.
NA = not applicable
NR = not recorded
Except as noted, all processing was downflow.

Table 2.6. Experimental Conditions for Column 3 Test, Resin #9

Process step	Solution	Total Volume			Flowrate		Time	T, °C
		BV[1]	AV[2]	mL	BV/h	mL/min	h	
In-situ Preconditioning (5/21/03)								
Water rinse	DI water	11.4	4.09	204	3.28	0.980	3.48	NR
Acid wash	0.5 M HNO_3	6.76	2.42	121	2.94	0.877	2.3	NR
Water rinse	DI water	8.12	2.90	145	2.96	0.882	2.75	NR
Cycle 1 (Start 5/27/03)								
Regeneration	0.25 M NaOH	5.23	1.87	93.6	2.41	0.720	2.17	24
Loading column	AZ-102 Simulant	202	NA	3617	1.41	0.419	141.7	22-24
Feed displacement	0.1 M NaOH	3.09	1.11	55.3	2.37	0.709	1.30	NR
Rinse	DI water	3.45	1.24	61.8	2.41	0.718	1.43	22
Elution	0.5 M HNO_3	5.34	1.91	95.7	1.77	0.529	3.57	23-25
Elution	0.5 M HNO_3	25.3	9.04	452	1.06	0.317	23..8	21-25
Rinse	DI water	2.58	0.92	46.2	1.20	0.358	2.15	NR
Cycle 2 (Start 6/5/03)								
Regeneration	1.0 M NaOH	4.86	1.74	87.0	2.37	0.707	2.05	21
Loading column	AZ-102 Simulant	189	NA	3390	1.55	0.464	121.0	20-24
Feed displacement	0.1 M NaOH	3.82	1.37	68.4	2.47	0.736	1.55	23
Rinse	DI water	3.28	1.18	58.8	2.14	0.639	1.53	23
Elution	0.5 M HNO_3	5.23	1.88	93.6	1.71	0.512	3.05	24
Elution	0.5 M HNO_3	8.96	3.20	160	1.21	0.360	7.43	21-24
Rinse	DI water	4.00	1.43	71.6	1.20	0.358	3.33	21
Cycle 3 (Start 6/13/03)								
Regeneration	1.0 M NaOH	6.36	2.28	114	2.36	0.704	2.70	23
Loading column	AZ-102 Simulant	173	NA	3100	1.42	0.425	121.0	20-23
Feed displacement	0.1 M NaOH	3.79	1.36	67.8	2.44	0.729	1.55	23
Rinse	DI water	4.14	1.48	74.1	2.51	0.749	1.65	23
Elution	0.5 M HNO_3	5.29	1.89	94.6	1.72	0.514	3.07	23
Elution	0.5 M HNO_3	16.5	5.92	296	1.17	0.348	14.17	20-23
Rinse	DI water	3.69	1.32	66.1	1.22	0.365	3.02	20
Cycle 4 (Start 6/20/03)								
Regeneration	1.0 M NaOH	5.70	2.04	102	2.46	0.735	2.32	21
Loading column	AZ-102 Simulant (2.40 E-7 M Cs)	71.8	NA	1285	0.61	0.181	116.0	20-24

(1) BV = bed volume (17.9 in mL Na form as loaded in column)
(2) AV = apparatus volume (50 mL)
NA = not applicable
NR = not recorded
All processing was downflow.

Table 2.7. Experimental Conditions for Column 4 Test, Resin #9

Process step	Solution	Total Volume			Flowrate		Time	T, °C
		BV[(1)]	AV[(2)]	mL	BV/h	mL/min	h	
In-situ Preconditioning (5/21/03)								
Water rinse	DI water	10.9	3.78	189	3.04	0.876	3.60	NR
Acid wash	0.5 M HNO_3	6.98	2.42	121	3.06	0.882	2.28	NR
Water rinse	DI water	8.37	2.90	145	3.03	0.874	2.77	NR
Cycle 1 (Start 5/27/03)								
Regeneration	0.25 M NaOH	6.35	2.20	110	3.00	0.865	2.12	24
Loading column	AP-101 Simulant	215.2	NA	3723	3.00	0.865	71.7	23-24
Feed displacement	0.1 M NaOH	3.30	1.14	57.1	3.19	0.921	1.03	24
Rinse	DI water	3.45	1.19	59.7	3.05	0.879	1.13	24
Elution	0.5 M HNO_3	5.69	1.97	98.4	1.90	0.546	3.00	23
Elution	0.5 M HNO_3	28.2	9.76	488	1.23	0.356	22.9	23
Rinse	DI water	5.19	1.79	89.7	1.30	0.374	4.00	NR
Cycle 2 (Start 6/7/03)								
Regeneration	1.0 M NaOH	5.60	1.94	96.9	2.71	0.781	2.07	23
Loading column	AP-101 Simulant	206.1	NA	3569	2.78	0.801	73.8	22-24
Feed displacement	0.1 M NaOH	4.04	1.40	69.9	3.15	0.908	1.28	23
Rinse	DI water	3.64	1.26	63.1	2.77	0.798	1.32	NR
Elution	0.5 M HNO_3	5.87	2.03	102	1.93	0.556	3.05	24
Elution	0.5 M HNO_3	9.70	3.38	169	1.32	0.379	7.43	22-24
Rinse	DI water	4.35	1.51	75.3	1.31	0.377	3.33	21
Cycle 3 (Start 6/13/03)								
Regeneration	1.0 M NaOH	7.95	2.75	138	2.95	0.849	2.70	23
Loading column	AP-101 Simulant	212.7	NA	3680	2.93	0.845	71.8	20-24
Feed displacement	0.1 M NaOH	4.12	1.42	71.2	2.81	0.809	1.47	21
Rinse	DI water	3.71	1.28	64.2	2.89	0.834	1.28	22
Elution	0.5 M HNO_3	6.13	2.12	106	2.00	0.577	3.07	23
Elution	0.5 M HNO_3	19.2	6.64	332	1.35	0.391	14.2	20-23
Rinse	DI water	4.19	1.45	72.5	1.40	0.403	3.00	20
Cycle 4 (Start 6/23/03)								
Regeneration	1.0 M NaOH	6.55	2.27	113.3	2.98	0.858	2.20	20
Loading column	AP-101 Simulant (1.06 E-7 M Cs)	67.2	NA	1163	1.47	0.424	46.0	21-24

(1) BV = bed volume (17.3 mL in Na form as loaded in column).
(2) AV = apparatus volume (50 mL).
NA = not applicable
NR = not recorded
All processing was downflow.

Table 2.8. Experimental Conditions for Column 5 Test, Resin #11

Process step	Solution	Total Volume			Flowrate		Time	T, °C
		BV[(1)]	AV[(2)]	mL	BV/h	mL/min	h	
In-situ Preconditioning (6/12/03)								
Water rinse	DI water	8.82	3.27	163	3.53	1.09	2.50	NR
Acid wash	0.5 M HNO_3	6.82	2.53	126	3.41	1.05	2.00	23
Water rinse	DI water	8.52	3.16	158	3.30	1.02	2.58	NR
Cycle 1 (Start 6/13/03)								
Regeneration	1 M NaOH	7.24	2.68	134	3.12	0.965	2.32	23
Loading column	AZ-102 Simulant	118.7	NR	2200	1.55	0.477	77.2	20-24
Feed displacement	0.1 M NaOH	4.50	1.67	83.3	3.41	1.05	1.32	22
Rinse	DI water	3.85	1.43	71.4	3.50	1.08	1.10	23
Elution (upflow)	0.5 M HNO_3	6.29	2.33	116.5	2.26	0.697	3.12	23
Elution (upflow)	0.5 M HNO_3	35.4	13.1	656.9	1.49	0.460	22.8	20-23
Rinse (upflow)	DI water	3.67	1.36	68.1	1.60	0.494	2.3	23
Cycle 2 (Start 6/23/03)								
Regeneration (upflow)	1.0 M NaOH	7.26	2.69	134	3.51	1.08	2.07	22
Loading column	AZ-102 Simulant	110.0	NA	2039	1.63	0.503	70.1	21-24
Feed displacement	0.1 M NaOH	4.04	1.50	74.8	3.23	1.00	1.25	23
Rinse	DI water	3.57	1.32	66.1	3.45	1.07	1.03	23
Elution	0.5 M HNO_3	6.51	2.42	121	2.17	0.670	3.00	23
Elution	0.5 M HNO_3	12.3	4.56	228	1.56	0.482	8.87	23-24
Rinse	DI water	3.23	1.20	59.8	1.55	0.478	2.08	24
Cycle 3 (Start 7/11/03)								
Regeneration	1.0 M NaOH	6.89	2.56	128	3.31	1.02	2.08	23
Loading column	AZ-102 Simulant	117.7	NA	2182	1.61	0.498	72.8	21-25
Feed displacement	0.1 M NaOH	3.63	1.34	67.2	3.30	1.02	1.10	21
Rinse	DI water	4.00	1.48	74.2	3.20	0.989	1.25	22
Elution	0.5 M HNO_3	6.86	2.54	127	2.28	0.703	3.02	22-23
Elution	0.5 M HNO_3	32.8	12.1	607	1.45	0.448	23.3	22-24
Rinse	DI water	3.65	1.35	67.7	1.47	0.454	2.48	23
Cycle 4 (Start 7/21/03)								
Regeneration	1.0 M NaOH	6.71	2.49	124.4	3.15	0.972	2.13	23
Loading column	AZ-102 Simulant (2.40 E-7 M Cs)	87.8	NA	1628	1.63	0.504	54.2	22-27

(1) BV = bed volume (18.5 mL in Na form as loaded in column)
(2) AV = apparatus volume (50 mL)
NA = not applicable
NR = not recorded
Except as noted, all processing was downflow.

Table 2.9. Experimental Conditions for Column 6 Test, Resin #1

Process step	Solution	Total Volume			Flowrate		Time	T, °C
		BV[(1)]	AV[(2)]	mL	BV/h	mL/min	h	
In-situ Preconditioning (7/10/03)								
Water rinse	DI water	7.82	3.19	160	2.84	0.968	2.75	NR
Acid wash	0.5 M HNO_3	6.28	2.57	128	2.79	0.950	2.25	NR
Water rinse	DI water	7.73	3.16	158	2.85	0.969	2.72	NR
Cycle 1 (Start 7/11/03)								
Regeneration	1 M NaOH	5.81	2.37	119	2.79	0.949	2.08	23
Loading column	AZ-102 Simulant	107.0	NA	2186	1.46	0.498	72.8	21-25
Feed displacement	0.1 M NaOH	3.06	1.25	62.6	2.79	0.948	1.10	22
Rinse	DI water	3.48	1.42	71.2	2.79	0.949	1.25	22
Elution	0.5 M HNO_3	6.19	2.52	126	2.07	0.703	3.00	22
Elution	0.5 M HNO_3	31.7	13.0	649	1.41	0.479	23.2	22-24
Rinse	DI water	3.57	1.46	72.9	1.42	0.483	2.52	23
Cycle 2 (Start 7/21/03)								
Regeneration	1.0 M NaOH	5.83	2.38	119	2.73	0.930	2.13	23
Loading column	AZ-102 Simulant	70.3	NA	1436	1.56	0.529	45.0	22-27
Feed displacement	0.1 M NaOH	3.24	1.32	66.1	2.78	0.945	1.17	23
Rinse	DI water	3.15	1.29	64.4	2.91	0.991	1.08	23
Test Cancelled								

(1) BV = bed volume (20.4 mL in Na form as loaded in column)
(2) AV = apparatus volume (50 mL)
NA = not applicable
NR = not recorded
All processing was downflow.

Table 2.10. Experimental Conditions for Column 7 Test, Resin #3

Process step	Solution	Total Volume			Flowrate		Time	T, °C
		BV[(1)]	AV[(2)]	mL	BV/h	mL/min	h	
In-situ Preconditioning (7/10/03)								
Water rinse	DI water	7.21	2.84	134	2.59	0.801	2.78	NR
Acid wash	0.5 M HNO_3	6.06	2.39	112	2.64	0.814	2.30	NR
Water rinse	DI water	7.91	3.12	146	2.65	0.819	2.98	NR
Cycle 1 (Start 7/11/03)								
Regeneration	1 M NaOH	6.53	2.58	121	2.53	0.781	2.58	23
Loading column	AZ-102 Simulant	152.5	NA	2827	1.56	0.483	95.8	22-26
Feed displacement	0.1 M NaOH	3.2	1.26	59.3	2.74	0.848	1.17	22
Rinse	DI water	3.74	1.48	69.3	2.81	0.867	1.33	22
Elution	0.5 M HNO_3	6.28	2.47	116	1.88	0.581	3.33	22
Elution	0.5 M HNO_3	32.2	12.7	597	1.48	0.456	21.8	22-24
Rinse	DI water	4.08	1.61	75.6	1.53	0.472	2.67	23
Cycle 2 (Start 7/21/03)								
Regeneration	1.0 M NaOH	5.92	2.34	109.8	2.69	0.832	2.20	23
Loading column	AZ-102 Simulant	152.7	NA	2830	1.60	0.496	119.1	21-27
Feed displacement	0.1 M NaOH	3.67	1.45	68.0	2.62	0.809	1.40	22
Rinse	DI water	3.70	1.46	68.5	3.00	0.926	1.23	22
Elution	0.5 M HNO_3	6.19	2.45	115	1.99	0.614	3.12	NR
Elution	0.5 M HNO_3	13.6	5.34	251	1.51	0.466	9.07	22
Rinse	DI water	3.06	1.20	56.6	1.49	0.460	2.05	22
Cycle 3 (Start 7/23/03)								
Regeneration	1.0 M NaOH	6.38	2.51	118	2.85	0.882	2.23	24
Loading column	AZ-102 Simulant	150.4	NA	2788	1.61	0.497	93.5	22-28
Feed displacement	0.1 M NaOH	3.22	1.27	59.6	2.88	0.889	1.12	23
Rinse	DI water	3.58	1.41	66.4	2.95	0.910	1.22	24
Elution	0.5 M HNO_3	5.98	2.36	111	2.02	0.623	2.97	25
Elution	0.5 M HNO_3	19.7	7.77	365	1.51	0.467	13.0	22-25
Rinse	DI water	3.08	1.22	57.2	1.46	0.450	2.12	22
Cycle 4 (Start 8/4/03)								
Regeneration	0.25 M NaOH	6.77	2.67	125	2.92	0.903	2.32	23
Loading column	AZ-102 Simulant (2.50 E-7 M Cs)	58.3	NA	1080	0.719	0.222	79.9	22-23

(1) BV = bed volume (18.5 mL in Na form as loaded in column)
(2) AV = apparatus volume (47 mL)
NA = not applicable
NR = not recorded
All processing was downflow.

Table 2.11. Experimental Conditions for Column 8 Test, Resin #6

Process step	Solution	Total Volume			Flowrate		Time	T, °C
		BV[(1)]	AV[(2)]	mL	BV/h	mL/min	h	
In-situ Preconditioning (7/10/03)								
Water rinse	DI water	8.11	3.31	156	2.88	0.920	2.82	NR
Acid wash	0.5 M HNO_3	6.51	2.65	125	2.85	0.910	2.28	NR
Water rinse	DI water	8.13	3.32	156	2.84	0.906	2.87	NR
Cycle 1 (Start 7/11/03)								
Regeneration	1 M NaOH	7.02	2.86	135	2.72	0.868	2.58	23
Loading column	AZ-102 Simulant	116.8	NA	2237	1.60	0.511	72.6	22-26
Feed displacement	0.1 M NaOH	3.37	1.37	64.6	2.81	0.897	1.20	21
Rinse	DI water	3.44	1.40	66.0	2.91	0.929	1.18	22
Elution	0.5 M HNO_3	6.59	2.68	126	2.00	0.639	3.28	22
Elution	0.5 M HNO_3	32.2	13.1	617	1.48	0.472	21.8	22-24
Rinse	DI water	4.25	1.73	81.4	1.59	0.509	2.67	23
Cycle 2 (Start 7/21/03)								
Regeneration	1.0 M NaOH	6.12	2.49	117.2	2.78	0.888	2.20	23
Loading column	AZ-102 Simulant	114.1	NA	2187	1.64	0.523	69.9	22-27
Feed displacement	0.1 M NaOH	3.14	1.28	60.2	2.81	0.898	1.12	22
Rinse	DI water	3.51	1.43	67.3	2.97	0.948	1.18	22
Elution	0.5 M HNO_3	6.29	2.57	121	2.02	0.644	3.12	NR
Elution	0.5 M HNO_3	13.3	5.40	254	1.48	0.472	9.07	22
Rinse	DI water	2.99	1.22	57.3	1.46	0.466	2.05	22
Cycle 3 (7/28/03)								
Regeneration	1.0 M NaOH	6.52	2.66	125	2.92	0.932	2.23	24
Loading column	AZ-102 Simulant	102.6	NA	1965	1.63	0.521	62.9	22-28
Feed displacement	0.1 M NaOH	3.51	1.43	67.2	2.77	0.884	1.27	22
Rinse	DI water	3.72	1.52	71.3	2.79	0.892	1.33	23
Elution	0.5 M HNO_3	6.29	2.55	120	2.06	0.658	3.05	25
Elution	0.5 M HNO_3	19.8	8.09	380	1.52	0.486	13.0	22-25
Rinse	DI water	3.21	1.31	61.4	1.51	0.484	2.12	22
Cycle 4 (Start 8/4/03)								
Regeneration	1.0 M NaOH	6.63	2.70	127	2.90	0.928	2.28	23
Loading column	AZ-102 Simulant (2.50 E-7 M Cs)	59.0	NA	1131	0.737	0.235	80.0	22-23

(1) BV = bed volume (19.2 mL in Na form as loaded in column)
(2) AV = apparatus volume (47 mL)
NA = not applicable
NR = not recorded
All processing was downflow.

Table 2.12. Experimental Conditions for Column 9 Test, SL-644 Resin, 20- to 30-Mesh

Process step	Solution	Total Volume			Flowrate		Time	T, °C
		BV[1]	AV[2]	mL	BV/h	mL/min	h	
In-situ Preconditioning (7/24/03)								
Water rinse	DI water	7.41	3.22	151	2.76	0.940	2.68	NR
Acid wash	0.5 M HNO_3	6.13	2.67	125	2.88	0.979	2.13	NR
Water rinse	DI water	7.51	3.26	153	2.89	0.983	2.60	NR
Cycle 1 (Start7/25/03)								
Regeneration	0.25 M NaOH	6.52	2.83	133	2.83	0.965	2.30	21
Loading column	AZ-102 Simulant	203.1	NA	4148	1.71	0.580	118.5	22-26
Feed displacement	0.1 M NaOH	3.72	1.61	75.9	3.05	1.04	1.22	22
Rinse	DI water	3.98	1.73	81.3	2.78	0.946	1.43	22
Elution	0.5 M HNO_3	6.33	2.74	129	2.17	0.739	2.92	25
Elution	0.5 M HNO_3	19.7	8.54	402	1.49	0.509	13.1	22-25
Rinse	DI water	3.12	1.35	63.7	1.50	0.509	2.08	22
Cycle 2 (Start 8/4/03)								
Regeneration	0.25 M NaOH	7.59	3.30	155	3.67	1.25	2.07	23
Loading column	AZ-102 Simulant (2.50E-7 M Cs)	63.4	NA	1295	0.784	0.267	80.1	21-23
End Test								

(1) BV = bed volume (20.4 mL in Na form as loaded in column)
(2) AV = apparatus volume (47 mL)
NA = not applicable; NR = not recorded

A photograph of two duplicate apparatuses is shown in Figure 2.4. The appearance of Resin #11 in Column 5 H-form and Resin #1 (Column 6) Na-form can be observed. Also shown are the fluid levels above the resin beds, which constituted the mixing areas during feed transitions. The fluid level remained at the same height during resin expansion and contraction. During up-flow elution (Columns 2 and 5), the entire cavity above the resin bed was filled with fluid.

2.10 Hydraulic Properties Testing

Hydraulic tests were performed to measure characteristics that affect the hydraulic performance of selected RF resins and SL-644 resin. These physical characteristics were evaluated under simulated process conditions and included the following: permeability, compressibility, angle of internal friction, and particle size and shape after multiple chemical cycling.

Figure 2.4. Photograph of Two Ion Exchange Column Assemblies (Column 5 in the H-form, left: Column 6 in the Na-form, right)

2.10.1 Permeability Testing

The permeability tests were performed with columns operating at similar pressure drops as those that would be experienced in one full-scale WTP column.[(a)] This was accomplished by increasing the superficial velocity in the small-scale column by the ratio of the full-scale to laboratory-scale column heights. To cover a range of possible conditions, columns with two height-to-diameter ratios were tested with a range of laminar flowrates. The pressure drop was measured as a function of flowrate, and the column permeability, K, was calculated according to Equation 2.12.

$$K = \frac{L\mu q}{\Delta p} \tag{2.12}$$

(a) Testing was conducted according to Test Instructions TI-RPP-WTP-287, Rev. 0, *Column Ion Exchange with Resins for Permeability Testing Test 1*, BS Augspurger, July 2003; TI-RPP-WTP-276, Rev. 0, *Column Ion Exchange with Resins for Permeability Testing Test 2*, BS Augspurger, July 2003; TI-RPP-WTP-277, Rev. 0, *Column Ion Exchange with Resins for Permeability Testing Test 3*, BS Augspurger, August 2003.

where L = resin bed height, m
q = superficial liquid velocity, m/s
μ = solution viscosity, kg/m/s
Δp = pressure drop measured across the column, kg/m/s^2.

Load cells were added to the configuration with placement on the bottom and side of the column (near the bottom). They were used to opportunistically measure the radial and axial forces generated by the resin during resin expansion.

The experimental setup for these tests is shown schematically in Figure 2.5. A photograph of the system is provided in Figure 2.6. The pumps and column assembly were duplicated to enable the testing of two column height-to-diameter ratios of 1.6 and 2.7 simultaneously. The reagent volumes were created in sufficient quantity to meet the flow requirements for the two column assemblies and multiple-cycle testing. The following is a description of the various components of the experimental setup.

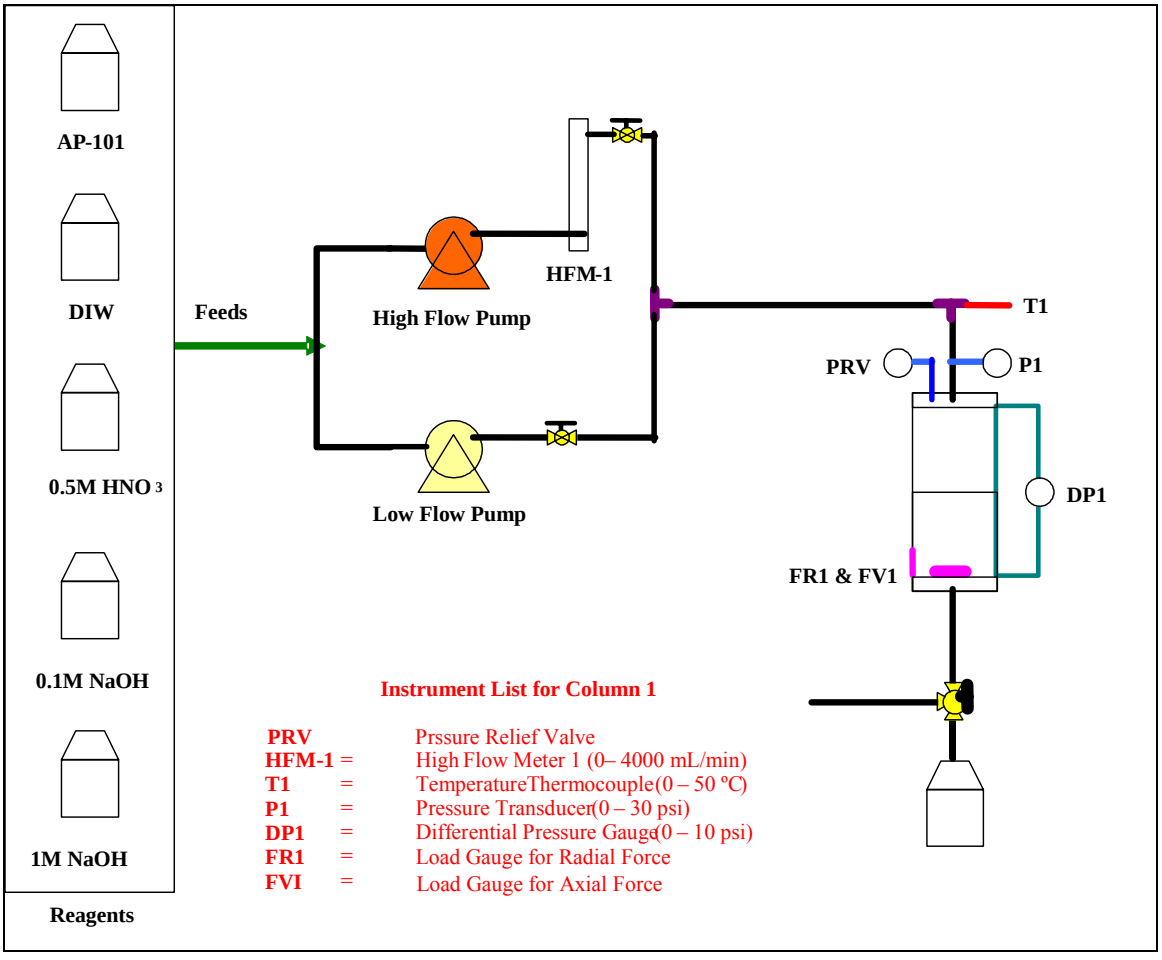

Figure 2.5. Schematic of the Permeability Test Equipment Showing One of the Two Ion Exchange Columns and its Associated Instruments

Figure 2.6. Photograph of the Permeability Testing System

Depending on the processing step, the solution from one of the reagent bottles was diverted either to the low-flow pump or the high-flow pump loop. The low-flow pump loop was used for the resin preconditioning, elution, and rinse/displacement steps of the ion exchange cycle. The high-flow pump loop was used for the resin loading and the regeneration steps of the ion exchange cycle. The pumps used in both loops were appropriately sized positive displacement pumps of FMI models QV and QVG50 (Syosset, NY) for the high and low flow requirements.

The high-flow loop was instrumented with Emerson MicroMotion Coriolis (Boulder, CO) mass-flow meters, which enabled measurement of the volumetric flowrate. The liquid temperature and line pressure were measured before entry into the ion exchange column. The temperature was measured with a Type K thermocouple. The line pressure was measured with a liquid-filled analog pressure gage (Model PGM-63L-30Psi, Omega, Stamford, CT). A pulsation damper (Model BH-07596-20, Cole Parmer, Vernon Hills, IL) was used to create a continuous smooth flow through the column.

The ion exchange columns were 5-cm ID, 20-cm-long glass columns (Part # 123974, Spectrum Chromatography, Houston, TX). Glass pressure ports were installed on the top and bottom of the column to measure the differential pressure across the resin bed using differential pressure transducers (Model PX2300-10DI, Omega, Stamford, CT). A pressure-relief valve (SS-RL3S4, Seattle Valve and Fitting, Seattle, WA) was installed on the top of the column to prevent column over-pressurization.

The resin bed was held in place on a porous polypropylene cylindrical plug (See Figure 2.7). This plug raised the resin up to the height of the bottom pressure port and housed the bottom load cell. A

0.25-in.-diameter pin was flush mounted with the resin bed. When force was exerted downward, the pin transferred the force to a miniature load cell within the plug (Model 13, Sensotec, Columbus, OH). A similar arrangement was also provided on the side of the column to measure radial forces (near the bottom of the resin bed). Neither load cell was calibrated; results were generated for indication only. The resin was prevented from passing through the porous plug by a plastic screen. A small amount of glass wool was inserted into the bottom pressure tap to prevent resin from passing. The top pressure tap was above the resin bed, so glass wool was not necessary. The resin-bed height was measured with a ruler.

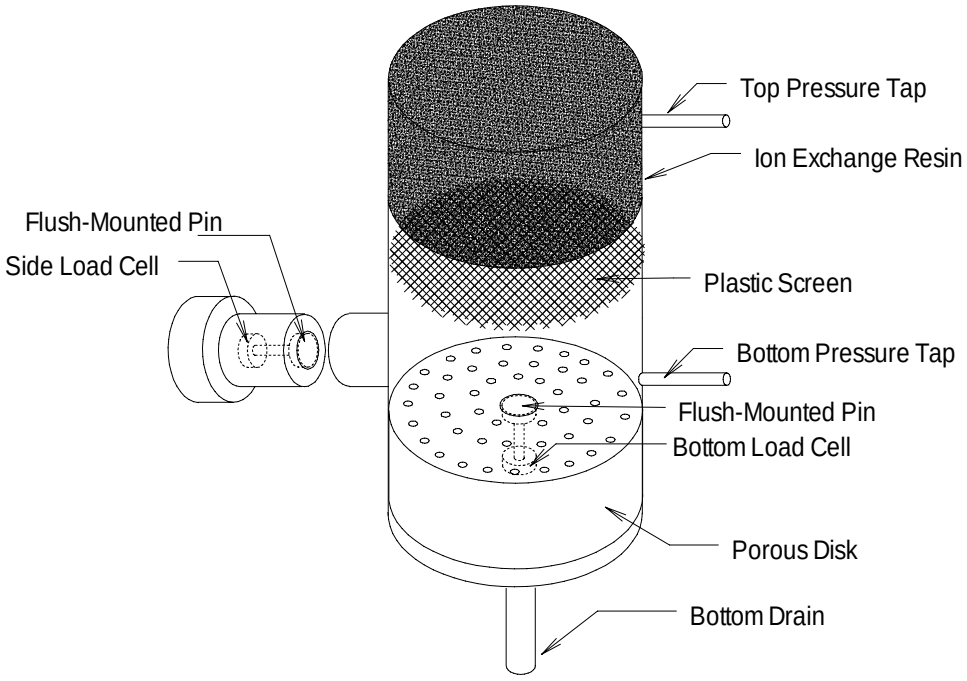

Figure 2.7. Schematic of the Ion Exchange Column Load Cell Placement

Electronic data were collected with IO Tech, Personal Daq/56, and PDQ2 data-acquisition software (Cleveland, OH) installed on a Micron Electronics TransPort TREK 2 computer. The data-acquisition board was an analog input/digital input/output (I/O) board. The Data Acquisition System (DAS) sampled all channels at 1-sec intervals. Data were recorded in the data log files in 10-sec intervals.

Specific processing conditions during the permeability testing are shown in Table 2.13. Preweighed resin was slurried into each column as the wet H-form. Each resin bed was pretreated using the steps described in Table 2.13. Following the pretreatment, the resin was cycled four times through a load/displace/elute/regenerate cycle. The rinse, elute, and displacement solutions were used only once and disposed of. The AP-101 simulant loading and NaOH regeneration solutions were recycled during a single step and reused for 2 to 4 cycles to minimize waste generation.

Table 2.13. Processing Steps for the Permeability Testing

Process Step	Flowrate(s)	Volume or Time	Measurements
Pretreatment			
Rinse: DI Water	3 BV/h	3 AV	Resin Height
Elute: 0.5 M HNO3	3 BV/h	6 BV	Resin Height
Rinse: DI Water	3 BV/h	3 AV	Resin Height
Regenerate: 1 M NaOH	3 BV/h	6 BV	Resin Height
Cycle 1			
Load: AP-101 Simulant	1600, 1200, 800 mL/min	30, 30, 30 min (re-circulated flow)	Flowrate Pressure Drop Load Cell Force Resin Height Temperature Viscosity/Density
Displacement: 0.1 M NaOH	3 BV/h	3 BV	Resin Height
Rinse: DI Water	3 BV/h	3 BV	Resin Height
Elute: 0.5 M HNO3	6 BV/h	12 BV	Resin Height
Rinse: DI Water	1.4 BV/h	3 BV	Resin Height
Regenerate: 1 M NaOH	1600, 1200, 800 mL/min	90, 30, 30 min (re-circulated flow)	Flowrate Pressure Drop Load Cell Force Resin Height Temperature Viscosity/Density
Cycle 2			
Same as Cycle 1, except only measure permeability at 1600 mL/min flowrate			
Cycle 3			
Same as Cycle 1, except only measure permeability at 1600 mL/min flowrate			
Cycle 4			
Same as Cycle 1			

Measurements required to calculate the permeability were taken during the loading and regeneration steps of each cycle. These measurements, including resin-bed height, liquid flowrate, and pressure drop, were taken manually every 5 min. These same measurements were also recorded every 10 seconds electronically with the data-acquisition system. The side and bottom load cell forces were similarly measured. Three flowrates were tested for the first and fourth cycles while a single flowrate was used to measure permeability for the second and third cycles. After each permeability test, samples were taken to measure the density and viscosity of the solution upon completion of the experiment to account for any dilution that may have occurred during solution reuse. For the DI water rinses, eluting, and displacement steps, only the total time and final resin height were measured.

A cross-reference of resins evaluated along with their Na-form volumes and height-to-diameter ratios are provided in Table 2.14. The resins were tested in the order presented in the table. Due to restrictions in the column-height measurement, the tests did not allow the original targeted height-to-diameter ratio of 3.2.

Table 2.14. Resins Evaluated for Permeability

Resin ID#	Resin Type	Resin Height-to-Diameter Ratio[(a)]		Resin Volume (mL)[(a)]	
		Column A	Column B	Column A	Column B
#12	SL-644, granular	1.88	2.72	184	267
#3	RF, spherical	1.56	2.8	153	274
#9	RF, granular	1.52	2.78	149	273
(a) Height and volume measured after the first displacement step of Cycle 1.					

Although the load cells provided some information about the resin expansion, this information has several caveats. First, the load-cell data are for indication only. Before the experiment was started, they were zeroed and then calibrated with a 100 g (~4.5 psi) weight. All data greater than 4.5 psi were extrapolated from this range. Secondly, due to difficulties in the load cells failing in the caustic environment, there is very little load-cell data for Resin #12. Before Cycle 1 with Resin #12, the load cell on the side of the Column B and the bottom of Column A failed. Then during Cycle 1, the bottom load cell of Column A failed. In the middle of Cycle 2, the resin was removed from Column B, and both load cells were replaced. The side load cell failed within a few hours and the bottom within one additional cycle. Thus, Cycle 4 data were only collected on the side of Column A. During subsequent resin tests, none of the load cells failed, and all data were collected. However, a final difficulty did exist. The load cells zero tended to drift over time, even when not installed in the column. Once the experiment was started, no adjustments were made to the load-cell-zero value since resin was present. This may have resulted in some additional error.

Following the permeability testing of the resins, representative samples of the material in the columns were collected for microscopy and PSD analysis. The results of the post-permeability tests were compared with the same batch of resins before permeability testing. To allow for resin comparison, the processed resins were converted to the H-form by soaking in 0.5 M HNO_3, rinsing with DI water, and then drying under nitrogen. Micrographs of the dried resins were taken at 10×, 25×, and 70×. The resin particles in this case were sprinkled on double-stick tape to reduce bias caused by large flat faces coming to rest downward on the support. The Na-form resin was used for PSD analysis following the same procedure, and instrumentation was applied to the pretreated resins, TPR-RPP-WTP-222, Rev. 1 (see Section 2.6). NIST-traceable 100-μm and 500-μm standards were used before and after the resin PSD measurements to assure the accuracy of the results.

2.10.2 Compressibility Testing

The compressibility test was designed to test compressive strength and angle of internal friction using compressive forces for each of the resins.[(a)] This test was performed by applying a known force on the top of a resin bed. The change in bed height provided the compressibility measurement. Load cells on the side and the bottom of the column provided the ratio of radial and axial forces. These were then used to calculate the angle of internal friction, α_m, based on Equation 2.13.

(a) Testing was conducted according to Test Instruction TI-RPP-WTP-278, Rev. 0, *Compressibililty Test of Resins for Hanford Ion Exchange Columns*, MJ Schweiger, August 2003.

$$\alpha_m = \sin^{-1}\left(\frac{\Delta P_{bottom} - \Delta P_{side}}{\Delta P_{bottom} + \Delta P_{side}}\right) \tag{2.13}$$

where ΔP_{side} is the side load-cell pressure, and ΔP_{bottom} is the bottom load-cell pressure [10].

A schematic of the test apparatus is shown in Figure 2.8. The test was performed by using the same 5-cm-diameter columns and apparatus as were used in the permeability studies. In addition, an elastic membrane above the bed was pressurized with water to produce force on the top of the resin bed. The resin itself was in AP-101 simulant solution. The plastic pressure disk at the bottom assured that the membrane applied an even distribution of pressure across the resin surface, and the pressure disk at the top prevented the water used to pressurize the membrane from mixing with the AP-101 simulant used in the resin. The bottom of the column allowed the simulant to flow out as the resin bed compressed. The pressure on the bed was increased stepwise to 20 psi by turning on and off the FMI positive-displacement pump. The pressure was decreased stepwise by opening a valve at the top of the column and allowing the AP-101 simulant solution forced out during the compression to flow back into the column.

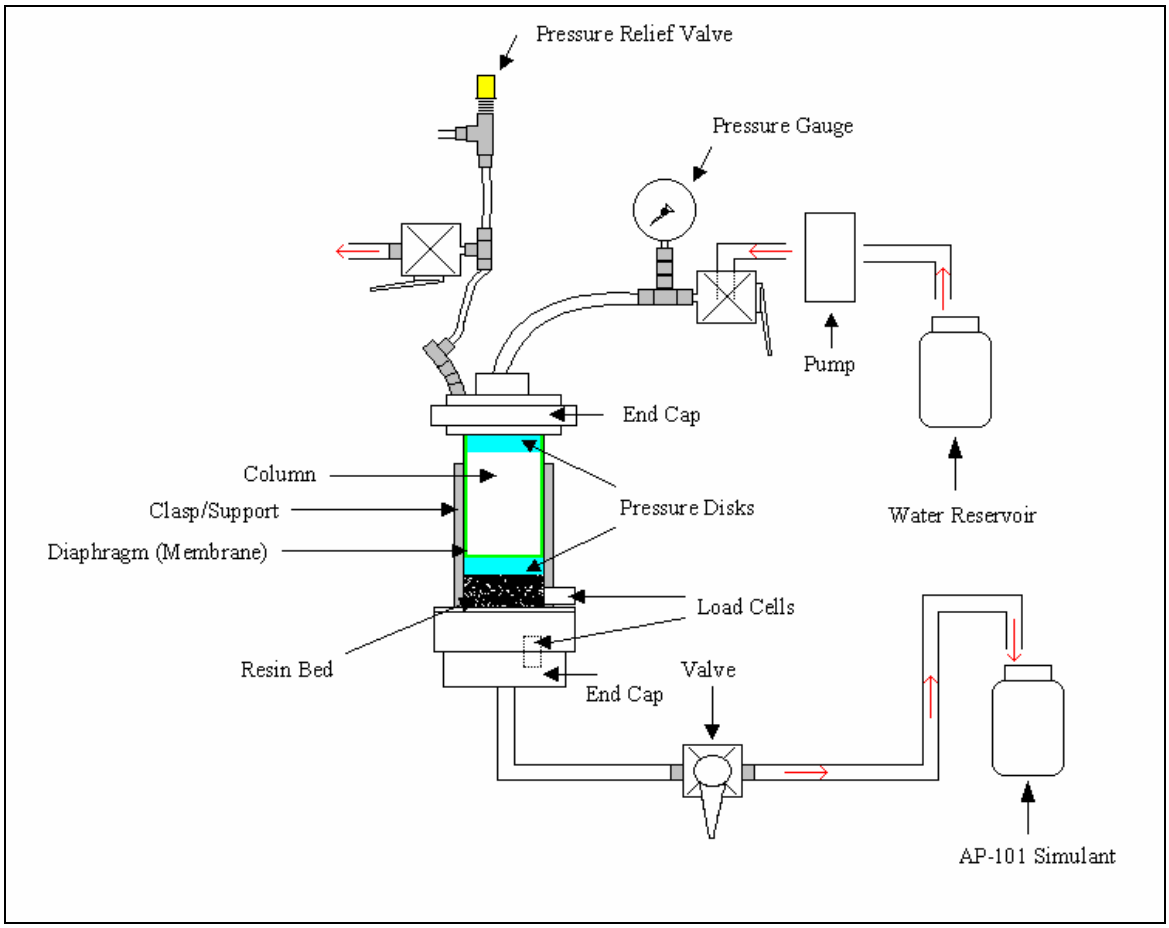

Figure 2.8. Schematic of the Compressibility Test Equipment. All resins were tested with a single apparatus.

Testing was performed using the same resins that were used in the permeability tests for the experiment with a length to diameter (L/D) ratio of 2.7. After permeability testing, these resins had been stored under DI water in the Na-form under N_2 before being used for the compressibility testing. Sufficient resin was added to the column to produce a resin-bed height 1 to 2 cm above the side load cell inlet (~4 cm tall). The column was filled with AP-101 simulant, the membrane was installed, and air pockets were removed from the column. The resin bed was then vibrated before the measurements to pack the resin so the particles obtained as tight a particle configuration as possible. Measurements of the resin height and load cells were taken at test initiation, at 5, 10, 15, 20, 15, 10, and 5 psi, with repeat cycling of these measurements for four to five cycles.

3.0 Bulk-Property Results

This section summarizes bulk-property test results, including resin morphology, water content, PSDs in hydrated H-form and Na-form, bed density, swollen-resin density, and, on selected samples, skeletal density and porosity.

3.1 As-Received Resin Properties

The resins were provided from the manufacturer with varying quantities of water, as determined by the F-factor measurements, summarized in Table 3.1. The relative percent differences between the duplicate measurements for Resins #3, #4, and #9 were higher than the other resins tested. This was attributed to sample heterogeneity. For the most part, the resins were easily manipulated. Resins #3, #4, #6, and #7 rolled very easily, a common test for resin sphericity. The distance rolled was not measured. Resins #10 and #11 were very sticky and difficult to process through the riffle sampler. This was probably due to the high water content of this material.

Table 3.1. As-Received Resin F-Factors

Resin ID	F-factor	Duplicate	Resin ID	F-factor	Duplicate
1	0.9828	0.9811	7	0.5182	0.5184
2	0.9111	0.9132	8	0.9468	0.9489
3	0.6459	0.6049	9	0.9244	0.9026
4	0.5800	0.5820	10	0.5247	0.5232
5	0.9212	0.9199	11	0.5479	0.5524
6	0.6037	0.5693	12	NA[(a)]	NA[(a)]
(a) NA = not applicable, Resin #12 was received as a wet slurry.					

The dry-sieve PSD results are shown in Table 3.2. The % mass fraction shown under the screen mesh size represents the mass fraction retained by that screen. Because of the high water content contributing to the sticky nature of Resins #10 and #11, aliquots of these resins were dried under vacuum until a free-flowing form was produced. The widest PSD and the most fines were noted with Resins #10 and #11. The tightest PSDs were noted with the spherical resins #3, #4, #6, and #7. The table cells have been shaded and outlined to indicate the size ranges comprising just ≥99% by mass of each resin sample.

The bulk, dry-resin-density results are shown in Table 3.3. The densities ranged from a high of 0.81 g/mL for Resin #1 to a low of 0.35 g/mL for Resin #7. Resins #1, #2, #5, #8, and #9 resulted in dry-bulk densities similar to SL-644 dry-bulk densities (0.74 to 0.84 g/mL) previously reported by Fiskum et al. [11]. Generally, the spherical resins were characterized with the lowest dry-mass density. This may be in part because they contained significant water (F-factor ≈0.55). The as-received Resins #10 and #11 were difficult to handle because the particles stuck to each other and to other contact surfaces. This behavior was attributed to the high water content. Aliquots of these resins were dried under vacuum until a free-flowing form was produced before determining the bulk density. Despite partial drying (F-factor ≈0.72), Resins #10 and #11 resulted in low densities, nearly as low as the spherical-form material.

Table 3.2. As-Received PSD, Dry-Sieve

Mesh size[(a)]	25	30	35	40	45	50	60	>60	F-factor
Pore size, μm:	710	600	500	425	355	300	250	<250	NA
Resin ID	*Mass %[(b)]*								*NA*
1	0.090	7.11	44.2	22.5	13.4	12.1	0.589	0.079	0.977
2	0.034	1.28	32.5	24.4	21.1	18.4	2.13	0.151	0.907
3	0.004	0.002	0.009	0.235	99.3	0.268	0.093	0.045	0.625
4	0.006	0.001	0.004	0.254	99.6	0.135	0.026	0.005	0.579
5	0.056	1.43	35.3	25.0	21.3	14.6	2.016	0.265	0.916
6	0.00	0.005	0.00	0.857	99.0	0.124	0.019	0.008	0.587
7	0.013	0.004	0.004	1.44	98.5	0.062	0.00	0.00	0.517
8	0.127	0.309	1.46	29.2	41.3	24.6	2.68	0.292	0.946
9	0.046	1.90	34.3	24.0	22.1	14.7	2.54	0.356	0.911
10	0.00	0.05	1.84	33.5	29.6	17.9	9.31	7.77	0.719
11	0.067	3.10	17.0	21.6	17.7	19.6	11.9	8.97	0.743

(a) U.S. standard sieve size corresponds to ASTM E-11 specification.
(b) The shaded cells indicate the size range comprising just ≥ 99% by mass of each resin sample.
NA = not applicable

Table 3.3. Bulk Dry-Resin Densities

Resin ID	Bulk dry density, g/mL	Duplicate density, g/mL	Average density, g/mL	Resin ID	Bulk dry density, g/mL	Duplicate density, g/mL	Average density, g/mL
1	0.817	0.814	0.816	7	0.359	0.355	0.357
2	0.771	0.780	0.776	8	0.714	0.702	0.708
3	0.430	0.428	0.429	9	0.754	0.764	0.759
4	0.403	0.407	0.405	10	0.460	0.464	0.462
5	0.796	0.792	0.794	11	0.495	0.494	0.494
6	0.397	0.393	0.395	12	NA[(a)]	NA[(a)]	NA[(a)]

(a) NA = not applicable, Resin #12 was received as a wet slurry.

3.2 Optical Microscopy

Optical micrographs were taken of each of the pretreated, dried resins in the H-form at 10×, 25×, and 70×. The 70× micrographs are shown in Figure 3.1 through Figure 3.3. See Appendix A for the 10× and 25× micrographs. Resins #3, #4, #6, and #7 were spherical and ranged from red-orange to brown-orange in color. They were similar in size and morphology. Resins #3, #6, and #7 appeared pitted or mottled on the surface whereas Resin #4 appeared to exhibit some smooth surface areas. Resins #1 and #8 through #12 had the appearance of broken-glass shards with sharp angular edges and shiny surfaces. They were composed of a variety of shapes, sizes, and shades of reddish-brown. Resin #11 was characteristically darker, nearly black. Of the spherical resins, Resin #6 was the only one that showed some fragmentation

of the spheres. However, based on the fact that a small amount of fines were present in all of the spherical resin sieve tests (see Table 3.2), a small amount of broken fragments was likely to exist in all samples. These micrographs support the particle-size measurements where Resins #3, #4, #6, and #7 had tight PSDs whereas the others had large PSDs.

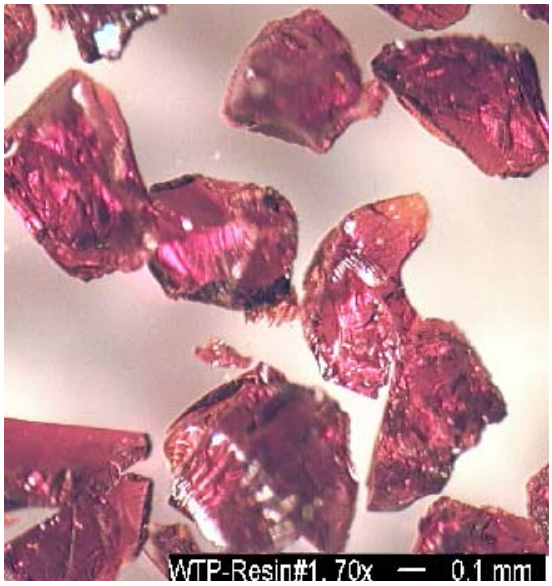

(a)

(b)

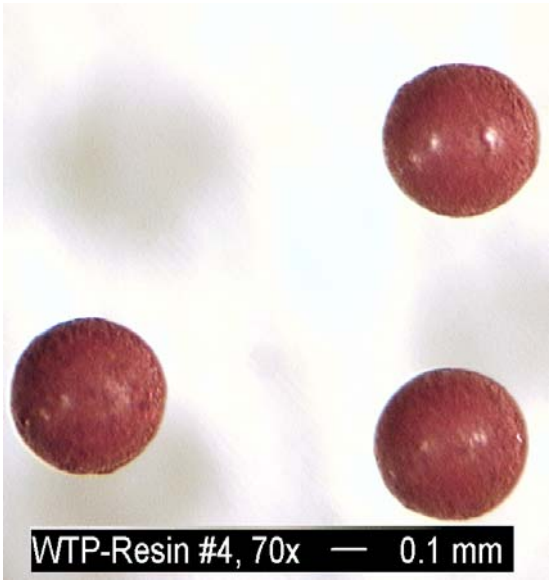

(c)

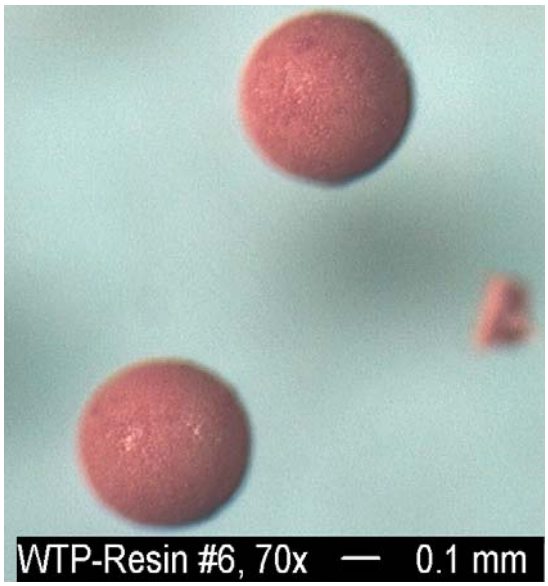

(d)

Figure 3.1. Micrographs of Pretreated H-Form Resin #1 (a), #3 (b), #4 (c), and #6 (d) at 70× Magnification

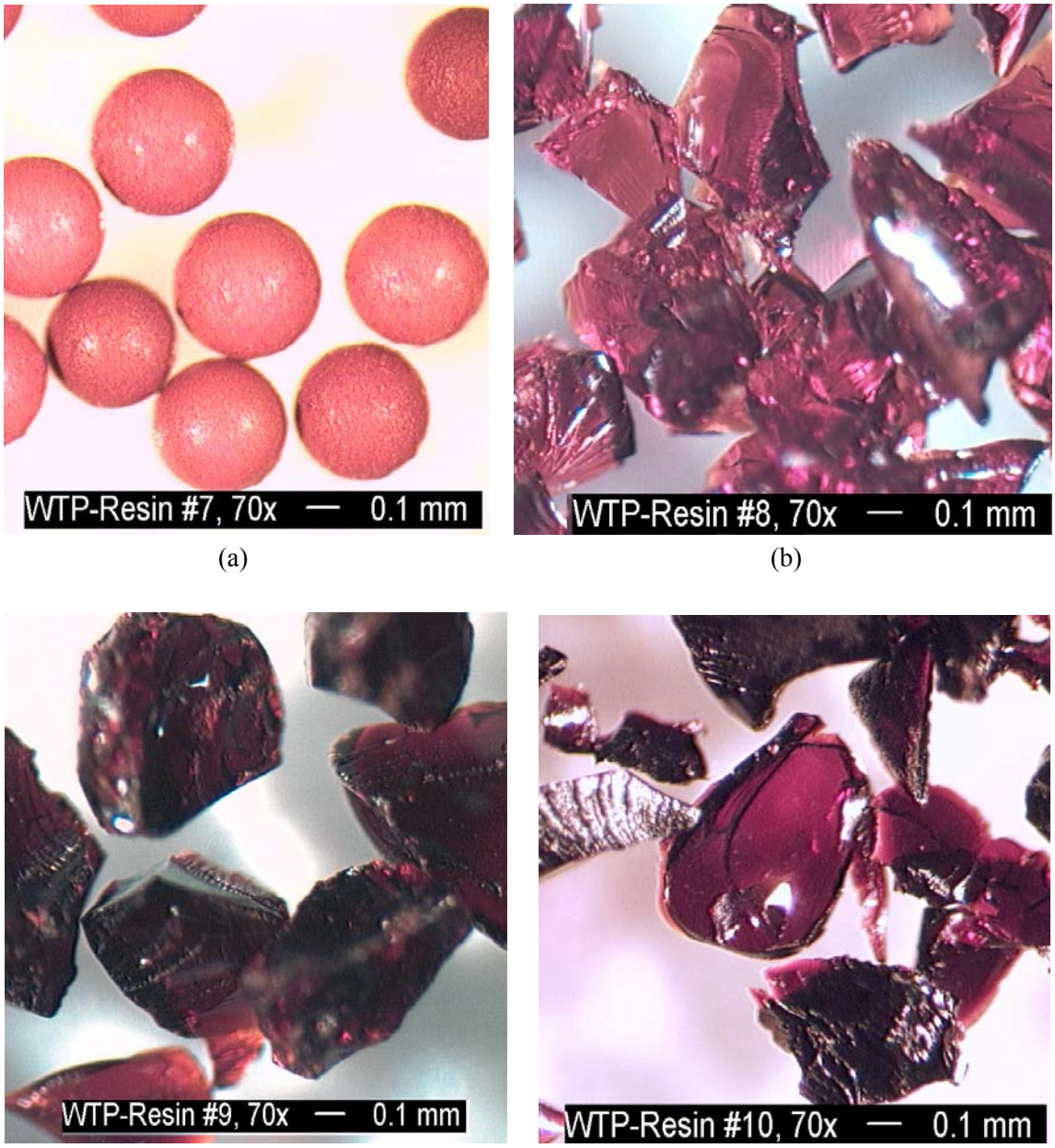

Figure 3.2. Micrographs of Pretreated H-Form, #7 (a), #8 (b), #9 (c), and #10 (d) at 70× Magnification

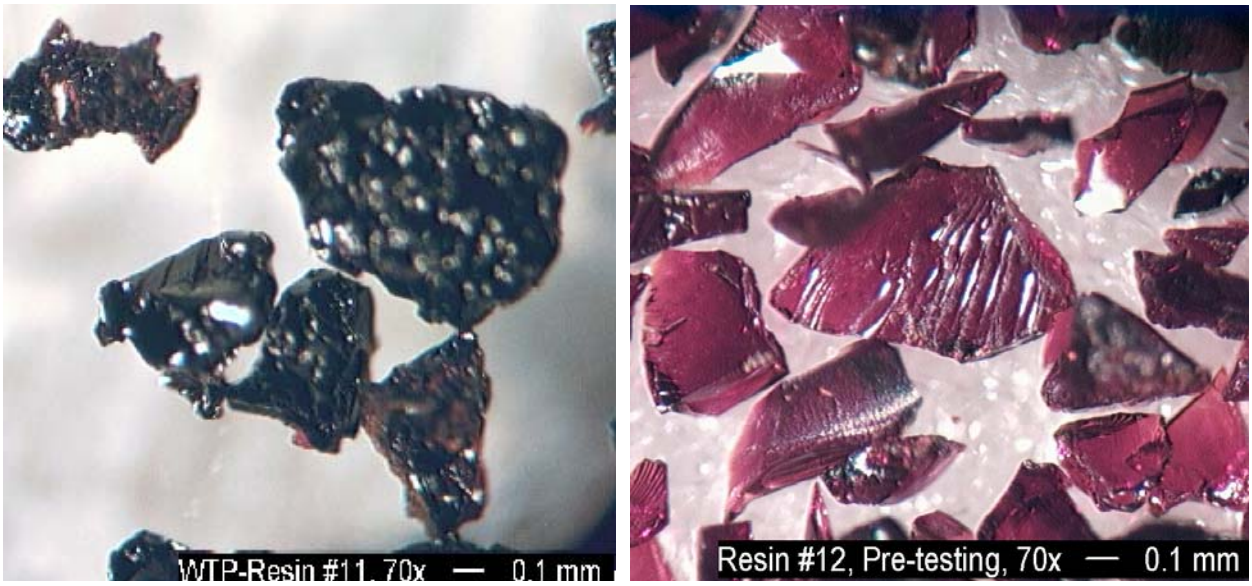

(a) (b)

Figure 3.3. Micrographs of Pretreated H-Form Resins #11 (a), and #12 (b) at 70× Magnification

3.3 Pretreated Bulk-Resin Properties

Bulk properties were evaluated for the RF resins and are compared, where possible, to the SL-644 resin from production batch C-01-05-28-02-35-60 (25-gal production batch). Bulk properties included F-factor determination as a function of drying temperature, dry-bed density as a function of solution matrix, wet-slurry density as a function of solution matrix, shrink-swell characteristic as a function of H-form volume and Na-form volume, swollen-resin density, bed porosity, and skeletal density.

3.3.1 F-Factor Determination

Table 3.4 shows the F-factor results of the pretreated resin for three different drying temperatures (22°C, 50°C, and 85°C) under vacuum. There was an average 7% change in the F-factor results between drying at 22°C and 50°C. The average F-factor dropped an additional 3% when the temperature was changed from 50°C to 85°C. No manifestation of physical damage was observed at any of the three drying temperatures. Therefore, it was decided to use the 50°C results for all calculations.

Table 3.4. Pretreated Resin F-Factors

	F-Factor as a Function of Temperature					
	22 °C		50 °C		85 °C	
Resin ID	Sample	Duplicate	Sample	Duplicate	Sample	Duplicate
1	0.7490	0.7503	0.6999	0.7015	0.6838	0.6838
3	0.6087	0.6118	0.5697	0.5718	0.5562	0.5589
4	0.9788	0.9807	0.9085	0.9153	0.8743	0.8791
6	0.6090	0.6082	0.5674	0.5677	0.5443	0.5459
7	0.7668	0.8166	0.7108	0.7578	0.6845	0.7305
8	0.7895	0.7831	0.7375	0.7333	0.7195	0.7125
9	0.7964	0.7917	0.7340	0.7306	0.7051	0.7033
10	0.7705	0.7740	0.7144	0.7182	0.6938	0.6950
11	0.8237	0.8210	0.7804	0.7751	0.7599	0.7521
12	1.0078	1.0060	0.9712	0.9694	0.9528	0.9473

The Resin #12 (SL-644) F-factor determined at 22ºC resulted in a value higher than 1. The resin starting material contained little water (note that the F-factor at 85ºC averaged 0.95). The duplicate Resin #12 samples apparently continued to accumulate water from the environment, despite the vacuum condition (probably from companion samples that were releasing water). This behavior indicated that the SL-644 material was somewhat hygroscopic.

3.3.2 Resin Dry-Bed Densities

The Na-form wetted resins displayed significantly different settling rates upon transfer to the AP-101 simulant matrix. Resins #3, #4, #6, and #7 were initially suspended in the top portion of AP-101 simulant. The resins gradually settled to the bottom of the graduated cylinder over a nominal 30-min settling period. Resins #1, #9, #10, #11, and #12 settled immediately when placed in the AP-101 simulant. The bulk of Resin #8 settled immediately; however, fines remained suspended for about 10 minutes. In all other media (DI water, 0.5 M HNO_3, and 0.25 M NaOH), the resins settled as soon as they were poured into the graduated cylinder.

The dry-bed densities of the H-form and Na-form resins expanded in solution are shown in Table 3.5 and Table 3.6, respectively. In all cases, the dry-bed density mass was based on the weighed H-form resin mass. The H-form density was determined with both DI water and 0.5 M HNO_3 as the liquid media. The Na-form density was determined with both 0.25 M NaOH and AP-101 simulant as the liquid media. The overall error was estimated to be ±5%. To calculate the Na-form resin dry-bed density relative to the Na-form mass, the resin-specific mass increase factor (I_{Na}) will need to be determined.[(a)] The measured volumes were based on the smallest settled resin-bed volume obtained from tapping and vibrating. These conditions were different than those applied to the actual column tests where the resin beds were not disturbed once processing was initiated, and packing resulted only from resin-bed shrinking and swelling in the course of normal pre-conditioning and processing steps.

(a) Determination of the I_{Na} mass increase factor was beyond the scope of the current testing.

Table 3.5. Dry-Bed Resin Densities (H-form)

Resin ID	Average Dry-Bed Density			
	DI Water Media, g/mL[(a)]	RPD	0.5M HNO_3 Media, g/mL[(a)]	RPD
1 (H-form)	0.414	3.7	0.409	1.3
3 (H-form)	0.407	5.1	0.399	0.46
4 (H-form)	0.412	2.3	0.410	1.4
6 (H-form)	0.410	1.0	0.402	0.90
7 (H-form)	0.411	5.6	0.409	4.7
8 (H-form)	0.470	2.8	0.461	1.0
9 (H-form)	0.499	4.0	0.497	3.2
10 (H-form)	0.450	5.1	0.454	3.1
11 (H-form)	0.486	1.1	0.481	2.5
12 (H-form)	0.542	0.53	0.537	1.4
(a) The resin mass was based on the measured dry H-form resin. RPD = relative percent difference.				

Table 3.6. Dry-Bed Resin Densities (Na-form)

Resin ID	Average Dry-Bed Density			
	0.25M NaOH Media, g/mL [(a)]	RPD	AP-101 Simulant Media, g/mL [(a)]	RPD
1 (Na-form)	0.301	2.2	0.314	1.7
3 (Na-form)	0.269	6.4	0.270	4.5
4 (Na-form)	0.246	2.7	0.248	1.4
6 (Na-form)	0.266	1.9	0.278	0.32
7 (Na-form)	0.236	4.8	0.238	4.3
8 (Na-form)	0.291	4.0	0.293	2.9
9 (Na-form)	0.303	0.67	0.303	0.67
10 (Na-form)	0.203	2.0	0.222	2.9
11 (Na-form)	0.219	0.44	0.231	1.3
12 (Na-form)	0.192	1.6	0.222	1.9
(a) The resin mass was based on the measured dry H-form resin. RPD = relative percent difference.				

There was no measurable change, within the error of the method, in dry-bed density of the H-form resin on conversion of the aqueous matrix from DI water to 0.5 M HNO_3. The Na-form resin dry-bed densities for Resins #1 through #9 and #11 did not change, within the error of the method, on conversion from 0.25 M NaOH to AP-101 simulant matrices. However, Na-form Resins #10 and #12 did show significant changes of 9% and 16%, respectively.

These values can be compared to the estimated dry-bed densities derived from the column ion exchange testing presented in Section 5.0. Densities based on the tapped, settled volume were higher than column-testing results where the resin beds were packed only as a result of normal swelling and shrinking during processing. This is especially apparent with respect to Resin #12 where the H-form resin-bed

density was calculated to be 0.31 g/mL (as opposed to 0.542 g/mL from Table 3.5), and the Na-form bed density was calculated to be 0.21 g/mL (nearly in agreement with 0.192 g/mL from Table 3.6). The relative expansion factors on conversion from H-form to Na-form resin are summarized in Table 3.7 for the bulk-property testing and the ion exchange column testing for comparison. For Resins #11 and #12, the compaction associated with the tapping/vibrating process of the H-form resin beds was significant.

Table 3.7. Relative Resin Volume Expansion on Conversion from H-Form to Na-Form

	Relative Expansion Factor on Conversion from H-form to Na-form									
Resin #:	***1***	***3***	***4***	***6***	***7***	***8***	***9***	***10***	***11***	***12***
Bulk property testing	1.38	1.51	1.67	1.54	1.74	1.62	1.65	2.22	2.22	2.82
Ion exchange column test[(a)]	1.3	1.3	NA	1.3	NA	NA	1.4	NA	1.5	1.5
(a) Extracted from Table 5.3. NA = not applicable, resins were not tested in the column format.										

3.3.3 Wet-Slurry Densities

The bulk, wet-slurry densities of the settled resins are shown in Table 3.8 (H-form) and Table 3.9 (Na-form). The slurry densities in all four matrices were surprisingly similar, given the difference in densities of the contact solutions (1.00 g/mL for DI water and 1.25 g/mL for AP-101 simulant). The H-form densities in 0.5 M HNO_3 of Resins #10 (0.956 g/mL) and #12 (0.984 g/mL) appeared to be biased low. The low bias may be attributable to the small sample sizes used for the determinations, which resulted in small measured volumes.[(a)] The resin slurry densities in the AP-101 simulant matrix were less than the AP-101 simulant density (1.25 g/mL). The resins, however, did not float. The reason for this discrepancy is not known.

(a) The sample sizes were nominally 2.2 g (#10) and 2.8 g (#12) dry H-form mass. These sample sizes represented half of the mass of the other samples processed. Visibly large sub-aliquots of the #10 and #12 as-received resins were processed; however, because of the large water contents of the as-received materials, the actual dry masses were small.

Table 3.8. Bulk Wet Slurry Resin Densities (H-Form)

Resin ID	Average Bulk Wet Density			
	DI Water Media, g/mL	RPD	0.5M HNO_3 Media, g/mL	RPD
1 (H-form)	1.11	1.0	1.08	0.76
3 (H-form)	1.09	0.55	1.02	2.4
4 (H-form)	1.10	1.4	1.06	1.9
6 (H-form)	1.10	1.5	1.06	0.70
7 (H-form)	1.12	0.73	1.07	0.02
8 (H-form)	1.10	0.52	1.10	1.9
9 (H-form)	1.11	2.5	1.08	0.41
10 (H-form)	1.05	3.0	0.956[(a)]	3.7
11 (H-form)	1.11	1.1	1.08	2.1
12 (H-form)	1.07	5.5	0.984	1.4

(a) The low density may be attributable to measured volume error associated with the small sample size.

Table 3.9. Bulk Wet Slurry Resin Densities (Na-Form)

Resin ID	Average Bulk Wet Density			
	0.25M NaOH Media, g/mL	RPD	AP-101 Simulant Media, g/mL	RPD
1 (Na-form)	1.14	0.55	1.13	1.3
3 (Na-form)	1.08	0.34	1.10	1.5
4 (Na-form)	1.11	0.65	1.08	1.6
6 (Na-form)	1.11	2.0	1.09	1.0
7 (Na-form)	1.10	0.87	1.10	0.26
8 (Na-form)	1.13	0.98	1.14	1.5
9 (Na-form)	1.12	0.70	1.11	1.6
10 (Na-form)	1.06	1.5	1.05	0.40
11 (Na-form)	1.09	1.0	1.10	0.20
12 (Na-form)	1.06	2.6	1.04	NA[(a)]

(a) NA = not applicable; one value was determined to be an outlier and therefore, only one value was reported.

3.3.4 Swollen-Resin Density

Table 3.10 shows the swollen-resin density of each resin for both the H-form and Na-form. The swollen-resin densities were determined for both the H-form (relative to H-form mass) and the Na-form (relative to Na-form mass) resins. All of the H-form densities were larger than the Na-form densities, consistent with the expansion noted for the Na-form resins relative to the H-form resins. Resin densities were generally consistent, ranging from 1.15 g/mL to 1.28 g/mL in the H-form and 1.08 g/mL to 1.19 g/mL in the Na-form. It is unclear why the swollen resin densities were so low. The resins did not float in the simulant matrices (AP-101 and AZ-102 simulants). The relative density ratios are also

provided in Table 3.10. The SL-644, #12, resulted in the highest difference (10%) in relative swollen-resin density.

Table 3.10. Swollen-Resin Densities

Resin ID	Average Swollen-Resin Density				
	H-Form, g/mL	RPD	Na-Form, g/mL	RPD	H-Form: Na-Form Ratio
1	1.20	0.28	1.15	1.5	1.05
3	1.21	0.39	1.15	0.87	1.05
4	1.15	0.10	1.13	0.97	1.02
6	1.18	0.91	1.14	0.23	1.03
7	1.16	0.59	1.13	0.41	1.02
8	1.20	3.7	1.16	2.9	1.04
9	1.25	1.68	1.19	0.09	1.06
10	1.17	0.47	1.12	1.1	1.04
11	1.21	2.8	1.11	0.28	1.09
12	1.28	2.5	1.08	0.46	1.10

3.3.5 Bed Porosity and Skeletal Density

The expanded H-form resin-bed porosities and particle densities were measured for Resins #3, #9, and #12. Their results are summarized in Table 3.11. The average calculated resin-bed porosities were similar, ranging from 0.37 to 0.42 for the three different types of resins tested. The SL-644 resin (#12) bed porosity (0.43) was 17% lower than that provided by SRTC at 0.49 on the same IBC SL-644 production batch.[(a)]

Table 3.11. Resin-Bed Porosity and Skeletal Density

Resin ID	Bed Porosity	Duplicate Bed Porosity	RPD	Skeletal Density, g/mL	Duplicate Skeletal Density, g/mL	RPD
3	0.39	0.36	9.0	1.286	1.535	17.6
9	0.38	0.38	0.24	1.415	NA[(a)]	NA[(a)]
12	0.43	0.41	3.6	1.426	1.405	1.5

NA = not applicable
(a) The duplicate was determined to be an outlier and therefore, only one value was used.

The average H-form skeletal densities for the three resins tested were essentially equivalent at 1.41 g/mL. The skeletal-density data may be limited because of the measurement sensitivity associated with the pycnometer. A 0.1% pycnometer volume change would change the H-form skeletal density by 3.7%. The skeletal density calculated for SL-644 Resin #12 was lower than those reported by Hassan et al. at 1.61 and 1.55 g/mL on as-received resins from SL-644 production batches 644BZ and

(a) Private communication, C Nash, January 2003.

981020MB48-563, respectively [12]. Resin #12 results agreed well with the result provided by SRTC (1.40 g/mL) determined previously on the same resin production batch.[(a)]

3.4 Particle-Size Distribution

Figure 3.4 shows the comparison between the average particle sizes for the pretreated resins in the H-form and in the Na-form. The reported values are based on the average of several runs to minimize errors associated with potential non-representative sampling. Results are presented on a mean volume basis. Resin #8 resulted in essentially the same average particle size in both the H- and Na-forms. This may have been due to non-representative sampling as the sampling technique remains an issue for this analysis. Other resin results showed that the Na-form was from 5% (#1 and #9) to 22% (#11) larger than the H-form. The mean particle size of the resins may be skewed slightly low because the instrument was only capable of measuring the particle size up to 1410 μm. This bias effect would more significantly affect the Na-form measurement than the H-form measurement. Based on the shape of the distribution plots, this bias appeared to be small. Resins #2 and #5 were combined and analyzed as Resin #9, as previously noted.

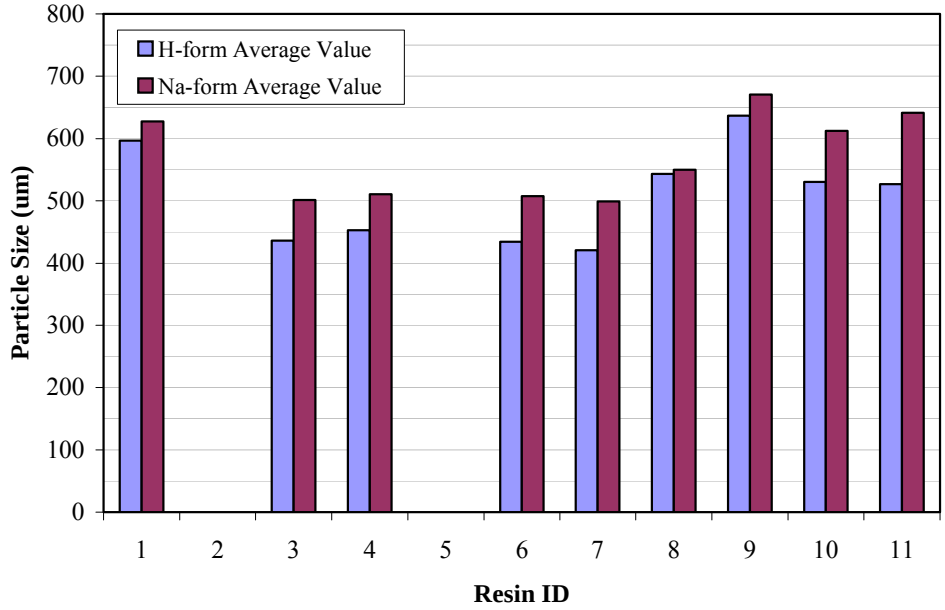

Figure 3.4. Average Particle-Size Distribution Comparison

Figure 3.5 and Figure 3.6 show the range of particle sizes for each resin in both the H-form and Na-form, respectively. The bars above and below the mean represent the particle-size ranges for the lower 10% and upper 90% on a volume basis. Resins #3, #4, #6, and #7 had fairly tight PSDs with a spread of ~170 μm in the H-form and a spread of 220 to 270 μm in the Na-form. Resins #1, #8, #9, #10, and #11 had large PSDs with a spread of ~450 μm in the H-form and an average spread of ~500 μm in the Na-form. These values are tabulated in Table 3.12.

(a) Private communication from C Nash, January 2003.

Table 3.12. Particle-Size-Distribution Summary for RF Resins

Resin ID:	1	3	4	6	7	8	9	10	11
H-Form									
Mean particle size, μm	597	436	453	434	421	544	637	530	527
Particle size, low 10%, μm	420	350	340	346	330	370	434	328	336
Particle size, high 90%, μm	866	522	512	515	499	780	892	812	794
Na-Form									
Mean particle size, μm	628	501	511	508	499	550	671	612	641
Particle size, low 10%, μm	372	397	397	394	396	352	438	352	384
Particle size, high 90%, μm	904	622	665	639	616	774	930	873	886

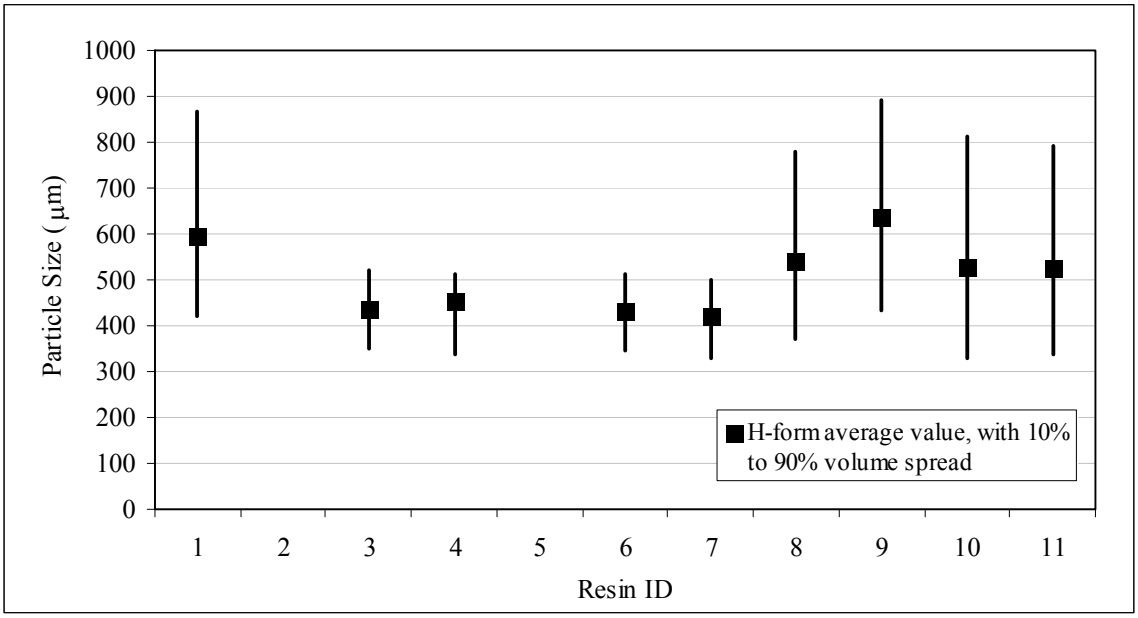

Figure 3.5. H-Form PSD

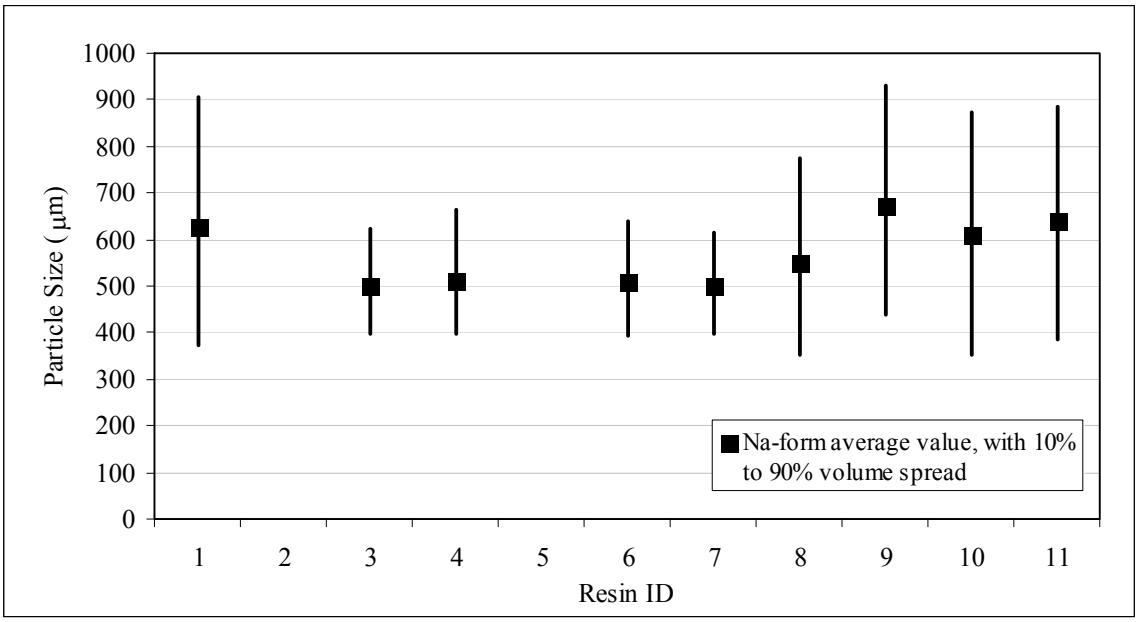

Figure 3.6. Na-Form PSD

Figure 3.7 through Figure 3.10 present representative distribution plots for spherical and granular resins in both the H-form and the Na-form. Figure 3.7 and Figure 3.8 show the PSD for Resin #3 (both H-form and Na-form), which is representative of a tight PSD. Figure 3.9 and Figure 3.10 show the PSDs for Resin #9 (both H-form and Na-form), which is representative of the broader PSD. In both cases, the shapes of the PSD profiles essentially remained the same and shifted higher as the resin was converted from the H-form to the Na-form. In all cases, the pretreated resins resulted in a single maximum despite the contractions and expansions associated with cycling during pretreatment.

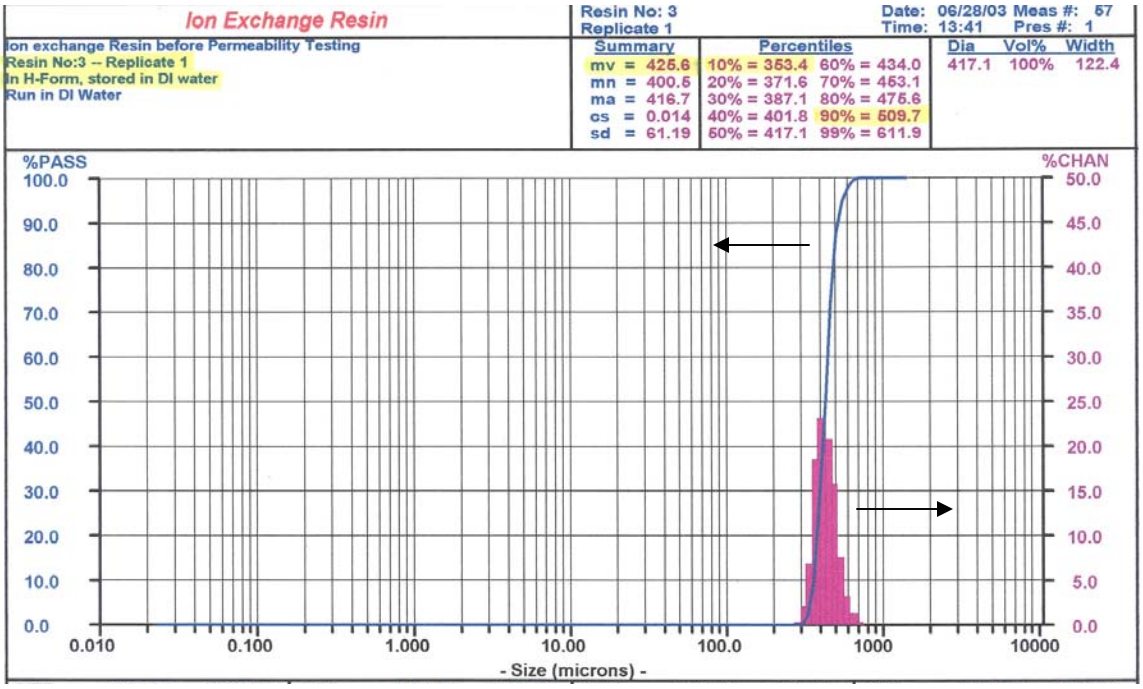

Figure 3.7. Resin #3 H-Form Representative of a Tight PSD

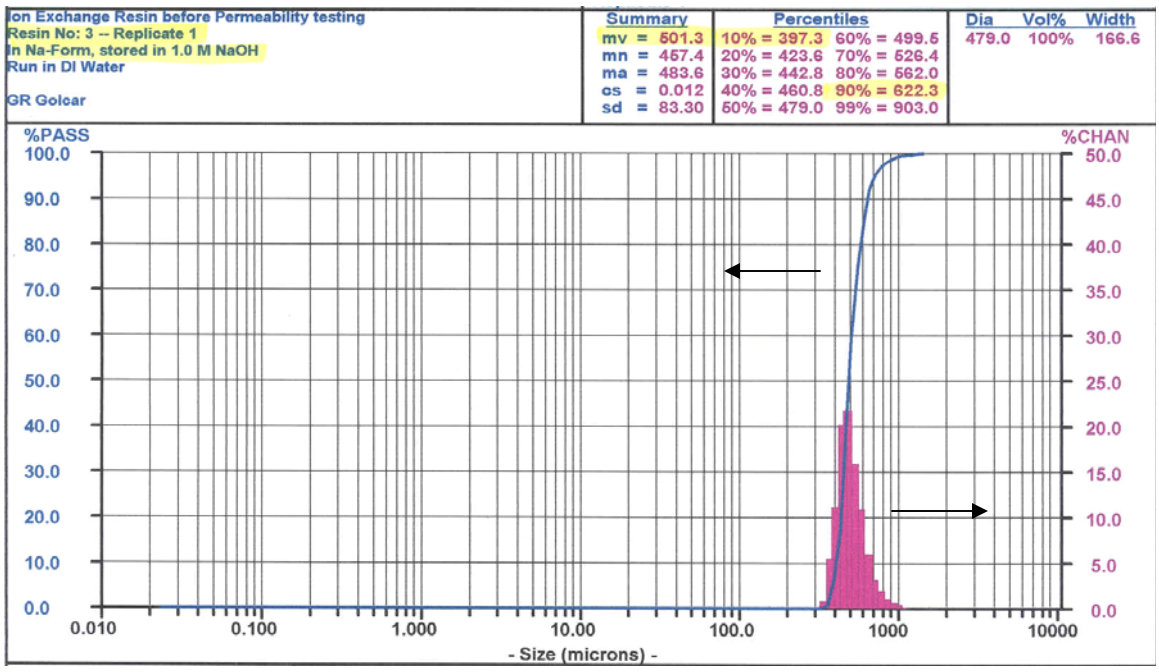

Figure 3.8. Resin #3 Na-Form Representative of a Tight PSD

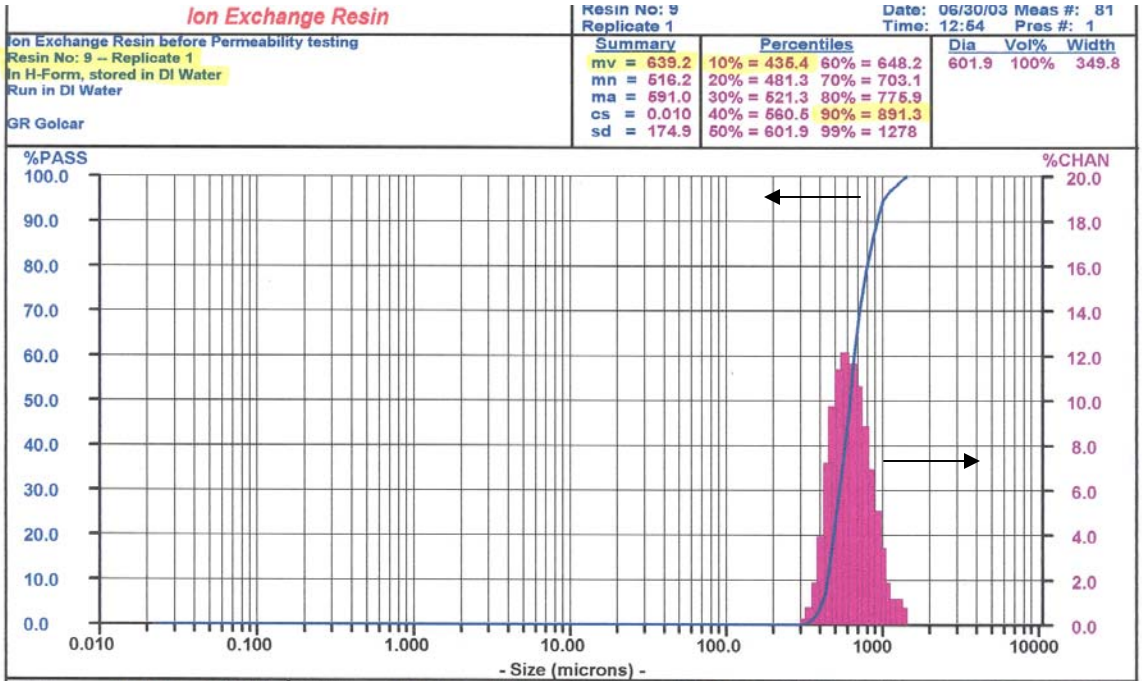

Figure 3.9. Resin #9 H-Form Representative of a Large PSD

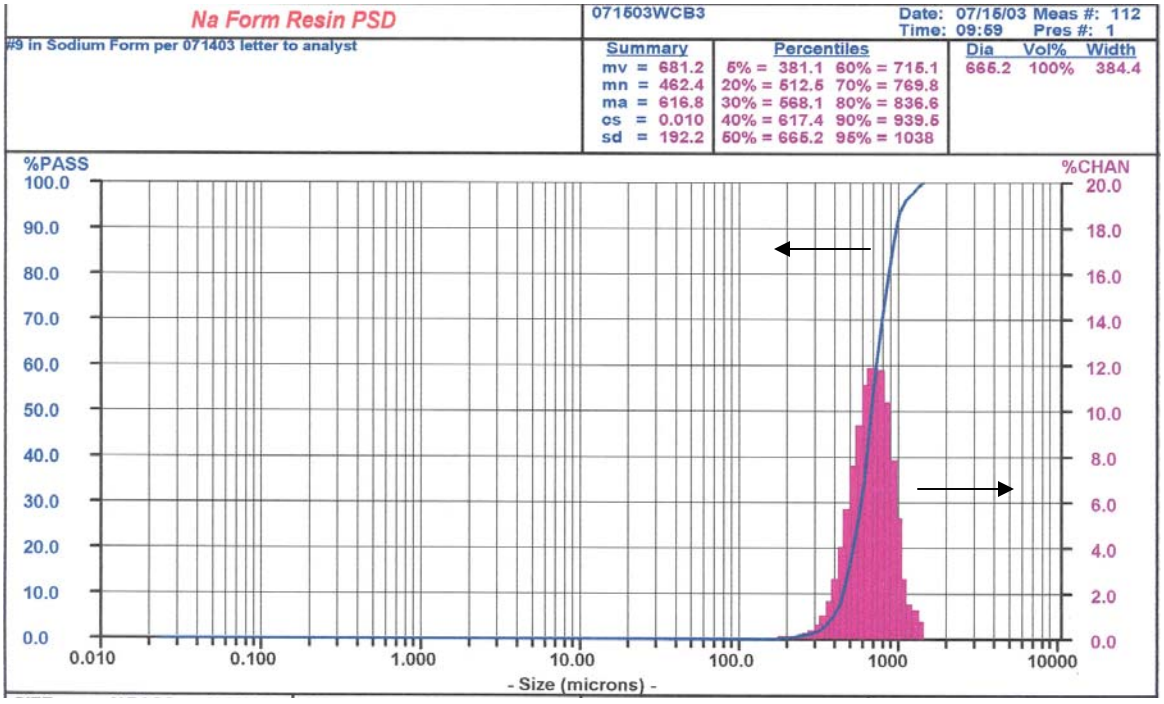

Figure 3.10. Resin #9 Na-Form Representative of a Large PSD

4.0 Batch-Contact Results

The following sections discuss the assessment of batch-contact equilibrium verification, equilibrium-distribution coefficient determinations, and isotherms for the various RF resins tested. Batch-contact details are provided in Appendix B.

4.1 Equilibrium Test

Achievement of batch-contact equilibrium was evaluated for each of the pretreated resins in duplicate at a high Cs concentration in the contact solution (681 mg/L Cs in AZ-102 simulant matrix). Samples were removed from the shaker at 24-, 48-, 72-, and 96-h processing times. The K_d results for each contact time are summarized in Table 4.1.

Table 4.1. Batch Equilibrium K_d Values as a Function of Contact Time

Initial [Cs] mg/L	Resin ID	Average K_d Values, mL/g[(a)] (Contact Time)			
		24 h	48 h	72 h	96 h
681	1	212	208	210	214
681	3	269	271	268	266
681	4	155	159	154	142
681	6	220	217	217	203
681	7	154	155	155	138
681	8	221	219	208	201
681	9	123	122	119	116
681	10	90	91	91	88
681	11	110	104	107	100

(a) Maximum uncertainties in the count data were ±1%, which corresponded to nominal ±2% uncertainties in the K_d values.

The measured K_d values remained constant with time, indicating that Cs quickly equilibrated with each resin (within 24 hours) and remained in the initial equilibrium condition through the 96-h contact time. For better clarity, these results are also shown graphically in Figure 4.1. These results were consistent with those reported by Brown et al. where Cs equilibrium conditions were established with RF resin in 20 hours [13]. Data analysis for the other Cs concentrations tested based on the average 96-h contact time were considered to represent equilibrium conditions.

4.2 Batch-Contact Testing as a Function of Cs Concentration

Various Cs concentrations in AZ-102 simulant were tested at the 96-h contact time. These K_d results are summarized in Table 4.2. The RPDs calculated from the duplicate results were generally over-conservative because the differences in some K_d values also were represented by different equilibrium Cs concentrations. The ultra-low Cs concentration was tested to evaluate polishing-column conditions.

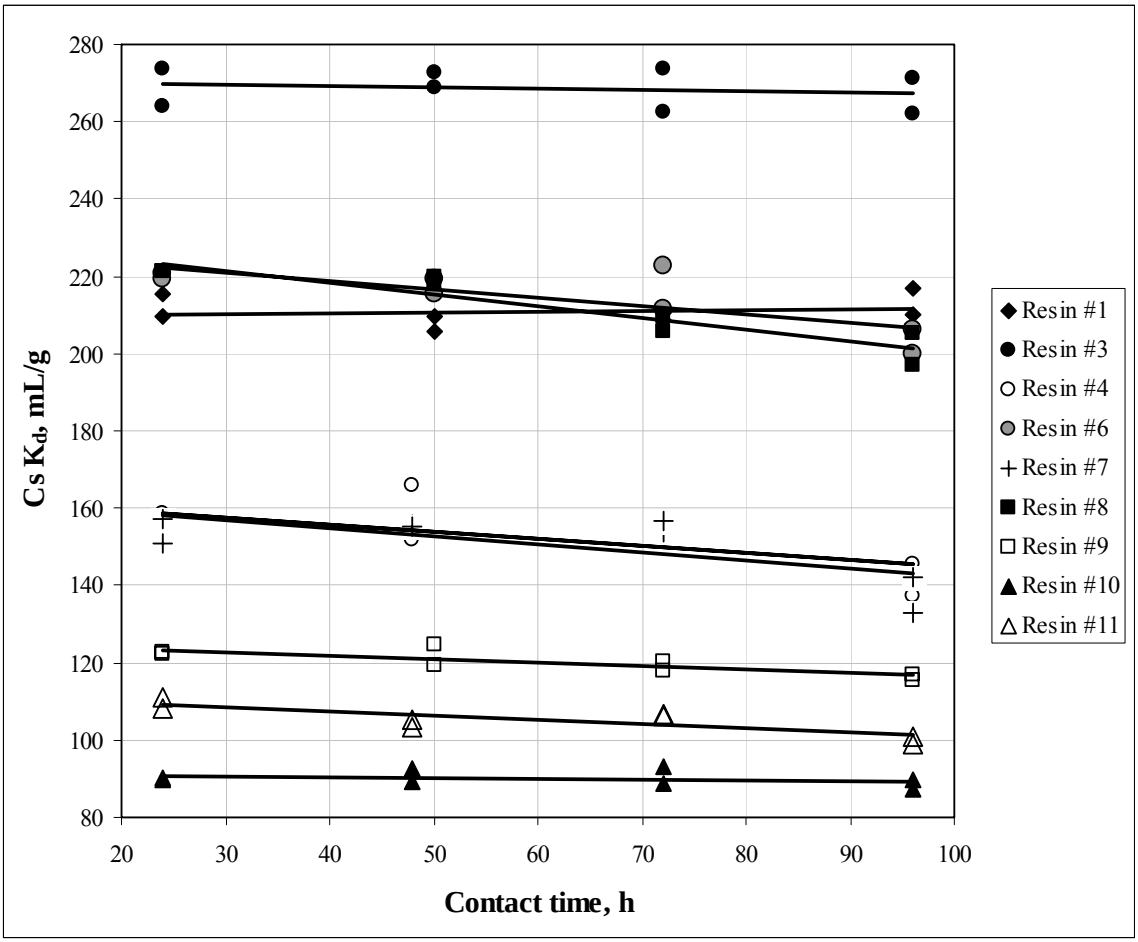

Figure 4.1. Equilibrium K_d Values as a Function of Contact Time

The K_d values versus Cs concentrations are plotted in Figure 4.2 and Figure 4.3 on a log-log scale to better indicate differences between the resins. All resin K_d responses appeared linear on the log-log plot where the Cs concentration was greater than ~3 μg/mL. As Cs concentrations decreased, the K_d curve bent sharply toward constant K_d values. The low Cs concentration values bracket the estimated input Cs concentration to the polishing column (2.4E-7 M Cs or 0.032 μg/mL). The K_d performance of Resins #4 and #7 were not distinguishable. Resins #1, #3, and #8 appeared to behave similarly, except at the very low Cs concentrations, where #3 dropped slightly in K_d value. Resins #10 and #11 appeared to have comparable K_d values at low Cs concentrations to #8 and #1, rising higher than Resin #9. However, Resin #9 performed similarly to Resins #10 and #11 at the higher Cs concentrations.

Data reported by Kurath et al. [3] for RF resin performance in neutralized current acid waste (NCAW) simulant (5 M Na), which is similar to the AZ tank wastes, are also shown in Figure 4.3 (RF resin produced by Boulder Scientific, production batch BSC-210). The Kurath-reported data were reported in units of lambda (K_d * ρ_{DRB}) as a function of Na:Cs mole ratios. The lambda values were converted to K_d values by dividing lambda by the reported dry-bed density, 0.34 g/mL, where mass was based on the Na-form resin. Across the equilibrium Cs concentration range, the Kurath-reported batch-contact results appeared superior (higher K_ds) to those obtained in the current test.

Table 4.2. Equilibrium Cs K_d Values in AZ-102 Simulant in Contact with Resins

Feed Spike ID	Resin ID	Equilibrium			Resin ID	Equilibrium		
		Cs, µg/mL	Cs K_d,, mL/g	RPD, %		Cs, µg/mL	Cs K_d,, mL/g	RPD, %
Spike 5	1	3.31E-4	2548	0.5	8	3.14E-4	2603	0.2
		3.38E-4	2535			3.14E-4	2598	
Spike 1		5.32	1149	1.8		4.45	1367	6.4
		5.40	1171			4.59	1282	
Spike 2		14.1	825	3.5		10.0	1029	5.6
		13.9	854			11.0	973	
Spike 3		34.1	586	5.7		25.0	725	6.8
		32.3	620			28.8	678	
Spike 4		268	210	3.2		258	209	6.6
		261	217			278	196	
Spike 5	3	5.32E-4	1943	7.1	9	7.14E-4	1036	0.6
		5.73E-4	1810			7.15E-4	1042	
Spike 1		7.61	994	5.0		8.31	642	9.0
		8.08	945			6.78	702	
Spike 2		20.2	702	11.2		22.8	443	2.7
		17.8	785			21.2	455	
Spike 3		37.8	602	4.1		55.1	305	8.7
		41.5	577			49.5	332	
Spike 4		280	262	3.5		360	117	0.4
		261	271			362	117	
Spike 5	4	6.37E-4	966	0.03	10	3.45E-4	2401	1.9
		6.35E-4	967			3.40E-4	2446	
Spike 1		7.75	519	2.1		7.55	743	4.5
		7.95	508			7.22	777	
Spike 2		19.7	396	2.1		21.4	464	0.1
		19.1	404			21.3	464	
Spike 3		45.5	289	3.3		54.0	292	3.5
		43.6	299			56.9	282	
Spike 4		278	146	5.9		407	87	3.1
		286	137			398	90	
Spike 5	6	6.64E-4	1556	12.7	11	2.59E-4	2545	11.2
		7.41E-4	1370			2.35E-4	2847	
Spike 1		10.2	707	3.7		4.88	967	1.1
		9.27	734			4.81	978	
Spike 2		22.4	574	4.2		14.4	599	2.1
		23.1	550			14.6	587	
Spike 3		54.3	408	1.2		40.2	359	1.4
		53.7	403			39.9	364	
Spike 4		296	206	3.3		349	99	1.9
		319	200			346	101	
Spike 5	7	7.45E-4	1006	3.0	No data			
		7.72E-4	977					
Spike 1		10.7	484	1.0				
		10.6	489					
Spike 2		24.7	383	2.3				
		25.0	374					
Spike 3		54.6	292	3.5				
		53.0	303					
Spike 4		336	133	6.7				
		228	142					

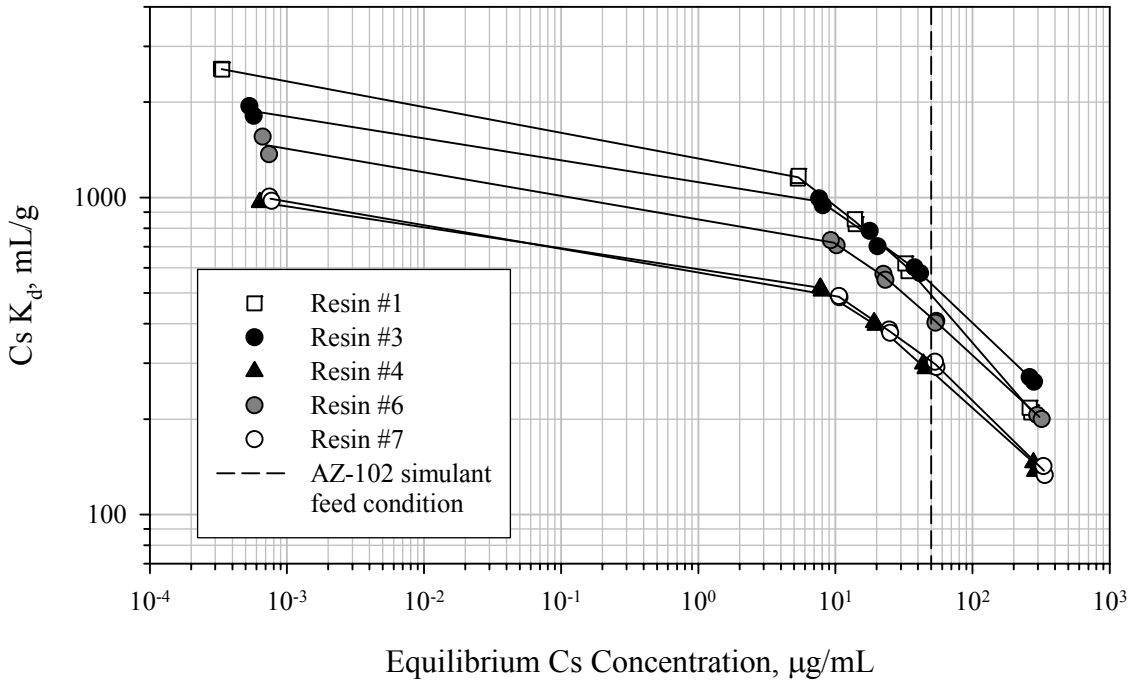

Figure 4.2. Equilibrium Cs K_d Values for Resins #1, #3, #4, #6, and #7

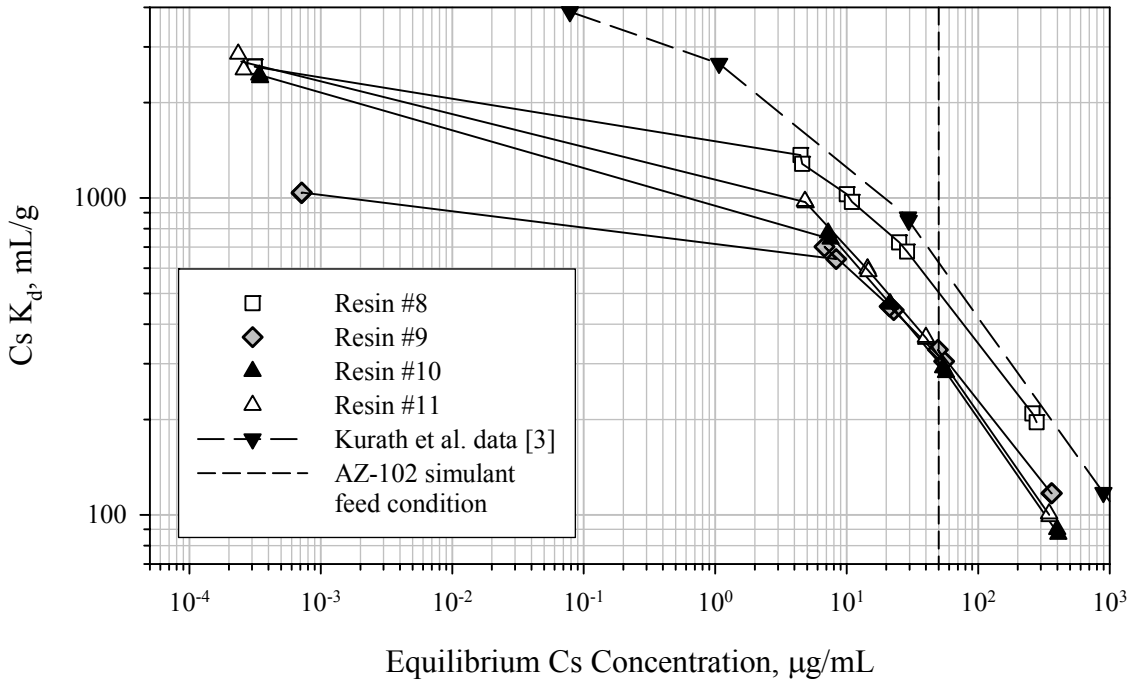

Figure 4.3. Equilibrium Cs K_d Values for Resins #8, #9, #10, #11, and Kurath et al. Data [3]

4.3 Isotherms

The equilibrium Cs concentrations in the supernatants were calculated according to Equation 2.8, and the Cs concentrations in the resins were calculated according to Equation 2.9. The calculated equilibrium concentrations are shown in Table 4.3.

The isotherms represented by these values are presented in Figure 4.4 and Figure 4.5. The equilibrium Cs concentrations in the resins are represented in two manners, concentration expressed as mg/g (left axis) and concentration expressed as mmoles/g (right axis). The AZ-102 simulant Cs concentration is 0.05 mg/mL. All resin masses were based on the H-form resin. To correct for the Na-form resin mass, the mass increase factor (I_{Na}) on conversion to Na-form would need to be incorporated.[(a)] This correction is expected to decrease the reported values. It is expected that the relative mass decrease would be similar for all resin forms.

The total Cs capacity for the given matrix (AZ-102 simulant) can be estimated from the isotherm where the curve levels off at a given Cs concentration in the resin. It appeared that the spherical form resins (#3 and #6) had not reached the Cs-capacity limit; their isotherm curves did not level off and appeared, instead, to continue to climb past the experimental limit with increasing Cs concentration in solution. Resin #3 performed the best, reaching a maximum (within the experimental constraints) of 73.4 mg Cs/g resin, equivalent to 0.552 mmoles Cs/g resin. Of the granular materials, Resin #1 and #8 appeared to perform the best, reaching maximum resin Cs concentrations of 56.7 and 54.4 mg/g (0.426 and 0.409 mmoles/g), respectively. The resins with the least capacity were #10 and #11 at 35.8 and 35.0 mg Cs/g resin (0.269 and 0.263 mmole Cs/g resin), respectively.

These values may be compared with the Cs capacity on SL-644 in contact with AZ-101 actual waste (0.44 mmoles/g) and AZ-102 actual waste (0.30 mmoles/g), calculated from previously reported batch-contact data by Fiskum et al. [14 and 15, respectively]. The ground-resin Cs capacities appeared similar to that of SL-644 in contact with AZ-101. The comparison, however, must be used with caution. The SL-644 used in these actual waste tests (IBC production batch 010319SMC-IV-73) used a smaller PSD (212- to 425-μm dry-sieved fraction) and had been stored nominally one year in the H-form in air before batch contact. Furthermore, the contact-solution headspace was not filled with an inert gas.

(a) Determination of I_{Na} factor was beyond the scope of current test requirements.

Table 4.3. Equilibrium Cs Concentrations for RF Resins in Contact with AZ-102 Simulant

Feed Spike ID	Resin ID	Equilibrium Cs Concentration		Resin ID	Equilibrium Cs Concentration	
		mg/mL	mg/g[(a)]		mg/mL	mg/g[(a)]
Spike 5	1	3.31E-7	8.44E-04	8	3.14E-7	8.18E-4
		3.38E-7	8.56E-04		3.14E-7	8.16E-4
Spike 1		5.32E-3	6.11E+0		4.44E-3	6.07E+0
		5.39E-3	6.32E+0		4.59E-3	5.88E+0
Spike 2		1.41E-2	1.16E+1		1.00E-2	1.03E+1
		1.39E-2	1.18E+1		1.09E-2	1.07E+1
Spike 3		3.41E-2	2.00E+1		2.50E-2	1.82E+1
		3.23E-2	2.01E+1		2.88E-2	1.95E+1
Spike 4		2.68E-1	5.64E+1		2.58E-1	5.39E+1
		2.61E-1	5.67E+1		2.78E-1	5.44E+1
Spike 5	3	5.32E-7	1.03E-3	9	7.14E-7	7.39E-4
		5.73E-7	1.04E-3		7.15E-7	7.45E-4
Spike 1		7.61E-3	7.56E+0		8.31E-3	5.33E+0
		8.08E-3	7.64E+0		6.78E-3	4.76E+0
Spike 2		2.02E-2	1.42E+1		2.28E-2	1.01E+1
		1.78E-2	1.39E+1		2.12E-2	9.65E+0
Spike 3		3.78E-2	2.27E+1		5.51E-2	1.68E+1
		4.15E-2	2.40E+1		4.95E-2	1.64E+1
Spike 4		2.80E-1	7.34E+1		3.60E-1	4.23E+1
		2.61E-1	7.08E+1		3.62E-1	4.24E+1
Spike 5	4	6.37E-7	6.16E-4	10	3.45E-7	8.29E-4
		6.35E-7	6.14E-4		3.40E-7	8.32E-4
Spike 1		7.75E-3	4.02E+0		7.55E-3	5.61E+0
		7.95E-3	4.04E+0		7.22E-3	5.61E+0
Spike 2		1.97E-2	7.79E+0		2.14E-2	9.93E+0
		1.91E-2	7.74E+0		2.13E-2	9.88E+0
Spike 3		4.55E-2	1.32E+1		5.40E-2	1.58E+1
		4.36E-2	1.30E+1		5.69E-2	1.61E+1
Spike 4		2.78E-1	4.05E+1		4.07E-1	3.55E+1
		2.86E-1	3.92E+1		3.98E-1	3.58E+1
Spike 5	6	6.64E-7	1.03E-3	11	2.59E-7	6.60E-4
		7.41E-7	1.01E-3		2.35E-7	6.68E-4
Spike 1		1.02E-2	7.21E+0		4.88E-3	4.71E+0
		9.27E-3	6.81E+0		4.81E-3	4.70E+0
Spike 2		2.24E-2	1.28E+1		1.44E-2	8.61E+0
		2.31E-2	1.27E+1		1.46E-2	8.57E+0
Spike 3		5.43E-2	2.21E+1		4.02E-2	1.44E+1
		5.37E-2	2.16E+1		3.99E-2	1.46E+1
Spike 4		2.96E-1	6.12E+1		3.49E-1	3.46E+1
		3.19E-1	6.37E+1		3.46E-1	3.50E+1
Spike 5	7	7.45E-7	7.49E-4	No Data		
		7.72E-7	7.55E-4			
Spike 1		1.07E-2	5.18E+0			
		1.06E-2	5.19E+0			
Spike 2		2.47E-2	9.45E+0			
		2.51E-2	9.37E+0			
Spike 3		5.46E-2	1.60E+1			
		5.30E-2	1.61E+1			
Spike 4		3.36E-1	4.46E+1			
		3.28E-1	4.66E+1			

(a) The Cs resin loading is in terms of mg Cs per gram of dry H-form resin.

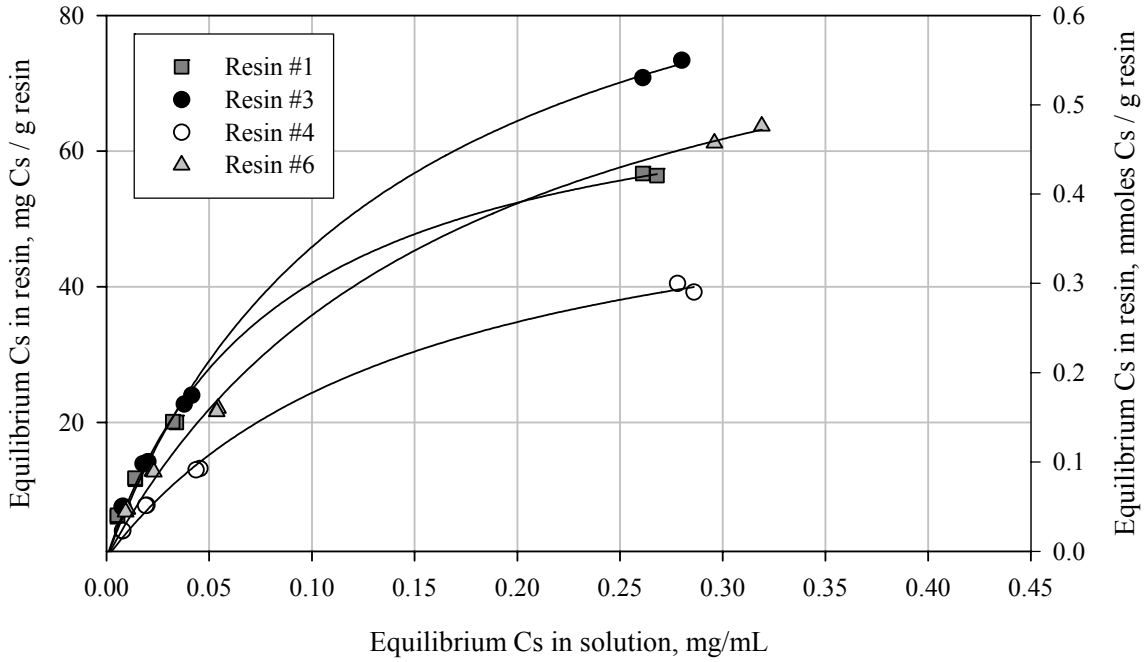

Figure 4.4. Equilibrium Cs Isotherm for Resins #1, #3, #4, and #6

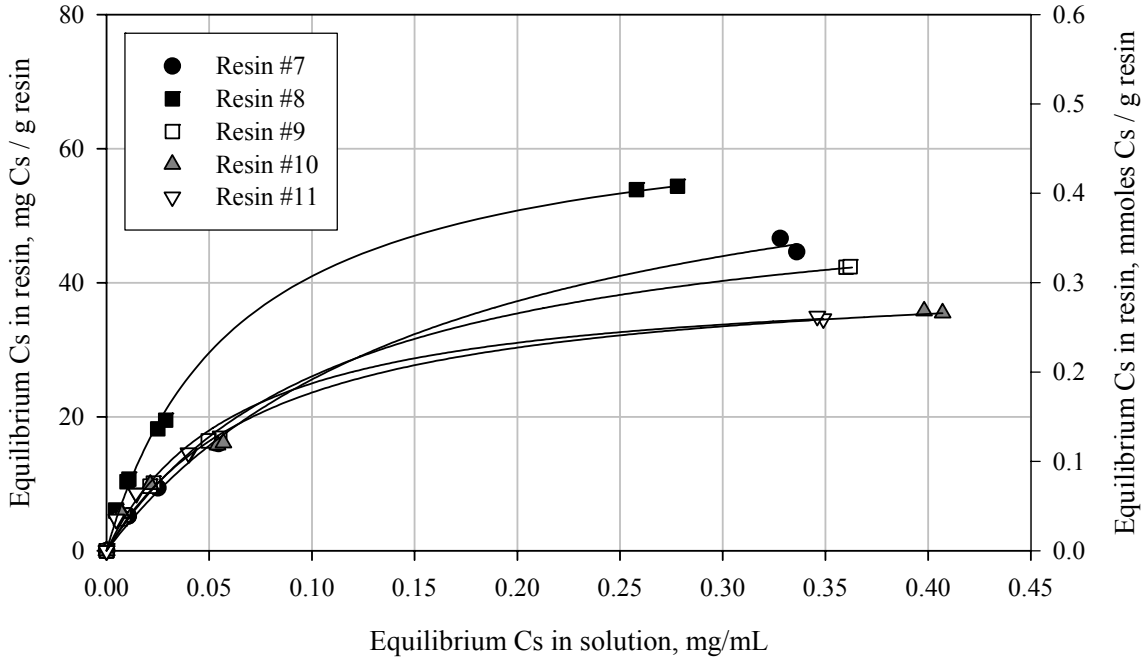

Figure 4.5. Cs Isotherms for Resins #7, #8, #9, #10, and #11

5.0 Column-Testing Results

The Cs load and elution behavior for the various resins tested is presented along with the estimated residual Cs on the resin beds after elution. Shrink-swell characteristics are also reported.

5.1 Load and Elute Behavior

The Cs load and elution profiles are provided in Sections 5.1.1 through 5.1.8 for all cycles tested. Each load profile is plotted as % C/C_o vs. the BVs of feed processed through each column. The abscissa reflects BVs as a function of the resin in the Na-form as originally loaded in the column.[(a)] The C_o value for the Cs tracer was determined for each feed condition. The C/C_o is plotted on a probability scale. A probability scale is the inverse of the Gaussian cumulative distribution function (characteristic of ideal ion exchange theory) such that a graph of the sigmoidally-shaped Gaussian cumulative distribution function appears as a straight line [16]. The probability scale has a couple of advantages, including making low C/C_o data easily readable such that the initial load performance is discernable, and extrapolation to 50% breakthrough can be easily estimated in the sigmoidal region. Less-than values are recorded on the breakthrough profiles as actual values. The less-than values can be identified from the data-input tables provided in Appendix C. Many of the % C/C_o values shown before significant breakthrough in the loading profiles were actually less-than values; thus, comparisons in these regions must be made carefully. Also shown on each load figure is the minimum Cs removal required for the effluent to meet design-basis ^{137}Cs loading in the vitrified glass product. For the AZ-102 actual tank waste, the maximum % C/C_o is 0.025, corresponding to a Cs decontamination factor (DF) of 4000. For the AP-101 actual tank waste, the maximum % C/C_o is 0.0992, corresponding to a DF of 1000.

Each elution profile is plotted as C/C_o versus the BVs of eluant processed through each column. As with the load profile, the BV represents the resin BV in the expanded Na-form. The C/C_o is plotted on a log scale to better discern the low relative Cs concentrations and the elution tailing effect.

5.1.1 Column 1, SL-644, Resin #12

Column 1 tested the SL-644 from C-01-05-28-02-35-60 (Resin #12) with 50 μg/mL Cs in the AZ-102 simulant matrix. Only 1.5 cycles were tested because of an experimental problem where the feed line was accidentally pulled out of the feed solution after processing 133 BVs of simulant during Cycle 2. The load and elution profiles are shown in Figure 5.1 and Figure 5.2, respectively. Cycle 1 Cs breakthrough did not begin until nominally 180 BVs had been processed, culminating in 50% breakthrough at 240 BVs. This performance was superior to that reported for actual tank waste AZ-102 (70 μg/mL total Cs) previously reported [15] where Cs breakthrough began at 68 BVs, and 50% breakthrough occurred at 93 BVs. The difference is attributed to a higher Cs concentration in the actual waste (70 mg/L) and to differences in the resin batches, ages, and processing histories. On this current test, there was no measurable evidence of Cs bleed from the first cycle into the second process cycle, corresponding to less than 3E-3% C/C_o Cs bleed.

(a) The bed volume fluctuated significantly during the various processing steps.

The elution resulted in the typical profile found with previous SL-644 testing. The peak C/C_o value was found at 5 BVs eluate, and 1% C/C_o was reached at 15 BVs. The 15 BVs required to reach 1% C/Co was probably biased high; it is the interpolated value obtained from a large sample effluent collection of 5.6 BVs. The eluted Cs concentration tailed significantly to a nearly constant 0.1% C/C_o.

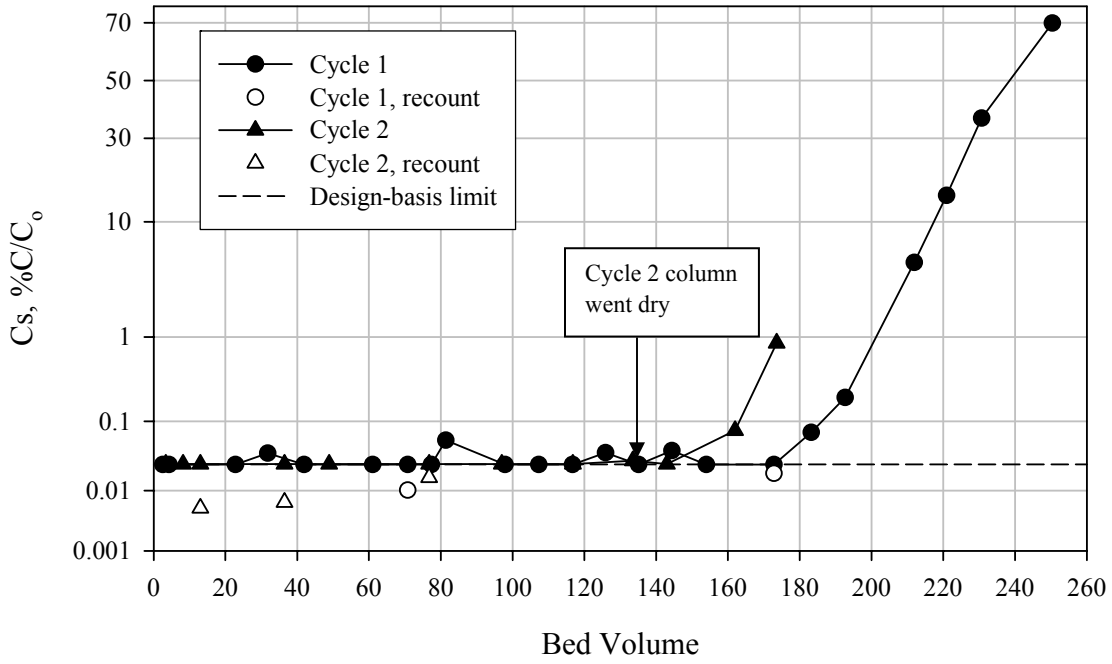

Figure 5.1. Column 1, Resin #12 (SL-644), Cs Load Profiles with AZ-102 Simulant

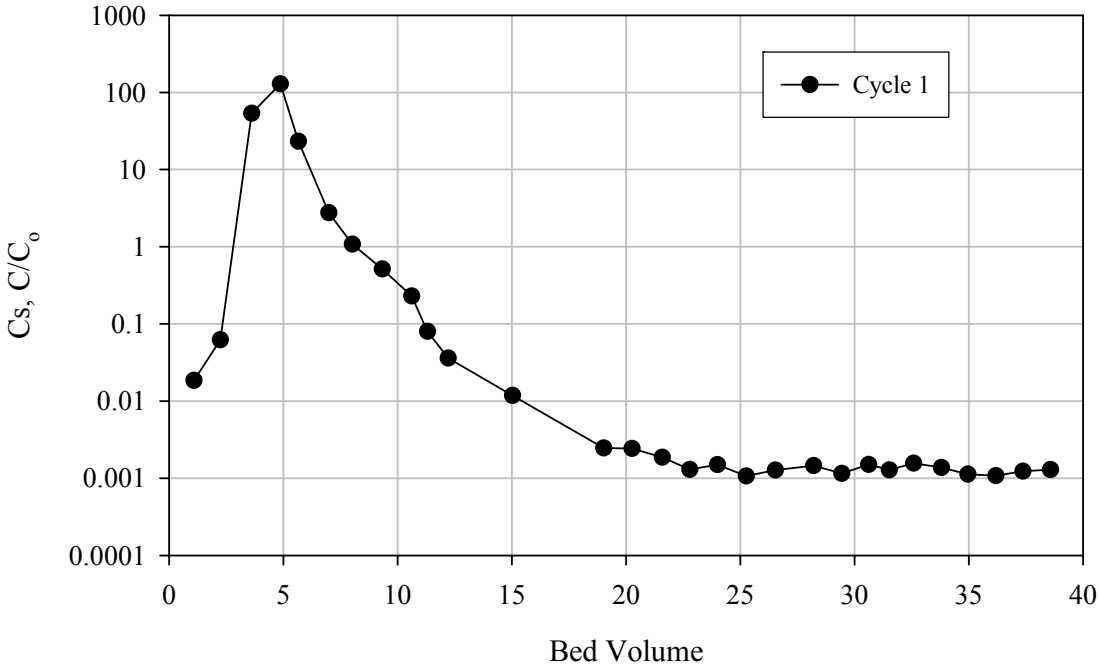

Figure 5.2. Column 1, Resin #12 (SL-644), Cs Elution Profile

5.1.2 Columns 2 and 3, Resin #9

Columns 2 and 3 each tested Resin #9 with the AZ-102 simulant. Column 2 was processed with upflow elution whereas Column 3 was processed exclusively downflow. During the first load cycle, after processing AZ-102 simulant for about 100 minutes, small bubbles were evident in the resin bed about a quarter of the distance from the bottom to about the midpoint. The bubbles were largest on Column 3 at about 3-mm maximum size. The total volume of bubbles in the bed was estimated to be less than 0.5 mL. As loading continued, the bubble size diminished. After loading for 3 days, the bubbles were no longer visible. Incomplete conversion of the resin to the Na-form was suspected to contribute to the formation of the observed bubbles. A more concentrated NaOH regenerant solution (1.0 M) was tested on Resin #9 on a quick bench test. Significant bubble production was not observed, so the 1.0 M NaOH was used in subsequent RF testing. No further bubble formation was observed.

The Column 2 and 3 load and elution profiles are shown in Figure 5.3 through Figure 5.6. The three breakthrough profiles for each column were almost identical above 0.1% C/C_o, indicating little or no degradation of the resin capacity. The downflow elution profiles (Figure 5.6) were almost identical, corroborating this observation. Differences in the upflow elution curves (Figure 5.4) were attributed to differences in the liquid head above the resin bed, described below.

The Cs load breakthrough began at about 120 to 130 BVs, and 50% breakthrough was reached at 170 to 190 BVs. Low levels of ^{134}Cs (3E-2% C/C_o) were detected on Column 2 Cycle 3 during the early load cycle, indicating that Cs from the previous process cycle(s) was bleeding into the product effluent.[(a)] This result was not surprising because the Cycle 2 elution was short, and the final Cs concentration did not drop below $C/C_o = 3.5$. The Cs bleed was not detected on Column 3 Cycle 3 (<8E-3% C/C_o). The Column 3 Cycle 2 elution used nominally the same volume of eluate as that of Column 2, but because of the downflow operation, the C/C_o final concentration was two orders of magnitude lower at 0.03.

The elution profiles for Column 2 were much broader than those of Column 3. During elution, the Column 2 headspace above the resin bed filled with eluate, a nominal 12-mL volume. As the resin shrank, the headspace expanded further. The peak C/C_o value was obtained at nominally 6 BVs of eluate. Cs concentrations continued to decline in a very slow manner, consistent with the behavior of a continuously stirred tank reactor (CSTR) model, as shown previously for SL-644 [17]. The C/C_o values continued to drop until at least 34 BVs were reached. Thus, for plant application, the upflow elution behavior may need to be modeled in conjunction with a changing-volume CSTR.

The elution profiles for Column 3 resulted in peak C/C_o values obtained at 5 BVs. A shoulder in the elution profiles was evident at around 8 BVs. The flowrate was reduced from 2 BV/h to 1.4 BV/h at nominally 5 to 6 BVs processing. The decrease in flowrate and the appearance of the shoulder may be related, indicating that Cs elution may be particle-diffusion-limited. The elution profile leveled off at 22 BVs to 0.1% C/C_o.

(a) Cycle 3 feeds were spiked with a different Cs tracer, ^{137}Cs.

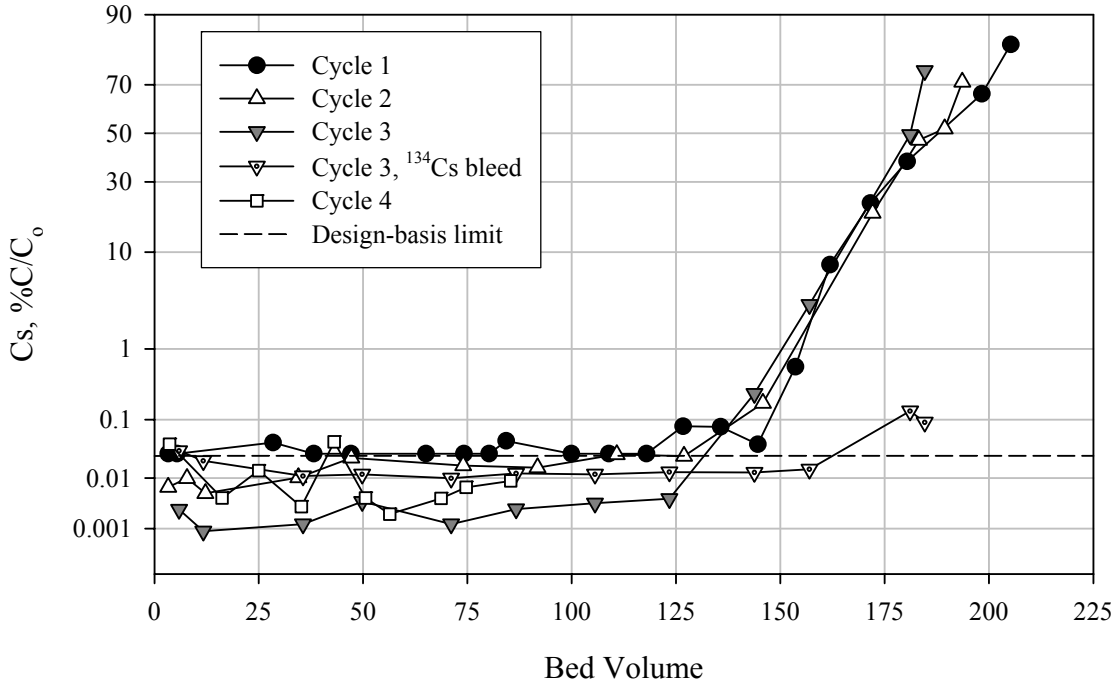

Figure 5.3. Column 2, Resin #9 Cs Load Profiles with AZ-102 Simulant

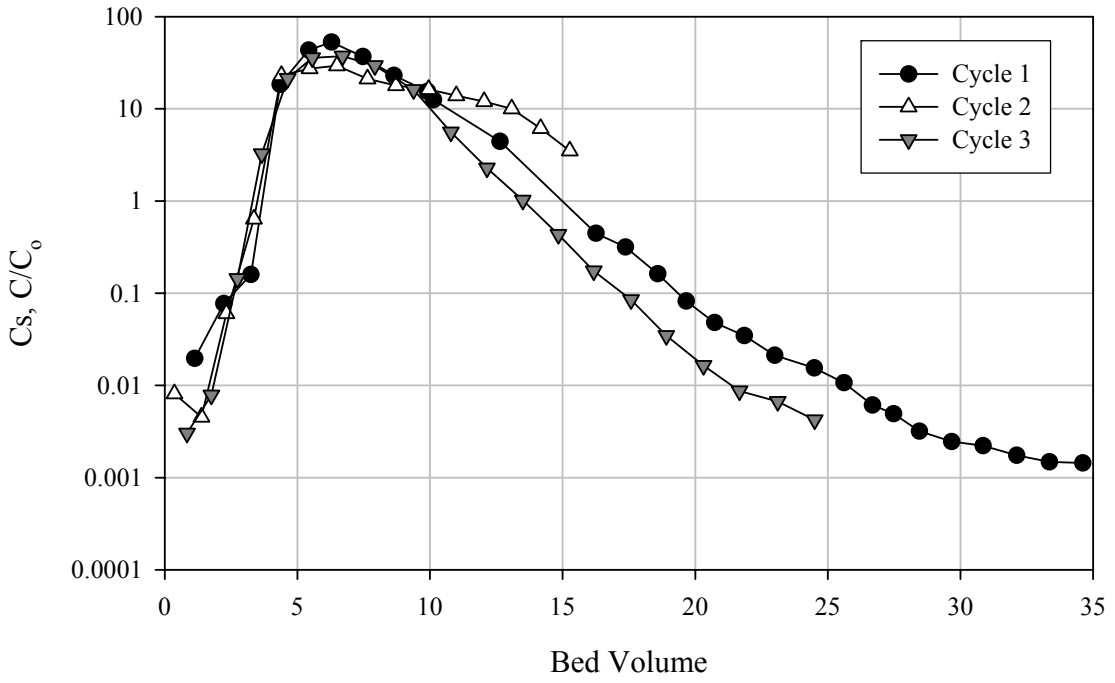

Figure 5.4. Column 2, Resin #9 Upflow Cs Elution Profiles

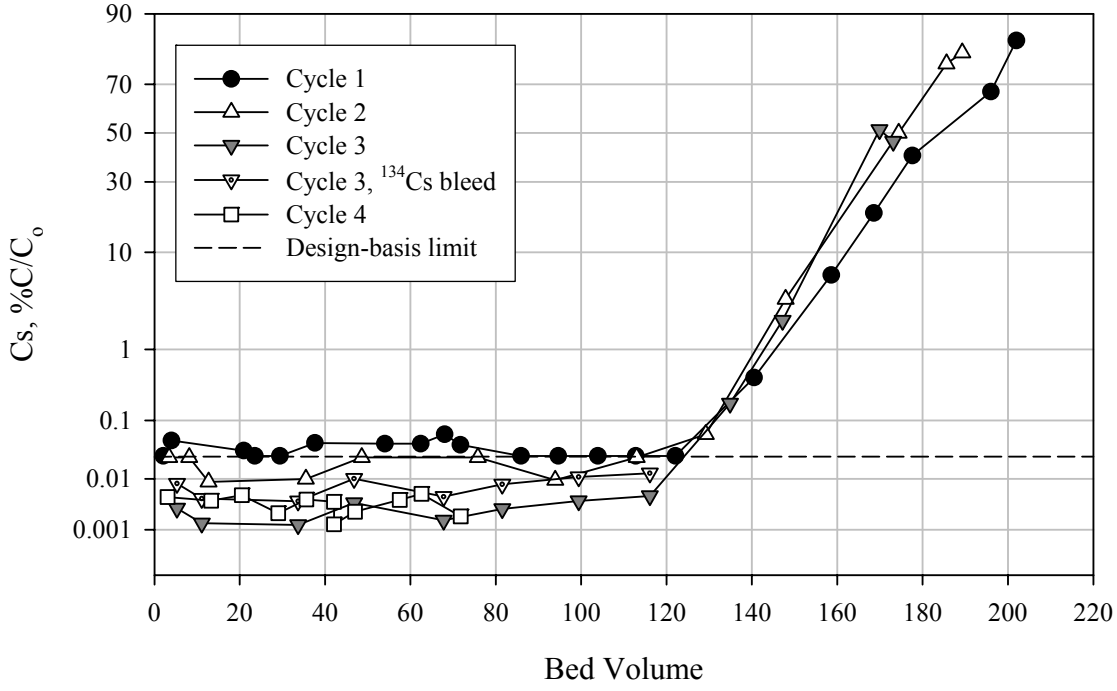

Figure 5.5. Column 3, Resin #9 Load Cs Profiles with AZ-102 Simulant

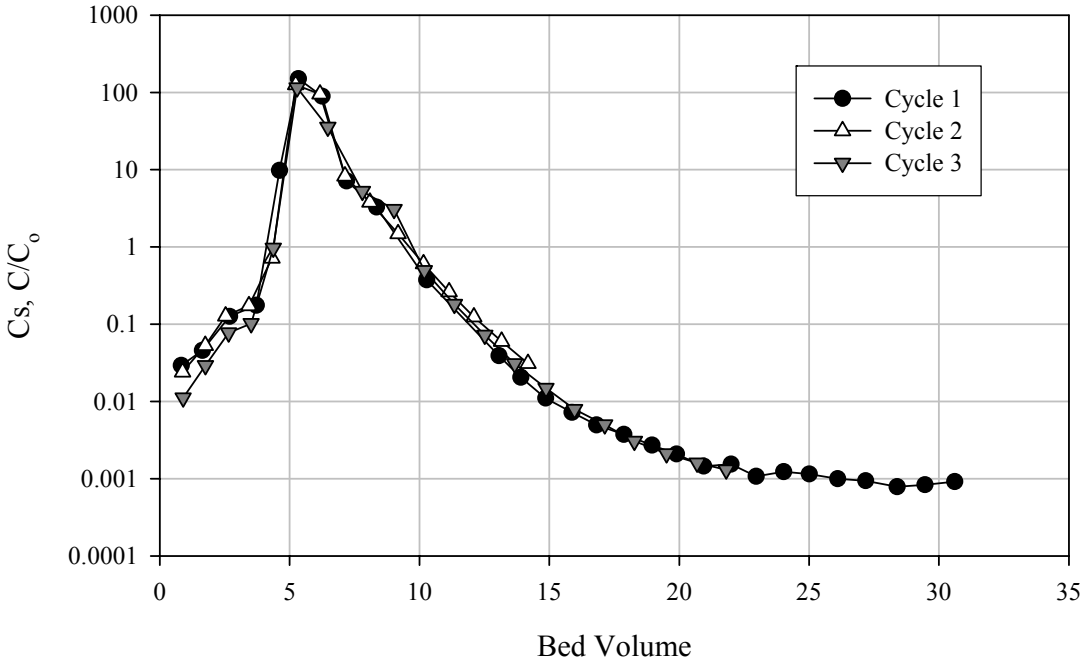

Figure 5.6. Column 3, Resin #9 Cs Elution Profiles

Process cycles subsequent to the first cycle did not result in a jump in the initial Cs effluent concentration (i.e., before significant breakthrough) as has been previously observed [14, 18]. The final (fourth) load cycle for each column was to demonstrate polishing-column conditions in that the feed Cs concentration was reduced to 0.031 μg/mL (2.4E-7 M). Even with the mistaken load direction (upflow feed) for Column 2, the effluent Cs concentration was generally below the design-basis limit for Cs removal, at nominally 4E-3% C/C_o (two samples exceeded the design-basis limit). Column 3 fourth cycle resulted in non-detected Cs, < 4E-3% C/C_o.

5.1.3 Column 4 Resin #9

Column 4 tested Resin #9 with AP-101 simulant. As in the case of Columns 2 and 3, bubbles were also evident in the Column 4 first cycle after processing AP-101 simulant feed for nominally 100 minutes; after processing for 3 days, the bubbles were no longer visible. As with Columns 2 and 3, the regenerant NaOH concentration was raised to 1.0 M after the first process cycle, and no more bubble formation was observed in subsequent load cycles.

The AP-101 simulant contained the highest K concentration expected in the tank-waste feeds (0.71 M K). The K is known to reduce Cs selectivity of RF resin as well as of SL-644. The Cs load profile, shown in Figure 5.7, dramatically shows the results of the K influence on the Cs load. The Cs breakthrough began early at nominally 25 BVs, culminating in a 50% breakthrough at nominally 205 BVs. The ^{134}Cs bleed from Cycles 1 and 2 into Cycle 3 was also apparent at nominally 2.5E-2% C/C_o. Cs bleed was also evident in Cycle 4 (loaded under polishing conditions) at ~1.4E-2% C/C_o. The high ^{134}Cs bleed in Cycle 3 resulted from Cs remaining on the resin from the previous load cycle (Cycle 2), since the feed for Cycle 3 contained only ^{137}Cs tracer (no ^{134}Cs). The ^{134}Cs C/C_o was at least an order of magnitude greater than the ^{137}Cs C/C_o for at least the first 23 BVs. This suggested that the Cs bleed resulted from residual Cs located at the bottom of the resin bed rather than at the top or homogeneously distributed throughout.

The elution of this resin was conducted virtually identical to that of Column 3. The elution profile, shown in Figure 5.8, was consistently broader than that of Column 3 with the peak C/C_o at 5 to 6 BVs. Tailing for the first cycle leveled off at nominally 3E-3 C/C_o. It was not clear if the third cycle reached a steady-state Cs elution concentration after processing 25 BVs.

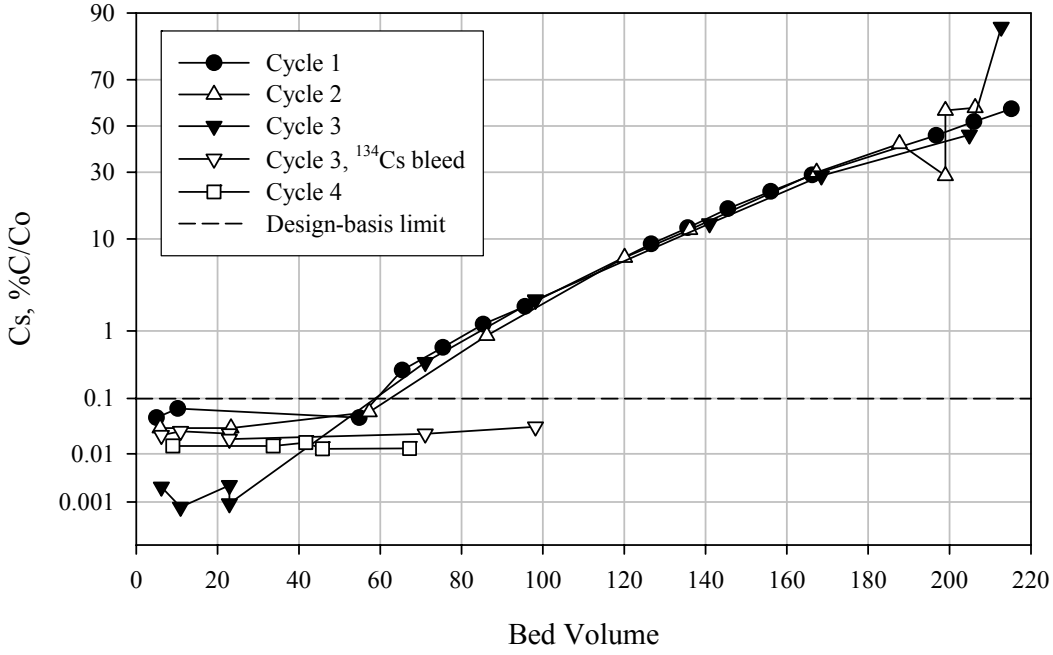

Figure 5.7. Column 4, Resin #9 Cs Load Profiles with AP-101 Simulant

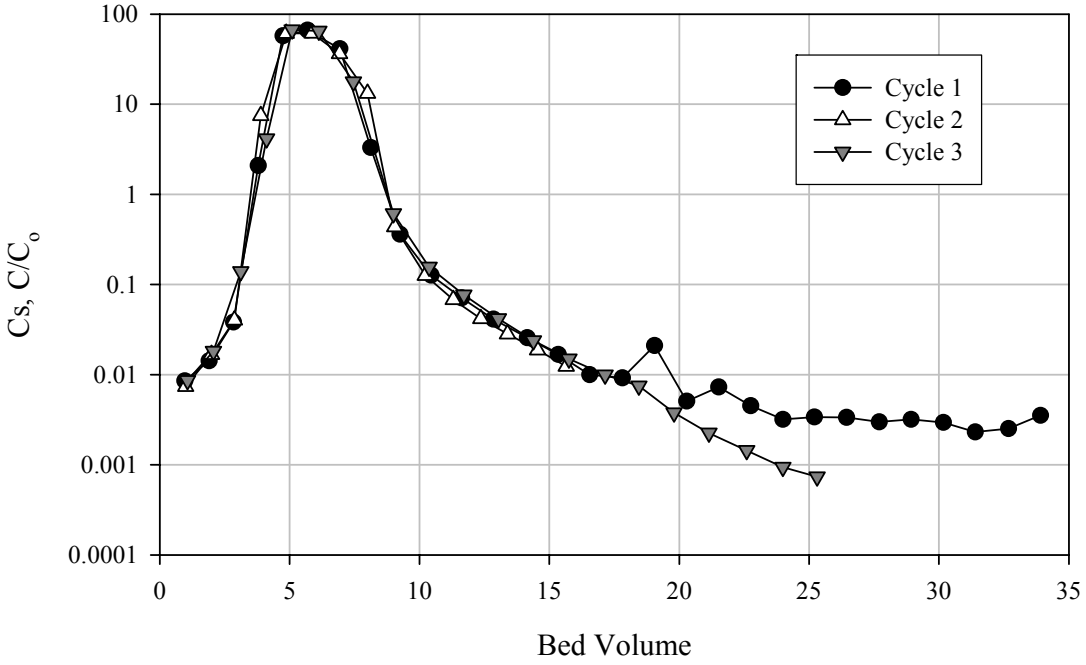

Figure 5.8. Column 4, Resin #9 Cs Elution Profiles

5.1.4 Column 5 Resin #11

Column 5 tested Resin #11 with AZ-102 simulant. The AZ-102 simulant effluent composite for Cycles 1 and 2 had a pale-green appearance, unlike the bright-yellow feed.[(a)] The effluent color change from yellow to green is indicative of Cr(IV) reduction to Cr(III). If the Cr was reduced, then another component (in the resin) would have been oxidized. The Cycle 3 effluent composite was the same color as the feed—yellow. The Cs load profiles are shown in Figure 5.9. The onset of Cs breakthrough was apparent after processing 70 BVs with 50% Cs breakthrough occurring at 110 BVs. Subsequent process cycles resulted in detectable amounts of Cs bleed at nominally 4.4E-3% C/C_o (Cycle 2), 8.8E-3% C/C_o (Cycle 3), and 3.4E-3% C/C_o (Cycle 4).

The Cycle 1 elution was conducted upflow, and Cycle 2 to 3 elutions were conducted downflow. The elution profiles are provided in Figure 5.10. In both cases, the peak C/C_o values were reached after processing 5 BVs. The downflow elution profiles resulted in a shoulder at nominally 7 BVs, similar to that observed with Resin #9. The effluent valve was inadvertently left closed during Cycle 3 for 50 minutes during the third-to-last sample collection. No change in effluent Cs concentration was noted corresponding to the stopped-flow condition. Downflow elution appeared to have reached a steady-state of 0.1% C/C_o after processing nominally 30 BVs. The upflow elution profile was similar to the Column 2 upflow elution profiles and the CSTR behavior. The upflow elution appeared to asymptotically approach 0.1% C/C_o, but did not quite reach that eluate concentration after processing 42 BVs. The resultant Cs bleed into the next process load cycle was slightly higher with the upflow elution than that associated with the downflow elution.

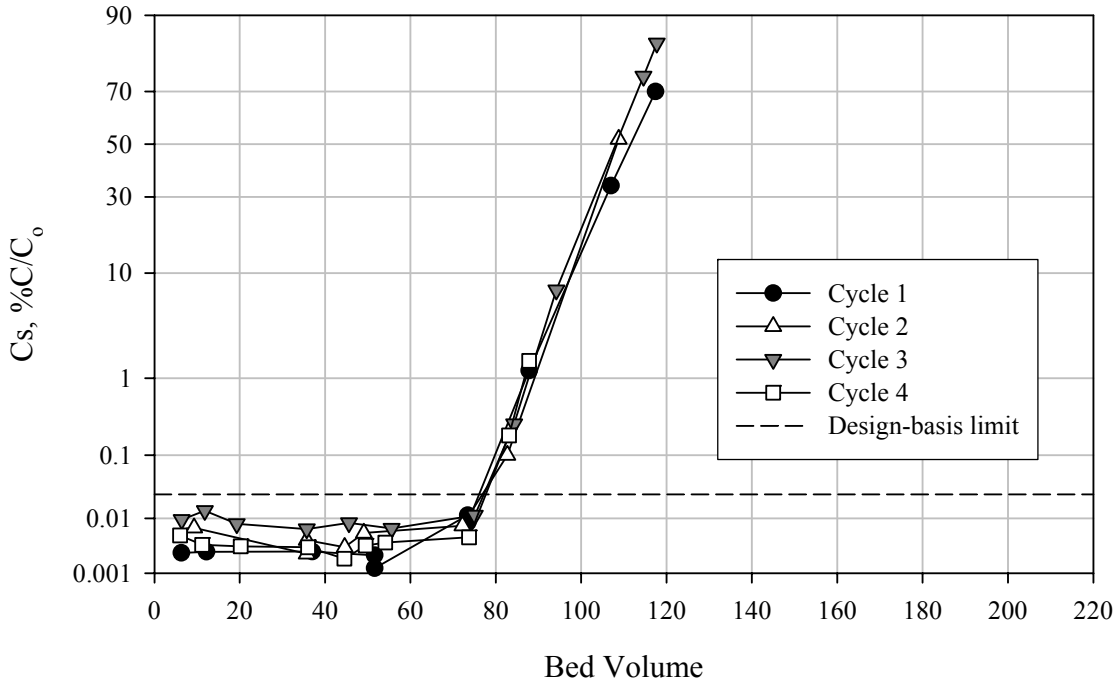

Figure 5.9. Column 5, Resin #11 Cs Load Profiles with AZ-102 Simulant

(a) The effluent from Resin #9 processing was bright yellow, the same color as the feed.

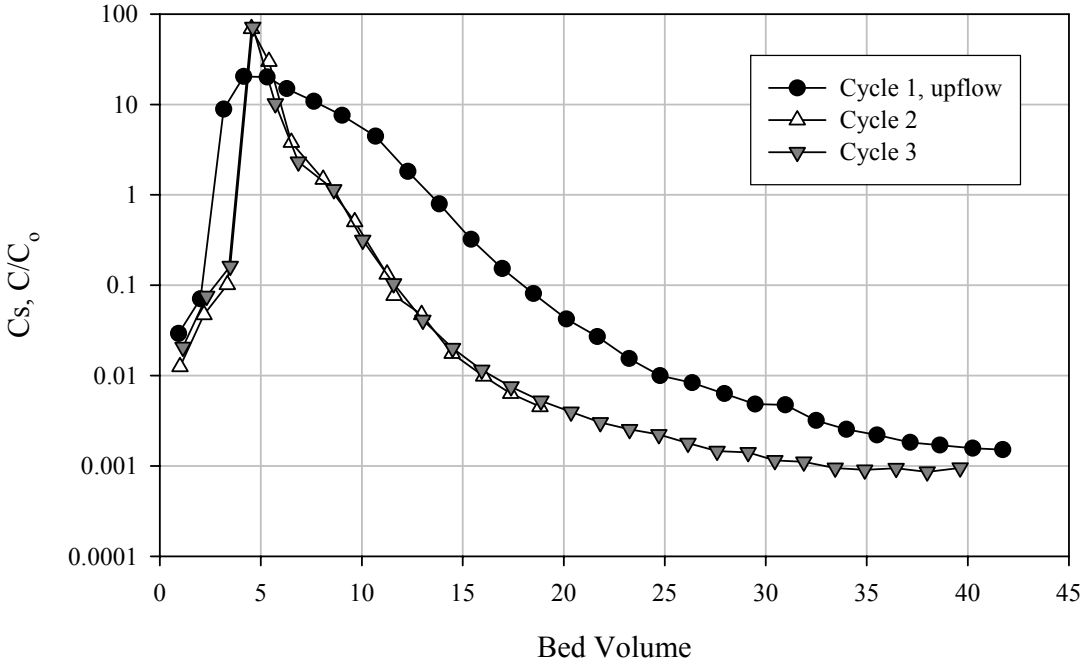

Figure 5.10. Column 5, Resin #11 Cs Elution Profiles

5.1.5 Column 6 Resin #1

Column 6 tested Resin #1 with AZ-102 simulant. The AZ-102 simulant effluent composite had a green hue, similar to that found with Column 5 effluent. The Cs load profiles are shown in Figure 5.11. Breakthrough was apparent at 20 BVs, and 50% C/C_o was reached at 50 BVs. The load profile was not linear on the probability scale, indicating non-ideal ion exchange load behavior. Because of the relatively low Cs capacity (low feed volume to reach 50% breakthrough relative to the other resins) and slow kinetics (non-linear breakthrough on the probability scale), testing with this resin was ceased after the second-cycle load.

Elution from this resin resulted in a typical elution profile (Figure 5.12). The peak C/C_o value was obtained at nominally 6 BVs, and tailing continued to a steady-state of nominally 2E-4 C/C_o. The rapid elution ($C/C_o = 0.001$ in just 15 BVs) was attributed to the relatively low amount of Cs loaded on the resin as a result of its low Cs capacity and slow kinetics (apparent from the loading curve). A small peak was found at nominally 36 BVs. Just before this point, the effluent valve was inadvertently left closed for 50 minutes. The slight rise in Cs concentration was attributed to continued elution from the resin into the interstitial fluid during the stopped-flow condition. The eluate sample colors were unique in that the second through fifth samples were progressively darker in color (brownish-green); the sixth sample was colorless (see Figure 5.13).

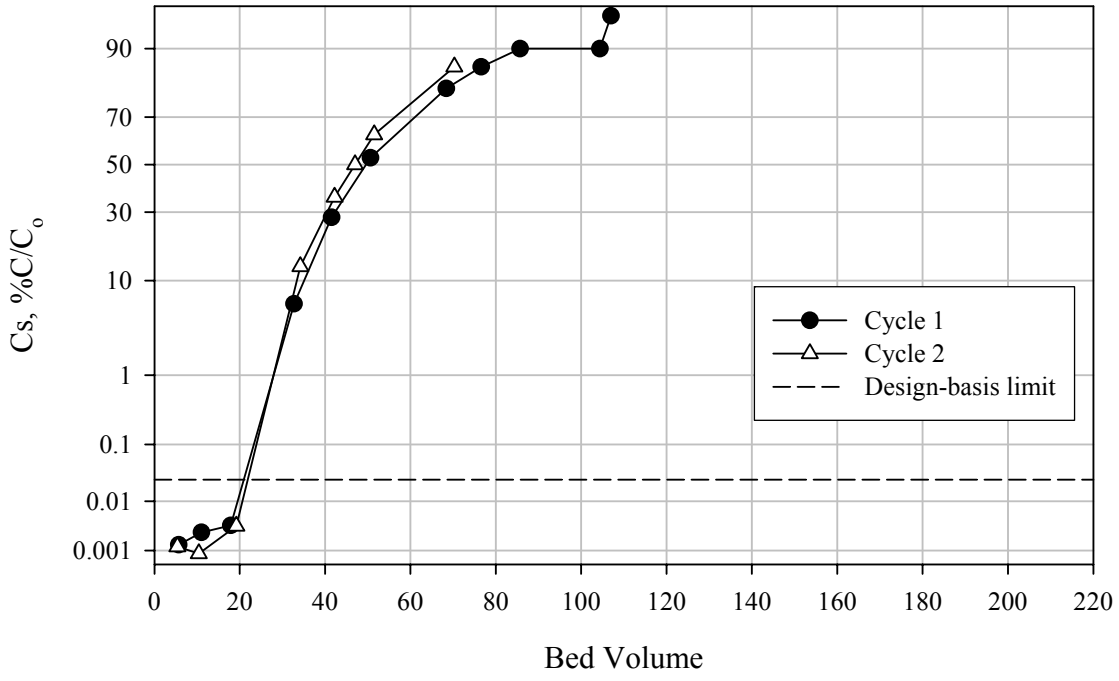

Figure 5.11. Column 6, Resin #1 Cs Load Profiles

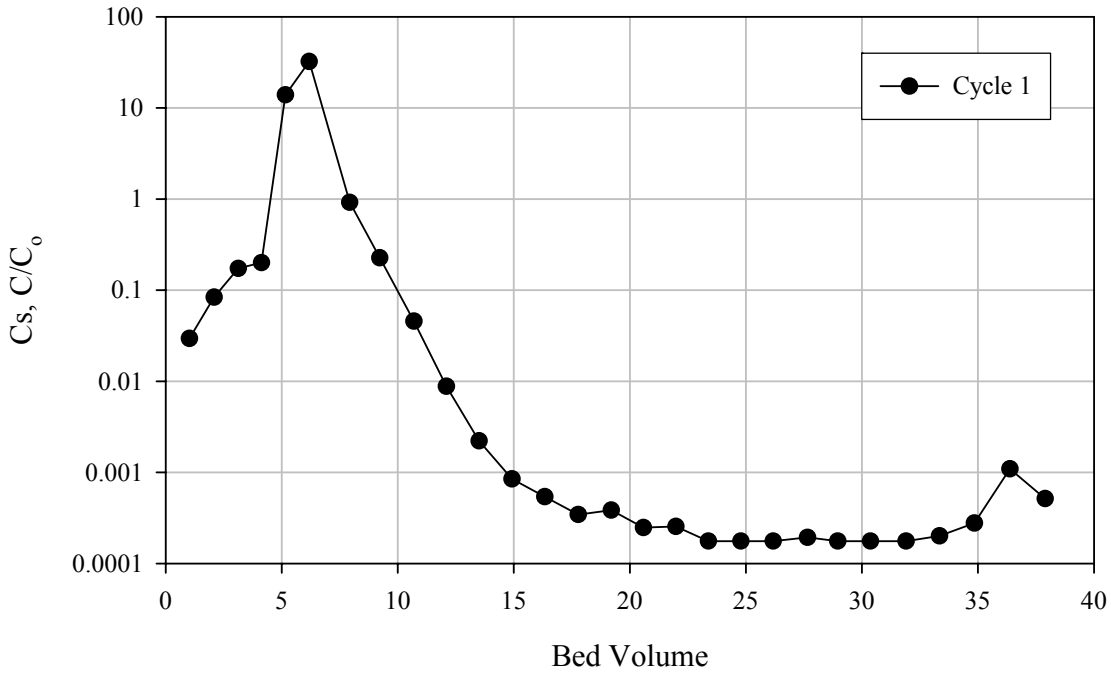

Figure 5.12. Column 6, Resin #1 Cs Elution Profile

Figure 5.13. Elution Samples from Column 6, Cycle 1, Showing Eluate Color Variations

5.1.6 Column 7 Resin #3

Column 7 tested Resin #3 with AZ-102 simulant. Because the resin changed colors on conversion from the H-form (reddish brown) to the Na-form (black) and vice versa, the conversion front through the column was observed. In all cases, the resin-form change appeared to occur horizontally across the bed; no channeling, angling, or protuberances of the resin conversion process were obvious.

The Cs load profiles are shown in Figure 5.14. The Cs breakthrough began at nominally 80 BVs, reaching 50% C/C_o at 143 BVs. The breakthrough profile appeared linear on the probability plot, thus manifesting ideal load behavior. The repeated cycle load profiles were virtually identical. Cs bleed into Cycles 2 and 3 was not detectable at <2E-3% C/C_o. Cs bleed into Cycle 4 was barely detectable (high uncertainties) at 2E-3% C/C_o.

The Cs elution from Resin #3 was well-reproduced for all three monitored cycles (Figure 5.15). The peak was found at 5 BVs, with tailing. A shoulder appeared at 6 BVs, corresponding to the reduction in flowrate from 2 BV/h to 1.4 BV/h. No experimental reason was attributed to the spike in C/C_o at 19 BVs for Cycle 1; it was most likely a slight cross-contamination into the sample. The elution tail Cs concentration leveled out at the instrument detection limit of 1.6 E-4 C/C_o.

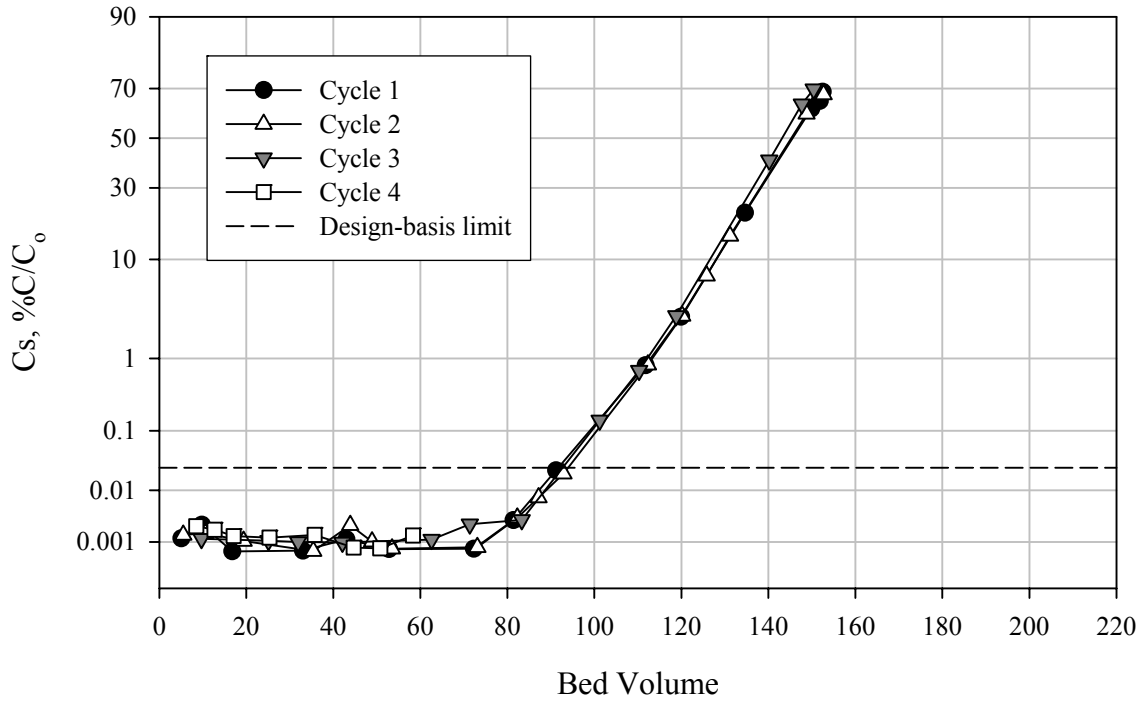

Figure 5.14. Column 7, Resin #3 Cs Load Profiles with AZ-102 Simulant

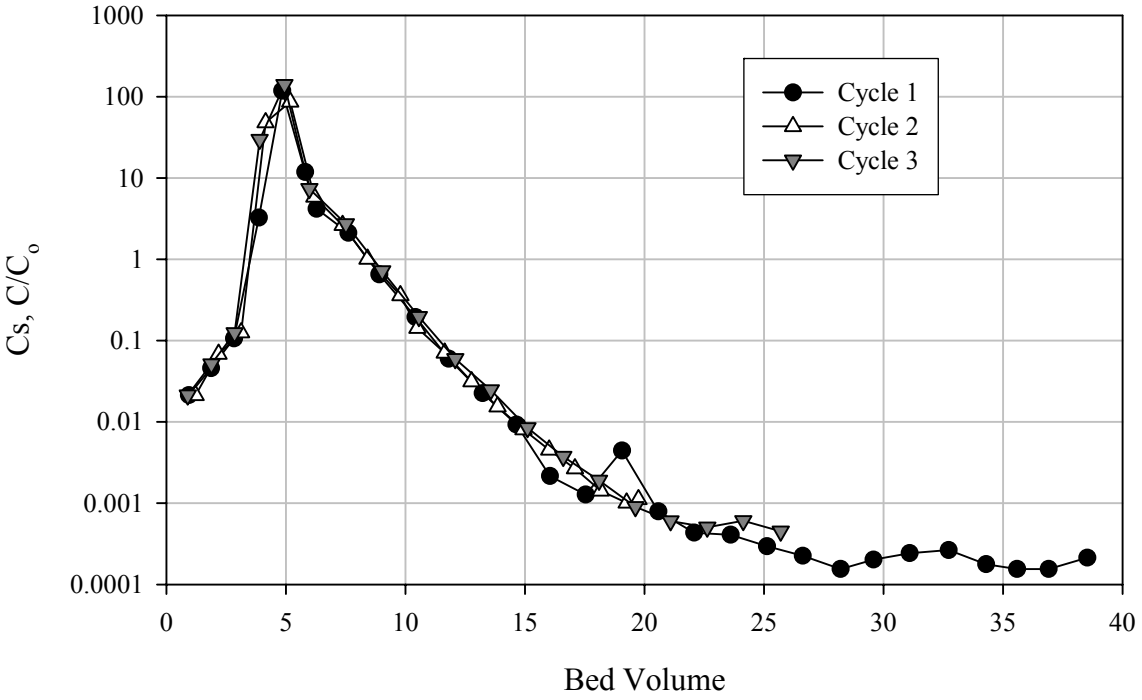

Figure 5.15. Column 7, Resin #3 Cs Elution Profiles

5.1.7 Column 8 Resin #6

Column 8 tested Resin #6 with AZ-102 simulant. The Cs load profiles are provided in Figure 5.16. The Cs breakthrough began at nominally 45 BVs, reaching 50% C/C_o at about 85 BVs. The breakthrough profile appeared linear on the probability plot, indicating ideal load behavior. The Cs bleed into subsequent load cycles (2 and 3) was <2E-3% C/C_o. The Cs bleed into the fourth load cycle was detected at long count times as high as 2.3 E-3% C/C_o. The fourth cycle did not show an increase in Cs concentration after processing 45 BVs because the feed Cs concentration was reduced to 0.032 μg/mL (significantly less than the 50 μg/mL for the first three load cycles).

The elution profiles (Figure 5.17) were similar to those obtained for Resin #3 (Column 7). The peak elution concentration was obtained at 5 BVs. The elution tailed quickly with a shoulder in the region where the flowrate was decreased. The eluate Cs concentration reduced to the instrument detection limit, 2E-4 C/C_o, after processing 21 BVs.

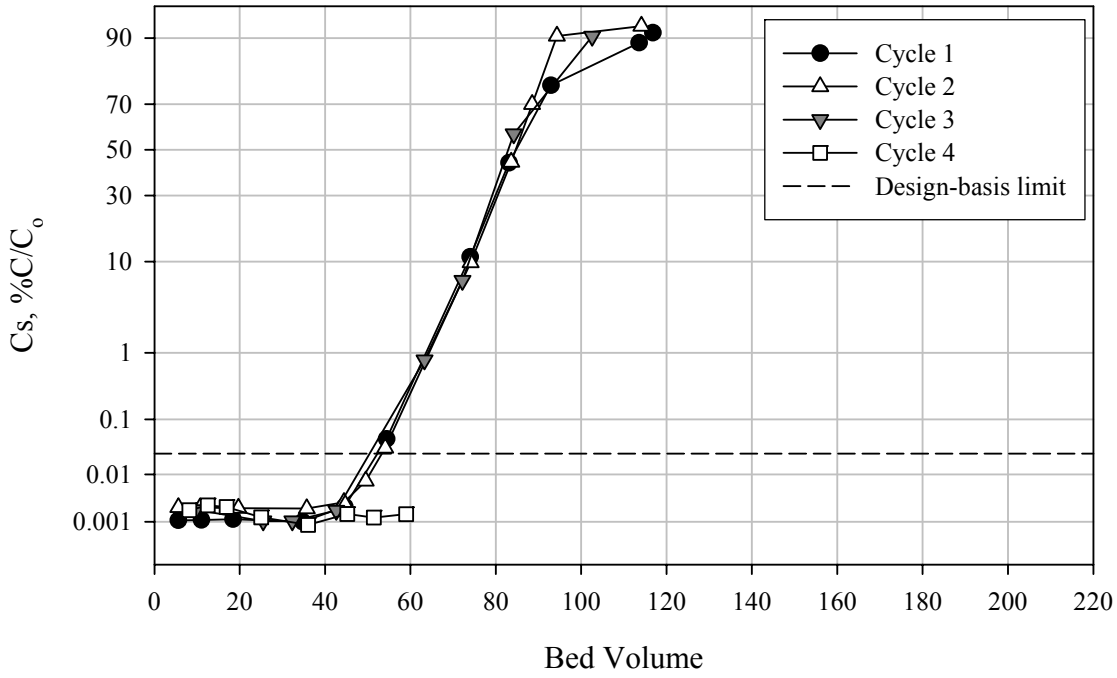

Figure 5.16. Column 8, Resin #6 Cs Load Profiles with AZ-102 Simulant

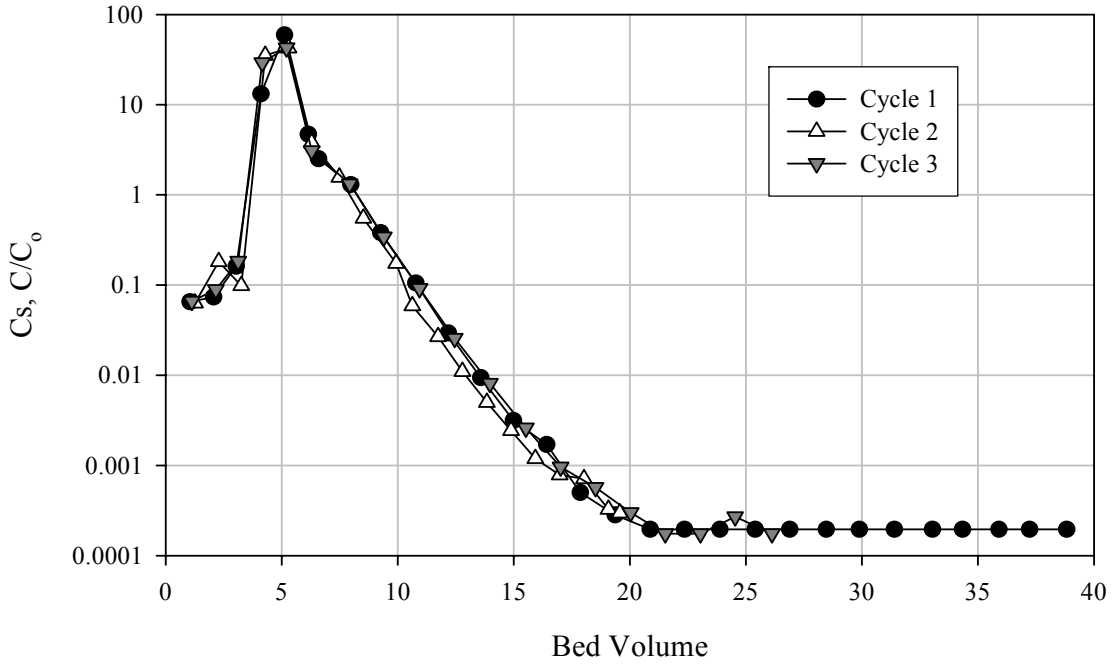

Figure 5.17. Column 8, Resin #6 Cs Elution Profiles

5.1.8 Column 9 Resin SL-644

Column 9 tested the wet-sieved 20- to 30-mesh fraction of the SL-644 resin provided by SRTC (production batch C-01-11-05-02-35-60)[(a)] with AZ-102 simulant. The Cs load profile is shown in Figure 5.18. The Cs breakthrough began at nominally 80 BVs, reaching 50% C/C_o at nearly 190 BVs. The load profile resulted in a linear shape on the probability scale, indicating ideal load behavior. The load profile was quite different from that generated with Column 1 (wider PSD) where the onset of breakthrough occurred much later at 150 BVs. The better performance of the Column 1 SL-644 may be attributable to the smaller particles providing more surface area for Cs exchange. Subsequent bleed into the second process cycle (AZ-102 simulant at 0.032 µg/mL Cs and 0.7 BV/h flowrate) was minimal at ≤3E-3% C/C_o.

The Cs elution profile is shown in Figure 5.19. The peak C/C_o value was obtained at nominally 4.2 BVs with rapid tailing to 4E-4 C/C_o. The Column 9 SL-644 (20- to 30-mesh) elution profile was not much different in shape or final C/C_o values as was found with Column 1 (SL-644 broader PSD). This indicated that the PSD may not be a significant factor for elution efficiency.

(a) Product specification delineated in e-mail from C Nash to S Fiskum July 16, 2003.

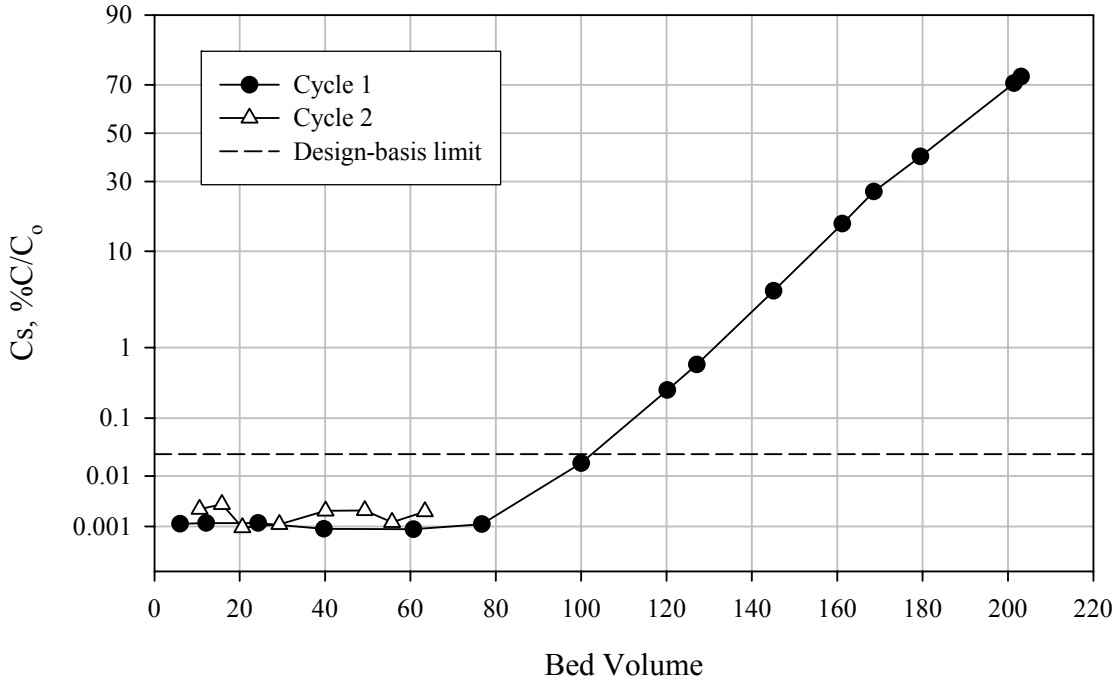

Figure 5.18. Column 9, SL-644 (20-30 mesh) Cs Load Profiles with AZ-102 Simulant

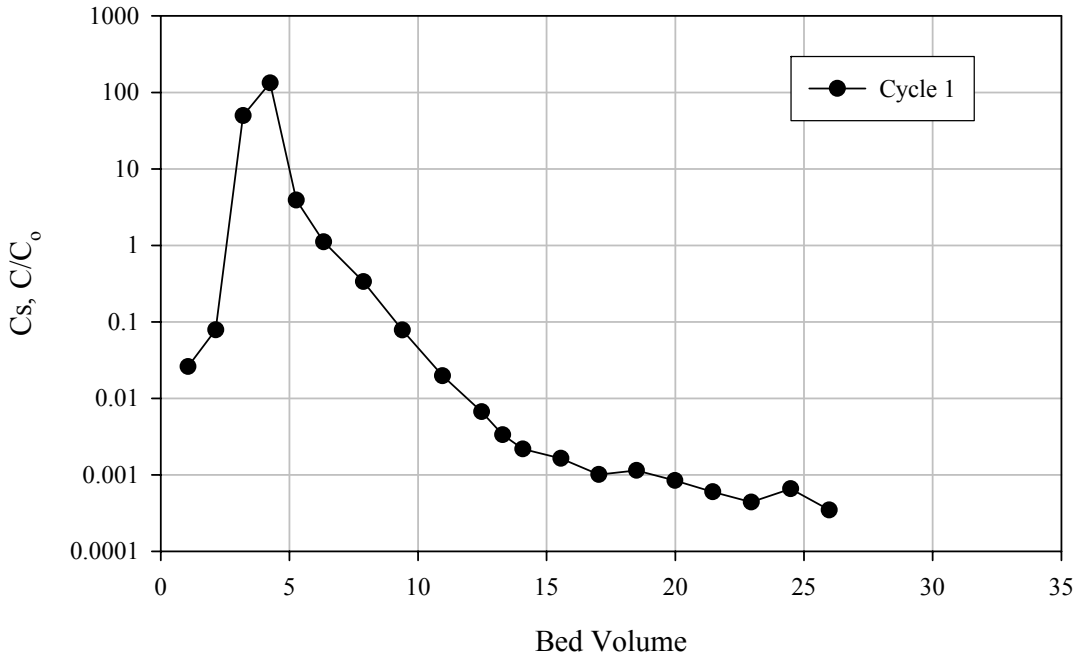

Figure 5.19. Column 9, SL-644 (20-30 mesh) Cs Elution Profile

5.1.9 Column-Testing Summary

The Cs load and breakthrough profiles are compared in Figure 5.20 for selected resins from the first process cycle using AZ-102 simulant. Three resin types are shown: ground gels (Resin #9 and Resin #11), spherical (Resin #3), and SL-644 (two different production batches). Resins #12 (SL-644) and #9 were spiked with less ^{134}Cs activity than were Resins #11, #3, and the 20 to 30 mesh SL-644. The plotted initial Cs concentrations from Resins #12 and #9 appeared to have higher activity than did the other plots; however, this was an artifact of the method detection limit. In all cases, the initial Cs concentrations were below the instrument detection limit (see Appendix C for tabulated data).

The SL-644 from production batch C-01-05028-02-35-60 (Resin #12) resulted in the most delayed onset for Cs breakthrough (180 BVs) as well as the largest volume processed before reaching 50% C/C_o at 235 BVs. From these plots, it was clear that the SL-644 from the 20- to 30-mesh wet-sieve fraction (production batch C-01-11-05-02-35-60) resulted in a much earlier Cs breakthrough at 80 BVs with 50% C/C_o reached at 190 BVs.

The ground-gel RF Resin #9 performance was intermediate between the two SL-644 ion exchange performances with breakthrough onset occurring at 120 BVs, and 50% breakthrough occurring at 190 BVs. The spherical resin (#3) Cs breakthrough occurred at nearly the same loading as for the SL-644 20 to 30 mesh and 50% breakthrough reached sooner after processing 145 BVs. The ground-gel Resin #11 clearly resulted in an earlier breakthrough at nominally 60 BVs and 50% breakthrough at 110 BVs.

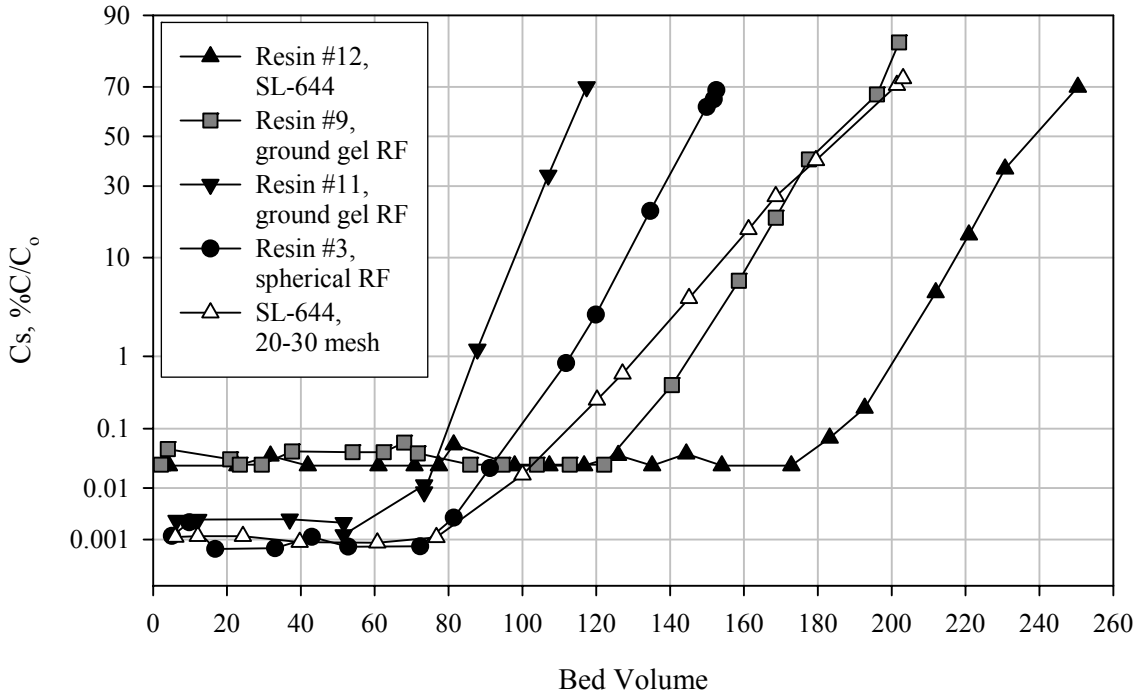

Figure 5.20. Load Profile Comparison

Estimates of the λ_{50} values in AZ-102 simulant, calculated from the product of the feed condition K_d and resin-bed densities, are provided in Table 5.1. The values are estimated because the correction for Na-form mass was neither determined nor applied. The experimentally determined 50% breakthrough for the spherical Resin #3 agreed well with the estimated λ_{50} value. The ground-gel resins, however, differed by 25% to 300%. It is not clear at this time why the ground-gel λ_{50} theoretical value differed significantly from the experimental values. The experimentally-measured 50% breakthroughs derived from the column testing are considered to be a more reliable indicator for plant performance.

Table 5.1 Estimated and Measured 50% Breakthrough in AZ-102 Simulant

Resin ID	Estimated K_d at Feed Condition, mL/g[(a)]	Estimated Bed Density, g/mL[(b)]	λ_{50}, BVs	Measured 50% Breakthrough, BVs
#1	500	0.30	150	50
#3	530	0.27	143	145
#6	420	0.27	113	83
#9	320	0.30	96	185
#11	330	0.22	73	110

(a) Determined from Figure 4.2 and Figure 4.3 interpolations.
(b) Taken from Table 3.6 Na-form dry bed densities.
The K_d and bed-density values are estimated because correction for Na-form mass was not determined and could not be applied.

The elution profiles from selected resins (resins as shown in Figure 5.20) are compared in Figure 5.21. In most cases, the first process cycles are shown. In the case of Resin #11, the third process cycle elution is shown because it was conducted downflow (the first cycle was conducted upflow). The Cs-elution profiles appeared generally similar with the peak Cs elution occurring at nearly 5 BVs and 1% C/C_o reached within 16 BVs. Differences are most apparent at the elution tail. Both the spherical RF and the 20 to 30 mesh SL-644 reached the lowest C/C_o values at nearly a factor of 5 lower than those of the ground-gel RF resins and SL-644 (Resin #12).

Except for Resins #1 (with low Cs loading) and #6, downflow elution of the RF resins required ≥25% more BVs to reach 1% C/C_o than with the 20- to 30-mesh SL-644. Resins #1 (with low Cs loading), #3, and #6 downflow elution volumes were equivalent to the 20- to 30-mesh SL-644 elution volume required to reach 0.1% C/C_o. The ground-gel RF resins generally required ≥35% more BVs to reach 0.1% C/C_o than that of the 20- to 30-mesh SL-644 resin. When taken with the residual Cs results (Sec. 5.2 below), these results indicate that the 20- to 30 mesh SL-644 resin elutes Cs to a lower final Cs concentration more efficiently than do the RF resins over the first 20 BVs. The spherical RF resins elute Cs to a lower final Cs concentration more efficiently than the ground-gel RF resins.

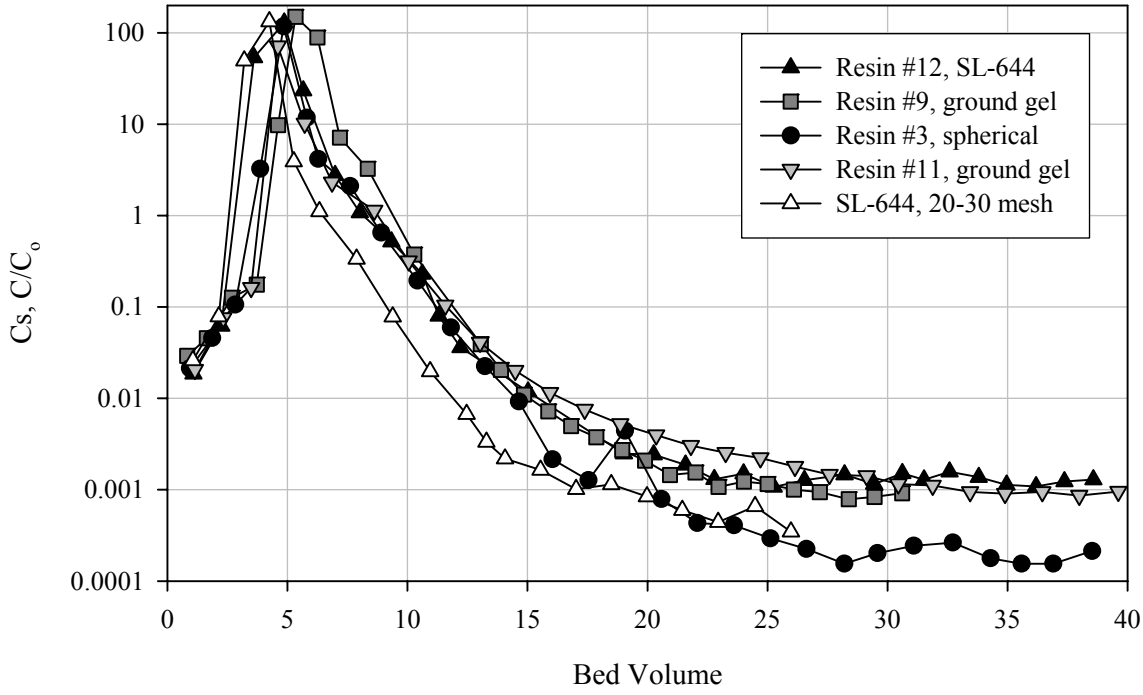

Figure 5.21. Elution Profile Comparison

5.2 Residual Cs on Resin Beds

Residual Cs was estimated from the approximate Cs tracer activity determined from direct counting of the resin beds in the columns. The sample geometry was imprecise because exact spatial loading of residual Cs in the resin was not known, and the column configuration was awkward in presentation to the side-looking detector. Because of these limitations, the relative accuracy of the calculated Cs activities was estimated to be within a factor of two.

For Columns 1 through 4, Cycles 1 and 2, the Cs tracer was ^{134}Cs (shaded cells); for Cycle 3 and 4, the Cs tracer was ^{137}Cs. Residual ^{134}Cs was found on Columns 2 through 4 after the third process cycle, albeit at much lower concentrations than the ^{137}Cs. This indicated that some Cs from process Cycle(s) 1 and/or 2 was still present on the resin after process Cycle 3 elution.

The ratios of Cs tracer to total Cs concentration were calculated from the measured Cs tracer concentrations and the measured feed Cs concentrations.[(a)] These ratios were applied to the Cs-tracer activity on the column to estimate the total micrograms of Cs remaining on the resin bed and associated apparatus. The estimates of total Cs remaining on the resin beds are provided in Table 5.2. The accuracy of the total Cs remaining on the resin beds was estimated to be within a factor of two, and the data are

(a) Nominally 0.013 μCi/mL ^{134}Cs and 0.075 μCi/mL ^{137}Cs were spiked into AZ-102 simulant (containing 50 μg/mL stable Cs). Nominally the same Cs tracer concentrations were spiked into the AP-101 simulant (which contained 6 μg/mL stable Cs).

labeled "for indication only." Also provided in Table 5.2 are the residual Cs concentrations relative to resin mass (dry H-form) loaded in the columns (again for indication only).

Table 5.2. Residual Cs on Column

Resin ID	Column Number	Cs Isotope	Cycle 1, total μg Cs	Cycle 1, μg Cs/ g resin	Cycle 2, total μg Cs	Cycle 2, μg Cs/ g resin	Cycle 3, total μg Cs	Cycle 3, μg Cs/ g resin
#12	Column 1	^{134}Cs	11	2.7	NA	NA	NA	NA
#9	Column 2	^{134}Cs	44	7.6	240	41	2.1	0.36
		^{137}Cs	NA	NA	NA	NA	18	3.1
#9	Column 3	^{134}Cs	34	6.0	43	7.5	3.3	0.58
		^{137}Cs	NA	NA	NA	NA	27	4.8
#9	Column 4	^{134}Cs	12	2.1	10	1.7	0.19	0.033
		^{137}Cs	NA	NA	NA	NA	7.1	1.2
#11	Column 5	^{137}Cs	64	14	60	13	46	11
#1	Column 6	^{137}Cs	5.4	0.85	NA	NA	NA	NA
#3	Column 7	^{137}Cs	1.7	0.34	2.7	0.55	2.6	0.52
#6	Column 8	^{137}Cs	1.4	0.28	2.1	0.41	2.1	0.41
SL-644 (20–30 mesh)	Column 9	^{137}Cs	16	3.5	NA	NA	NA	NA

NA = not applicable
Results are for indication only; overall accuracy was estimated to be within a factor of two.
Shaded cells highlight the use and measurement of ^{134}Cs tracer.
Mass of resin is based on dry H-form resin mass placed in the column.
Eluant BVs and flow direction varied between Columns and Cycles. Tables 2.4 through 2.12 provide the eluant BV data and flow direction. For Columns 1 through 8, Cycle 1 eluant BVs varied between 30 and 40; Cycle 2 eluant BVs varied between 14 and 20; Cycle 3 eluant BVs varied between 22 and 40. All cycles of Column 2 were eluted upflow. Only the first process cycle of Column 5 was eluted upflow.

The spherical resins #3 and #6 retained the least Cs after elution. Resin #11 retained the highest Cs after elution. Ground-gel Resin #9 retained Cs ranging from nominally 20 to 44 μg after processing the AZ-102 simulant. The high Cs value (240 μg) for Resin #9, Column 2 was associated with the short (15 BV) upflow elution where Cs was incompletely rinsed free from the mixing volume above the resin bed. The longer upflow elution volumes (34.6 BVs and 24.5 BVs associated with Cycle #1 and Cycle #3, respectively) resulted in improved Cs removal. Resin #9 retained only 7 to 12 μg Cs after processing the AP-101 simulant (Column 4). Two conditions may have contributed to the smaller residual Cs mass associated with the AP-101 simulant processing. Less total Cs was actually loaded onto the resin relative to Columns 2 and 3. The AP-101 simulant contained a high potassium concentration, which has been shown previously to be a competitor for ion exchange sites [3]. The competitive behavior may contribute in some manner to more effective Cs elution behavior.

The residual Cs (total) remaining on each ion exchange column, normalized to resin mass, is summarized in Figure 5.22. The relative trends between resins and process cycle are readily apparent. The spherical RF resins resulted in clearly less retained Cs than the ground-gel resins (RF and SL-644). The spherical Resin #3 retained approximately a factor of seven less Cs than the SL-644 (20- to

30-mesh)[a] and approximately a factor of ten less Cs than the ground-gel RF Resin #9 after the third process cycle.

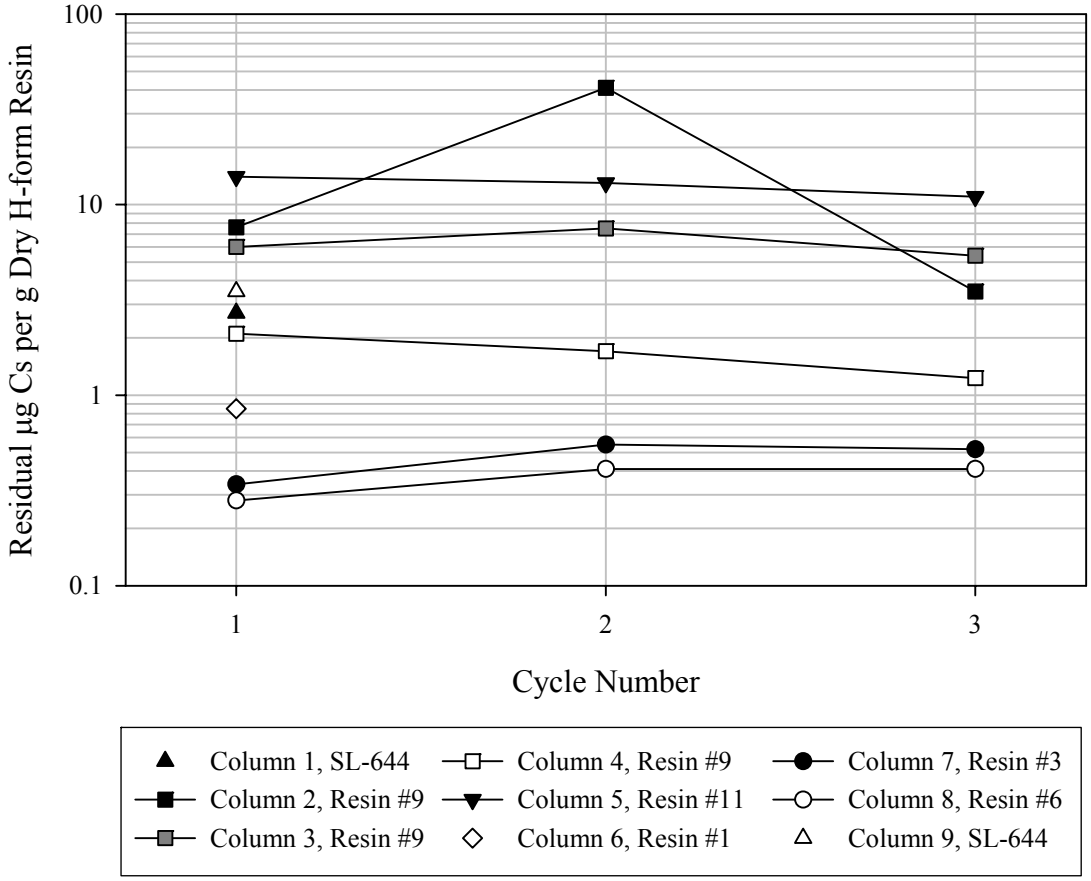

Figure 5.22. Residual Cs (Total) Remaining on Eluted Resin Beds per Gram Dry Resin

The WTP design-basis limit for ^{137}Cs activity in spent resin is 60 µCi/g (acid-form resin).[b] This value, based on processing with SL-644 with a bulk density of 0.66 g/mL,[c] corresponds to a ^{137}Cs concentration per unit volume basis of 40 µCi/mL. This volume-basis activity limit is the primary driver for WTP spent-resin handling. In conjunction with the ^{137}Cs isotopic fraction, this volume-basis limit can be used to determine allowable total Cs concentrations on the spent resins (mass basis). The Envelope B tank wastes, represented by AZ-102 simulant, contain nominally 31% ^{137}Cs [14, 15]. The total residual Cs concentration limits for the RF resins after processing Envelope B tank wastes can be calculated according to Equation 5.1.

(a) Comparison of Cycle 1 of Column 9 with Cycle 3 of Column 7, each with nominally 26 BVs eluate.
(b) WTP meeting minutes CCN 055152, 4/24/03.
(c) Spent resin bulk density values were not available. As-received bulk densities were used as a rough estimate of the spent resin bulk density.

$$C = \frac{L_m}{\delta * A * SpA} \tag{5.1}$$

where C = total Cs concentration limit (μg/g)
L_m = ^{137}Cs concentration limit, volume basis (40 μCi/mL)
δ = bulk dry-resin density (g/mL, from Table 3.3)[(a)]
A = ^{137}Cs isotopic fraction (0.31)
SpA = specific activity of ^{137}Cs (87 μCi/μg).

After processing Envelope B tank waste, the mass-basis limit for total Cs on spent SL-644 is calculated to be 2.2 μg/g. The corresponding limit for spherical RF Resin #3 is 3.4 μg/g and for ground-gel RF Resin #9, it is 2.0 μg/g. The estimated total residual Cs remaining on the SL-644 and ground-gel RF (3.5 and 5.4 μg/g, respectively) exceeded the calculated allowable Cs concentrations. The residual Cs on the spherical RF Resin #3 (0.52 μg/g) was less than the calculated allowable Cs concentration.

5.3 Eluate Composition

One eluate from processing Column 7 Cycle 3 (Resin #3) was selected for further analysis of metals, anions, and organic carbon. The eluate composite analytical results are summarized in Table 5.3. Nominally 95% of the Cs processed through Column 7 Cycle 3 was exchanged onto the resin bed. The remaining 5% of the Cs broke through the column and was collected in the effluent. Within experimental uncertainties, all of the Cs that was loaded on the resin bed was eluted and collected in the eluate.

Other cation and anion constituents in the eluate were dominated by Na and K. The mmole sum of the K, Na, and Cs was 29.8, corresponding to an estimated total capacity of 6.0 mmoles per gram of dry H-form resin. The corresponding capacity for SL-644 was calculated to be 3.5 mmoles per gram of dry H-form resin, based on the mmoles of recovered metals from AZ-102 actual tank waste processing [15].

The Cr concentration in the eluate was small; only 0.018 mmoles were eluted. Based on the 5-g resin bed and assuming full elution of Cr, the Cr capacity corresponded to 3.6E-3 mmoles/g. In contrast, the SL-644 eluate resulted in higher Cr concentrations, corresponding to 0.015 to 0.11 mmoles Cr per gram of H-form resin mass (based on a 2-g H-form resin-bed mass) [14, 15, 18, 19]. The presence of Ba, Ni, and Pb in the RF resin eluate was attributed to reagent impurities most likely in the feed.

(a) Spent resin bulk density values were not available. As-received bulk densities were used as a rough estimate of the spent resin bulk density.

Table 5.3. Column 7 Cycle 3 Composite Eluate Composition

Analyte	MRQ	Sample, µg/mL	Average mmoles[(a)]	% of Feed
ICP-AES				
Al	75	2.73	4.82E-2	0.034
Ba	78	0.025	8.7E-5	NA
Ca	150	[1.3] J[(b)]	[1.6E-2] J[(b)]	[0.30] J[(b)]
Cd	7.5	<0.038	ND	NA
Cr	15	1.93	1.77E-2	0.023
Cs[(c)]	0.5	272	9.75E-1	95.5[(c)]
Fe	150	0.459	3.91E-3	[2.1]
K	75	243	2.96E+0	0.73
Mo	90	[0.023]	[1.1E-4]	[0.0033]
Na	75	1250	2.59E+1	0.18
Ni	30	[0.042]	[3.4E-4]	NA
Pb	300	[0.032]	[7.4E-5]	NA
Zn	16.5	<0.05	ND	NA
IC				
Chloride	30	[7.4]	[9.9E-2]	[3.2]
Nitrate	2300	30,500	Eluant matrix	Eluant matrix
Sulfate	2300	120	5.95E-1	0.068
Phosphate	2500	<2.5	ND	<0.05
TOC				
TOC (as C) HP	1500	<2	ND	ND
TOC (as C) F	1500	<46	ND	ND

(a) Based on a total eluate volume of 476 mL.
(b) J = estimated value; the Ca result failed the serial dilution test.
(c) Calculated from tracer recovery. The remaining 5% of the Cs was in the composite effluent.
Notes:
The overall uncertainty for these analytes of interest was ±15%.
Bracketed results indicate that the analyte concentration uncertainty exceeded ±15%. Less-than (<) results indicate that the analyte concentrations were below the instrument detection limit (IDL); the dilution-corrected IDLs are given.
Samples were submitted under ASR 6835, Radiochemical Processing Laboratory (RPL) Sample ID 03-1471.
HP = hot-persulfate oxidation method
F = furnace oxidation method
MRQ = minimum reportable quantity
NA = not applicable, element was not part of feed composition.
ND = not detected
TOC = total organic carbon.

5.4 Resin Volume Changes

The SL-644 and RF resins changed volume as a function of feed composition. The volume change was calculated relative to the initial Na-form resin volume as loaded into the ion exchange column according to Equation 5.1:

$$R_v = \frac{V_s}{V_i} \tag{5.1}$$

where R_v is the relative bed volume, V_s is the bed volume in a given matrix, and V_i is the resin-bed volume as initially loaded in the column (Na-form).

The error associated with the volume measurement was driven by the uncertainty in the resin-bed height measurement of ±0.2 cm. At the smallest resin BV (H-form), this corresponded to an uncertainty of nominally 5%.

The relative BV changes and associated matrix are provided in Table 5.4. Each process step is numbered. The BV change is shown graphically in Figure 5.23 through Figure 5.25 as a function of the process step number. The resin-bed changes for Column 1 SL-644 are incorporated in all figures as a point of reference.

The SL-644 in Column 1 (25-gal production batch) and Resin #11 had the greatest shrink swell behavior at 57% volume change from H-form to Na-form. The SL-644 in Column 9 (250-gal production batch) changed the next most dramatically at a 48% volume change. Resins #9, #1, #3, and #6 each changed nominally 32% on expansion from H-form to Na-form. The changes in the Na-form on conversion from 1 M NaOH, to feed, to feed displacement, and then to DI water rinse were generally less dramatic for Resin #9 than were observed for Resins #3 and #6.

Table 5.4. Relative Bed Volumes as a Function of Feed Matrix

Feed matrix	Step Number	Column 1 SL-644[a]	Column 9 SL-644[b]	Column 2 Resin #9	Column 3 Resin #9	Column 4 Resin #9	Column 5 Resin #11	Column 6 Resin #1	Column 7 Resin #3	Column 8 Resin #6
Initial volume, mL	NA	16.3	20.4	17.3	17.9	17.3	18.5	20.4	18.5	19.2
1M NaOH soak/DI rinse	1	1.000	1.000	1.000	1.000	1.000	1.000	1.000	1.000	1.000
0.5M HNO_3	2	0.808	0.769	0.855	0.789	0.800	0.763	0.769	0.864	0.852
DI water	3	0.827	0.738	0.855	0.781	0.800	0.746	0.754	0.831	0.820
0.25M/1M NaOH[c]	4	1.173	1.092	0.982	0.895	0.945	1.119	1.046	1.085	1.082
feed, AZ102 simulant	5	1.077	0.954	1.091	1.035	1.073[d]	1.017	1.015	0.966	0.951
feed displacement	6	1.077	1.031	1.055	nr	1.091	1.085	1.031	1.034	1.066
DI water	7	1.077	1.031	1.055	nr	1.091	1.136	1.031	1.017	1.066
0.5M HNO_3	8	0.788	0.754	0.800	0.772	0.800	0.746	0.800	0.814	0.820
DI water	9	0.750	0.738	Nr	0.789	0.891	0.712	0.785	0.814	0.820
0.25M/1M NaOH[c]	10	1.192	1.077	1.109	1.053	1.109	1.119	1.046	1.068	1.066
feed, AZ102 simulant	11	1.019	0.985	1.036	1.018	1.055[d]	1.017	1.031	0.966	0.967
feed displacement	12	1.192	1.077	1.073	1.035	1.091	1.085	1.046	1.051	1.082
DI water	13	1.173	1.062	Nr	1.035	1.073	1.085	1.031	1.034	1.033
0.5M HNO_3	14	0.846	0.754	0.818	0.789	0.818	0.712	0.800	0.814	0.836
DI water	15	0.827	0.754	0.818	0.789	0.818	0.712	0.800	0.814	0.836
0.25M/1M NaOH[c]	16	NA	NA	1.091	1.088	1.127	1.119	NA	1.068	1.066
feed, AZ102 simulant	17	NA	NA	1.036	1.018	1.055[d]	1.017	NA	0.983	0.967
feed displacement	18	NA	NA	1.036	1.035	1.073	1.102	NA	1.051	1.082
DI water	19	NA	NA	1.055	1.035	1.055	1.085	NA	1.000	1.066
0.5M HNO_3	20	NA	NA	0.800	0.772	0.818	0.712	NA	0.814	0.836
DI water	21	NA	NA	0.800	0.772	0.818	0.712	NA	0.814	0.836
0.25M/1M NaOH[c]	22	NA	NA	1.109	1.053	1.091	1.136	NA	1.085	1.049
feed, AZ102 simulant	23	NA	NA	1.073	1.018	1.055[d]	1.034	NA	1.000	0.984
feed displacement	24	NA	NA	1.073	1.018	1.055	1.102	NA	1.051	1.098
DI water	25	NA	NA	1.091	1.018	1.036	1.085	NA	1.119	1.066
0.5M HNO_3	26	NA	NA	nr	0.789	0.818	0.712	NA	0.847	0.836
DI water	27	NA	NA	nr	nr	nr	0.695	NA	0.847	0.852

(a) SL-644, Resin #12, from production batch C-01-05-28-02-35-60.
(b) SL-644 from production batch C-01-11-05-02-35-60, 20- to 30-mesh wet-sieve fraction.
(c) The 0.25 M NaOH regeneration solution was used in the first cycle for Columns 1 through 4 and for SL-644. The 1 M NaOH was used for all subsequent RF testing.
(d) Column 4 tested AP-101 simulant.
NA = not applicable; nr = not recorded

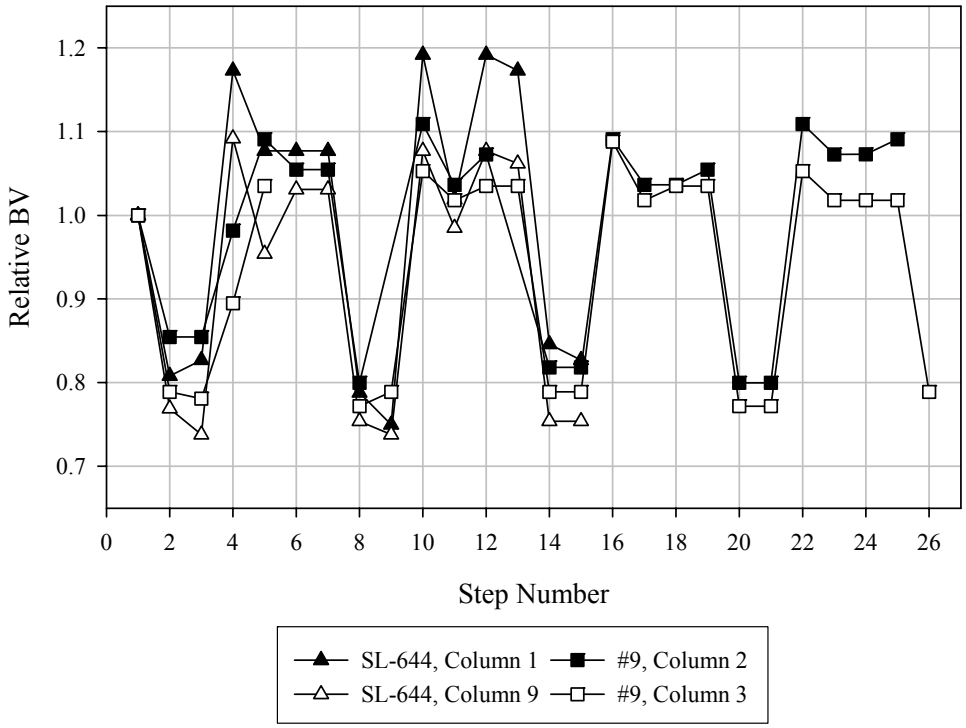

Figure 5.23. Relative Resin BV Changes, Resins #12 (SL-644), #9

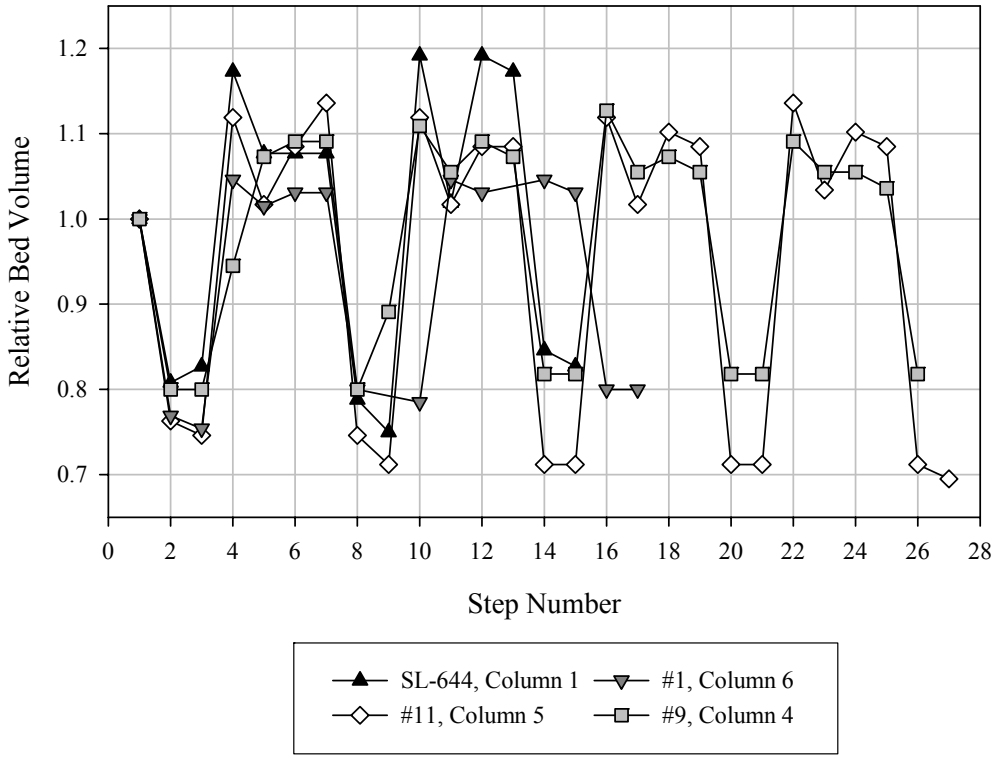

Figure 5.24. Relative Resin BV Changes, Resins #12 (SL-644), #11, #1, and #9

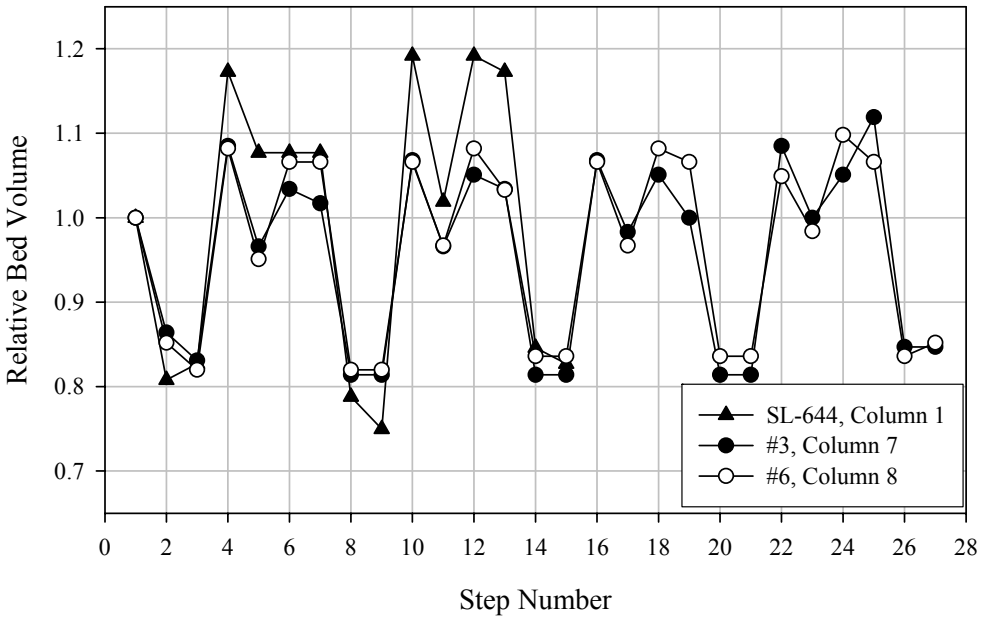

Figure 5.25. Relative Resin BV Changes, Resins#12 (SL-644), #3, and #6

6.0 Hydraulic Properties Test Results

This section discusses the results of permeability and compressibility testing of the two RF resins forwarded for testing, #3 and #9, and SL-644, Resin #12, as a relative measure to the RF resins.

6.1 Permeability Test

The results of the permeability tests during the first and last cycles with Resins #3, #9, and #12 are shown in Figure 6.1. For the three resins and the two height-to-diameter ratios, the resin permeability during NaOH regeneration was lower than observed during AP-101 simulant processing. This result would indicate that as the resins expanded, the resin bed had reduced voids between particles. Based on the Ergun equation (Equation 6.1), as void space is reduced, pressure drop increases:

$$\frac{\Delta P}{L} = \frac{150\mu(1-\varepsilon)^2 u_0}{\varepsilon^3 d_p^2} + \frac{1.75\rho(1-\varepsilon)u_0^2}{\varepsilon^3 d_p} \tag{6.1}$$

where ΔP = pressure drop (Pa)
L = bed height (m)
μ = fluid viscosity (kg/m/s)
ε = void fraction
u_0 = fluid superficial velocity (m/s)
d_p = particle diameter (m)
ρ = fluid density (kg/m^3).

System A with an L/D ratio of approximately 1.6 had higher permeability values than System B with an L/D ratio of approximately 2.7. Because permeability should account for differences in resin heights, the differences were either associated with higher compressive forces generated in the tall bed or with channeling in the shorter bed.

For laminar flow in a packed bed of incompressible material, the permeability should be constant as a function of flowrate. In most cases, the permeability decreased with increasing flowrates. This is what would be expected of a compressible resin where void fraction decreases with higher pressure drop.

The permeability appeared also to be a function of resin type. The lowest permeability measurements were found with the granular resin form. The highest permeability material was found with the spherical Resin #3. Based on the wide range of particle sizes seen in Resin #12 and Resin #9 (described in Section 6.3), it was not surprising that these two resins would have lower bed permeablities than the nearly mono-disperse Resin #3.

Figure 6.2 illustrates the change in permeability as a function of cycle number for the column with an L/D ratio of 2.7. All resins showed a general decreasing trend in permeability from Cycle 1 to Cycle 4. Resin #9 showed the largest decrease in permeability through the four cycles, but Resin #12 remained as the lowest permeability resin. However, the results of Resin #12 may not be directly comparable to the

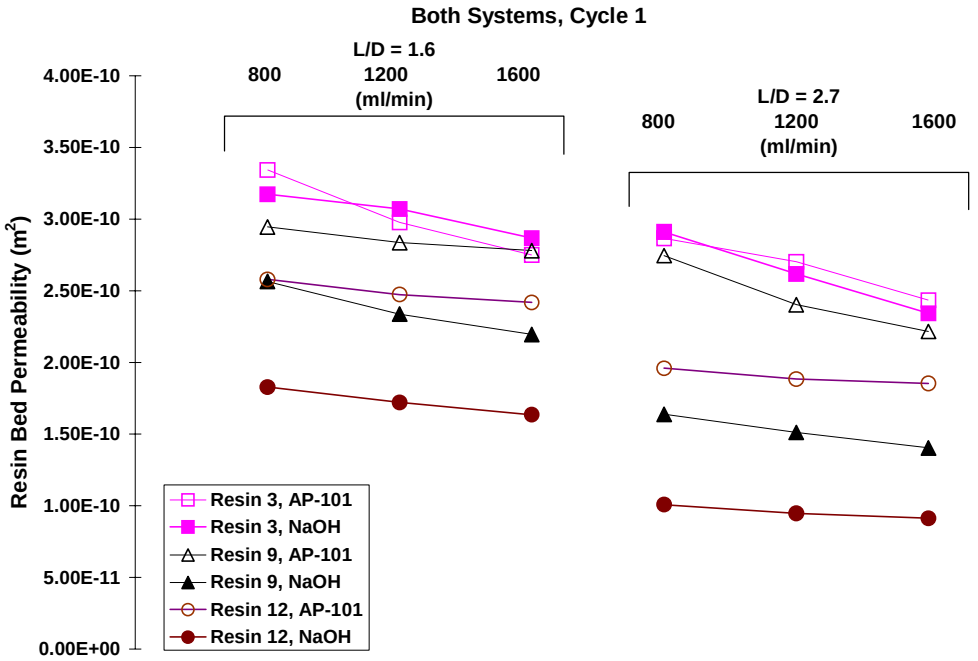

(a)

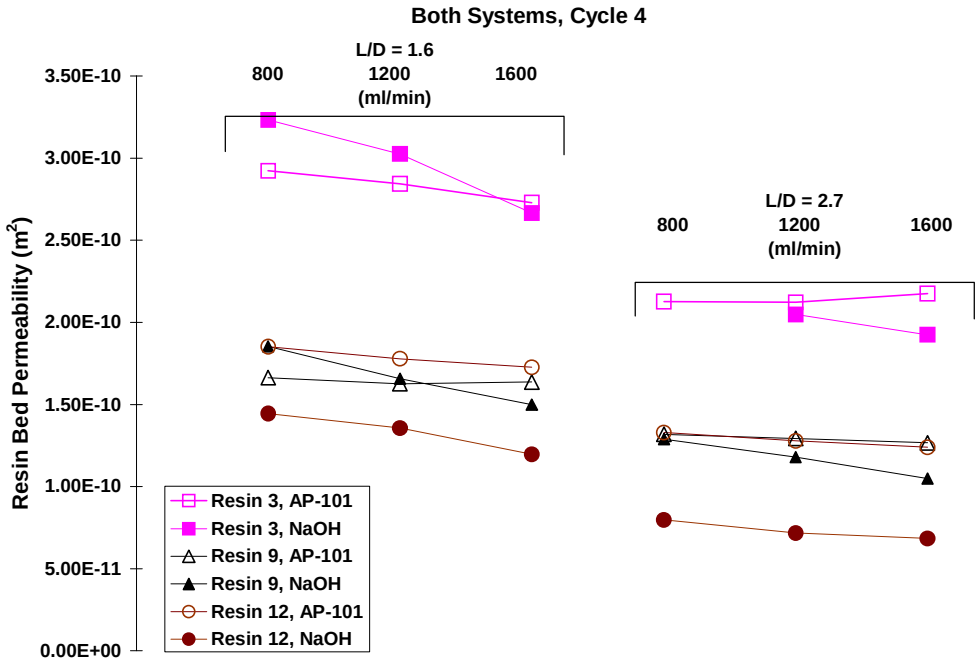

(b)

Figure 6.1. Permeability Results from (a) Cycle 1 and (b) Cycle 4 Provided as a Function of Resin Type, Cycle Step, and Flowrate. Note: Cycle 4, Resin 3, NaOH, 800 mL/min data point was not taken.

other resins. Resin #12 was removed from the column after the second cycle to repair the load cells. This potentially allowed changes in the resin-bed characteristics, including resin packing, residual stress, and fines distribution. The increase in permeability between Cycle 2 and Cycle 3 for Resin #12 suggested that the resin removal did change these bed characteristics.

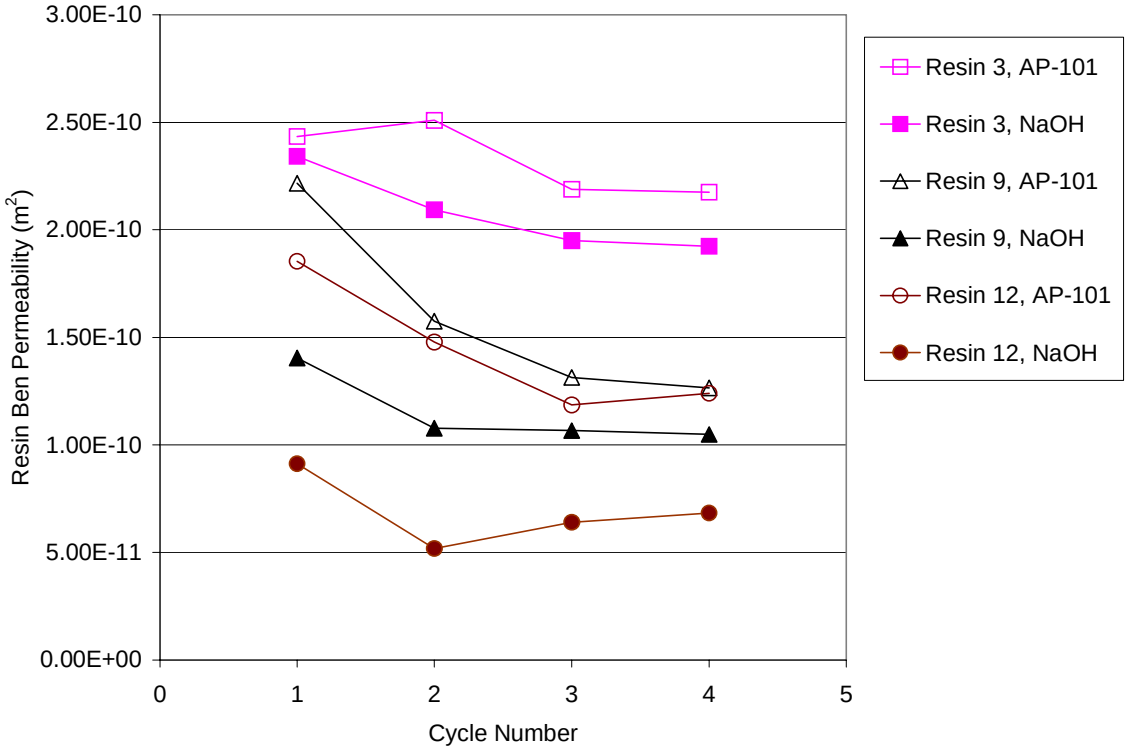

Figure 6.2. The Change in Resin-Bed Permeability over the Course of the Four Cycles for the Column with L/D = 2.7, 1600 mL/min Flowrate. The column with L/D 1.6 shows similar trends but more data scatter.

6.2 Load-Cell Results

The maximum liquid differential, radial, and axial pressures measured for each of the resins for Column B (L/D = 2.7) are shown in Figure 6.3 through Figure 6.5. In all cases, the load-cell pressures during regeneration were significantly higher than the liquid differential pressure. The liquid differential pressure was generally higher during AP-101 simulant loading than during the NaOH regeneration for all resins tested. Conversely, the load-cell pressures (both axial and radial) were higher during the regeneration than during AP-101 simulant column loading. The load-cell data also indicated that axial pressures were higher than radial pressures during AP-101 simulant loading whereas radial pressures were generally higher than axial pressures during regeneration.

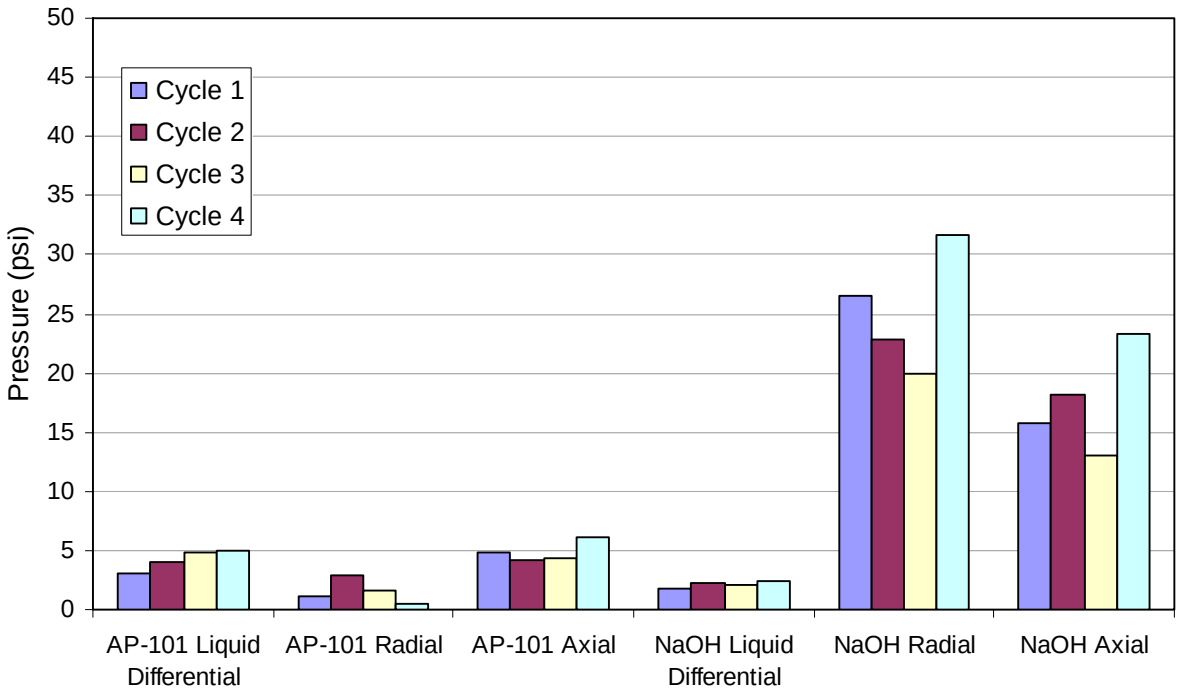

Figure 6.3. Comparison of Maximum Liquid Differential, Radial, and Axial Pressure for Resin #9 in Column B

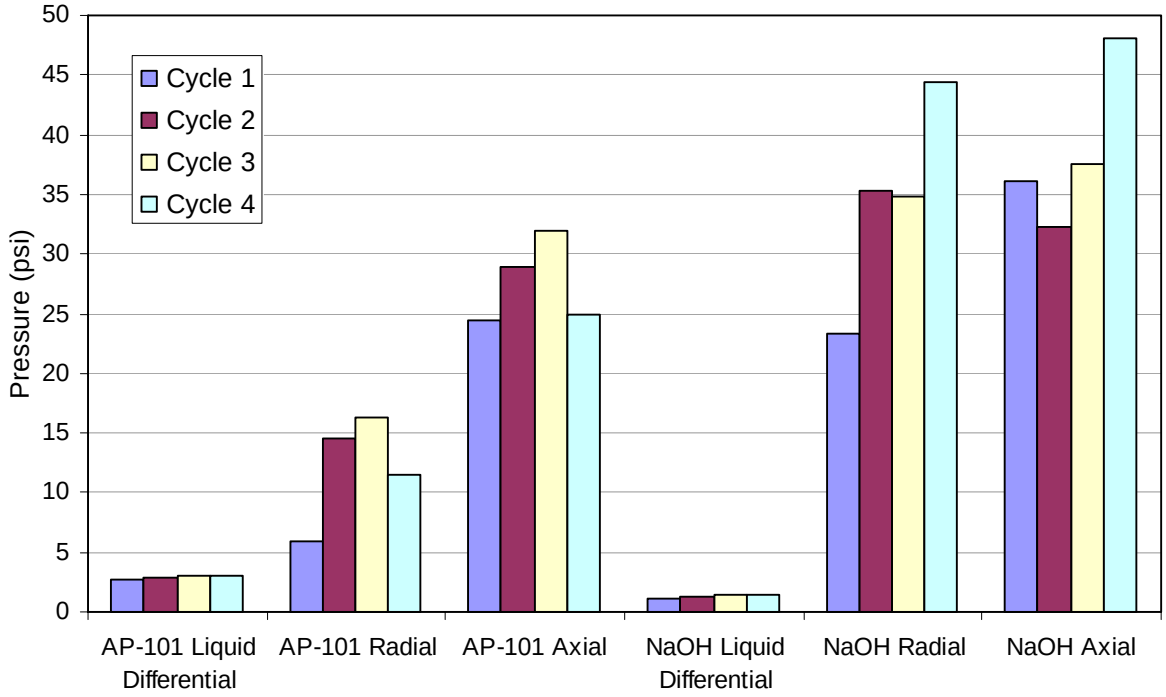

Figure 6.4. Comparison of Maximum Liquid Differential, Radial, and Axial Pressure for Resin #3 in Column B

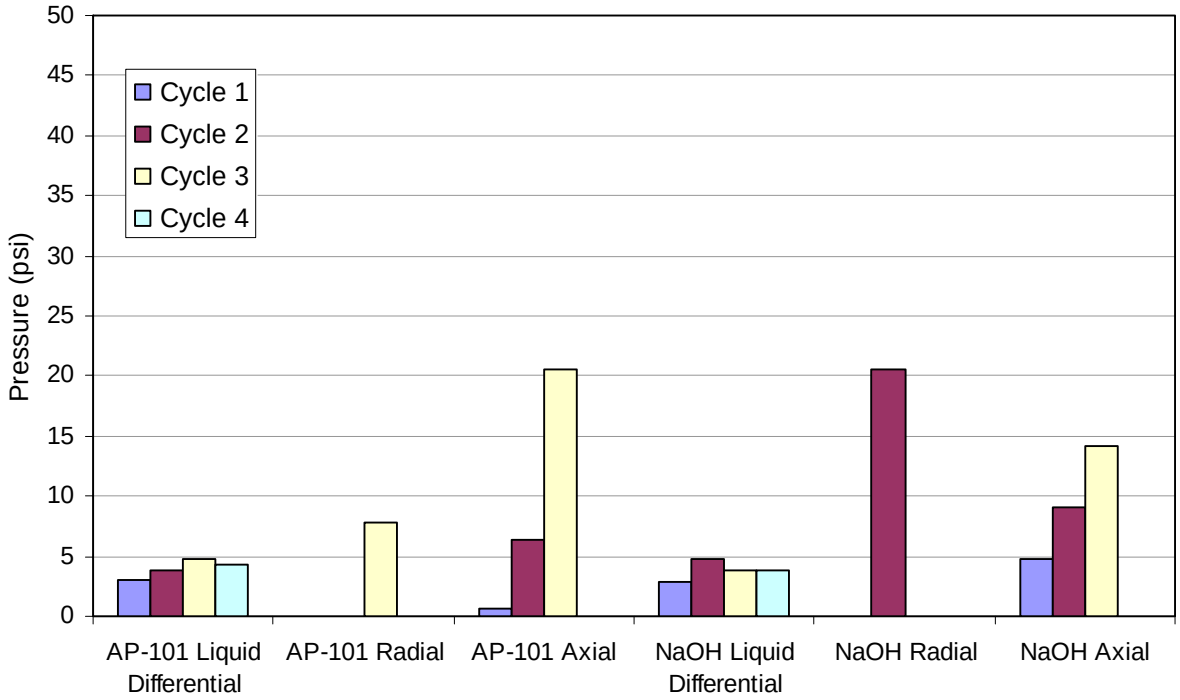

Figure 6.5. Comparison of Maximum Liquid Differential, Radial, and Axial Pressure for Resin #12 in Column B

The higher liquid-differential pressure during AP-101 simulant loading was simply the result of a higher viscosity solution. However, the higher load-cell pressures during regeneration indicated that the resins were expanding faster than the resin height was increasing, resulting in outward forces on the bottom and side of the column. The higher radial versus axial forces suggested that a larger fraction of the axial forces were relieved by increased bed height.

Unlike Resin #9 that produced bottom and side load-cell pressures during AP-101 simulant loading similar to the liquid pressure drop, Resin #3 load cells indicated large increases in axial and radial pressure. This result is believed to be due to the expansion of this resin during the loading cycle. Unlike the other resins, whose level remained relatively constant during loading, adding AP-101 simulant to Resin #3 caused a sudden decrease in column level followed by a slow rise similar to that seen during regeneration. However, unlike the expansion during the regeneration step that caused higher radial pressures, the AP-101 simulant expansion for Resin #3 resulted primarily in higher axial pressures. The reason for this difference was not clear.

Typical load-cell plots for Resin #9 and Resin #3 for one entire cycle are shown in Figure 6.6 and Figure 6.7, respectively. Load-cell plots for all resins and cycles are provided in Appendix D. The system with the greater L/D (System B) tended to take longer to equilibrate than the system with lower L/D (System A). Therefore, the permeability testing on System B with NaOH and AP-101 simulant was generally longer in an effort to reach a constant pressure value. The horizontal lines are guides to denote the duration of each of these processing steps.

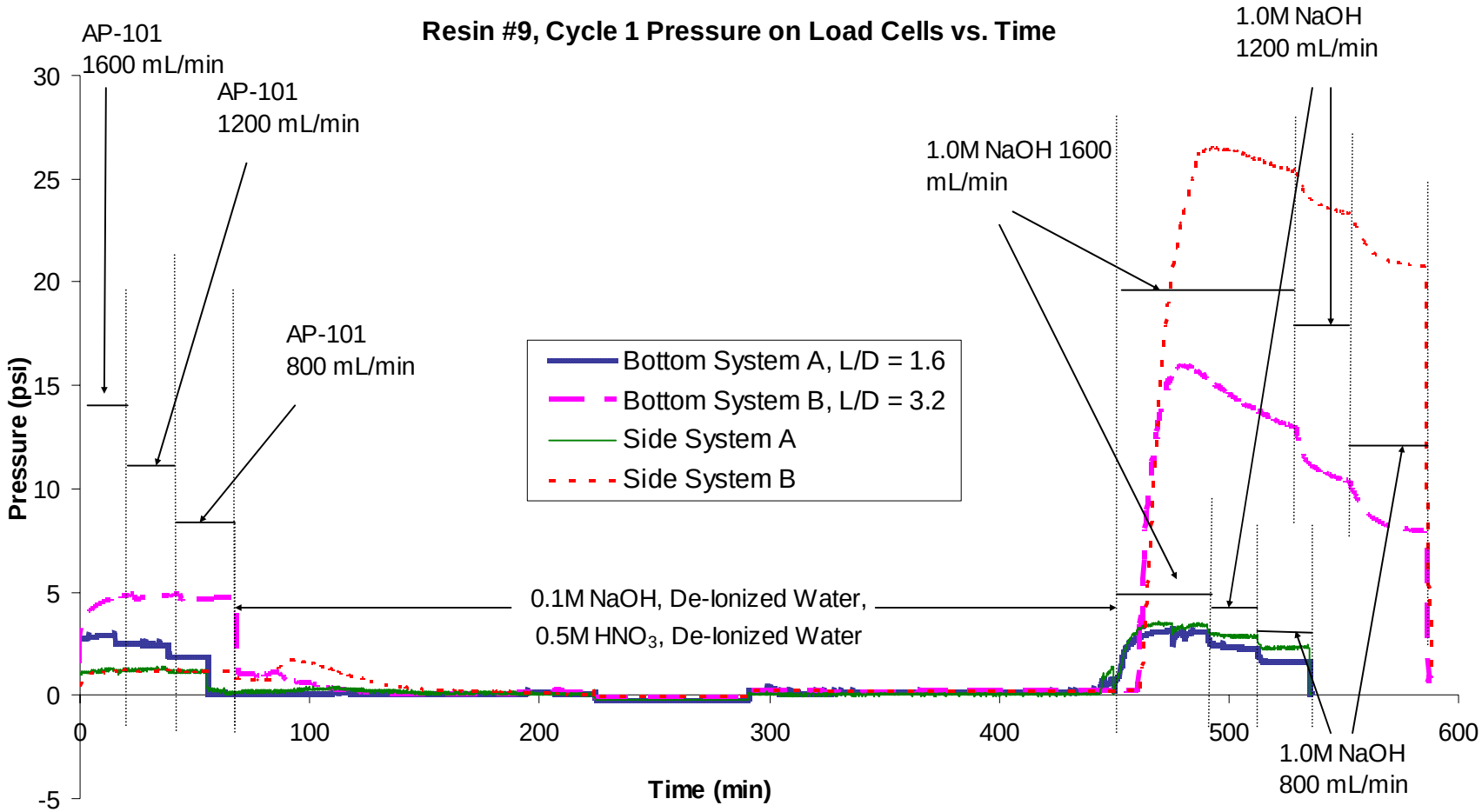

Figure 6.6. Typical Load Cell Data During one Load/Elute/Regenerate Cycle for Resin #9

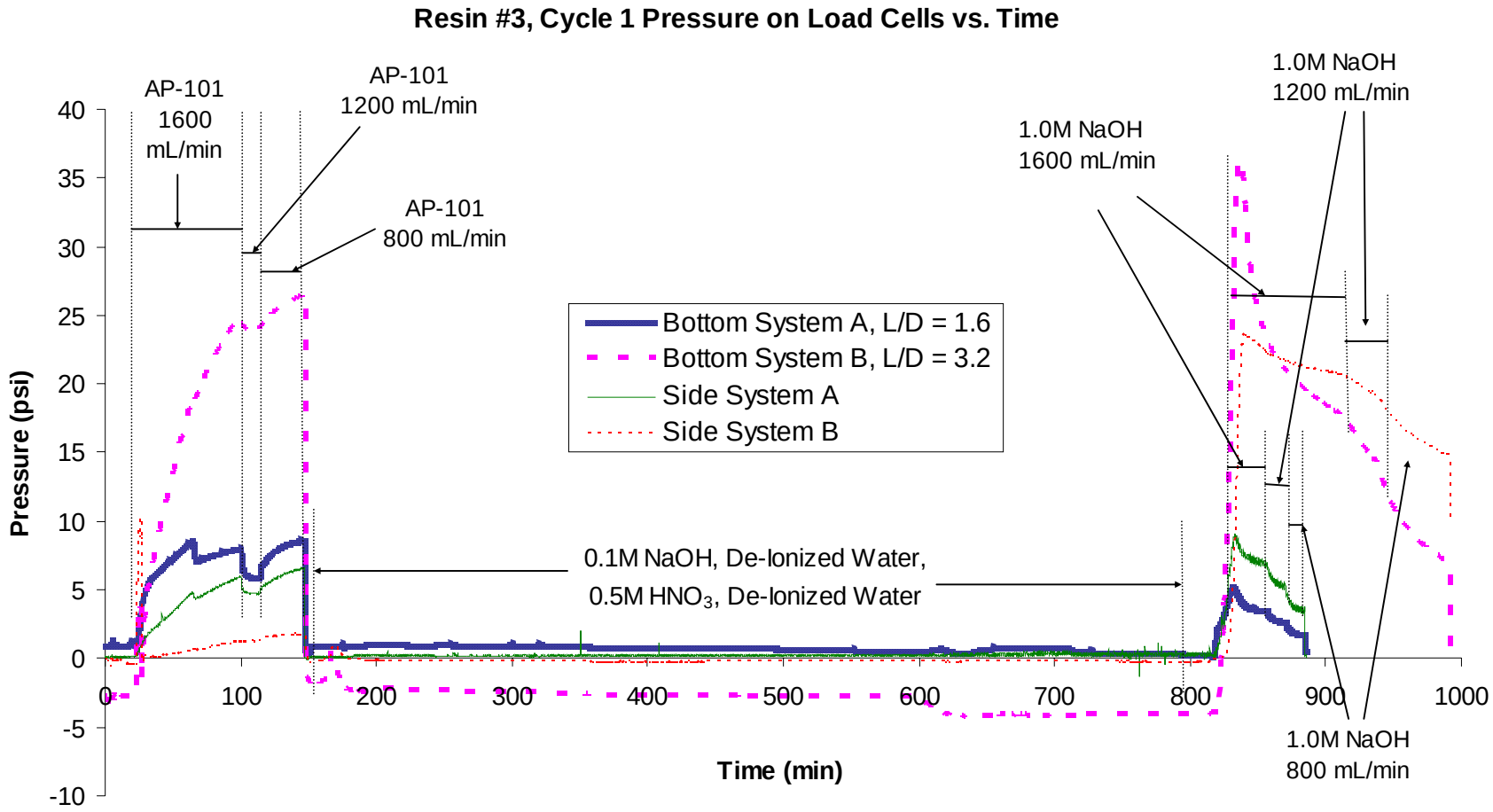

Figure 6.7. Typical Load Cell Data During one Load/Elute/Regenerate Cycle for Resin #3

In all cases, once flow was stopped, the load-cell pressure dropped quickly to zero (within less than a minute). It appeared that a small liquid differential pressure on the bed held the resin in place and allowed higher load-cell pressures in the bottom of the column. Without the liquid-differential pressure, the bed quickly expanded in the vertical direction, relieving all internal pressure. This sudden decrease in load-cell pressure, not seen in previous work performed at SRTC, may occur because of the low coefficient of friction for the glass-column sides as compared to the plastic columns used in previous research.

In some cases, the resin bed appeared to relax during an expansion, resulting in a sudden reduced side or bottom pressure. This can be seen in Figure 6.7 for the side load cell of System B just inside of the AP-101 simulant 1600 mL/min region. Both Resin #3 (Cycle #1 and 3) and Resin #12 (Cycle #3) show load-cell traces where pressure increases and then suddenly drops before increasing once again. It was possible that vibration or a sudden jarring of the column caused the resin bed to shift, reducing the measured pressures. Based on these observations, efforts were made to reduce vibration and to not touch the columns during subsequent permeability testing.

6.3 Particle-Size Distribution and Microscopy Data

Both the PSD and the microscopy data indicated that a reduction in particle size occurred during the testing of Resins #9 and #12. Figure 6.8 shows the mean particle-size results for the resins before and after testing in the two columns. For the L/D ratio = 1.6 column (System A), Resin #9 resulted in a decrease of approximately 80 microns (12% average size reduction), and Resin #12 resulted in a decrease of approximately 150 microns (19% average size reduction) in the mean particle size from the beginning to end of the testing. For the L/D ratio of 2.7 (System B), Resin #9 resulted in a decrease of approximately 150 microns (22% average size reduction), and Resin #12 resulted in a decrease of 160 microns (21% average size reduction). The post-testing PSD for Resin #12 had a large variability, and subsampling consistently was difficult, resulting in the need for averaging many subsample results to obtain a consistent mean value. However, the size distribution for Resin #12 was generally bimodal (see Figure 6.9). Before testing, the ~800 micron peak accounted for 60% (by volume) of the particles, and the ~400 micron peak accounted for 14%. After testing, the larger particle-fraction decreased to 52%, and the smaller particle fraction increased to 35% (see Figure 6.10).

The generation of smaller particles in the resin bed may be attributed to physical and chemical stresses. The physical stress on the resin could occur during expansion from the H-form to the Na-form. In this case, the expanding particles could be swelling against each other, as indicated by the radial forces measured in the resin bed. Particle breakage would occur by larger compressive forces pushing against each other or the grinding of one particle against another as the bed expands. The chemical stress resulting in attrition of the resin particles could also be related to the osmotic shock of cycling the resin between the base and acid forms. Uneven or rapid expansions from the chemical changes could result in particle fracture.

There was a significant difference in the particle-size change between the two Resin #9 column tests. The larger reduction in particle size for the higher L/D ratio was probably due to physical stresses due to the greater internal pressures in the taller column. These higher pressures would result in increased particle breakage than in the lower L/D ratio column.

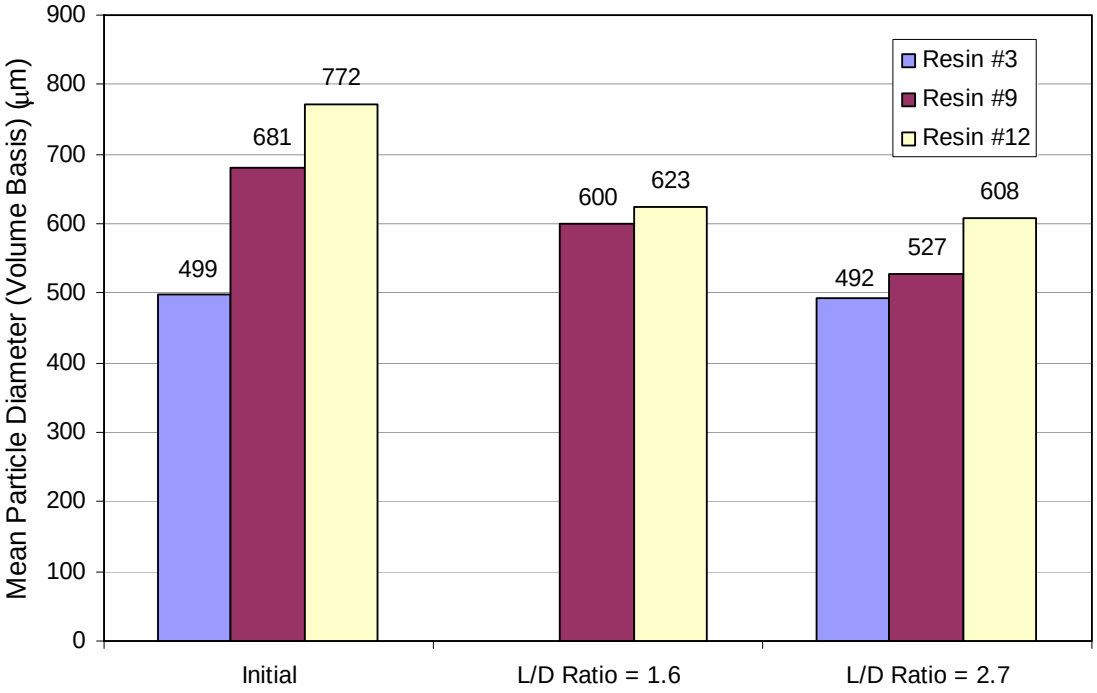

Figure 6.8. Comparison of Mean Particle Size Before and after Testing, Na-Form Resins. (No PSD measurement was taken for Resin #3, L/D = 1.6.)

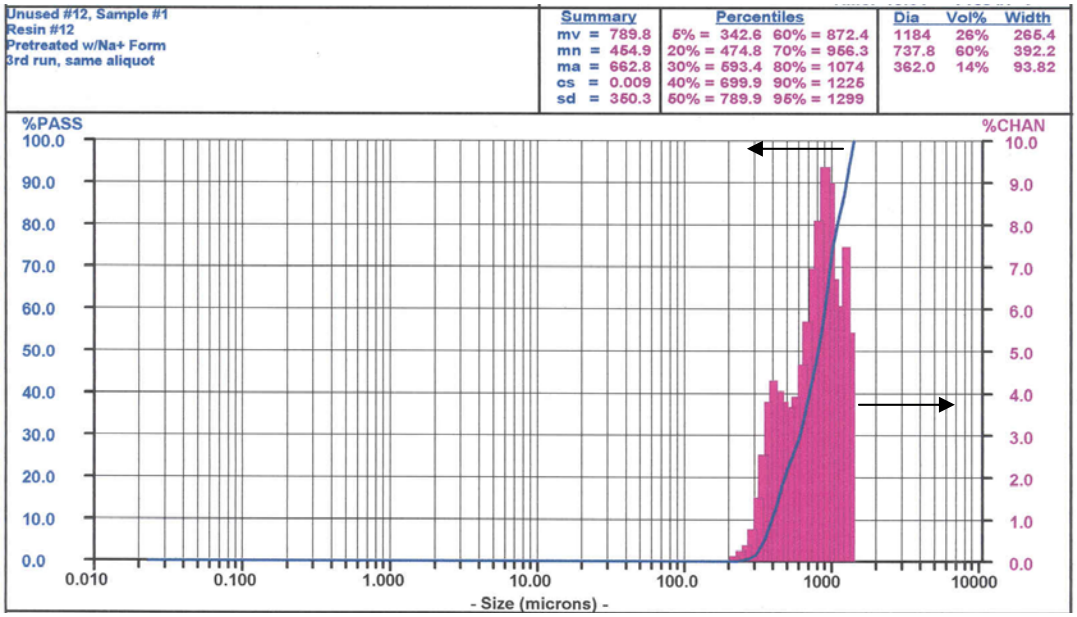

Figure 6.9. PSD of Resin #12 Na-Form (before permeability testing)

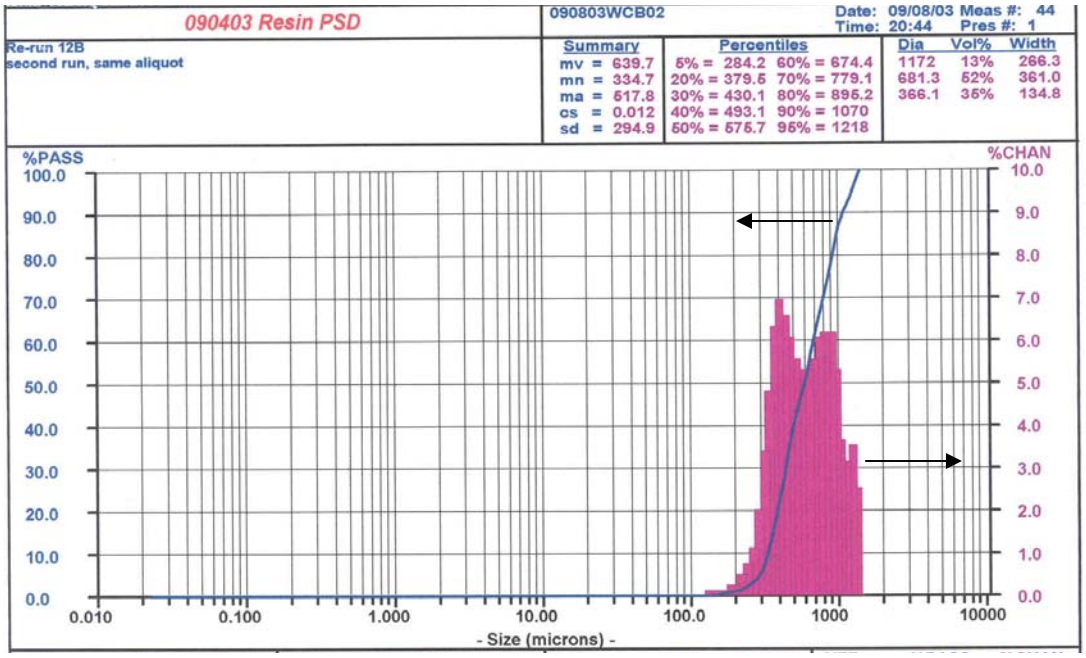

Figure 6.10. PSD of Resin #12 Na-Form (after permeability testing, Column B)

In contrast, the average particle size for Resin #12 was virtually the same for both L/D ratio columns. Because there is not a significant difference in final particle size between the column L/D ratios, the resin breakage for this resin could be related solely to the osmotic shock of cycling between the acid to the base forms of the resin. However, Resin #12 was removed from the higher L/D ratio column after the second cycle, and the larger compressive forces that might have built up in this column due to resin cycling were relieved. Thus, the amount of particle breakage due to these physical stresses may have been artificially reduced. Therefore, no conclusions can be drawn from a comparison of particle sizes for Resin #12 at the higher L/D.

The mean particle size of Resin #3 shown in Figure 6.8 indicated no decrease in PSD in spite of the large forces exerted on the resin during testing. The micrographs, shown in Figure 6.11, confirmed this result. The number of broken spheres was roughly similar for both the pre-testing and post-testing results. This is in contrast to the micrographs of Resins #9 and #12 where many of the particles appear significantly smaller (see Figure 6.12 and Figure 6.13). PSD measurements were not taken on Resin #3 for Column A (L/D ratio = 1.6), so no PSD comparison could be made. However, the micrographs seem to indicate no additional particle breakage from the higher L/D ratio of Column B over Column A.

Because there was little particle breakage for Resin #3, the decrease in permeability after multiple cycles would be caused by compaction of the bed as it shrinks and swells. In contrast, with Resin #9 and #12, the decrease in permeability after multiple process cycles would also be caused by increased resin fines. These fines not only reduce the overall particle size, but also decrease the void fraction in the bed. Both of these factors contribute to decreased permeability.

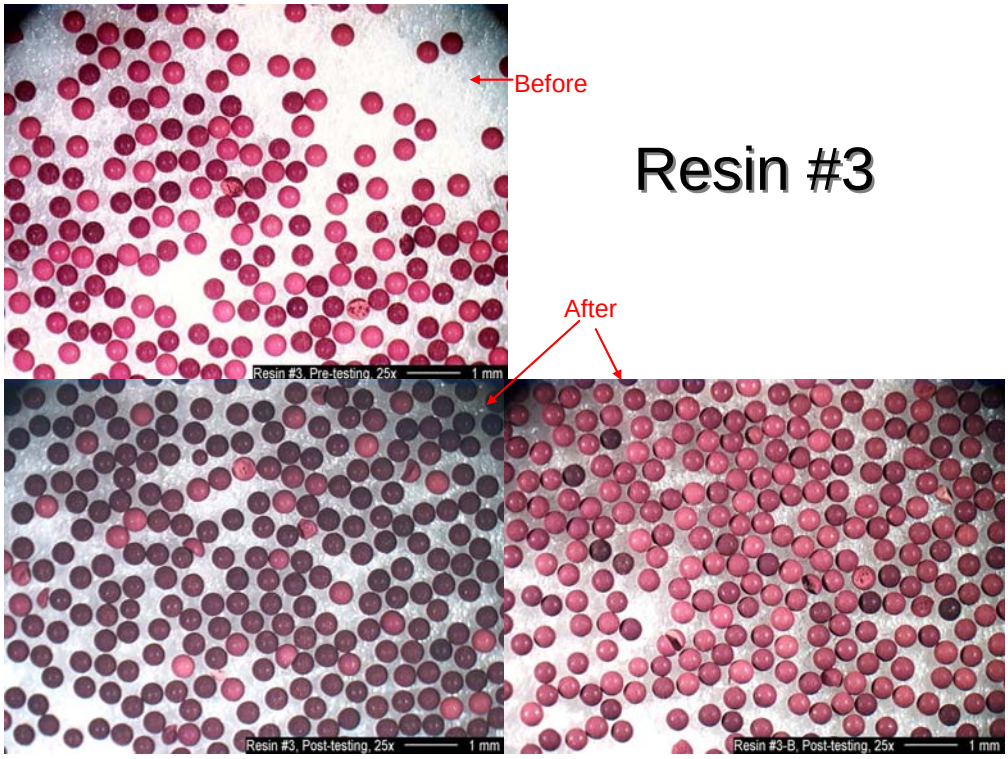

Figure 6.11. Micrographs of Resin #3 Before (upper left) and After Testing for Columns with L/D = 1.6 (lower left) and L/D = 2.7 (lower right) H-Form Resin

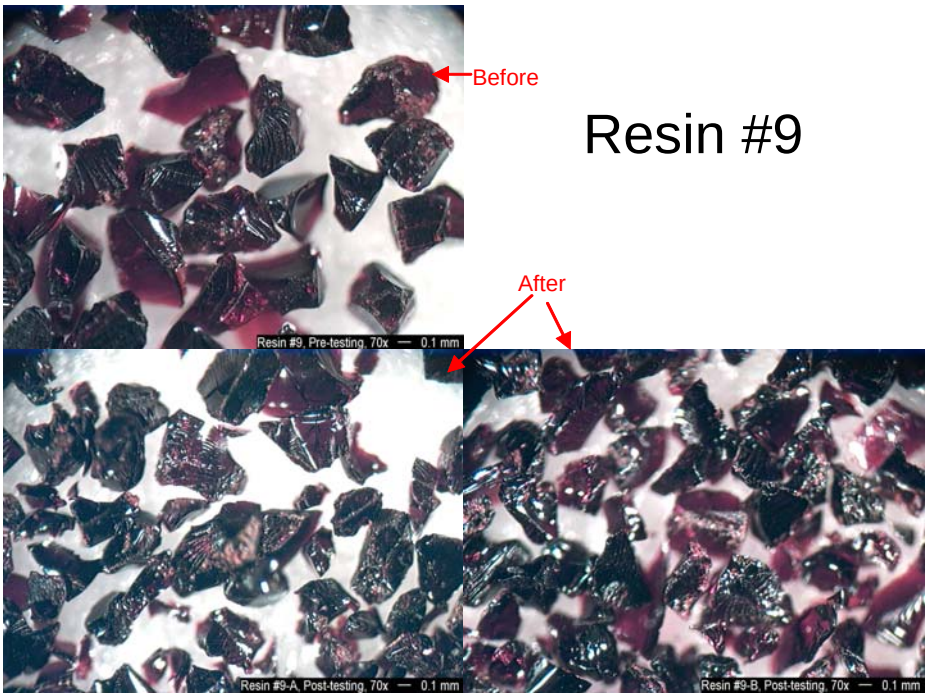

Figure 6.12. Micrographs of Resin #9 Before (upper left) and After Testing for Columns with L/D = 1.6 (lower left) and L/D = 2.7 (lower right) H-Form Resin

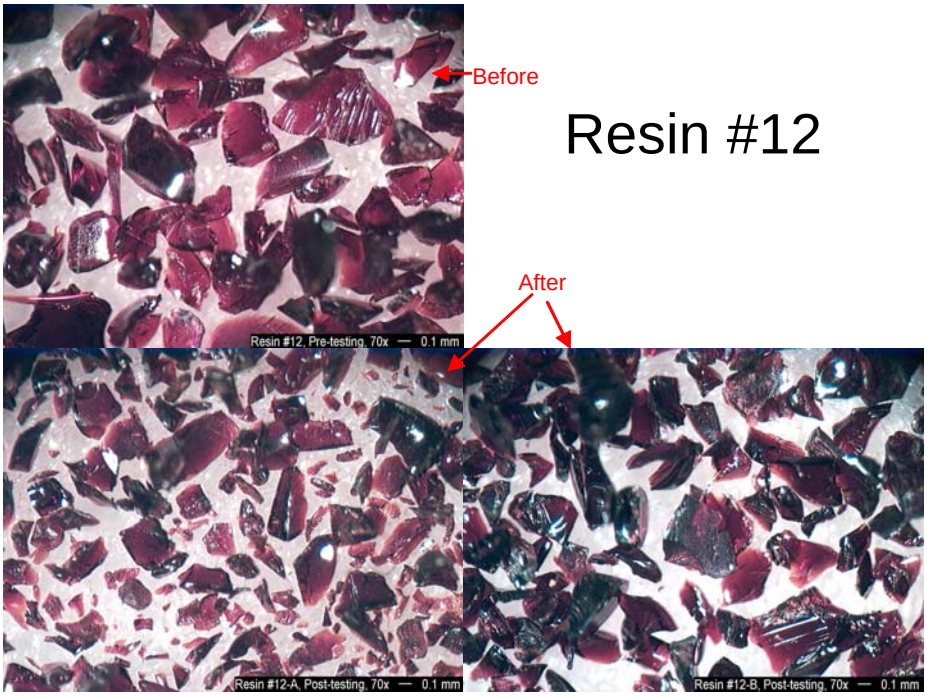

Figure 6.13. Micrographs of Resin #12 Before (upper left) and After Testing for Columns with L/D = 1.6 (lower left) and L/D = 2.7 (lower right) H-Form Resin

6.4 Compressibility Testing

Five successive compressibility cycles from 0 to 20 psig were performed for each ion exchange resin to allow the bed height to equilibrate. Both the resin height and the force on the side (radial pressure) and the bottom load cells (axial pressure) changed over all five cycles. The resin heights for the final loading cycle are presented in Figure 6.14. These results are fairly consistent with previous cycles in that Resin #3 showed the least compression (~0.2 mm), and Resin #12 showed the greatest compression (~6.3 mm) over the pressure range studied. Figure 6.15 shows the expected pressure drop (ΔP) using the resin compressibility to adjust the bed void fraction (ε) based on the Blake-Kozeny relationship [20] between pressure drop and void fraction for laminar flow:

$$\Delta P \propto \frac{(1-\varepsilon)^2}{\varepsilon^3} \tag{6.2}$$

These results indicate that if the column-height reduction results in a proportional reduction in bed-void fraction, the compressibility of Resin #12 could result in a significantly higher pressure drop across the column as compared to Resins #3 and #9. This significant compressibility could be a concern in a full-scale column.

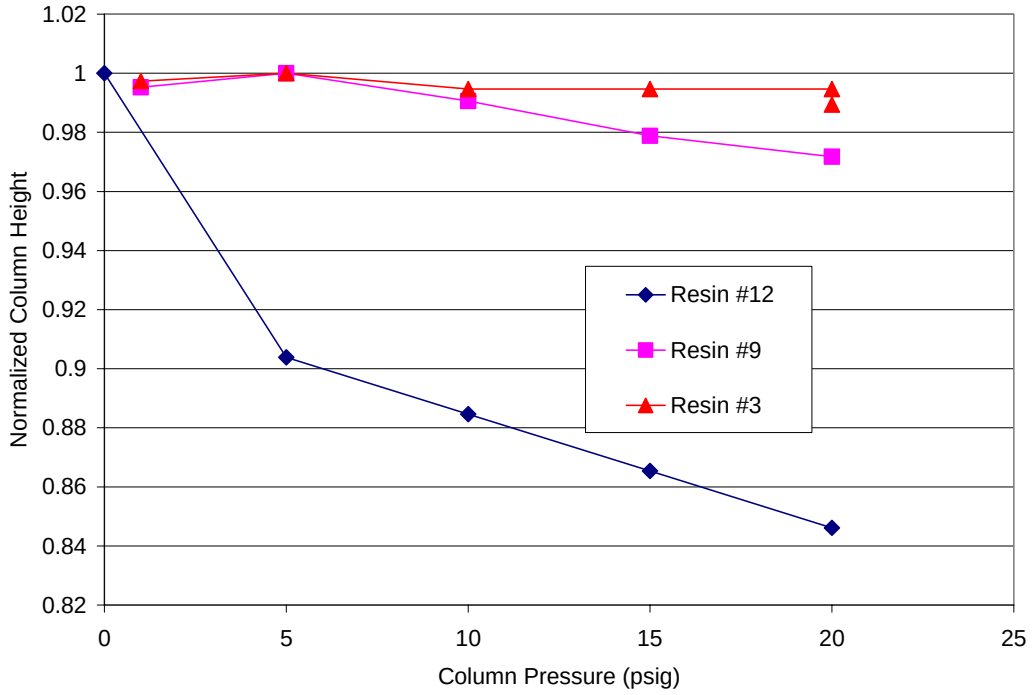

Figure 6.14. Resin-Bed Height Compression as a Function of Exerted Axial Pressure

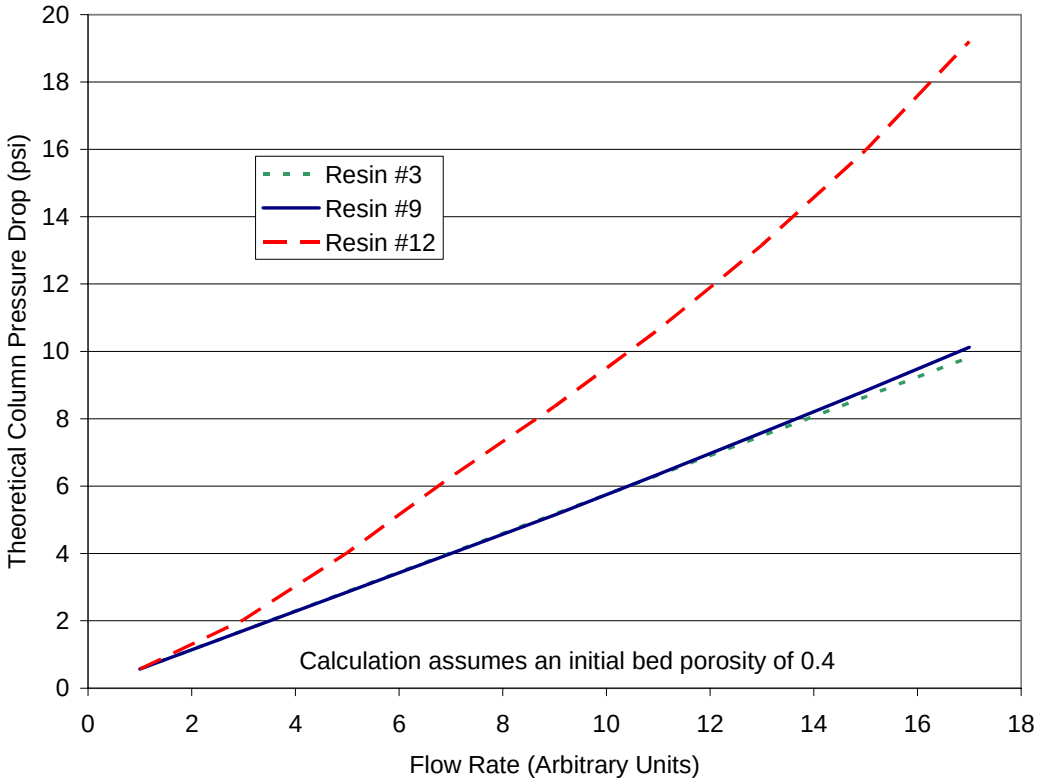

Figure 6.15. Calculated Pressure Drop as a Function of Flow, Including Resin Compressibility

The compressibility testing also included the effects of pressure on the load cells at the bottom and side of the column. A typical result of these multiple cycling tests is shown in Figure 6.16. As expected, in all cases, the load-cell pressure increased linearly with exerted pressure on the top of the bed. As the pressure was decreased, however, the load-cell pressure remained higher than during the pressure increase. This hysteresis effect was especially significant for Resin #3 where there was an ~40% increase in bottom load-cell pressure during the column relaxation as in the column compression (See Appendix D). This result might suggest that the resin bead structure of Resin #3 builds up pressures that are not quickly released, even after the axial pressure is removed. Such a result would be consistent with the higher pressures seen with Resin #3 during the regeneration step of the permeability testing. Once all pressure was released from the top of the column, the axial and radial pressures dropped back to zero within less than a minute. This result was also similar to the observation that the axial and radial pressure went to zero when the flowrate was stopped during permeability testing (see Figure 6.7).

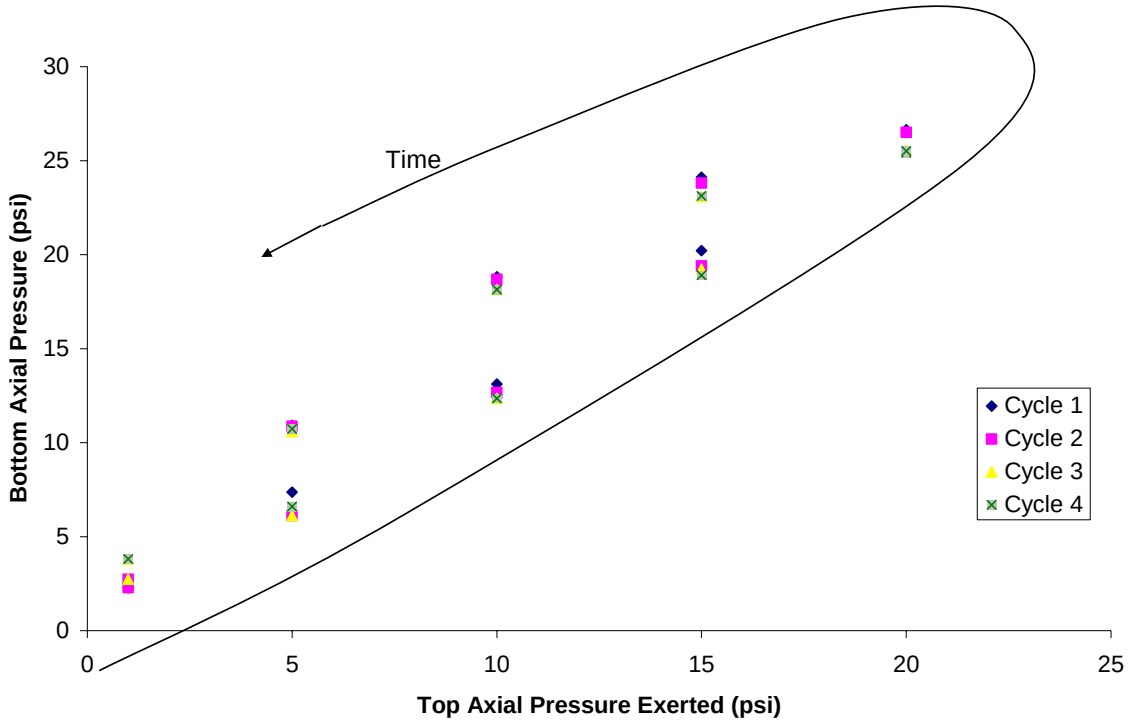

Figure 6.16. Typical Compression Versus Bottom-Load-Cell Pressure Plot During the Compressibility Study. This graph presents data from Resin #3.

A comparison of the final compression of the bottom and side load cells for the three resins is presented in Figure 6.17. In all cases, the bottom axial pressure reading exceeded the pressure exerted at the top of the column. It is possible that this result was caused by forces due to resin expansion; however, it was more likely caused by the load-cell mass inaccuracies. Since the load cell was calibrated at only 0 and ~4.5 psi, the higher values may have errors in their extrapolation. However, the results still indicate that most of the downward force for this sized column remained in the downward direction, and only a small fraction could be seen in the radial direction. It may be that a larger column or a higher resin bed would produce higher radial forces.

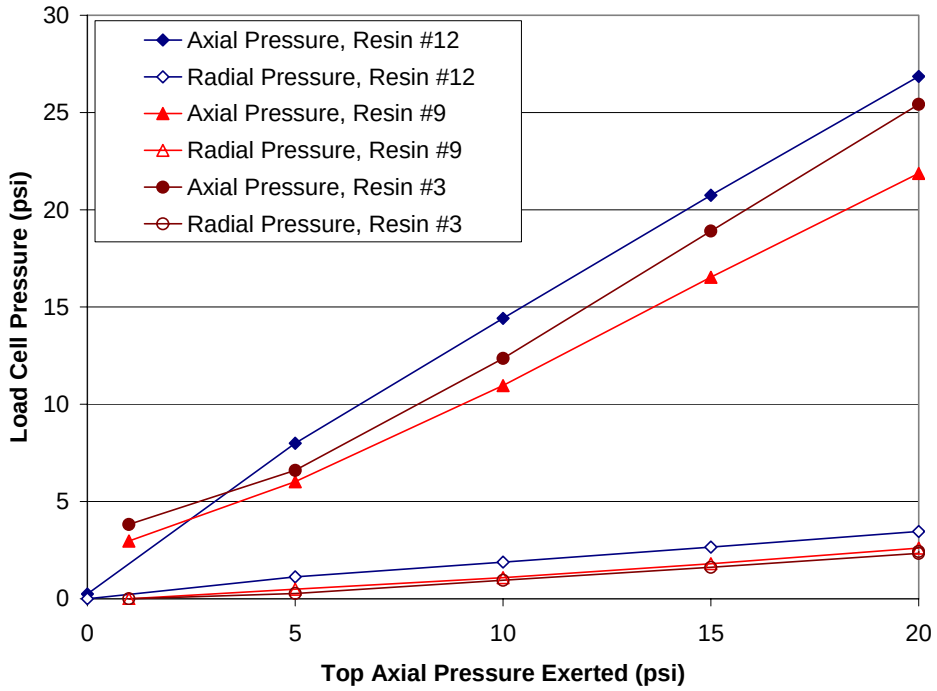

Figure 6.17. Cycle 5 Load Cell Results from the Resin Compressibility Study

The results of the angle of internal friction analysis are provided in Figure 6.18. As can be seen in the figure, the angles of internal friction for the three resins were nearly identical. The small radial forces observed during this testing corresponded to high angles of internal friction. These angles were much higher than would be expected for a free-flowing, granular material that is generally between 15° and 30°. The much higher values indicated that either the particles were sticky, or the experimental setup did not allow accurate measurement of this angle.

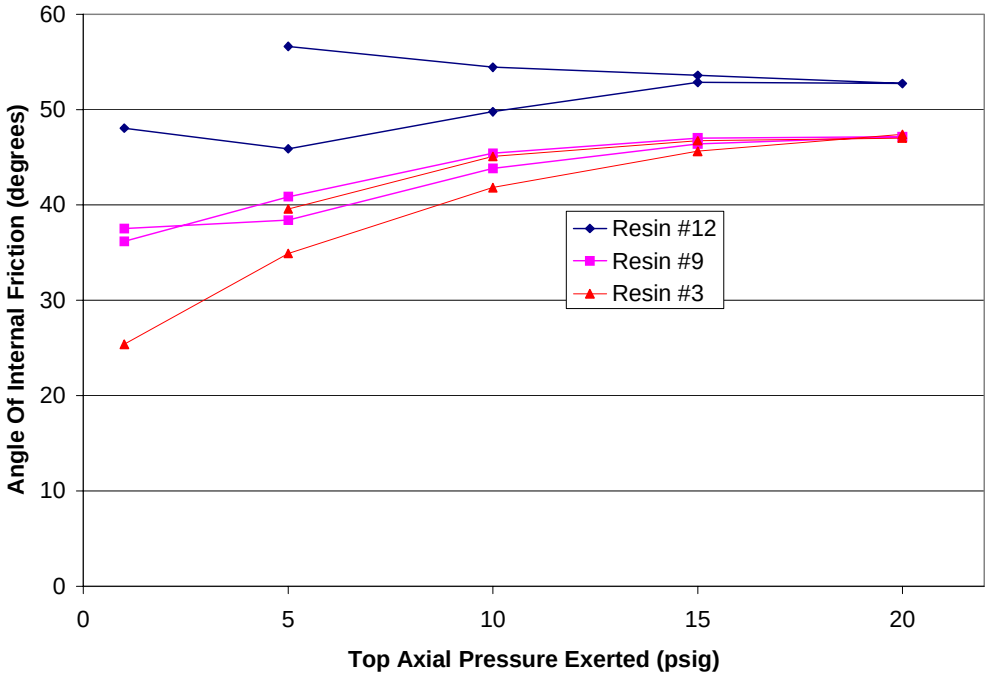

Figure 6.18. Angle of Internal Friction as a Function of Exerted Axial Column Pressure

7.0 Quality Control

This section describes the quality assurance (QA) and QC requirements and implementation.

7.1 Quality-Assurance Requirements

PNWD implemented the RPP-WTP quality requirements by performing work in accordance with the PNWD Waste Treatment Plant Support Project quality assurance project plan (QAPjP) approved by the RPP-WTP QA organization. This work was performed to the quality requirements of NQA-1-1989 Part I, Basic and Supplementary Requirements, and NQA-2a-1990, Part 2.7. These quality requirements were implemented through PNWD's *Waste Treatment Plant Support Project (WTPSP) Quality Assurance Requirements and Description Manual* and to the approved Test Plan, TP-RPP-WTP-210, Rev. 0 and Test Exceptions 24590-WTP-TEF-RT-03-022 and 24590-WTP-TEF-RT-03-031. The analytical requirements were implemented through PNWD's *Conducting Analytical Work in Support of Regulatory Programs* requirements document.

Experiments that were not method-specific were performed in accordance with PNWD's procedures QA-RPP-WTP-1101 "Scientific Investigations" and QA-RPP-WTP-1201 "Calibration Control System," assuring that sufficient data were taken with properly calibrated measuring and test equipment (M&TE) to obtain quality results.

As specified in Test Specification 24590-PTF-TSP-RT-02-016, Rev. 0, "Develop Requirements for Resorcinol Formaldehyde Alternate Resin," BNI's QAPjP, PL-24590-QA00001, was not applicable since the work was not performed in support of environmental/regulatory testing, and the data should not be used as such.

PNWD addressed internal verification and validation activities by conducting an independent technical review of the final data report in accordance with PNWD's procedure QA-RPP-WTP-604. This review verified that the reported results were traceable, that inferences and conclusions were soundly based, and that the reported work satisfied the test-plan objectives. This review procedure is part of PNWD's *WTPSP Quality Assurance Requirements and Description Manual*.

7.2 ASO Analytical Results

Samples were submitted to the ASO under ASRs 6769, 6835, and 6852. Data quality and QC are discussed for each analytical method. Analytical instrument calibration data are maintained in the ASO project files at PNWD with cross-reference to the ASR number. All raw and reduced data are maintained in data files associated with Project 42365 at PNWD.

7.2.1 Inductively-Coupled Plasma-Atomic Emission Spectrometry

The ICP-AES analyses were conducted on acid-digested simulant sample aliquots and on one elution composite aliquot. All batch and instrument QC requirements were met. The QC results of the simulant analyses are summarized: RPDs of analytes of interest (Al, Cr, K, Na, and P) were within 2.5%; the BS

recoveries ranged from 97% to 106%; the MS recoveries and post-matrix spike recoveries ranged from 101% to 115%; the serial dilution resulted in a maximum percent difference of 7%.

The ICP-AES analyses were conducted directly on the Cs composite eluate (Column 7, Cycle 3). All batch and instrument QC requirements were met. Because the analysis was a direct determination, preparation batch QC samples (reagent blank, duplicate, BS, and MS) were not required. The serial dilution test results on all analytes of interest passed except for Ca. The serial dilution calculated percent difference for Ca was 195%. However, the Ca result (1.3 μg/mL) was well below the MRQ (150 μg/mL).

7.2.2 Inductively Coupled Plasma-Mass Spectrometry

The ICP-MS analyses for Cs concentrations in the AZ-102 and AP-101 simulants were conducted using duplicate acid-digested sample aliquots. All batch QC requirements were met. The BS recovered at 100%, and the matrix spike recovered at 102%. The RPDs for the two duplicate samples were within 4%. All instrument QC requirements were met except that a post-matrix spike was inadvertently not performed. However, because the matrix-spike recovery met the batch QC success criteria, reanalysis was not required.

7.2.3 Gamma-Energy Analysis

All samples submitted for GEA were prepared in calibrated geometries for direct measurement. Therefore, batch QC was not applicable. All instrument QC parameters were met.

7.2.4 Ion Chromatography

The IC analyses were conducted directly on simulant sample aliquots. All batch and instrument QC requirements were met. Precision was assessed with one simulant sample run in duplicate. All anions of interest met the RPD acceptance criterion of <15%. The laboratory control sample (LCS)/BS produced recoveries (107% to 110%) well within the acceptance criteria of 80% to 120%. The MS recoveries for all anions except flouride recovered 104% to 110%, within the 75% to 125% acceptance criteria. The fluoride MS recovered at 129%, exceeding slightly the upper-bound criterion. Interfering, co-eluting anions significantly impact the MS measurement and recovery calculation. Because the sample was analyzed directly, no preparation was required, and thus no preparation blank was prepared.

An IC analysis was conducted directly on the composite Cs eluate. All batch and instrument QC requirements were met. The LCS/BS and MS recoveries (90% to 109%) were well within the acceptance criteria (80% to 120% for the LCS/BS and 75% to 125% for the MS). Two other samples (LAW matrix and eluate matrix) were run in duplicate as part of the analytical batch. Analyte precision was well within the acceptance criterion of <15% RPD for the analytes greater than 10× the method detection limit (MDL) (chloride, nitrite, and nitrate for the LAW and nitrate only for the eluate). Neither sulfate nor phosphate precision was evaluated because the duplicate sample sulfate and phosphate concentrations were less than 10× the MDL.

7.2.5 Hydroxide

The hydroxide concentrations were determined in both AZ-101 and AP-101 tank-waste simulants using acid titration. Hydroxide was calculated based on response at the first inflection point. All QC performance criteria were met. The BS and MS recoveries were 100% and 94%, respectively. The relative percent differences for duplicate analyses of AZ-102 and AP-101 simulants were 4.5% and 0.3%, respectively.

7.2.6 Total Organic Carbon and Total Inorganic Carbon

The TOC and TIC analyses were conducted on both simulants using the hot-persulfate method; only the TOC determination was conducted on the composite eluate sample using both the hot-persulfate and furnace-oxidation methods . All batch and instrument QC requirements were met. The QC results associated with the simulants are summarized as follows: RPDs were 0% and 1% TIC and TOC respectively; the BS recoveries were 101% and 97%, for TIC and TOC, respectively; the MS recoveries were 102% and 99% for TIC and TOC, respectively. The QC results associated with the composite eluate are summarized as follows: RPDs were not calculated because results were less than detectable; the hot persulfate method MS recovery was 108%, and the BS recovery was 100%. The furnace-oxidation method MS recovery was 106%, and the two BS recoveries were 97 to 99%.

7.3 Particle-Size Distribution

PSD measurements were performed on all resins, H-form and Na-form. The MicroTrac 3000 PSD measurement equipment was user-calibrated with NIST-certified particle-size standards. The standards were tested before and after sample analyses to verify instrument control.

7.4 Batch-Contact Results

Gamma measurements (for the 20-mL batch-contact samples) were taken on benchtop GEAs (high-purity germanium and sodium iodide detectors) for comparative measurements (i.e., indication). The equipment was user-calibrated to determine that the equipment was working properly. The gamma counters were energy-calibrated with vendor-supplied control samples. Because relative measurements were taken, absolute efficiency calibration of the benchtop gamma counters was not required; however, system stability was required. Detector stability was established each day the systems were in use by counting the control samples and background before and after the associated sample set. Batch-contact duplicate controls and duplicate samples were processed for each simulant at each Cs concentration. The results and measure of precision (RPD) are reported in Section 4.0, Batch-Contact Results.

7.5 Load and Elution Performance

The load and elution profiles were developed as relative measures using “for-indication only” measurement systems. Because relative Cs ratios were determined with these systems, absolute Cs activities did not need to be determined. Gamma measurements were taken on benchtop GEAs (high-purity germanium and sodium iodide detectors) for comparative measurements. The equipment was user-calibrated. The gamma counters were energy-calibrated with vendor-supplied control samples. Because

relative measurements were taken, absolute efficiency calibration of the benchtop gamma counters was not required; however, system stability was required. Detector stability was established each day the systems were in use by counting the control samples and background count rate before and after the associated sample set.

To confirm these analyses, selected samples from Column 3 Cycle 1 and Column 7 Cycle 2 were re-prepared in calibrated geometries and submitted to the ASO for analysis. Because these were direct measurements, the LCS, BS, and MS QC samples were not required. The ASO results agreed well with the "for-indication only" results as shown in Figure 7.1 and Figure 7.2 for the Cs load and elution profiles, respectively.

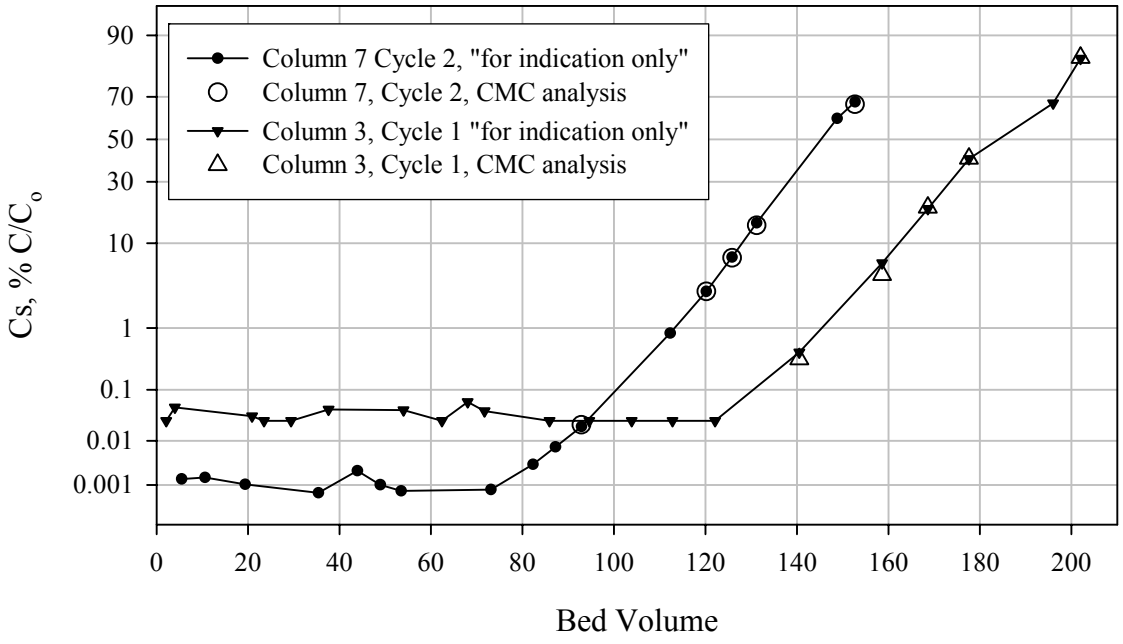

Figure 7.1. Confirmatory Analysis for Cs-Load Results

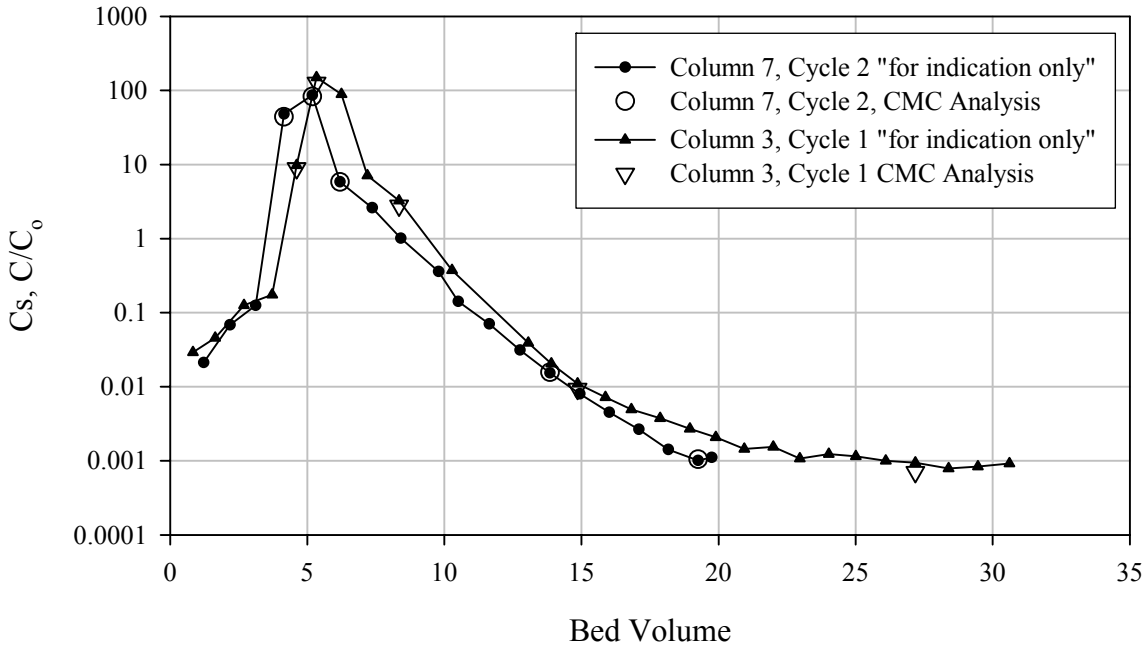

Figure 7.2. Confirmatory Analyses for Cs-Elution Results

7.6 Permeability and Compressibility Test

Measuring equipment used during the permeability and compressibility tests included flowmeters, thermocouples, differential pressure transducers, pressure gauges, particle-size analysis, viscometers, and rulers. The Micromotion flowmeters were calibrated by the Colorado Engineering Experiment Station, Inc. (Nunn, CO). The thermocouples and differential pressure transducers, along with the data-acquisition system, were calibrated by the Instrumentation Services & Technology Group at PNWD. Viscosity and PSD equipment was user-calibrated based on NIST-certified viscosity and particle-size standards. Load cells and total system pressure were for indication-only measurements. Resin-bed height was measured with standard laboratory equipment.

7.7 Miscellaneous Equipment

Additional equipment included thermometers, clocks, and balances. The thermometers and clocks were standard laboratory equipment for use as indicators only. Balances are calibrated annually by a certified contractor, QC Services, Portland, OR. Balance operations were checked each day of use with check weights.

8.0 Conclusions

Resorcinol-Formaldehyde resin performance data were generated to support the WTP's selection of RF resins for further development work. Physical properties and batch-contact Cs-distribution coefficients were measured for nine RF resins, including granular forms and spherical forms. Based on the initial testing results of these nine resins, five resins were selected for further column testing of Cs load and elution performance, and two resins were selected for further hydraulic properties testing. In some cases, SL-644 was tested in parallel with the RF resins.

Physical-Property Testing. Physical-property testing was conducted on nine RF resins and included PSD, shrink-swell behavior, and settled-resin-bed density. The spherical resins demonstrated the tightest PSDs. The settled BV swell from H-form to Na-form varied from 1.4 to 2.8 without correlation to resin type. Skeletal density and bed porosity were determined on one granular and one spherical resin. The skeletal densities were found to be virtually identical for both resin types (1.4 g/mL), as were the bed porosities (0.38).

Batch-Distribution Performance. Determination of batch-distribution coefficients, as a function of Cs concentration and resin type, were determined on nine RF resins. Batch equilibrium was established within a 24-h contact time for all resins tested. Equilibrium batch-distribution coefficients (K_d values) ranged from 300 to 600 mL/g in the AZ-102 simulant feed at a Cs concentration of 50 mg/L. The batch-distribution behavior was not necessarily a good indicator for resin performance in the column. Some resins resulted in high K_ds at the Cs simulant feed condition, but resulted in poor load behavior; the opposite was found with other resins. From the batch-contact data, isotherms were developed to estimate the Cs capacity of the various resins in AZ-102 simulant. Capacities ranged from 0.26 to 0.54 mmoles Cs per gram of dry resin. The Cs capacities were also compared to previously-reported SL-644 capacities (0.3 mmoles/g in AZ-102 actual waste and 0.44 mmoles/g in AZ-101 actual waste).

Load and Elution Performance. Multi-cycle Cs load and elution behavior was evaluated for selected granular and spherical resin forms using AZ-102 simulant. Two SL-644 resins were tested simultaneously. Only one granular resin was tested with AP-101 simulant that contained a high K concentration. The onset of Cs breakthrough and the number of BVs of feed processed at 50% C/C_o were determined. Considerable variations in Cs load profiles between resins were observed. The onset of Cs breakthrough ranged from 20 BVs to 130 BVs; 50% C/C_o ranged from 50 BVs to 190 BVs. There was good reproducibility of Cs load behavior as a function of process cycle for each individual resin. The high K concentration in AP-101 simulant interfered with Cs exchange onto the granular resin manifested by early Cs breakthrough and a small (gradual) slope in the Cs-breakthrough profile. The significant reduction in the amount of Cs removed per BV of AP-101 simulant processed, relative to AZ-102 simulant processing, was attributed to competition from K.

Peak elution Cs concentrations as a function of BVs processed, volume to reach 1% C/C_o, and steady-state Cs elution concentrations in terms of C/C_o were determined. Elution profiles were generally consistent for the resins tested. Each resin's elution behavior was highly reproducible for the three cycles tested. The spherical resin forms reached lower steady-state C/C_o elution values (4.5E-4 C/C_o) than did the granular forms (1.3E-3 C/C_o) after processing 22 BVs 0.5 M HNO_3. The AP-101 simulant processing resin resulted in a broadened elution peak. Residual Cs concentrations remaining on the eluted resin beds

were also determined. The spherical resins resulted in the least residual Cs on the resin beds after elution at nominally 2 μg after processing 39 BVs eluant in the downflow direction. The highest residual Cs remaining on the column was associated with a ground-gel resin at nominally 60 μg after processing 42 BVs eluant.

Shrink-swell behavior was determined in the column format for each resin. The SL-644 (Resin #12 with the broad PSD) resulted in the highest BV swings (40%) followed closely by one of the granular RF resin forms. The other granular resins, spherical resins, and SL-644 (20 to 30-mesh) were characterized by lower BV changes at nominally 30% change from Na-form to H-form.

The spherical RF resins eluted faster, had lower residual Cs after elution, and had lower initial C/C_o values on loading than the granular RF resins. These results suggest that the spherical RF beads contain pores or other characteristics that allow greater access to active sites within the particles.

For approximately the same or greater elution volumes, upflow elution of Resin #9 resulted in approximately the same or higher residual Cs on the resin bed, and the same or higher initial loading C/C_o values, than downflow elution.

Comparison of ^{134}Cs and ^{137}Cs tracer data indicate that Cs "bleed" on loading is almost exclusively from residual Cs located at the downstream end of the resin bed.

More NaOH is required for RF than for SL-644, per unit bed volume, for complete conversion of the resin to the Na form. Incomplete conversion results in gas generation (bubble formation) in the resin bed during subsequent feed loading.

Hydraulic Testing. Multi-cycle bed permeability was determined on one each of granular, spherical, and SL-644 resins. Radial and axial pressures were monitored during permeability testing as a function of process step and process cycle; comparisons between granular and spherical resins were provided. The permeability for the spherical resin was higher than that found for the ground-gel RF and SL-644 resins. Hydraulic distinctions between the RF and SL-644 resins were confounded by technical problems associated with SL-644 testing and the required SL-644 resin-bed manipulations.

Particle-size distributions were determined after processing, and were compared with pre-processing PSDs. The spherical resin did not change significantly in PSD; however, the granular materials (including SL-644) resulted in a bimodal distribution indicative of significant particle breakage. The observed ground-gel resin breakage may contribute to the lowered permeability and associated pressure drops in the column by enhancing resin packing.

Compressibility testing was conducted on the three resins after permeability testing; at 20 psig, the SL-644 compressed volume (15% compression) was significantly greater than the RF resin types (2% to 4% compression). The angle of internal friction was calculated as a function of exerted pressure (up to 20 psig) for each of the three resins. The SL-644 (Resin #12) resulted in the highest angle of internal friction. The spherical and granular RF resin's angles of internal friction were similar to each other and lower than that of SL-644.

Preliminary RF Purchase Specification. A preliminary RF purchase specification will be provided in a separate document from this report. It is anticipated that attributes in the preliminary purchase specifications will evolve/change as additional data are gathered in separate RF testing activities. The specification and anticipated changes would be better managed separately from the current report.

9.0 References

1. JP Bibler, RM Wallace, and LA Bray. 1989. "Testing a New Cesium-Specific Ion Exchange Resin for Decontamination of Alkaline High-Activity Waste." In: *Proceedings of the Symposium on Waste Management '90*. Feb 25–Mar 1, 1990, pp 747–751, Tucson, AZ.

2. LA Bray, RJ Elovich, and KJ Carson. 1990. *Cesium Recovery Using Savannah River Laboratory Resorcinol-Formaldehyde Ion Exchange Resin.* PNL-7273, Pacific Northwest Laboratory, Richland, WA.

3. DE Kurath, LA Bray, KP Brooks, GN Brown, SA Bryan, CD Carlson, KJ Carson, JR DesChane, RJ Elovich, and AY Kim. 1994. *Experimental Data and Analysis to Support the Design of an Ion-exchange Process for the Treatment of Hanford Tank Waste Supernatant Liquids.* PNL-10187, Pacific Northwest Laboratory, Richland, WA.

4. GN Brown, LA Bray, and RJ Elovich. 1995. *Evaluation and Comparison of SuperLig® 644, Resorcinol-Formaldehyde and CS-100 Ion Exchange Materials for the Removal of Cesium from Simulated Alkaline Supernate.* PNL-10486, Pacific Northwest Laboratory, Richland, WA.

5. TL Hubler, JA Franz, WJ Shaw, SA Bryan, RT Hallen, GN Brown, LA Bray, and JC Linehan. 1995. *Synthesis, Structural Characterization, and Performance Evaluation of Resorcinol-Formaldehyde (R-F) Ion-Exchange Resin.* PNL-10744, Pacific Northwest Laboratory, Richland, WA.

6. LA Bray, CD Carlson, KJ Carson, JR DesChane, RJ Elovich, and DE Kurath. 1996. *Initial Evaluation of Two Organic Resins and Their Ion Exchange Column Performance for the Recovery of Cesium from Hanford Alkaline Wastes.* PNNL-11124, Pacific Northwest National Laboratory, Richland, WA.

7. RL Russell, SK Fiskum, AP Poloski, and LK Jagoda. 2002. *AP-101 Diluted Feed (Envelope A) Simulant Development Report.* WTP-RPT-057, Battelle—Pacific Northwest Division, Richland, WA.

8. NM Hassan, and CA Nash. 2002. *Evaluating Residence Time for SuperLig® 644 Columns with Simulated LAW Envelope B Solution.* WSRC-TR-2002-00163, Savannah River Technology Center, Aiken, SC.

9. SK Fiskum, LA Snow, and DL Blanchard, Jr. 2003. *AP-101 Simulant Validation for Cesium Ion Exchange Processing Using SuperLig® 644*. WTP-RPT-088, Rev. 0, Battelle—Pacific Northwest Division, Richland, WA.

10. WL McCabe, and JC Smith. 1976. *Unit Operations of Chemical Engineering*, 3rd Edition. McGraw-Hill, NY.

11. SK Fiskum, ST Arm, and DL Blanchard. 2002. *Aging Study and Small Column Ion Exchange Testing of SuperLig® 644 for Removal of ^{137}Cs from Simulated AW-101 Hanford Tank Waste*, PNWD-3195, Battelle—Pacific Northwest Division, Richland, WA.

12. NM Hassan, WD King, and DJ McCabe. 1999. *SuperLig® Ion Exchange Resin Swelling and Buoyancy Study*. BNF-003-98-0051, Savannah River Technology Center, Aiken, SC.

13. GN Brown, LA Bray, CD Carlson, KJ Carson, JR DesChane, RJ Elovich, FV Hoopes, DE Kurath, LL Nenninger, and PK Tanaka. 1996. *Comparison of Organic and Inorganic Ion Exchangers for Removal of Cesium and Strontium from Simulated and Actual Hanford 241-AW-101 DSSF Tank Waste*, PNL-10920, Pacific Northwest National Laboratory, Richland, WA.

14. SK Fiskum, ST Arm, and DL Blanchard, Jr. 2003. *Small Column Ion Exchange Testing of SuperLig® 644 for Removal of ^{137}Cs from Hanford Waste Tank 241-AZ-101 (Envelope B)*, PNWD-3266, Rev. 0, Battelle—Pacific Northwest Division, Richland, WA.

15. SK Fiskum, DL Blanchard, and ST Arm. 2003. *Small Column Ion Exchange Testing of SuperLig® 644 for Removal of ^{137}Cs from Hanford Waste Tank 241-AZ-102 Concentrate (Envelope B).* PNWD-3267, Battelle—Pacific Northwest Division, Richland, WA.

16. JS Buckingham. 1967. *Waste Management Technical Manual*. ISO-100 DEL, Hanford Atomic Products Operation, Richland, WA.

17. ST Arm, SK Fiskum, DL Blanchard. 2002. Effect of Eluant Flow Direction on the Elution Characteristics of SuperLig-644 Ion Exchange Resin, PNWD-3202, Battelle-Pacific Northwest Division, Richland, WA.

18. SK Fiskum, DL Blanchard, and ST Arm. 2003. *Small Column Ion Exchange Testing of SuperLig® 644 for Removing ^{137}Cs from Hanford Waste Tank 241-AN-102 Supernate (Envelope C) Mixed with Tank 241-C-104 Solids (Envelope D) Wash and Permeate Solutions.* PNWD-3240, Battelle—Pacific Northwest Division, Richland, WA.

19. SK Fiskum, ST Arm, DL Blanchard, Jr., and BM Rapko. 2002. *Small Column Ion Exchange Testing of SuperLig® 644 for Removal of ^{137}Cs from Hanford Waste Tank 241-AP-101 Diluted Feed (Envelope A)*. PNWD-3198, Battelle—Pacific Northwest Division, Richland, WA.

20. RB Bird, WE Stewart, and EN Lightfoot. 1960. *Transport Phenomena.* John Wiley & Sons, NY.

Appendix A

Micrographs of Pretreated Resin

Appendix A: Micrographs of Pretreated Resin

All resin pictures were taken after pretreatment.

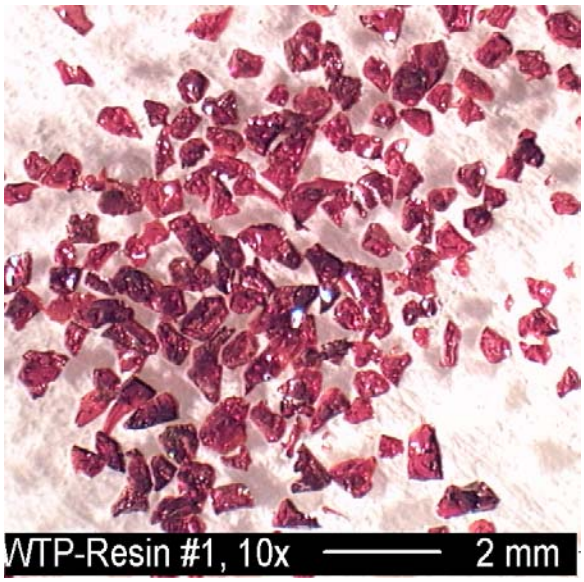

Resin #1 10x Magnification

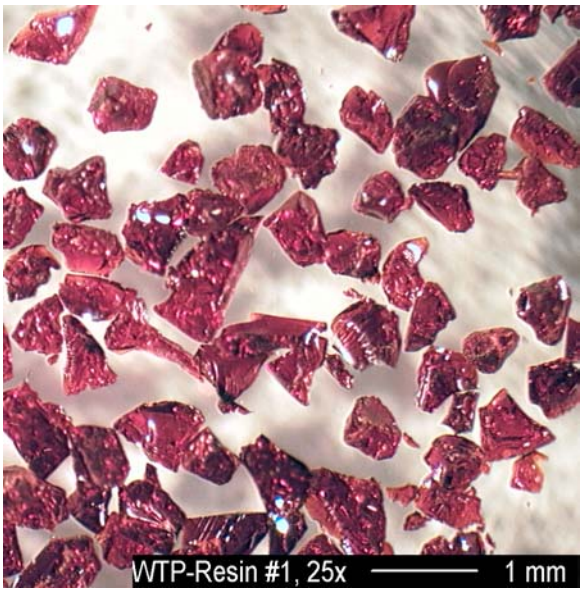

Resin #1 25x Magnification

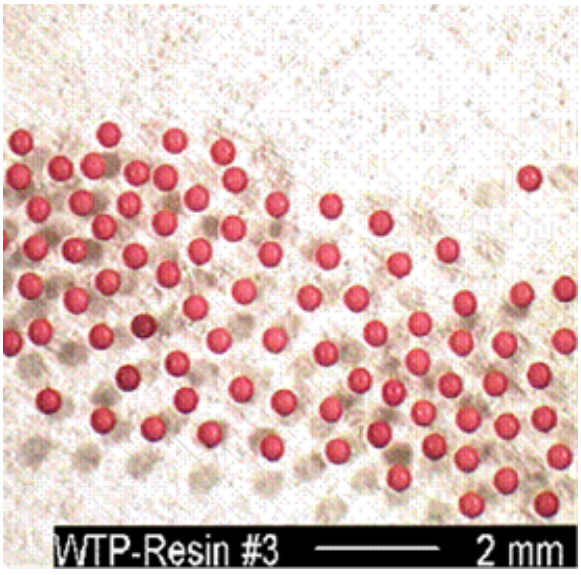

Resin #3 at 10x Magnification

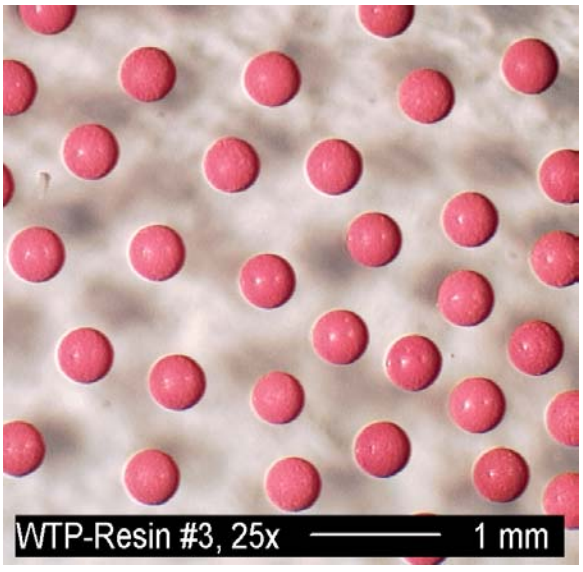

Resin #3 at 25x Magnification

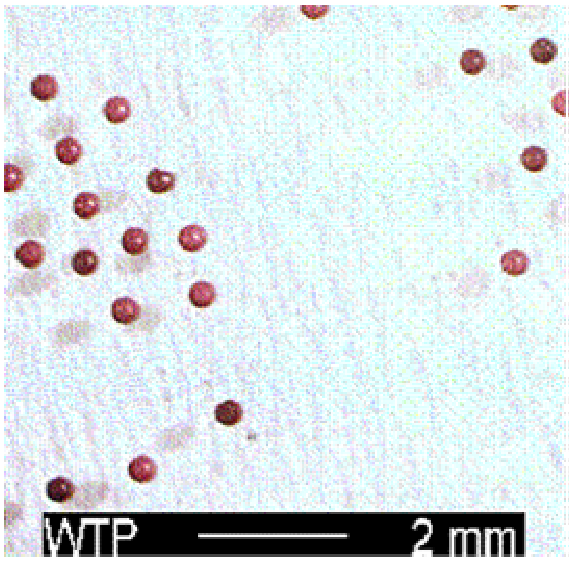

Resin #4 10x Magnification

Resin #4 at 25x Magnification

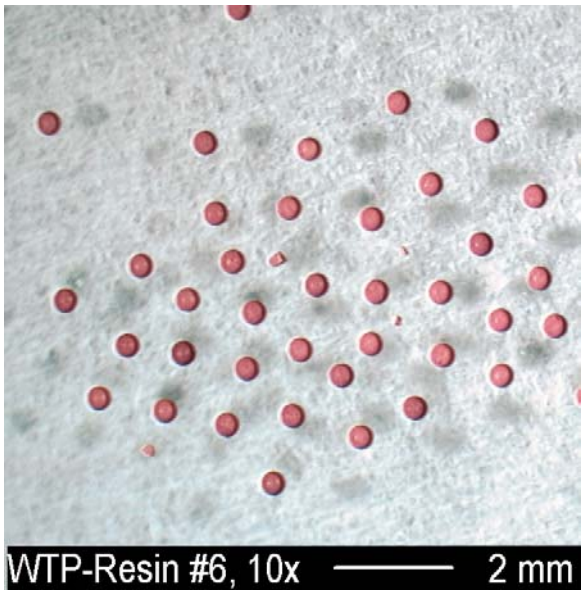

Resin #6 at 10x Magnification

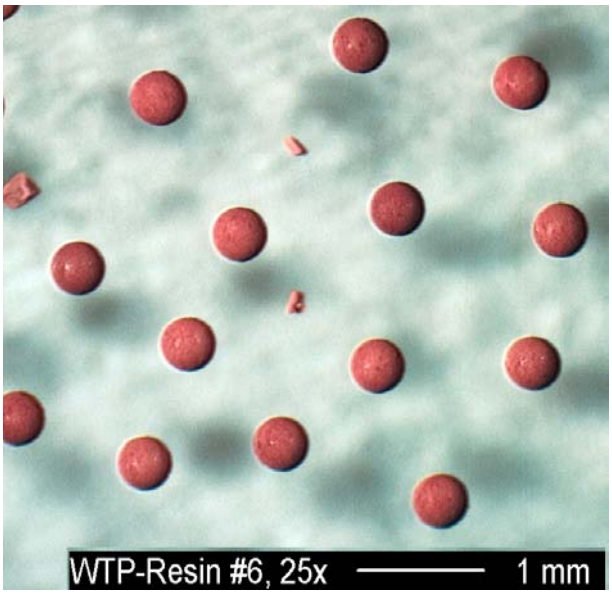

Resin #6 at 25x Magnification

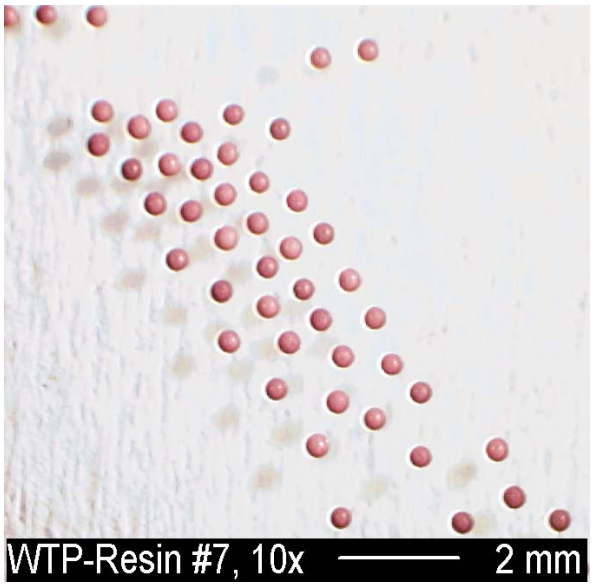

Resin #7 at 10x Magnification

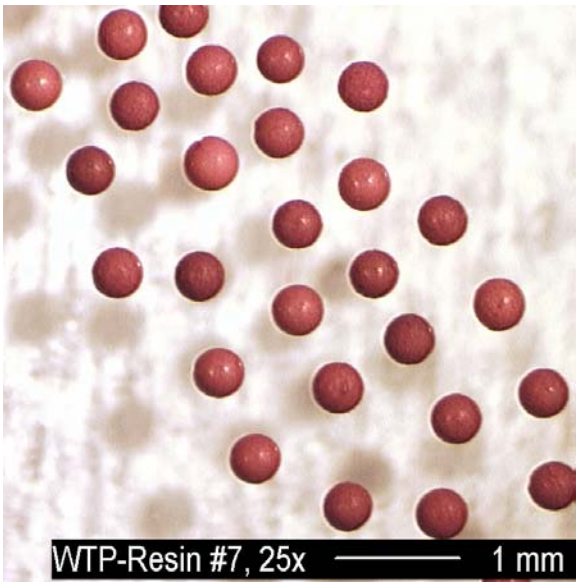

Resin #7 at 25x Magnifiction

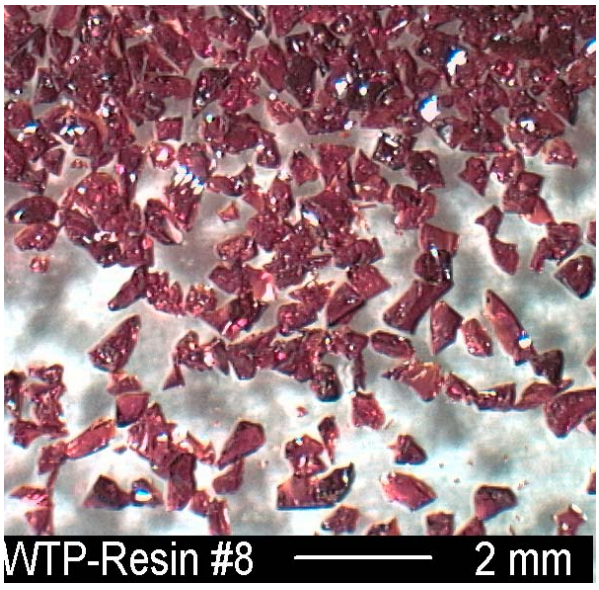

Resin #8 at 10x Magnification

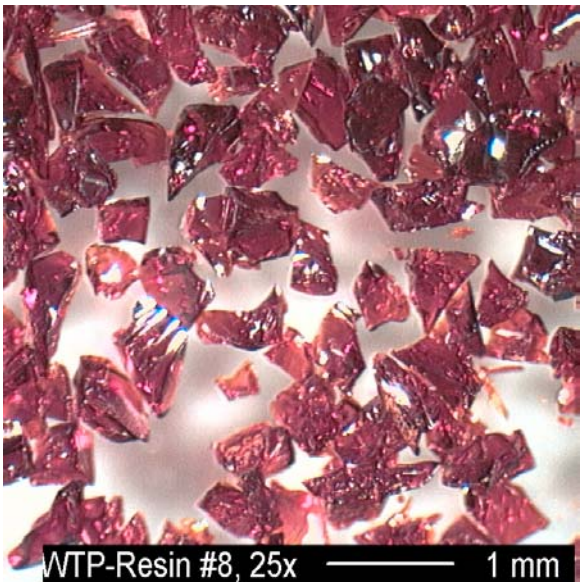

Resin #8 at 25x Magnification

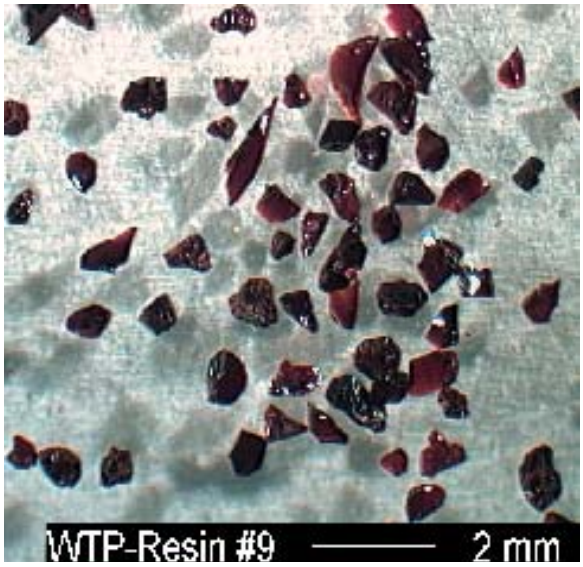

Resin #9 10x Magnification

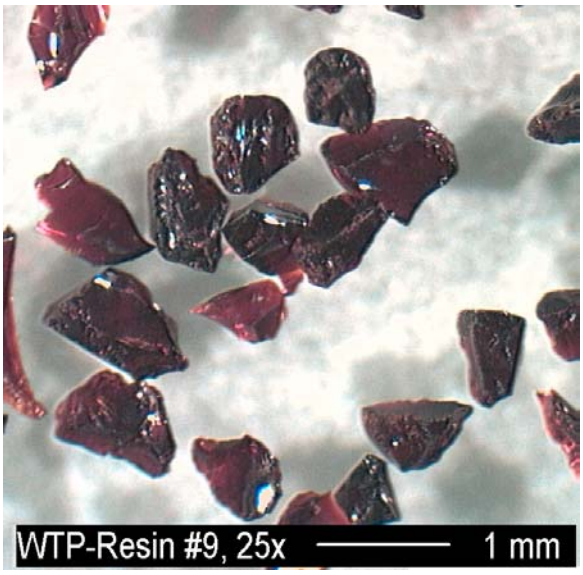

Resin #9 at 25x Magnification

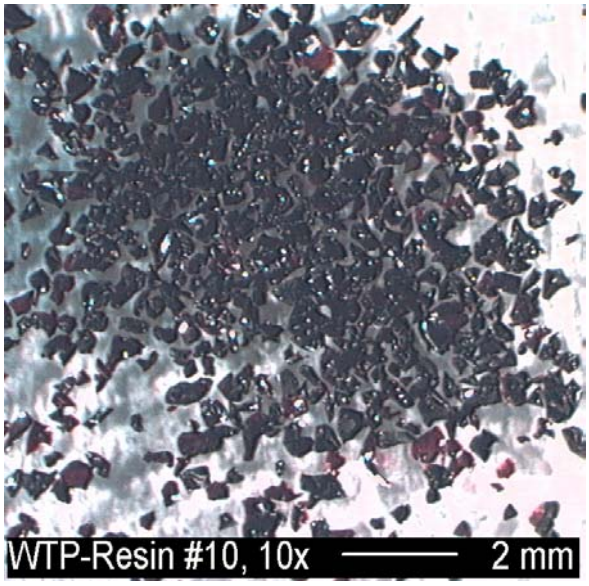

Resin #10 10x Magnification

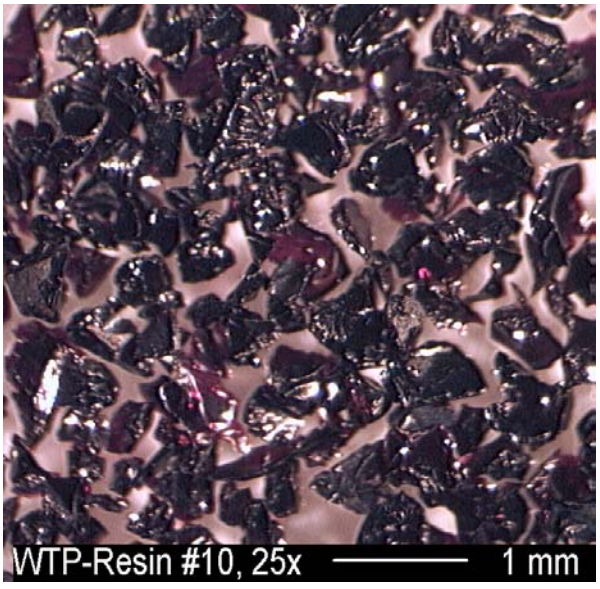

Resin #10 25x Magnification

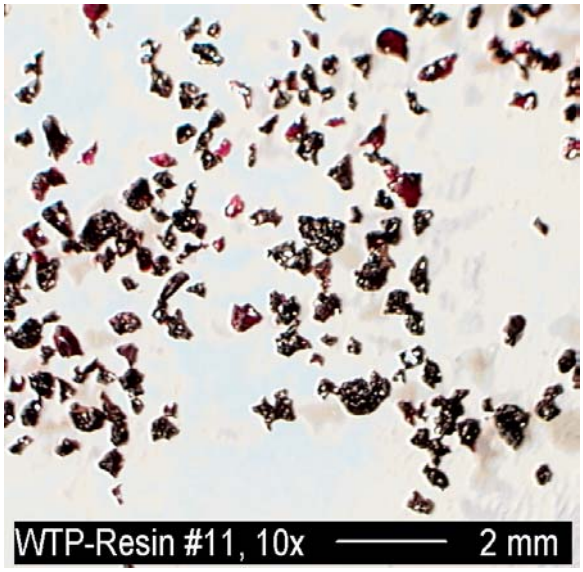

Resin #11 10x Magnification

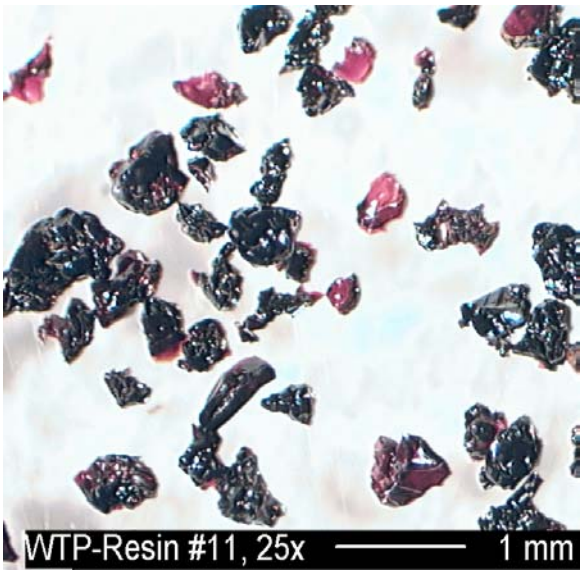

Resin #11 25x Magnification

Appendix B

Batch-Contact Testing

Appendix B: Batch-Contact Testing

Batch-Contact Equilibrium Confirmation

Table B.1 summarizes the batch-contact equilibrium data input values obtained as a function of time for resins #1, 3, 4, 6, 7, 8, 9, 10, and 11. The contact solution was composed of AZ-102 simulant at an initial Cs concentration of 681 mg/L. The data support the summaries presented in Table 4.1 and Figure 4.1. The raw data used to generate these data points are maintained in the project file 42365 at Battelle—Pacific Northwest Division.

Table B.1. Equilibrium Confirmation of Batch Contacts

Sample ID	IX Material	Resin mass, g	F factor	Corrected resin mass, g	Simulant volume[(a)], mL	Mass: volume ratio	Comparitor ^{137}Cs cpm/mL	Sample ^{137}Cs cpm/mL	Contact time, h	K_d, mL/g
249-AZ-S4-1T1A	1	0.2148	0.6672	0.1433	19.8290	138	9943	3891	24	215
249-AZ-S4-1T1B	1	0.2160	0.6672	0.1441	19.8449	138	9943	3943	24	210
249-AZ-S4-1T2A	1	0.2132	0.6672	0.1422	20.0342	141	9943	3997	50	210
249-AZ-S4-1T2B	1	0.2064	0.6672	0.1377	20.0323	145	9943	4119	50	206
249-AZ-S4-1T3A	1	0.2308	0.6672	0.1540	20.0071	130	9943	3796	72	210
249-AZ-S4-1T3B	1	0.2226	0.6672	0.1485	19.9778	135	9943	3896	72	209
249-AZ-S4-1	1	0.2198	0.6672	0.1466	20.0348	137	9943	3917	96	210
249-AZ-S4-1D	1	0.2191	0.6672	0.1462	19.7538	135	9943	3815	96	217
249-AZ-S4-3T1A	3	0.2161	0.5103	0.1103	19.8024	180	9943	4024	24	264
249-AZ-S4-3T1B	3	0.2180	0.5103	0.1112	19.7382	177	9943	3911	24	274
249-AZ-S4-3T2A	3	0.2248	0.5103	0.1147	20.0295	175	9943	3883	50	273
249-AZ-S4-3T2B	3	0.2280	0.5103	0.1163	19.9445	171	9943	3872	50	269
249-AZ-S4-3T3A	3	0.2092	0.5103	0.1068	19.6643	184	9943	4100	72	263
249-AZ-S4-3T3B	3	0.2191	0.5103	0.1118	19.6652	176	9943	3891	72	274
249-AZ-S4-3	3	0.2141	0.5103	0.1093	20.0028	183	9943	4090	96	262
249-AZ-S4-3D	3	0.2329	0.5103	0.1188	20.0200	168	9943	3808	96	271
249-AZ-S4-4T1A	4	0.2211	0.8987	0.1987	20.0506	101	424.2	164.8	24	159
249-AZ-S4-4T1B	4	0.2249	0.8987	0.2021	20.0437	99	424.2	168.7	24	150
249-AZ-S4-4T2A	4	0.2153	0.8987	0.1935	20.0845	104	426.4	173.2	48	152

Table B.1 (Contd)

Sample ID	IX Material	Resin mass, g	F factor	Corrected resin mass, g	Simulant volume[(a)], mL	Mass: volume ratio	Comparitor ^{137}Cs cpm/mL	Sample ^{137}Cs cpm/mL	Contact time, h	K_d, mL/g
249-AZ-S4-4T2B	4	0.2261	0.8987	0.2032	20.0759	99	426.4	159.1	48	166
249-AZ-S4-4T3A	4	0.2211	0.8987	0.1987	20.0784	101	426.4	168.0	72	155
249-AZ-S4-4T3B	4	0.2231	0.8987	0.2005	20.1054	100	426.4	169.4	72	152
249-AZ-S4-4	4	0.2218	0.8987	0.1993	20.0274	100	421.7	172.1	96	146
249-AZ-S4-4D	4	0.2260	0.8987	0.2031	20.1323	99	421.7	176.8	96	137
249-AZ-S4-6T1A	6	0.2206	0.5192	0.1145	19.9774	174	9943	4386	24	221
249-AZ-S4-6T1B	6	0.2206	0.5192	0.1145	19.9436	174	9943	4402	24	219
249-AZ-S4-6T2A	6	0.2313	0.5192	0.1201	19.8829	166	9943	4280	50	219
249-AZ-S4-6T2B	6	0.2249	0.5192	0.1168	19.8570	170	9943	4384	50	216
249-AZ-S4-6T3A	6	0.2189	0.5192	0.1136	19.5467	172	9943	4460	72	211
249-AZ-S4-6T3B	6	0.2521	0.5192	0.1309	19.5817	150	9943	3993	72	223
249-AZ-S4-6	6	0.2391	0.5192	0.1241	19.7348	159	9943	4327	96	206
249-AZ-S4-6D	6	0.2162	0.5192	0.1122	19.7413	176	9943	4656	96	200
249-AZ-S4-7T1A	7	0.2225	0.6932	0.1542	20.0996	130	424.2	192.3	24	157
249-AZ-S4-7T1B	7	0.2186	0.6932	0.1515	20.2109	133	424.2	198.9	24	151
249-AZ-S4-7T2A	7	0.2246	0.6932	0.1557	20.0595	129	426.4	193.1	48	156
249-AZ-S4-7T2B	7	0.2213	0.6932	0.1534	19.9580	130	426.4	194.6	48	155
249-AZ-S4-7T3A	7	0.2176	0.6932	0.1508	19.9390	132	426.4	197.0	72	154
249-AZ-S4-7T3B	7	0.2180	0.6932	0.1511	20.0114	132	426.4	195.3	72	157
249-AZ-S4-7	7	0.2241	0.6932	0.1553	20.0480	129	421.7	207.8	96	133
249-AZ-S4-7D	7	0.2194	0.6932	0.1521	20.0619	132	421.7	203.0	96	142
249-AZ-S4-8T1A	8	0.2500	0.6864	0.1716	19.8586	116	9972	3422	24	221
249-AZ-S4-8T1B	8	0.2483	0.6864	0.1704	19.4626	114	9972	3392	24	221
249-AZ-S4-8T2A	8	0.2404	0.6864	0.1650	19.8636	120	9972	3550	50	218
249-AZ-S4-8T2B	8	0.2282	0.6864	0.1566	19.9657	127	9972	3660	50	220
249-AZ-S4-8T3A	8	0.2181	0.6864	0.1497	19.8861	133	9972	3913	72	206
249-AZ-S4-8T3B	8	0.2239	0.6864	0.1537	19.9306	130	9972	3814	72	209

Table B.1 (Contd)

Sample ID	IX Material	Resin mass, g	F factor	Corrected resin mass, g	Simulant volume[(a)], mL	Mass: volume ratio	Comparitor ^{137}Cs cpm/mL	Sample ^{137}Cs cpm/mL	Contact time, h	K_d, mL/g
249-AZ-S4-8	8	0.2288	0.6864	0.1570	20.0257	128	9972	3821	96	205
249-AZ-S4-8D	8	0.2165	0.6864	0.1486	20.0350	135	9972	4052	96	197
249-AZ-S4-9T1A	9	0.2198	0.6838	0.1503	19.9503	133	9972	5182	24	123
249-AZ-S4-9T1B	9	0.2322	0.6838	0.1588	19.9310	126	9972	5049	24	122
249-AZ-S4-9T2A	9	0.2207	0.6838	0.1509	19.9044	132	9972	5233	50	119
249-AZ-S4-9T2B	9	0.2355	0.6838	0.1610	19.8699	123	9972	4963	50	125
249-AZ-S4-9T3A	9	0.2128	0.6838	0.1455	19.8639	137	9972	5349	72	118
249-AZ-S4-9T3B	9	0.2147	0.6838	0.1468	19.7772	135	9972	5267	72	120
249-AZ-S4-9	9	0.2189	0.6838	0.1497	19.7085	132	9972	5313	96	115
249-AZ-S4-9D	9	0.2178	0.6838	0.1489	19.8140	133	9972	5310	96	117
249-AZ-S4-10T1A	10	0.2202	0.6888	0.1517	20.0133	132	424.2	252.5	24	90
249-AZ-S4-10T1B	10	0.2220	0.6888	0.1529	20.0834	131	424.2	251.4	24	90
249-AZ-S4-10T2A	10	0.2274	0.6888	0.1566	20.1238	128	426.4	251.9	48	89
249-AZ-S4-10T2B	10	0.2214	0.6888	0.1525	20.0089	131	426.4	250.1	48	93
249-AZ-S4-10T3A	10	0.2213	0.6888	0.1524	20.0342	131	426.4	249.9	72	93
249-AZ-S4-10T3B	10	0.2231	0.6888	0.1537	20.0385	130	426.4	253.8	72	89
249-AZ-S4-10	10	0.2245	0.6888	0.1546	19.9995	129	421.7	251.9	96	87
249-AZ-S4-10D	10	0.2298	0.6888	0.1583	20.0372	127	421.7	246.6	96	90
249-AZ-S4-11T1A	11	0.2189	0.8674	0.1899	20.0437	106	424.2	209.5	24	108
249-AZ-S4-11T1B	11	0.2208	0.8674	0.1915	20.0352	105	424.2	206.0	24	111
249-AZ-S4-11T2A	11	0.2220	0.8674	0.1926	20.0342	104	426.4	214.2	48	103
249-AZ-S4-11T2B	11	0.2231	0.8674	0.1935	20.0166	103	426.4	211.3	48	105
249-AZ-S4-11T3A	11	0.2211	0.8674	0.1918	20.0875	105	426.4	211.6	72	106
249-AZ-S4-11T3B	11	0.2205	0.8674	0.1913	20.0879	105	426.4	211.3	72	107
249-AZ-S4-11	11	0.2226	0.8674	0.1931	20.0940	104	421.7	216.1	96	99
249-AZ-S4-11D	11	0.2218	0.8674	0.1924	20.0712	104	421.7	214.3	96	101

Equilibrium Batch-Contact Values as a Function of Cesium Concentration

Table B.2 summarizes the initial Cs concentrations in the five batch-contact solutions. Table B.3 summarizes the input data used for calculating the batch-contact equilibrium value (K_d) for resins #1, 3, 4, 6, 7, 8, 9, 10, and 11 in the AZ-102 simulant matrix. The data supports the summaries presented in Tables 4.2 and 4.3 and Figures 4.2 through 4.5. Samples were contacted for nominally 96 h. The raw data used to generate these data points are maintained in the project file 42365 at Battelle, PNWD.

Table B.2. AZ-102 Stock Contact Solutions

Sample ID	Cs conc., mg/L	Cs conc., M
249-AZ-S5-C	6.55E-03	4.93E-08
249-AZ-S5-CD	6.55E-03	4.93E-08
249-AZ-S1-C	49.9	4.48E-04
249-AZ-S1-CD	49.9	4.48E-04
249-AZ-S2-C	96.6	7.27E-04
249-AZ-S2-CD	96.6	7.27E-04
249-AZ-S3-C	177.7	1.34E-03
249-AZ-S3-CD	177.7	1.34E-03
249-AZ-S4-C	681.1	5.12E-03
249-AZ-S4-CD	681.1	5.12E-03

Table B.3. AZ-102 Simulant Batch-Contact Data

Sample ID	IX Material	Resin mass, g	F factor	Corrected resin mass, g	Simulant volume[(a)], mL	Mass: Volume ratio	Comparitor ^{137}Cs cpm/mL	Sample ^{137}Cs cpm/mL	Fraction Cs in solution	Equil. Cs molarity	Equil. Cs, mg/mL	Equil. Cs in resin, mg/g	K_d, mL/g
249-AZ-S5-1	1	0.2258	0.6533	0.1475	20.0055	136	3252	164.3	0.051	2.49E-09	3.31E-07	8.44E-04	2548
249-AZ-S5-1D	1	0.2180	0.6533	0.1424	19.6030	138	3252	167.5	0.051	2.54E-09	3.38E-07	8.56E-04	2535
249-AZ-S1-1	1	0.2219	0.6672	0.1480	20.3005	137	394.3	42.0	0.107	4.00E-05	5.32E-03	6.11	1149
249-AZ-S1-1D	1	0.2144	0.6672	0.1430	20.2961	142	394.3	42.6	0.108	4.06E-05	5.39E-03	6.32	1171
249-AZ-S2-1	1	0.2149	0.6672	0.1434	20.1537	141	398.8	58.1	0.146	1.06E-04	1.41E-02	11.6	825
249-AZ-S2-1D	1	0.2107	0.6672	0.1406	20.1310	143	398.8	57.2	0.144	1.04E-04	1.39E-02	11.8	854
249-AZ-S3-1	1	0.2155	0.6672	0.1438	20.0146	139	397.7	76.4	0.192	2.57E-04	3.41E-02	20.0	586
249-AZ-S3-1D	1	0.2171	0.6672	0.1448	19.9852	138	397.7	72.4	0.182	2.43E-04	3.23E-02	20.1	620
249-AZ-S4-1	1	0.2198	0.6672	0.1466	20.0348	137	9943	3917	0.394	2.02E-03	2.68E-01	56.4	210
249-AZ-S4-1D	1	0.2191	0.6672	0.1462	19.7538	135	9943	3815	0.384	1.97E-03	2.61E-01	56.7	217
249-AZ-S5-3	3	0.2195	0.5210	0.1144	19.6287	172	3223	261.7	0.081	4.00E-09	5.32E-07	1.03E-03	1943
249-AZ-S5-3D	3	0.2176	0.5210	0.1134	19.6552	173	3223	281.7	0.087	4.31E-09	5.73E-07	1.04E-03	1810
249-AZ-S1-3	3	0.2230	0.5103	0.1138	20.3505	179	394.3	60.1	0.152	5.73E-05	7.61E-03	7.56	994
249-AZ-S1-3D	3	0.2179	0.5103	0.1112	20.3138	183	394.3	63.9	0.162	6.08E-05	8.08E-03	7.64	945
249-AZ-S2-3	3	0.2115	0.5103	0.1079	20.0682	186	398.8	83.6	0.210	1.52E-04	2.02E-02	14.2	702
249-AZ-S2-3D	3	0.2220	0.5103	0.1133	20.0270	177	398.8	73.3	0.184	1.34E-04	1.78E-02	13.9	785
249-AZ-S3-3	3	0.2382	0.5103	0.1215	19.7463	162	397.7	84.6	0.213	2.48E-04	3.78E-02	22.7	602
249-AZ-S3-3D	3	0.2181	0.5103	0.1113	19.5789	176	397.7	92.9	0.234	3.12E-04	4.15E-02	24.0	577
249-AZ-S4-3	3	0.2141	0.5103	0.1093	20.0028	183	9943	4090	0.411	2.11E-03	2.80E-01	73.4	262
249-AZ-S4-3D	3	0.2329	0.5103	0.1188	20.0200	168	9943	3808	0.383	1.96E-03	2.61E-01	70.8	271
249-AZ-S5-4	4	0.2202	0.8847	0.1948	20.2814	104	3223	313.5	0.097	4.80E-09	6.38E-07	6.16E-04	966
249-AZ-S5-4D	4	0.2214	0.8847	0.1959	20.3089	104	3223	312.2	0.097	4.78E-09	6.35E-07	6.14E-04	967
249-AZ-S1-4	4	0.2362	0.8987	0.2123	20.2679	95	435.5	67.6	0.155	5.83E-05	7.75E-03	4.02	519
249-AZ-S1-4D	4	0.2332	0.8987	0.2096	20.2075	96	435.5	69.4	0.159	5.99E-05	7.95E-03	4.04	508
249-AZ-S2-4	4	0.2217	0.8987	0.1992	20.1979	101	423.3	86.3	0.204	1.48E-04	1.97E-02	7.79	396
249-AZ-S2-4D	4	0.2246	0.8987	0.2019	20.1827	100	423.3	83.9	0.198	1.44E-04	1.91E-02	7.74	404

Table B.3 (Contd)

Sample ID	IX Material	Resin mass, g	F factor	Corrected resin mass, g	Simulant volume[(a)], mL	Mass: Volume ratio	Comparitor ^{137}Cs cpm/mL	Sample ^{137}Cs cpm/mL	Fraction Cs in solution	Equil. Cs molarity	Equil. Cs, mg/mL	Equil. Cs in resin, mg/g	K_d, mL/g
249-AZ-S3-4	4	0.2231	0.8987	0.2005	19.9442	99	420.9	107.7	0.256	3.42E-04	4.55E-02	13.2	289
249-AZ-S3-4D	4	0.2283	0.8987	0.2052	19.9436	97	420.9	103.3	0.245	3.28E-04	4.36E-02	13.0	299
249-AZ-S4-4	4	0.2218	0.8987	0.1993	20.0274	100	421.7	172.1	0.408	2.09E-03	2.78E-01	40.5	146
249-AZ-S4-4D	4	0.2260	0.8987	0.2031	20.1323	99	421.7	176.8	0.419	2.15E-03	2.86E-01	39.2	137
249-AZ-S5-6	6	0.2193	0.5276	0.1157	20.2924	175	3223	326.5	0.101	5.00E-09	6.64E-07	1.03E-3	1556
249-AZ-S5-6D	6	0.2202	0.5276	0.1162	20.2792	175	3223	364.2	0.113	5.57E-09	7.41E-07	1.01E-03	1370
249-AZ-S1-6	6	0.2159	0.5192	0.1121	20.3615	182	394.3	80.6	0.204	7.67E-05	1.02E-02	7.21	707
249-AZ-S1-6D	6	0.2339	0.5192	0.1214	20.3370	167	394.3	73.2	0.186	6.97E-05	9.27E-03	6.81	734
249-AZ-S2-6	6	0.2214	0.5192	0.1149	19.8949	173	398.8	92.4	0.232	1.68E-04	2.24E-02	12.8	574
249-AZ-S2-6D	6	0.2203	0.5192	0.1144	19.7985	173	398.8	95.5	0.239	1.74E-04	2.31E-02	12.7	550
249-AZ-S3-6	6	0.2151	0.5192	0.1117	20.0300	179	397.7	121.4	0.305	4.08E-04	5.43E-02	22.1	408
249-AZ-S3-6D	6	0.2189	0.5192	0.1136	19.8296	174	397.7	120.1	0.302	4.04E-04	5.37E-02	21.6	403
249-AZ-S4-6	6	0.2391	0.5192	0.1241	19.7348	159	9943	4327	0.435	2.23E-03	2.96E-01	61.2	206
249-AZ-S4-6D	6	0.2162	0.5192	0.1122	19.7413	176	9943	4656	0.468	2.40E-03	3.19E-01	63.7	200
249-AZ-S5-7	7	0.2214	0.7077	0.1567	20.2076	129	3223	366.1	0.114	5.60E-09	7.45E-07	7.49E-04	1006
249-AZ-S5-7D	7	0.2189	0.7077	0.1549	20.2168	130	3223	379.8	0.118	5.81E-09	7.72E-07	7.55E-04	977
249-AZ-S1-7	7	0.2200	0.6932	0.1525	20.1458	132	435.5	93.4	0.214	8.05E-05	1.07E-02	5.18	484
249-AZ-S1-7D	7	0.2205	0.6932	0.1528	20.1687	132	435.5	92.5	0.213	7.98E-05	1.06E-02	5.19	489
249-AZ-S2-7	7	0.2210	0.6932	0.1532	20.1480	132	423.3	108.3	0.256	1.86E-04	2.47E-02	9.45	383
249-AZ-S2-7D	7	0.2210	0.6932	0.1532	20.0695	131	423.3	109.8	0.259	1.88E-04	2.51E-02	9.37	374
249-AZ-S3-7	7	0.2229	0.6932	0.1545	20.0277	130	420.9	129.3	0.307	4.11E-04	5.46E-02	16.0	292
249-AZ-S3-7D	7	0.2235	0.6932	0.1549	19.9735	129	420.9	125.7	0.299	3.99E-04	5.30E-02	16.1	303
249-AZ-S4-7	7	0.2241	0.6932	0.1553	20.0480	129	421.7	207.8	0.493	2.53E-03	3.36E-01	44.6	133
249-AZ-S4-7D	7	0.2194	0.6932	0.1521	20.0619	132	421.7	203.0	0.481	2.47E-03	3.28E-01	46.6	142
249-AZ-S5-8	8	0.2204	0.6991	0.1541	20.2010	131	3182	152.6	0.048	2.36E-09	3.14E-07	8.18E-04	2603

Table B.3 (Contd)

Sample ID	IX Material	Resin mass, g	F factor	Corrected resin mass, g	Simulant volume[a], mL	Mass: Volume ratio	Comparitor ^{137}Cs cpm/mL	Sample ^{137}Cs cpm/mL	Fraction Cs in solution	Equil. Cs molarity	Equil. Cs, mg/mL	Equil. Cs in resin, mg/g	K_d, mL/g
249-AZ-S5-8D	8	0.2214	0.6991	0.1548	20.2408	131	3182	152.5	0.048	2.36E-09	3.14E-07	8.16E-04	2598
249-AZ-S1-8	8	0.2205	0.6864	0.1514	20.2258	134	10292	916.8	0.089	3.34E-05	4.44E-03	6.07	1367
249-AZ-S1-8D	8	0.2270	0.6864	0.1558	20.2148	130	10292	946.1	0.092	3.45E-05	4.59E-03	5.88	1282
249-AZ-S2-8	8	0.2453	0.6864	0.1684	20.0217	119	10084	1044.8	0.104	7.53E-05	1.00E-02	10.3	1029
249-AZ-S2-8D	8	0.2357	0.6864	0.1618	20.1274	124	10084	1143.5	0.113	8.24E-05	1.09E-02	10.7	973
249-AZ-S3-8	8	0.2467	0.6864	0.1693	20.1491	119	10169	1433.1	0.141	1.88E-04	2.50E-02	18.2	725
249-AZ-S3-8D	8	0.2235	0.6864	0.1534	20.0952	131	10169	1647.0	0.162	2.17E-04	2.88E-02	19.5	678
249-AZ-S4-8	8	0.2288	0.6864	0.1570	20.0257	128	10032	3802.0	0.379	1.94E-03	2.58E-01	53.9	209
249-AZ-S4-8D	8	0.2165	0.6864	0.1486	20.0350	135	10032	4092.3	0.408	2.09E-03	2.78E-01	54.4	196
249-AZ-S5-9	9	0.2214	0.7217	0.1598	20.2220	127	3262	355.2	0.109	5.37E-09	7.14E-07	7.39E-04	1036
249-AZ-S5-9D	9	0.2199	0.7217	0.1587	20.2613	128	3262	356.0	0.109	5.38E-09	7.15E-07	7.45E-04	1042
249-AZ-S1-9	9	0.2300	0.6838	0.1573	20.1606	128	10292	1714	0.167	6.25E-05	8.31E-03	5.33	642
249-AZ-S1-9D	9	0.2671	0.6838	0.1826	20.1627	110	10292	1399	0.136	5.10E-05	6.78E-03	4.76	702
249-AZ-S2-9	9	0.2115	0.6838	0.1446	19.7970	137	10084	2380	0.236	1.71E-04	2.28E-02	10.1	443
249-AZ-S2-9D	9	0.2247	0.6838	0.1537	19.6746	128	10084	2214	0.220	1.60E-04	2.12E-02	9.65	455
249-AZ-S3-9	9	0.2124	0.6838	0.1452	19.8827	137	10169	3153	0.310	4.15E-04	5.51E-02	16.8	305
249-AZ-S3-9D	9	0.2259	0.6838	0.1545	19.8001	128	10169	2831	0.278	3.72E-04	4.95E-02	16.4	332
249-AZ-S4-9	9	0.2189	0.6838	0.1497	19.7085	132	10032	5302	0.529	2.71E-03	3.60E-01	42.3	117
249-AZ-S4-9D	9	0.2178	0.6838	0.1489	19.8140	133	10032	5338	0.532	2.73E-03	3.62E-01	42.4	117
249-AZ-S5-10	10	0.2217	0.6829	0.1514	20.2185	134	3262	171.9	0.053	2.60E-09	3.45E-07	8.29E-04	2401
249-AZ-S5-10D	10	0.2210	0.6829	0.1509	20.2101	134	3262	169.3	0.052	2.56E-09	3.40E-07	8.32E-04	2446
249-AZ-S1-10	10	0.2206	0.6888	0.1519	20.1123	132	435.5	65.9	0.151	5.68E-05	7.55E-03	5.61	743
249-AZ-S1-10D	10	0.2224	0.6888	0.1532	20.1252	131	435.5	63.0	0.145	5.43E-05	7.22E-03	5.61	777
249-AZ-S2-10	10	0.2212	0.6888	0.1524	20.1362	132	423.3	93.9	0.222	1.61E-04	2.14E-02	9.93	464
249-AZ-S2-10D	10	0.2226	0.6888	0.1533	20.1129	131	423.3	93.3	0.220	1.60E-04	2.13E-02	9.88	464

Table B.3 (Contd)

Sample ID	IX Material	Resin mass, g	F factor	Corrected resin mass, g	Simulant volume[(a)], mL	Mass: Volume ratio	Comparitor ^{137}Cs cpm/mL	Sample ^{137}Cs cpm/mL	Fraction Cs in solution	Equil. Cs molarity	Equil. Cs, mg/mL	Equil. Cs in resin, mg/g	K_d, mL/g
249-AZ-S3-10	10	0.2282	0.6888	0.1572	20.0754	128	420.9	128.0	0.304	4.06E-04	5.40E-02	15.8	292
249-AZ-S3-10D	10	0.2189	0.6888	0.1508	20.0571	133	420.9	134.8	0.320	4.28E-04	5.69E-02	16.1	282
249-AZ-S4-10	10	0.2245	0.6888	0.1546	19.9995	129	421.7	251.9	0.597	3.06E-03	4.07E-01	35.5	87
249-AZ-S4-10D	10	0.2298	0.6888	0.1583	20.0372	127	421.7	246.6	0.585	3.00E-03	3.98E-01	35.8	90
249-AZ-S5-11	11	0.2228	0.8635	0.1924	20.1828	105	3262	129.1	0.040	1.95E-09	2.59E-07	6.60E-04	2545
249-AZ-S5-11D	11	0.2212	0.8635	0.1910	20.1823	106	3262	116.8	0.036	1.77E-09	2.35E-07	6.68E-04	2847
249-AZ-S1-11	11	0.2223	0.8674	0.1928	20.1860	105	435.5	42.5	0.098	3.67E-05	4.88E-03	4.71	967
249-AZ-S1-11D	11	0.2230	0.8674	0.1934	20.1480	104	435.5	41.9	0.096	3.62E-05	4.81E-03	4.70	978
249-AZ-S2-11	11	0.2212	0.8674	0.1919	20.0940	105	423.3	63.0	0.149	1.08E-04	1.44E-02	8.61	599
249-AZ-S2-11D	11	0.2211	0.8674	0.1918	20.0635	105	423.3	64.0	0.151	1.10E-04	1.46E-02	8.57	587
249-AZ-S3-11	11	0.2201	0.8674	0.1909	20.0633	105	420.9	95.3	0.226	3.03E-04	4.02E-02	14.4	359
249-AZ-S3-11D	11	0.2195	0.8674	0.1904	20.1090	106	420.9	94.6	0.225	3.00E-04	3.99E-02	14.6	364
249-AZ-S4-11	11	0.2226	0.8674	0.1931	20.0940	104	421.7	216.1	0.512	2.63E-03	3.49E-01	34.6	99
249-AZ-S4-11D	11	0.2218	0.8674	0.1924	20.0712	104	421.7	214.3	0.508	2.60E-03	3.46E-01	35.0	101

Appendix C

Breakthrough and Elution Testing

Appendix C: Breakthrough and Elution Testing

The following data tables provide the data points shown in Figures 5.1 through 5.19. The raw data used to generate these data points are maintained in the Project File 42365 at Battelle—Pacific Northwest Division.

Table C.1. Column 1 Load and Elution Data, SL-644 with AZ-102 Simulant

Cycle 1 Load			Cycle 1 Elution		Cycle 2 Load		
BV	% C/C_o	Extended Count % C/C_o	BV	C/C_o	BV	% C/C_o	Extended Count % C/C_o
2.5	<2.49E-2	--	1.08	1.85E-2	3.4	<2.53E-2	--
4.3	<2.49E-2	--	2.24	6.21E-2	8.2	<2.53E-2	--
22.8	<2.49E-2	--	3.61	5.37E+1	13.0	<2.53E-2	<5.29E-3
31.8	3.63E-2	--	4.87	1.29E+2	36.5	<2.53E-2	<6.57E-3
41.9	<2.49E-2	--	5.66	2.33E+1	48.9	<2.53E-2	--
61.0	<2.49E-2	--	6.99	2.76E+0	76.8	<2.53E-2	<1.59E-2
70.8	<2.49E-2	<1.02E-2	8.02	1.08E+0	97.0	<2.53E-2	--
77.4	<2.49E-2	--	9.33	5.17E-1	116.8	<2.53E-2	--
81.4	5.55E-2	--	10.62	2.30E-1	133.5	2.83E-2	--
97.9	<2.49E-2	--	12.00	7.99E-2	Catastrophic column loss		
107.3	<2.49E-2	--	12.21	3.61E-2	143.0	<2.53E-2	--
116.7	<2.49E-2	--	17.85	1.18E-2	162.0	7.55E-2	--
125.9	3.71E-2	--	19.02	2.47E-3	173.6	8.67E-1	--
135.1	<2.49E-2	--	20.26	2.42E-3			
144.4	3.96E-2	--	21.59	1.87E-3			
154.0	<2.49E-2	--	22.79	1.30E-3			
172.8	<2.49E-2	1.84E-2	24.00	1.50E-3			
183.2	7.12E-2	--	25.26	1.07E-3			
192.7	2.03E-1	--	26.54	1.27E-3			
211.9	4.95E+0	--	28.21	1.46E-3			
220.9	1.49E+1	--	29.44	1.15E-3			
230.7	3.66E+1	--	30.62	1.51E-3			
250.4	6.99E+1	--	31.52	1.28E-3			
			32.59	1.57E-3			
			33.80	1.37E-3			
			34.96	1.13E-3			
			36.19	1.08E-3			
			37.37	1.23E-3			
			38.58	1.29E-3			

Table C.2. Column 2 Load and Elution Data, Resin #9 with AZ-102 Simulant

Cycle 1					Cycle 2				Cycle 3					Cycle 4	
Load			Elution (upflow)		Load		Elution (upflow)		Load			Elution (upflow)		Load (upflow)	
BV	% C/C_o	Extended Count % C/C_o	BV	C/C_o	BV	% C/C_o	BV	C/C_o	BV	Cs-137 % C/C_o	Cs-134 % C/C_o	BV	C/C_o	BV	% C/C_o
3.3	<2.74E-2	--	1.13	1.96E-2	3.3	<6.75E-3	0.37	8.12E-3	5.9	<2.47E-3	3.07E-2	0.84	3.03E-3	3.6	4.00E-2
5.4	<2.74E-2	--	2.23	7.70E-2	7.8	<9.94E-3	1.38	4.53E-3	11.7	<8.87E-4	2.05E-2	1.76	7.81E-3	16.2	4.17E-3
28.4	4.25E-2	--	3.25	1.59E-1	12.2	<5.17E-3	2.33	6.02E-2	35.6	<1.24E-3	1.09E-2	2.74	1.44E-1	25.0	1.37E-2
38.2	<2.74E-2	--	4.35	1.84E+1	34.5	<1.02E-2	3.36	6.36E-1	49.8	<3.56E-3	<1.17E-2	3.66	3.24E+0	35.2	2.81E-3
47.1	<2.74E-2	--	5.43	4.33E+1	47.2	<2.32E-2	4.40	2.29E+1	71.1	<1.24E-3	9.89E-3	4.64	2.13E+1	43.1	4.36E-2
65.1	<2.74E-2	--	6.29	5.29E+1	74.0	<1.69E-2	5.46	2.72E+1	86.7	<2.53E-3	1.22E-2	5.56	3.57E+1	50.6	4.16E-3
74.2	<2.74E-2	<1.51E-2	7.47	3.68E+1	91.8	<1.55E-2	6.49	2.94E+1	105.6	<3.28E-3	<1.17E-2	6.70	3.73E+1	56.4	2.00E-3
80.2	<2.74E-2	--	8.64	2.29E+1	110.8	<2.67E-2	7.65	2.11E+1	123.4	<4.04E-3	<1.29E-2	7.92	2.94E+1	68.7	4.12E-3
84.3	4.54E-2	--	9.91	1.54E+1	126.9	<2.48E-2	8.72	1.79E+1	143.8	2.49E-1	1.27E-2	9.38	1.61E+1	74.7	6.71E-3
99.9	<2.74E-2	--	10.13	1.25E+1	145.8	1.80E-1	9.95	1.62E+1	157.0	3.23E+0	<1.45E-2	10.79	5.58E+0	85.4	8.84E-3
108.9	<2.74E-2	--	12.64	4.42E+0	172.1	1.95E+1	10.99	1.39E+1	181.1	4.94E+1	1.37E-1	12.15	2.27E+0		
117.9	<2.74E-2	--	16.26	4.46E-1	183.2	4.71E+1	12.04	1.20E+1	184.6	7.50E+1	<9.14E-2	13.50	1.02E+0		
126.7	7.91E-2	<1.65E-2	17.37	3.17E-1	189.4	5.20E+1	13.08	1.00E+1	--	--	--	14.84	4.34E-1		
135.7	7.70E-2	--	18.59	1.62E-1	193.6	7.10E+1	14.17	6.12E+0	--	--	--	16.17	1.74E-1		
144.6	3.98E-2	--	19.66	8.22E-2	--	--	15.27	3.49E+0	--	--	--	17.58	8.47E-2		
153.6	5.91E-1	--	20.73	4.79E-2					--	--	--	18.91	3.46E-2		
161.9	7.83E+0	--	21.85	3.47E-2					--	--	--	20.31	1.64E-2		
171.6	2.26E+1	--	23.00	2.12E-2					--	--	--	21.67	8.71E-3		
180.4	3.81E+1	--	24.49	1.55E-2					--	--	--	23.11	6.69E-3		
198.3	6.65E+1	--	25.61	1.07E-2					--	--	--	24.50	4.22E-3		
205.2	8.31E+1	--	26.68	6.11E-3											
--	--	--	27.48	4.92E-3											
--	--	--	28.45	3.19E-3											
--	--	--	29.67	2.46E-3											
--	--	--	30.85	2.22E-3											
--	--	--	32.12	1.74E-3											
--	--	--	33.35	1.48E-3											
--	--	--	34.61	1.44E-3											

Table C.3. Column 3 Load and Elution Data, Resin #9 with AZ-102 Simulant

Cycle 1					Cycle 2				Cycle 3					Cycle 4	
Load			Elution		Load		Elution		Load			Elution		Load	
BV	% C/C_o	Extended Count % C/C_o	BV	C/C_o	BV	% C/C_o	BV	C/C_o	BV	Cs-137 % C/C_o	Cs-134 % C/C_o	BV	C/C_o	BV	% C/C_o
2.1	<2.59E-2	--	0.83	2.91E-2	3.45	<2.43E-2	0.88	0.024	5.3	<2.73E-3	<8.20E-3	0.90	1.11E-2	3.10	<4.55E-3
4.0	4.72E-2	--	1.64	4.56E-2	8.15	<2.43E-2	1.75	0.053	11.1	<1.37E-3	<4.25E-3	1.76	2.91E-2	13.3	<3.86E-3
20.9	3.18E-2	--	closed valve[a]		12.69	<8.85E-3	2.54	0.127	33.7	<1.26E-3	<3.76E-3	2.65	7.73E-2	20.5	<4.95E-3
23.5	<2.59E-2	--	2.69	1.26E-1	35.5	<9.96E-3	3.43	0.173	46.8	<3.50E-3	<1.01E-2	3.52	1.02E-1	29.0	2.17E-3
29.4	<2.59E-2	--	3.72	1.75E-1	48.6	<2.43E-2	4.32	0.713	67.8	<1.56E-3	<4.62E-3	4.37	9.66E-1	35.6	<4.08E-3
37.6	4.30E-2	--	4.61	9.74E+0	75.8	<2.43E-2	5.23	125.011	81.5	<2.66E-3	<7.94E-3	5.29	1.15E+2	42.1	<3.68E-3
54.0	4.18E-2	<8.61E-3	5.34	1.50E+2	93.9	<9.49E-3	6.17	94.891	99.4	<3.80E-3	<1.09E-2	6.47	3.55E+1	42.1	<1.30E-3
62.4	<4.18E-2	--	6.25	8.91E+1	113.0	<2.43E-2	7.13	8.254	116.1	<4.79E-3	<1.27E-2	7.80	5.23E+0	47.0	2.33E-3
68.0	6.00E-2	--	7.19	7.13E+0	129.2	<6.01E-2	8.09	3.779	134.9	1.83E-1	--	9.02	3.06E+0	57.5	<4.01E-3
71.7	4.02E-2	--	8.35	3.26E+0	147.9	3.71E+0	9.17	1.485	147.2	2.19E+0	--	10.19	4.96E-1	62.6	<5.22E-3
85.9	<2.59E-2	--	10.28	3.74E-1	174.4	5.00E+1	10.15	0.601	169.9	5.14E+1	--	11.34	1.81E-1	71.8	1.88E-3
94.6	<2.59E-2	--	13.06	3.91E-2	185.6	7.72E+1	11.14	0.262	173.1	4.64E+1	--	12.51	7.21E-2		
103.9	<2.59E-2	--	13.90	2.05E-2	189.3	8.06E+1	12.09	0.124	--	--	--	13.67	3.07E-2		
112.8	<2.59E-2	--	14.86	1.10E-2	--	--	13.16	0.060	--	--	--	14.87	1.48E-2		
122.1	2.59E-2	9.94E-2	15.87	7.20E-3	--	--	14.18	0.031	--	--	--	15.97	7.91E-3		
140.5	4.28E-1	3.07E-1	16.82	4.96E-3					--	--	--	17.13	4.98E-3		
158.6	6.34E+0	--	17.87	3.75E-3					--	--	--	18.27	3.06E-3		
168.6	1.95E+1	--	18.95	2.71E-3					--	--	--	19.51	2.11E-3		
177.6	4.04E+1	--	19.90	2.08E-3					--	--	--	20.69	1.60E-3		
196.0	6.72E+1	--	20.94	1.45E-3					--	--	--	21.81	1.30E-3		
202.0	8.40E+1	--	22.00	1.54E-3											
--	--	--	22.96	1.07E-3											
--	--	--	24.02	1.23E-3											
--	--	--	25.01	1.15E-3											
--	--	--	26.10	1.00E-3											
--	--	--	27.18	9.40E-4											
--	--	--	28.39	7.86E-4											
--	--	--	29.46	8.33E-4											
--	--	--	30.61	9.16E-4											

(a) Effluent valve was accidentally left closed causing system to pressurize to 10 psi.

Table C.4. Column 4 Load and Elution Data, Resin #9 with AP-101 Simulant

Cycle 1					Cycle 2				Cycle 3					Cycle 4	
Load			Elution		Load		Elution		Load			Elution		Load	
BV	% C/C_o	Extended Count % C/C_o	BV	C/C_o	BV	% C/C_o	BV	C/C_o	BV	Cs-137 % C/C_o	Cs-134 % C/C_o	BV	C/C_o	BV	% C/C_o
4.97	<4.68E-2	--	0.96	8.52E-3	5.86	<3.04E-2	1.00	7.40E-3	6.18	<2.11E-3	2.26E-2	1.07	8.61E-3	9.0	1.42E-2
10.2	6.71E-2	--	1.90	1.42E-2	23.3	<3.04E-2	1.99	1.67E-2	10.9	7.62E-4	2.66E-2	2.07	1.82E-2	33.7	1.41E-2
54.8	<4.68E-2	5.33E-2	2.84	3.83E-2	57.3	5.86E-2	2.87	4.03E-2	22.9	<2.28E-3	2.41E-2	3.12	1.39E-1	41.7	1.64E-2
65.4	2.80E-1	2.04E-1	3.79	2.08E+0	86.2	8.70E-1	3.89	7.49E+0	22.9*	9.23E-4	1.91E-2	4.11	4.14E+0	45.8	1.25E-2
75.4	6.00E-1	--	4.74	5.73E+1	120.1	6.78E+0	4.87	6.10E+1	71.1	3.67E-1	2.40E-2	5.10	6.70E+1	67.2	1.27E-2
85.3	1.23E+0	--	5.69	6.62E+1	136.1	1.20E+1	5.87	6.13E+1	98.2	2.44	3.21E-2	6.13	6.49E+1		
95.6	2.03E+0	--	6.93	4.13E+1	167.3	2.99E+1	6.92	3.64E+1	98.2*	2.42	<2.75E-2	7.46	1.77E+1		
126.6	9.05E+0	--	8.12	3.30E+0	187.7	4.20E+1	8.00	1.32E+1	141.0	13.40	<2.52E-2	9.00	6.13E-1		
135.6	1.24E+1	--	9.25	3.61E-1	199.0	2.86E+1	9.05	4.36E-1	168.5	28.6	<6.07E-2	10.37	1.56E-1		
145.5	1.74E+1	--	10.45	1.27E-1	199.0	5.70E+1	10.22	1.26E-1	204.9	46.0	<5.03E-2	11.71	7.68E-2		
156.0	2.29E+1	--	11.62	7.10E-2	206.3	5.82E+1	11.30	6.79E-2	212.7	86.9	NA	13.04	4.17E-2		
166.2	2.89E+1	--	12.85	4.12E-2	--	--	12.36	4.18E-2	--	--	--	14.39	2.38E-2		
196.7	4.57E+1	--	14.15	2.57E-2	--	--	13.39	2.83E-2	--	--	--	15.75	1.50E-2		
206.0	5.20E+1	--	15.34	1.67E-2	--	--	14.55	1.88E-2	--	--	--	17.15	9.94E-3		
215.2	5.77E+1	--	16.55	1.00E-2	--	--	15.65	1.24E-2	--	--	--	18.45	7.49E-3		
--	--	--	17.81	9.17E-3					--	--	--	19.80	3.77E-3		
--	--	--	19.05	2.10E-2					--	--	--	21.14	2.25E-3		
--	--	--	20.29	5.07E-3					--	--	--	22.60	1.44E-3		
--	--	--	21.52	7.29E-3					--	--	--	23.99	9.40E-4		
--	--	--	22.75	4.51E-3					--	--	--	25.31	7.36E-4		
--	--	--	23.99	3.19E-3											
--	--	--	25.20	3.39E-3											
--	--	--	26.44	3.35E-3											
--	--	--	27.70	2.99E-3											
--	--	--	28.93	3.19E-3											
--	--	--	30.17	2.95E-3											
--	--	--	31.40	2.31E-3											
--	--	--	32.68	2.52E-3											
--	--	--	33.91	3.53E-3											

* Sample was counted twice.

Table C.5. Column 5 Load and Elution Data, Resin #11 with AZ-102 Simulant

Cycle 1				Cycle 2				Cycle 3				Cycle 4	
Load		Elution		Load		Elution		Load		Elution		Load	
BV	% C/C_o	BV	C/C_o	BV	% C/C_o	BV	C/C_o	BV	% C/C_o	BV	C/C_o	BV	% C/C_o
6.31	<2.43E-3	0.93	2.92E-2	**9.3**	6.88E-3	1.00	1.25E-2	**6.4**	9.46E-3	1.15	2.06E-2	**6.0**	5.03E-3
12.2	<2.54E-3	2.01	7.05E-2	**35.7**	2.33E-3	2.19	4.72E-2	**11.8**	1.35E-2	2.33	7.55E-2	**11.2**	3.40E-3
37.0	<2.56E-3	3.16	8.85E+0	**35.7**	4.15E-3	3.34	1.01E-1	**19.3**	8.02E-3	3.49	1.62E-1	**20.2**	3.21E-3
51.6	<2.18E-3	4.15	2.03E+1	**44.6**	3.08E-3	4.54	6.88E+1	**35.7**	6.54E-3	4.60	7.14E+1	**36.0**	3.08E-3
51.6	1.25E-3	5.31	2.01E+1	**49.1**	5.57E-3	5.40	2.98E+1	**45.6**	8.34E-3	5.72	1.02E+1	**44.5**	1.89E-3
73.4	1.13E-2	6.29	1.49E+1	**72.2**	7.47E-3	6.51	3.80E+0	**55.6**	6.66E-3	6.86	2.31E+0	**49.5**	3.31E-3
73.4	8.44E-3	7.63	1.08E+1	**82.7**	9.99E-2	8.09	1.48E+0	**75.1**	1.12E-2	8.62	1.14E+0	**54.1**	3.74E-3
87.8	1.22E+0	9.02	7.56E+0	**108.8**	5.20E+1	9.65	5.03E-1	**84.3**	2.71E-1	10.05	3.16E-1	**73.7**	4.67E-3
107.0	34	10.68	4.45E+0	**--**	--	11.25	1.32E-1	**94.2**	7.35E+0	11.58	1.04E-1	**83.1**	0.189
117.4	70	12.28	1.81E+0	**--**	--	Valve closed[a]		**114.6**	7.50E+1	13.03	4.10E-2	**87.8**	1.569
118.7	105	13.84	7.91E-1	**--**	--	11.60	7.68E-2	**117.7**	8.42E+1	14.49	2.01E-2		
--	--	15.41	3.21E-1	**--**	--	12.96	4.71E-2	**--**	--	15.94	1.15E-2		
--	--	16.95	1.53E-1	**--**	--	14.48	1.75E-2	**--**	--	17.39	7.53E-3		
--	--	18.50	8.05E-2	**--**	--	16.03	9.84E-3	**--**	--	18.87	5.24E-3		
--	--	20.13	4.22E-2	**--**	--	17.37	6.33E-3	**--**	--	20.36	3.96E-3		
--	--	21.66	2.69E-2	**--**	--	18.82	4.52E-3	**--**	--	21.81	3.03E-3		
--	--	23.23	1.54E-2					**--**	--	23.26	2.54E-3		
--	--	24.76	9.99E-3					**--**	--	24.71	2.23E-3		
--	--	26.36	8.33E-3					**--**	--	26.15	1.79E-3		
--	--	27.95	6.30E-3					**--**	--	27.59	1.46E-3		
--	--	29.47	4.82E-3					**--**	--	29.13	1.41E-3		
--	--	30.96	4.75E-3					**--**	--	30.45	1.15E-3		
--	--	32.49	3.18E-3					**--**	--	31.88	1.11E-3		
--	--	33.99	2.54E-3					**--**	--	33.44	9.47E-4		
--	--	35.50	2.20E-3					**--**	--	34.90	9.04E-4		
--	--	37.15	1.82E-3					**--**	--	Valve closed[a]			
--	--	38.61	1.70E-3					**--**	--	36.45	9.45E-4		
--	--	40.24	1.57E-3					**--**	--	37.99	8.61E-4		
--	--	41.73	1.51E-3					**--**	--	39.62	9.54E-4		

(a) Effluent valve was accidentally left closed causing system to pressurize to 10 psi.

Table C.6. Column 6 Load and Elution Data, Resin #1 with AZ-102 Simulant

Cycle 1				Cycle 2	
Load		Elution		Load	
BV	% C/C_o	BV	C/C_o	BV	% C/C_o
5.70	<1.33E-3	1.03	2.96E-2	**5.4**	<1.22E-3
11.0	<2.41E-3	2.09	8.38E-2	**10.4**	<8.61E-4
17.9	3.35E-3	3.13	1.73E-1	**19.2**	<3.25E-3
32.7	6.2	4.13	2.00E-1	**34.2**	13
41.5	28	5.16	1.39E+1	**42.2**	36
50.6	53	6.19	3.23E+1	**47.0**	50
68.4	80	7.93	9.19E-1	**51.5**	63
76.6	86	9.23	2.26E-1	**70.3**	86
85.7	90	10.70	4.56E-2		
104.4	90	12.10	8.79E-3		
107.0	95	13.51	2.22E-3		
--	--	14.92	8.48E-4		
--	--	16.34	5.39E-4		
--	--	17.78	3.45E-4		
--	--	19.20	3.86E-4		
--	--	20.59	2.48E-4		
--	--	21.99	2.55E-4		
--	--	23.39	1.24E-4		
--	--	24.79	1.44E-4		
--	--	26.18	1.66E-4		
--	--	27.66	1.93E-4		
--	--	28.96	1.11E-4		
--	--	30.37	1.71E-4		
--	--	31.91	1.27E-4		
--	--	33.35	2.01E-4		
--	--	Valve closed[a]			
--	--	34.85	2.78E-4		
--	--	36.38	1.09E-3		
--	--	37.90	5.15E-4		

(a) Effluent valve was accidentally left closed causing system to pressurize to 10 psi.

Table C.7. Column 7 Load and Elution Data, Resin #3 with AZ-102 Simulant

Cycle 1				Cycle 2				Cycle 3				Cycle 4	
Load		Elution		Load		Elution		Load		Elution		Load	
BV	% C/C_o	BV	C/C_o	BV	% C/C_o	BV	C/C_o	BV	% C/C_o	BV	C/C_o	BV	% C/C_o
5.1	<1.18E-3	0.94	2.13E-2	5.5	<1.39E-3	1.22	2.12E-2	9.7	<1.16E-3	0.89	2.13E-2	8.5	2.08E-3
9.8	2.23E-3	1.87	4.57E-2	10.6	1.51E-3	2.18	6.83E-2	25.1	<1.06E-3	1.88	5.12E-2	12.7	1.77E-3
16.8	<6.34E-4	2.83	1.06E-1	19.4	<1.04E-3	3.12	1.25E-1	31.9	<1.00E-3	2.85	1.24E-1	17.1	<1.32E-3
33.0	<6.59E-4	3.87	3.25E+0	35.4	<6.45E-4	4.15	4.81E+1	42.1	<9.80E-4	3.90	2.97E+1	25.3	1.23E-3
43.0	<1.13E-3	4.84	1.18E+2	43.9	<2.18E-3	5.18	8.61E+1	62.6	<1.12E-3	4.94	1.40E+2	35.7	1.39E-3
52.8	<7.14E-4	5.80	1.18E+1	48.9	<1.02E-3	6.19	5.84E+0	71.4	<2.28E-3	5.98	7.35E+0	44.7	<7.65E-4
72.3	<7.22E-4	6.28	4.16E+0	53.5	<7.24E-4	7.37	2.61E+0	83.3	<2.77E-3	7.51	2.72E+0	50.8	<7.36E-4
81.4	2.73E-3	7.61	2.11E+0	73.1	<7.79E-4	8.41	1.01E+0	101.2	1.44E-1	9.03	7.16E-1	58.3	<1.36E-3
91.2	2.26E-2	8.91	6.49E-1	82.3	3.03E-3	9.79	3.59E-1	110.3	7.03E-1	10.56	1.96E-1		
111.8	8.21E-1	10.42	1.94E-1	87.2	7.37E-3	10.50	1.42E-1	118.8	3.02E+0	12.08	5.97E-2		
119.9	2.97E+0	11.81	5.97E-2	92.9	1.98E-2	11.64	7.04E-2	140.2	40.8	13.57	2.46E-2		
134.6	2.15E+1	13.23	2.25E-2	112.3	8.38E-1	12.76	3.13E-2	147.7	64.0	15.11	8.44E-3		
149.9	6.22E+1	14.64	9.24E-3	120.2	3.02	13.85	1.54E-2	150.4	69.8	16.60	3.75E-3		
151.8	6.53E+1	16.04	2.15E-3	125.8	7.31	14.94	8.03E-3	--	--	18.10	1.90E-3		
152.5	6.88E+1	17.54	1.27E-3	131.2	15.09	16.01	4.53E-3	--	--	19.62	9.01E-4		
--	--	19.06	4.42E-3	148.8	60.16	17.09	2.66E-3	--	--	21.09	6.02E-4		
--	--	20.58	7.90E-4	152.7	67.77	18.17	1.42E-3	--	--	22.63	5.03E-4		
--	--	22.08	4.32E-4	--	--	19.25	1.01E-3	--	--	24.13	6.07E-4		
--	--	23.60	4.07E-4	--	--	19.75	1.11E-3	--	--	25.70	4.50E-4		
--	--	25.12	2.94E-4										
--	--	26.62	2.25E-4										
--	--	28.20	1.30E-4										
--	--	29.58	2.02E-4										
--	--	31.09	2.43E-4										
--	--	32.72	2.64E-4										
--	--	34.29	1.77E-4										
--	--	35.59	1.23E-4										
--	--	36.91	1.34E-4										
--	--	38.52	2.13E-4										

Table C.8. Column 8 Load and Elution Data, Resin #6 with AZ-102 Simulant

Cycle 1				Cycle 2				Cycle 3				Cycle 4	
Load		Elution		Load		Elution		Load		Elution		Load	
BV	% C/C_o	BV	C/C_o	BV	% C/C_o	BV	C/C_o	BV	% C/C_o	BV	C/C_o	BV	% C/C_o
5.6	<1.08E-3	1.05	6.52E-2	5.6	<2.08E-3	1.27	6.32E-2	9.7	1.84E-3	1.13	6.60E-2	8.2	<1.81E-3
11.0	<1.10E-3	2.07	7.36E-2	10.7	<2.06E-3	2.29	1.82E-1	25.5	<1.04E-3	2.16	8.90E-2	12.5	2.30E-3
18.4	<1.15E-3	3.04	1.61E-1	19.7	<2.01E-3	3.26	9.87E-2	32.3	<1.04E-3	3.13	1.84E-1	16.9	2.12E-3
34.8	<1.00E-3	4.11	1.32E+1	35.7	<1.97E-3	4.29	3.53E+1	42.6	1.79E-3	4.16	2.93E+1	25.0	1.26E-3
44.6	2.16E-3	5.12	5.94E+1	44.4	2.66E-3	5.29	4.24E+1	63.3	7.98E-1	5.21	4.26E+1	36.0	8.56E-4
54.4	4.62E-2	6.15	4.69E+0	49.5	7.36E-3	6.29	3.80E+0	72.2	6.71E+0	6.29	3.10E+0	45.2	1.50E-3
74.0	11	6.59	2.51E+0	54.1	3.17E-2	7.48	1.57E+0	84.2	5.72E+1	7.93	1.32E+0	51.4	<1.25E-3
83.1	44	7.98	1.30E+0	74.1	9.82E+0	8.52	5.51E-1	102.6	9.03E+1	9.40	3.43E-1	59.0	1.49E-3
92.9	77	9.27	3.81E-1	83.6	4.44E+1	9.93	1.74E-1	--	--	10.94	9.17E-2		
113.6	89	10.78	1.05E-1	88.5	6.99E+1	10.63	5.88E-2	--	--	12.46	2.57E-2		
116.8	91	12.18	2.93E-2	94.3	9.04E+1	11.74	2.67E-2	--	--	13.97	8.14E-3		
--	--	13.58	9.39E-3	114.1	9.22E+1	12.79	1.10E-2	--	--	15.52	2.60E-3		
--	--	14.99	3.15E-3	--	--	13.84	5.00E-3	--	--	17.02	9.61E-4		
--	--	16.42	1.70E-3	--	--	14.88	2.43E-3	--	--	18.52	5.68E-4		
--	--	17.87	5.00E-4	--	--	15.93	1.19E-3	--	--	20.04	3.00E-4		
--	--	19.37	2.82E-4	--	--	16.98	7.84E-4	--	--	21.53	1.75E-4		
--	--	20.88	<1.96E-4	--	--	18.03	7.12E-4	--	--	23.04	1.54E-4		
--	--	22.36	<1.96E-4	--	--	19.08	3.26E-4	--	--	24.54	2.69E-4		
--	--	23.88	<1.96E-4	--	--	19.57	2.97E-4	--	--	26.13	1.38E-4		
--	--	25.40	<1.96E-4										
--	--	26.89	<1.96E-4										
--	--	28.47	<1.96E-4										
--	--	29.89	<1.96E-4										
--	--	31.40	<1.96E-4										
--	--	33.04	<1.96E-4										
--	--	34.34	<1.96E-4										
--	--	35.91	<1.96E-4										
--	--	37.23	<1.96E-4										
--	--	38.83	<1.96E-4										

Table C.9. Column 9 Load and Elution Data, SL-644 (20- to 30-mesh) with AZ-102 Simulant

Cycle 1				Cycle 2	
Load		Elution		Load	
BV	% C/C_o	BV	C/C_o	BV	% C/C_o
6.0	<1.13E-3	1.06	2.60E-2	10.60	<2.28E-3
12.1	<1.17E-3	2.14	7.85E-2	15.80	2.84E-3
24.3	<1.17E-3	3.20	4.96E+1	20.60	9.48E-4
39.7	<8.83E-4	4.25	1.33E+2	29.30	<1.10E-3
60.7	<8.66E-4	5.27	3.91E+0	40.10	<2.10E-3
76.7	<1.11E-3	6.33	1.11E+0	49.30	<2.13E-3
100.0	1.72E-2	7.88	3.35E-1	55.70	<1.22E-3
120.2	2.66E-1	9.39	7.83E-2	63.40	2.02E-3
127.1	6.04E-1	10.95	1.97E-2		
145.1	4.35E+0	12.47	6.69E-3		
161.2	1.63E+1	13.29	3.33E-3		
168.6	2.63E+1	14.07	2.18E-3		
179.5	4.00E+1	15.55	1.64E-3		
201.4	7.06E+1	17.03	1.01E-3		
203.1	7.30E+1	18.49	1.14E-3		
--	--	19.98	8.41E-4		
--	--	21.45	5.98E-4		
--	--	22.95	4.41E-4		
--	--	24.48	6.58E-4		
--	--	25.98	3.46E-4		

Appendix D

Hydraulic Testing

Appendix D: Hydraulic Testing

Table D.1. Permeability Results for Resin #3

Cycle #	System	Flow (mL/min)	Solution	Permeability (m^2)
1	A	800	AP-101	3.34E-10
1	A	1200	AP-101	2.98E-10
1	A	1600	AP-101	2.75E-10
2	A	1600	AP-101	2.67E-10
3	A	1600	AP-101	2.73E-10
4	A	800	AP-101	2.92E-10
4	A	1200	AP-101	2.84E-10
4	A	1600	AP-101	2.73E-10
1	A	800	NaOH	3.17E-10
1	A	1200	NaOH	3.07E-10
1	A	1600	NaOH	2.87E-10
2	A	1600	NaOH	3.41E-10
3	A	1600	NaOH	2.67E-10
4	A	800	NaOH	3.23E-10
4	A	1200	NaOH	3.03E-10
4	A	1600	NaOH	2.67E-10
1	B	800	AP-101	2.87E-10
1	B	1200	AP-101	2.70E-10
1	B	1600	AP-101	2.43E-10
2	B	1600	AP-101	2.51E-10
3	B	1600	AP-101	2.19E-10
4	B	800	AP-101	2.13E-10
4	B	1200	AP-101	2.12E-10
4	B	1600	AP-101	2.17E-10
1	B	800	NaOH	2.91E-10
1	B	1200	NaOH	2.62E-10
1	B	1600	NaOH	2.34E-10
2	B	1600	NaOH	2.09E-10
3	B	1600	NaOH	1.95E-10
4	B	1200	NaOH	2.05E-10
4	B	1600	NaOH	1.92E-10

Table D.2. Permeability Results for Resin #9

Cycle #	System	Flow (mL/min)	Solution	Permeability (m^2)
1	A	800	AP-101	2.94E-10
1	A	1200	AP-101	2.84E-10
1	A	1600	AP-101	2.78E-10
2	A	1600	AP-101	2.02E-10
3	A	1600	AP-101	1.84E-10
4	A	800	AP-101	1.66E-10
4	A	1200	AP-101	1.63E-10
4	A	1600	AP-101	1.64E-10
1	A	800	NaOH	2.57E-10
1	A	1200	NaOH	2.34E-10
1	A	1600	NaOH	2.20E-10
2	A	1600	NaOH	3.73E-10
3	A	1600	NaOH	1.60E-10
4	A	800	NaOH	1.85E-10
4	A	1200	NaOH	1.66E-10
4	A	1600	NaOH	1.50E-10
1	B	800	AP-101	2.74E-10
1	B	1200	AP-101	2.40E-10
1	B	1600	AP-101	2.22E-10
2	B	1600	AP-101	1.58E-10
3	B	1600	AP-101	1.31E-10
4	B	800	AP-101	1.32E-10
4	B	1200	AP-101	1.29E-10
4	B	1600	AP-101	1.27E-10
1	B	800	NaOH	1.64E-10
1	B	1200	NaOH	1.51E-10
1	B	1600	NaOH	1.40E-10
2	B	1600	NaOH	1.08E-10
3	B	1600	NaOH	1.07E-10
4	B	800	NaOH	1.29E-10
4	B	1200	NaOH	1.18E-10
4	B	1600	NaOH	1.05E-10

Table D.3. Permeability Results for Resin #12

Cycle #	System	Flow (mL/min)	Solution	Permeability (m^2)
1	A	800	AP-101	2.58E-10
1	A	1200	AP-101	2.47E-10
1	A	1600	AP-101	2.42E-10
2	A	1600	AP-101	2.08E-10
3	A	1600	AP-101	1.85E-10
4	A	800	AP-101	1.85E-10
4	A	1200	AP-101	1.78E-10
4	A	1600	AP-101	1.73E-10
1	A	800	NaOH	1.83E-10
1	A	1200	NaOH	1.72E-10
1	A	1600	NaOH	1.64E-10
2	A	1600	NaOH	1.38E-10
3	A	1600	NaOH	1.28E-10
4	A	800	NaOH	1.44E-10
4	A	1200	NaOH	1.36E-10
4	A	1600	NaOH	1.20E-10
1	B	800	AP-101	1.96E-10
1	B	1200	AP-101	1.88E-10
1	B	1600	AP-101	1.85E-10
2	B	1600	AP-101	1.48E-10
3	B	1600	AP-101	1.19E-10
4	B	800	AP-101	1.33E-10
4	B	1200	AP-101	1.28E-10
4	B	1600	AP-101	1.24E-10
1	B	800	NaOH	1.01E-10
1	B	1200	NaOH	9.47E-11
1	B	1600	NaOH	9.12E-11
2	B	1600	NaOH	5.20E-11
3	B	1600	NaOH	6.40E-11
4	B	800	NaOH	7.96E-11
4	B	1200	NaOH	7.18E-11
4	B	1600	NaOH	6.83E-11

Table D.4. Density Results from Permeability Testing Samples During Loading and Regeneration

System A				System B			
Sample ID	Weight (g)	Volume (mL)	Density (g/mL)	Sample ID	Weight (g)	Volume (mL)	Density (g/mL)
R9-AP-c1[(a)]	61.76	50	1.2352	R9-AP-c1[(a)]	62.32	50	1.2464
R9-AP-c2	61.79	50	1.2358	R9-AP-c2	61.46	50	1.2292
R9-AP-c3	61.42	50	1.2284	R9-AP-c3	61.99	50	1.2398
R9-AP-c4	61.25	50	1.225	R9-AP-c4	61.89	50	1.2378
R9-Na-c1	51.89	50	1.0378	R9-Na-c1	51.27	50	1.0254
R9-Na-c2	51.04	50	1.0208	R9-Na-c2	50.92	50	1.0184
R9-Na-c3	50.93	50	1.0186	R9-Na-c3	50.67	50	1.0134
R9-Na-c4	51.22	50	1.0244	R9-Na-c4	51.66	50	1.0332
R3-AP-c1	61.97	50	1.2394	R3-AP-c1	61.96	50	1.2392
R3-AP-c2	61.27	50	1.2254	R3-AP-c2	Not Measured		
R3-AP-c3	60.67	50	1.2134	R3-AP-c3	61.77	50	1.2354
R3-AP-c4	60.19	50	1.2038	R3-AP-c4[(b)]	68.41	50	1.3682
R3-Na-c1	51.49	50	1.0298	R3-Na-c1	51.4	50	1.028
R3-Na-c2	51.44	50	1.0288	R3-Na-c2	51.02	50	1.0204
R3-Na-c3	51.57	50	1.0314	R3-Na-c3	51.63	50	1.0326
R3-Na-c4	51.07	50	1.0214	R3-Na-c4	51.32	50	1.0264
R12-AP-c1	61.92	50	1.2384	R12-AP-c1	61.84	50	1.2368
R12-AP-c2	61.74	50	1.2348	R12-AP-c2	62.09	50	1.2418
R12-AP-c3	61.05	50	1.221	R12-AP-c3	61.29	50	1.2258
R12-AP-c4	61.09	50	1.2218	R12-AP-c4	61.20	50	1.224
R12-Na-c1	51.51	50	1.0302	R12-Na-c1	51.58	50	1.0316
R12-Na-c2	51.70	50	1.034	R12-Na-c2	51.20	50	1.024
R12-Na-c3	51.54	50	1.0308	R12-Na-c3	51.44	50	1.0288
R12-Na-c4	51.63	50	1.0326	R12-Na-c4	51.45	50	1.029

(a) Nomenclature: RX-YY-cZ where X is Resin #, YY is either AP-101 loading or NaOH regeneration, Z is cycle #

(b) Result is suspect.

Table D.5. Viscosity Results from Permeability Testing Samples During Loading and Regeneration

Sample ID	Temperature (°C)	Viscosity (cp)
12-AP-101-A-c1	24.4	2.64
12-AP-101-A-c4	24.3	2.49
12-AP-101-B-c1	24.4	2.77
12-AP-101-B-c2	24.4	2.80
12-AP-101-B-c3	24.4	2.69
12-AP-101-B-c4	24.4	2.65
12-NaOH-A-c1	23.9	1.14
12-NaOH-A-c4	23.9	1.12
12-NaOH-B-c1	22.9	1.16
12-NaOH-B-c2	23.9	1.11
12-NaOH-B-c3	24.0	1.12
3-AP-101-A-c1	24.6	2.64
3-AP-101-A-c2	23.8	2.59
3-AP-101-B-c1	24.4	2.81
3-AP-101-B-c3	23.9	2.72
3-NaOH-A-c1	23.9	1.11
3-NaOH-A-c3	24.0	1.13
3-NaOH-B-c1	23.9	1.12
3-NaOH-B-c4	23.9	1.12
9-AP-101-A-c1	24.6	2.62
9-AP-101-A-c2	24.7	2.56
9-AP-101-A-c3	24.7	2.60
9-AP-101-A-c4	24.6	2.52
9-AP-101-B-c1	24.7	2.92
9-AP-101-B-c2	24.6	2.67
9-AP-101-B-c3	23.9	2.78
9-AP-101-B-c4	24.7	2.72
9-NaOH-A-c1	23.4	1.10
9-NaOH-A-c2	23.9	1.08
9-NaOH-B-c1	23.4	1.13
9-NaOH-B-c2	23.9	1.09
9-NaOH-B-c3	23.4	1.04
Nomenclature: X-YYYY-Z-cN where X is Resin #, YYYY is either AP-101 loading or NaOH regeneration, Z is the system and N is the cycle #.		

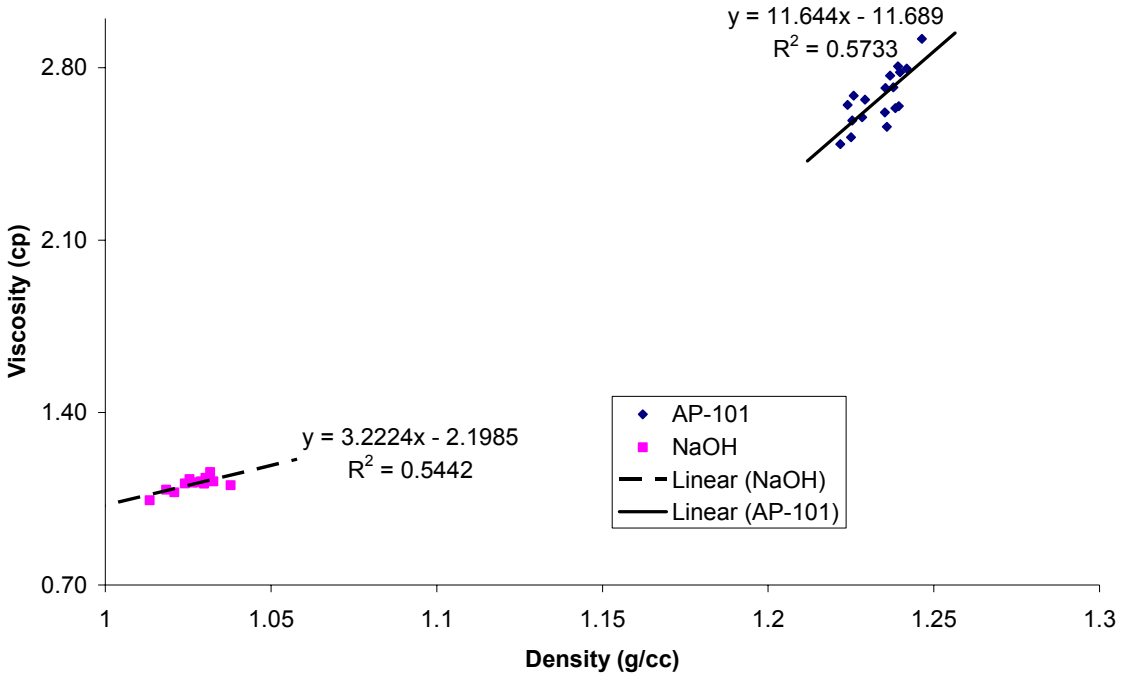

Figure D.1. Correlation between Density and Viscosity for Permeability Samples

Table D.6. Compressibility Results for Resin #3

Cycle 1							
Pressure (psi)	**Height[(a)] (mm)**	**Time (min)**	**Side Load (g)**	**Bottom Load (g)**	**Height[(b)] (mm)**	**Side (psi)**	**Bottom (psi)**
0	37.3	0	5	-5	38.3	0.22	-0.22
5	37.3	1	10	164	37.6	0.45	7.37
10	36.5	2	22	292	37.2	0.99	13.11
15	36.5	3	41	450	36.8	1.84	20.21
20	35.7	5	60	593	36.4	2.69	26.63
15	35.7	7	62	537	36.5	2.78	24.12
10	36.5	8	52	419	37.0	2.34	18.82
5	36.5	10	34	243	37.1	1.53	10.91
1	37.3	11	19	51	38.2	0.85	2.29
Cycle 2							
1	37.3	0	19	51	38.2	0.85	2.29
5	37.3	2	26	136	37.9	1.17	6.11
10	36.5	3	39	282	37.2	1.75	12.67
15	36.5	5	55	432	37.1	2.47	19.40
20	36.5	6	73	590	37.1	3.28	26.50
15	36.5	8	68	530	37.1	3.05	23.80
10	36.5	9	57	416	37.1	2.56	18.68
5	36.5	12	46	242	37.5	2.07	10.87
1	37.3	13	28	61	38.3	1.26	2.74
Cycle 3							
1	37.3	0	28	61	38.3	1.26	2.74
5	37.3	2	35	136	37.5	1.57	6.11
10	37.3	3	48	275	37.3	2.16	12.35
15	36.5	4	64	428	37.2	2.87	19.22
20	36.5	6	80	569	37.0	3.59	25.56
15	36.5	7	73	514	37.1	3.28	23.08
10	36.5	8	63	404	37.2	2.83	18.14
5	36.5	9	48	236	37.2	2.16	10.60
1	37.3	10	34	85	37.6	1.53	3.82
Cycle 4							
1	37.3	0	34	85	37.6	1.53	3.82
5	37.3	1	40	147	37.7	1.80	6.60
10	36.5	3	55	275	37.5	2.47	12.35
15	36.5	4	70	421	37.5	3.14	18.91
20	36.5	5	86	566	37.5	3.86	25.42
20	36.5	10	88	568	37.3	3.95	25.51
15	36.5	11	81	515	37.3	3.64	23.13
10	36.5	12	69	404	37.3	3.10	18.14
5	36.5	13	53	239	37.3	2.38	10.73
0	38.1	14	7	6	39.0	0.31	0.27

(a) Height was measured both with a ruler.
(b) Height was measured with a caliper.

Table D.7. Compressibility Results for Resin #9

Pressure (psi)	Height[(a)] (mm)	Time (min)	Side Load (g)	Bottom Load (g)	Height[(b)] (mm)	Side (psi)	Bottom (psi)
Cycle 1 1.5	43.7	0	-3	27	44	-0.13	1.21
5	42.9	5	2	83	43	0.09	3.73
10	42.1	7	7	176	42	0.31	7.90
15	41.3	14	17	269	41	0.76	12.08
20	40.5	15	27	381	41	1.21	17.11
15	41.3	16	25	333	41	1.12	14.96
10	41.3	17	20	234	41	0.90	10.51
5	41.3	18	13	123	41	0.58	5.52
1	42.9	19	6	38	42	0.27	1.71
Cycle 2 1	42.9	0	6	38	42	0.27	1.71
5	42.1	1	10	100	42	0.45	4.49
10	41.3	2	19	198	42	0.85	8.89
15	41.3	3	29	309	42	1.30	13.88
20	40.5	4	42	440	41	1.89	19.76
15	40.5	5	38	386	41.2	1.71	17.34
10	41.3	6	31	274	41.7	1.39	12.31
5	41.3	7	24	152	41.9	1.08	6.83
1	42.1	8	10	51	43	0.45	2.29
Cycle 3 1	42.1	0	10	51	43	0.45	2.29
5	42.1	1	15	111	42.5	0.67	4.99
10	41.3	3	25	211	42.1	1.12	9.48
15	41.3	4	37	330	41.6	1.66	14.82
20	40.5	5	51	455	41.3	2.29	20.44
15	40.5	6	46	406	41.5	2.07	18.23
10	40.5	7	37	287	41.8	1.66	12.89
5	41.3	8	30	158	41.9	1.35	7.10
1	42.1	10	13	58	42.9	0.58	2.60
Cycle 4 1	42.1	0	13	58	42.9	0.58	2.60
5	41.3	1	21	120	42.5	0.94	5.39
10	41.3	2	34	228	42	1.53	10.24
15	40.5	3	47	348	42	2.11	15.63
20	40.5	4	64	475	41.5	2.87	21.33
15	40.5	6	62	407	41.6	2.78	18.28
10	40.5	7	52	304	41.6	2.34	13.65
5	41.3	8	37	168	41.8	1.66	7.55
1	42.1	9	17	66	42.3	0.76	2.96
Cycle 5 1	42.1	0	17	66	42.3	0.76	2.96
5	42.1	1	28	134	42.5	1.26	6.02
10	41.3	2	41	244	42.1	1.84	10.96
15	40.5	3	57	368	41.6	2.56	16.53
20	40.5	4	75	487	41.3	3.37	21.87
15	40.5	5	68	425	41.5	3.05	19.09
10	40.5	6	57	314	41.8	2.56	14.10
5	41.3	6.5	43	184	41.9	1.93	8.26
1	42.1	7	17	70	42.9	0.76	3.14

(a) Height was measured both with a ruler.
(b) Height was measured with a caliper.

Table D.8. Compressibility Results for Resin #12

Pressure (psi)		Height (mm)	Time (min)	Side Load (g)	Bottom Load (g)	Side (psi)	Bottom (psi)
Cycle 1	0	41.3	0	-9	5.4	-0.40	0.24
	5	38.1	1	-1	194	-0.04	8.71
	10	37.3	2	12	350	0.54	15.72
	15	36.5	4	33	485	1.48	21.78
	20	35.7	5	55	624	2.47	28.03
	15	35.7	5.5	42	521	1.89	23.40
	10	36.5	6	32	382	1.44	17.16
	5	36.5	7	19	218	0.85	9.79
	1	41.3	8	-3	6	-0.13	0.27
Cycle 2	0	41.3	0	-9	5.4	-0.40	0.24
	5	38.1	1	4	179	0.18	8.04
	10	36.5	2	20	332	0.90	14.91
	15	35.7	2.5	37	474	1.66	21.29
	20	34.9	3	54	610	2.43	27.40
	15	34.9	4	43	507	1.93	22.77
	10	35.7	5	35	362	1.57	16.26
	5	36.5	5.5	25	217	1.12	9.75
	1	38.9	6	-1	16	-0.04	0.72
Cycle 3	0	41.3	0	-9	5.4	-0.40	0.24
	5	37.3	1	9	182	0.40	8.17
	10	36.5	2	26	324	1.17	14.55
	15	35.7	3	44	469	1.98	21.06
	20	34.9	3.5	63	603	2.83	27.08
	15	34.9	4	50	503	2.25	22.59
	10	35.7	5	42	361	1.89	16.21
	5	36.5	6	29	207	1.30	9.30
	1	38.1	8	1	21	0.04	0.94
Cycle 4	0	41.3	0	13	5.4	0.58	0.24
	5	37.3	1	31	174	1.39	7.81
	10	35.7	2	50	230	2.25	10.33
	15	35.7	3	67	465	3.01	20.88
	20	34.9	4	55	605	2.47	27.17
	15	34.9	4.5	48	502	2.16	22.55
	10	35.7	5	33	352	1.48	15.81
	5	36.5	6	3	205	0.13	9.21
	1	38.1	7	-3	27	-0.13	1.21
Cycle 5	0	41.3	0	-9	5.4	-0.40	0.24
	5	37.3	1	16	178	0.72	7.99
	10	36.5	2	33	321	1.48	14.42
	15	35.7	3	50	462	2.25	20.75
	20	34.9	4	68	598	3.05	26.86
	15	34.9	5	56	496	2.52	22.28
	10	35.7	5.5	48	358	2.16	16.08
	5	36.5	6	33	201	1.48	9.03
	1	36.5	7	5	34	0.22	1.53

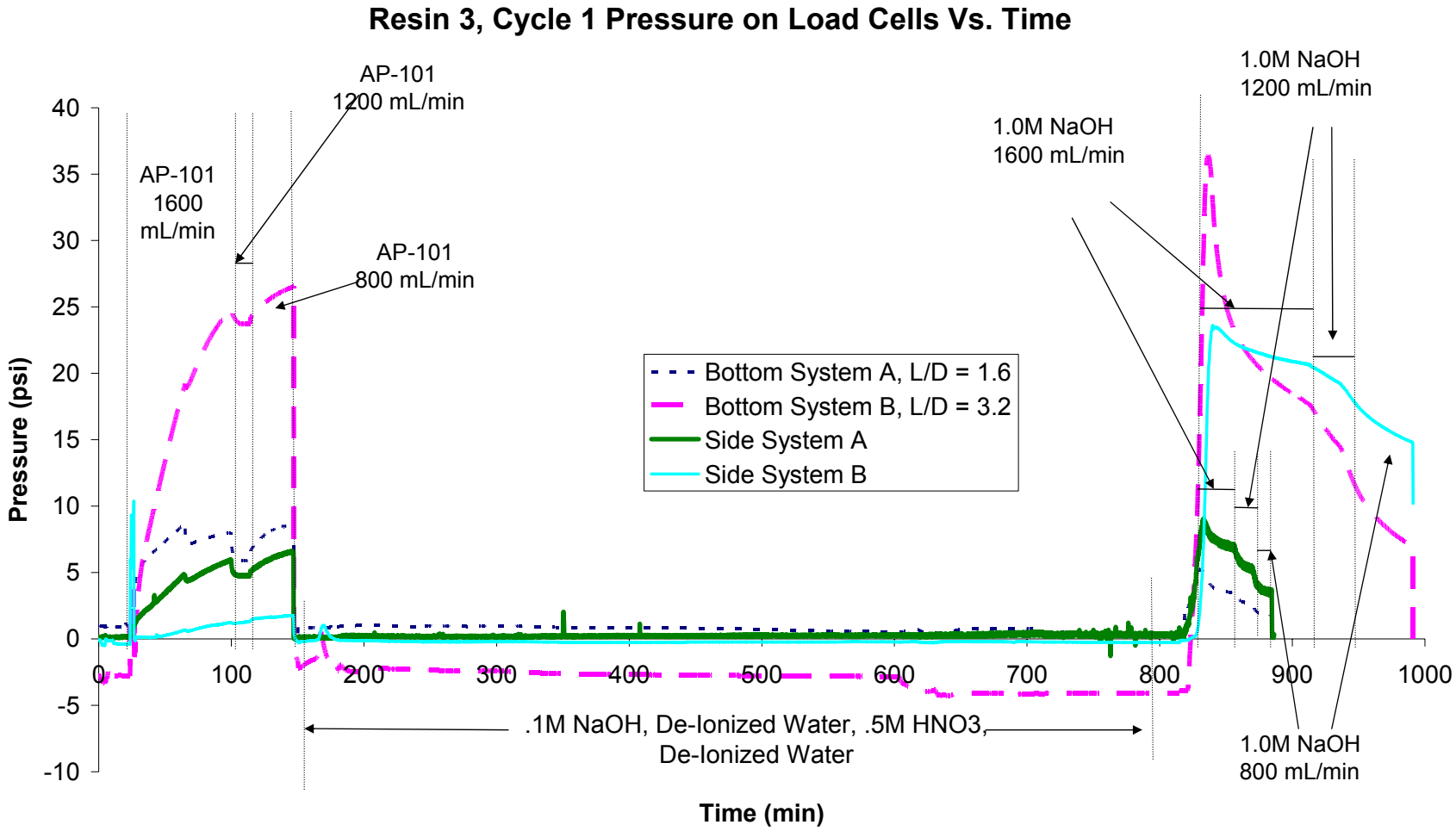

Figure D.2. Resin #3, Cycle #1, Load Cell Pressures

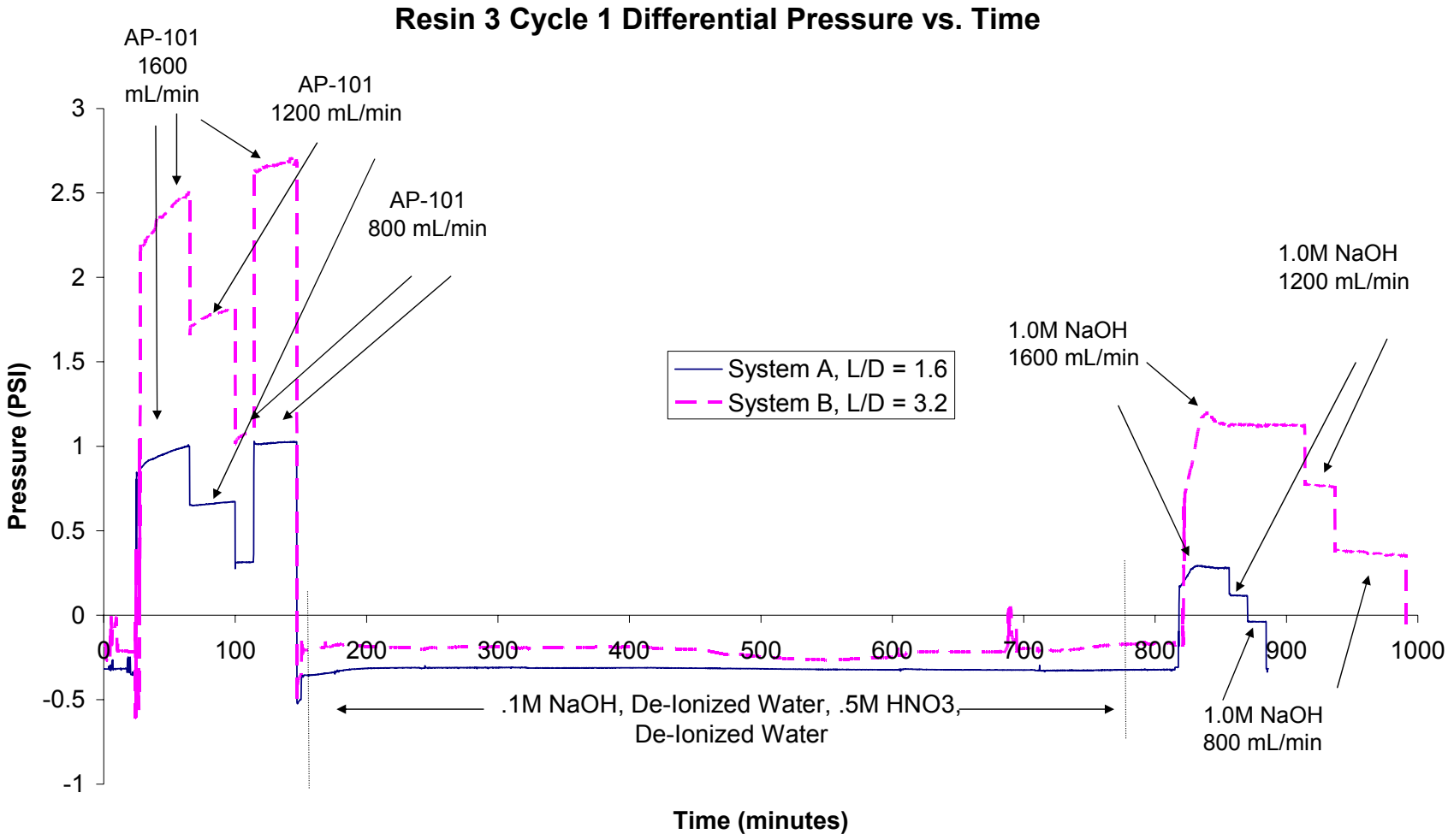

Figure D.3. Resin #3, Cycle #1, Liquid Differential Pressure

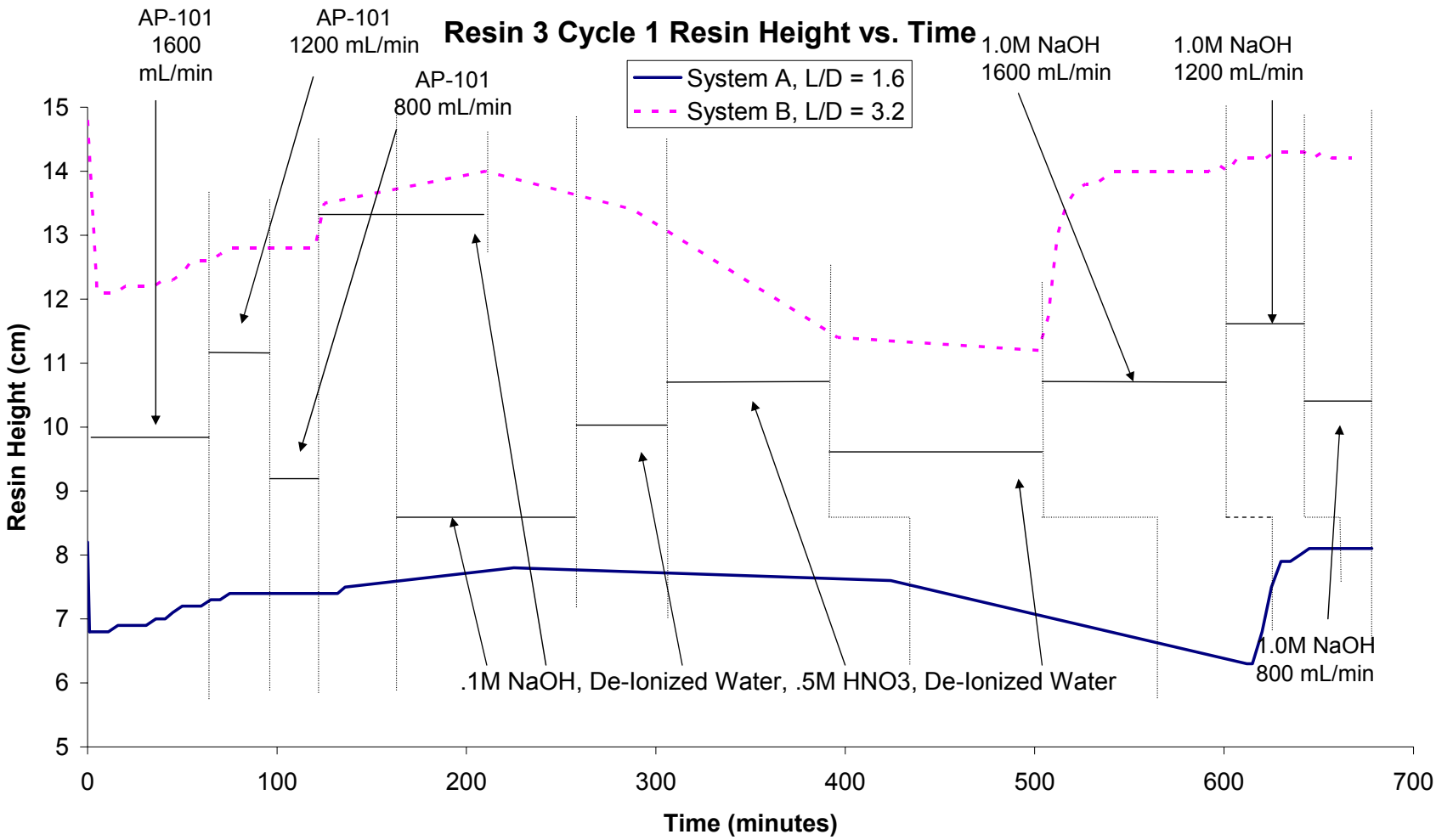

Figure D.4. Resin #3, Cycle #1, Resin Height

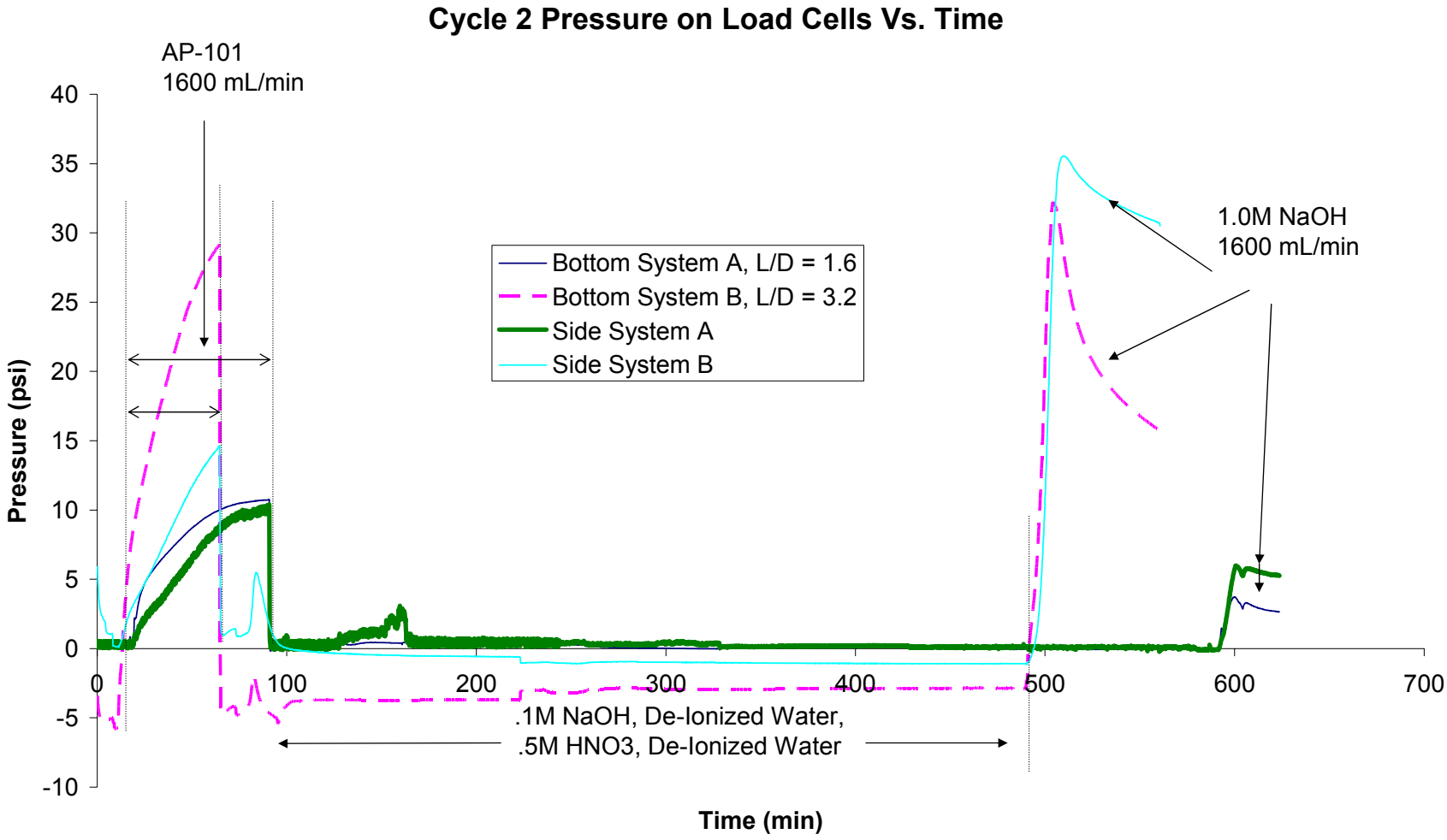

Figure D.5. Resin #3, Cycle #2, Load Cell Pressures

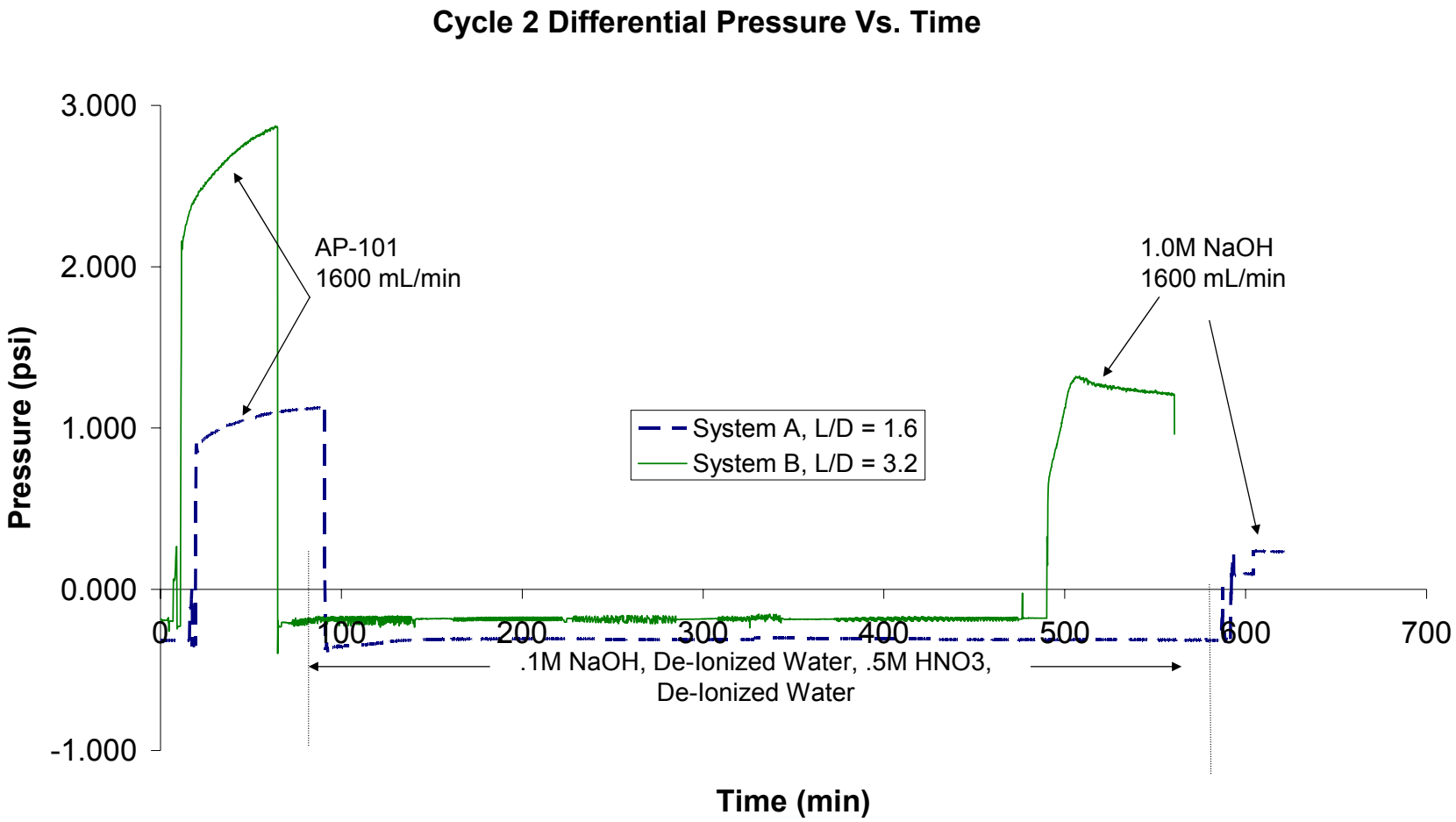

Figure D.6. Resin #3, Cycle #2, Liquid Differential Pressure

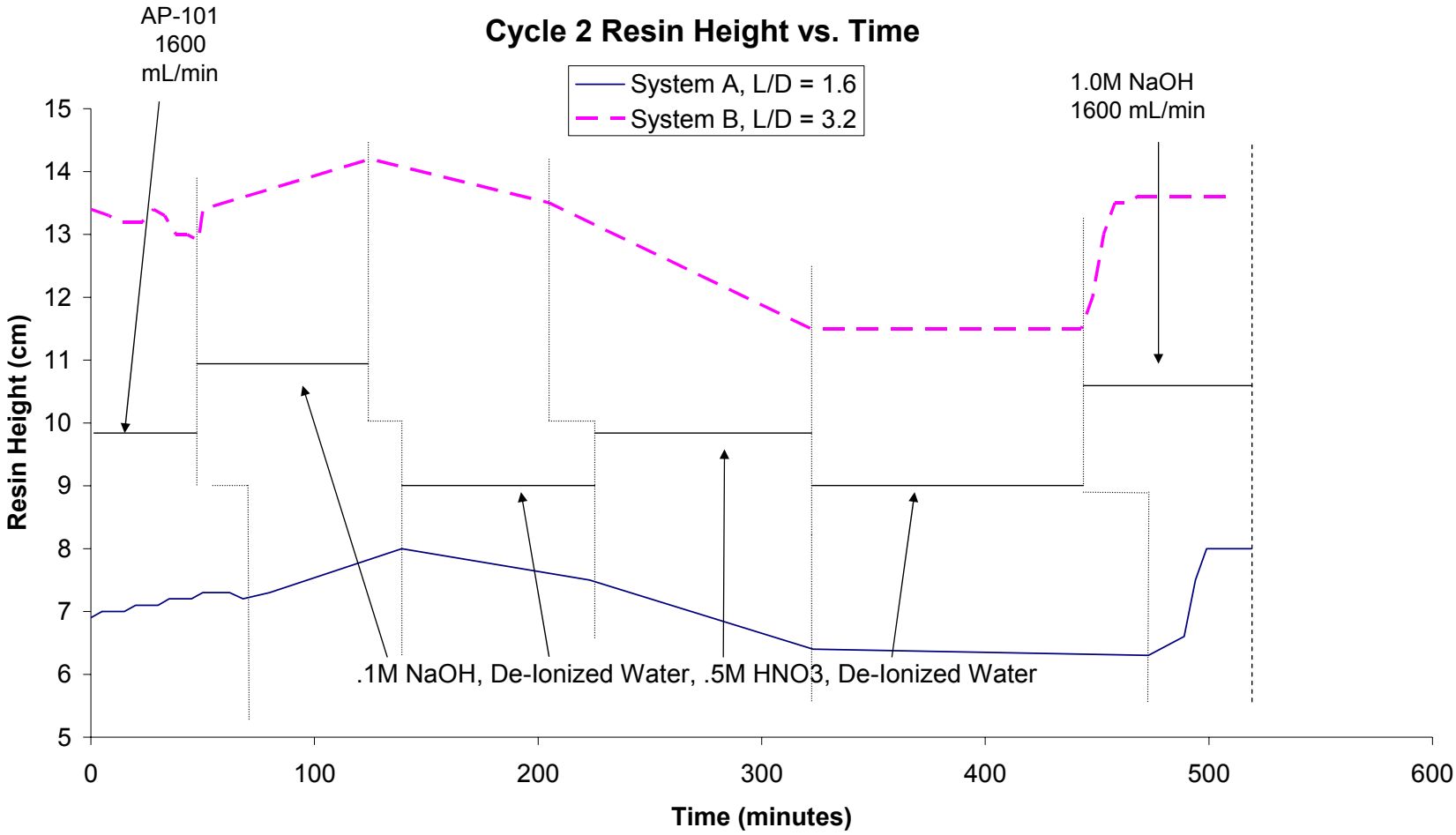

Figure D.7. Resin #3, Cycle #2, Resin Bed Height

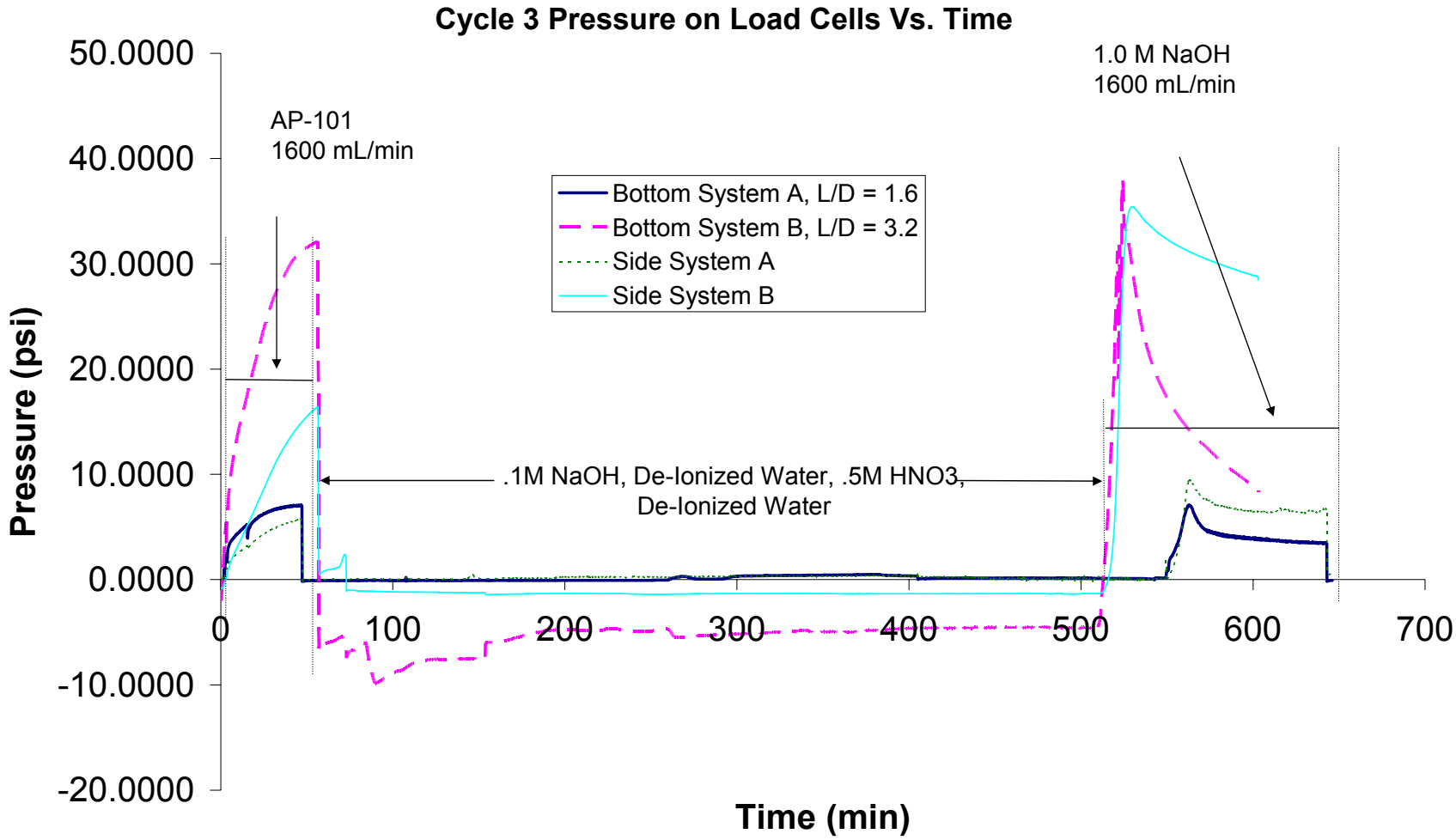

Figure D.8. Resin #3, Cycle #3, Load Cell Pressures

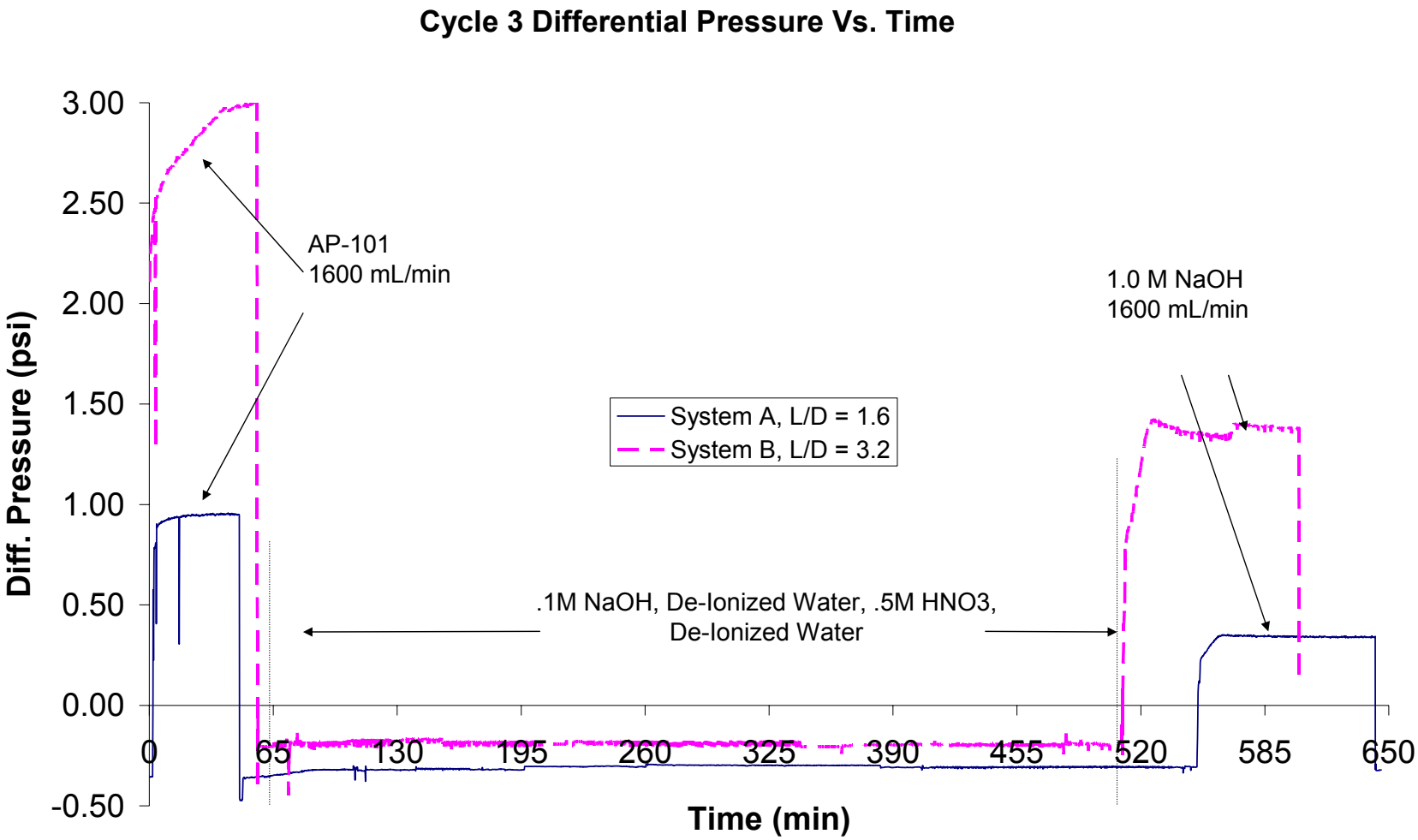

Figure D.9. Resin #3, Cycle #3, Liquid Differential Pressure

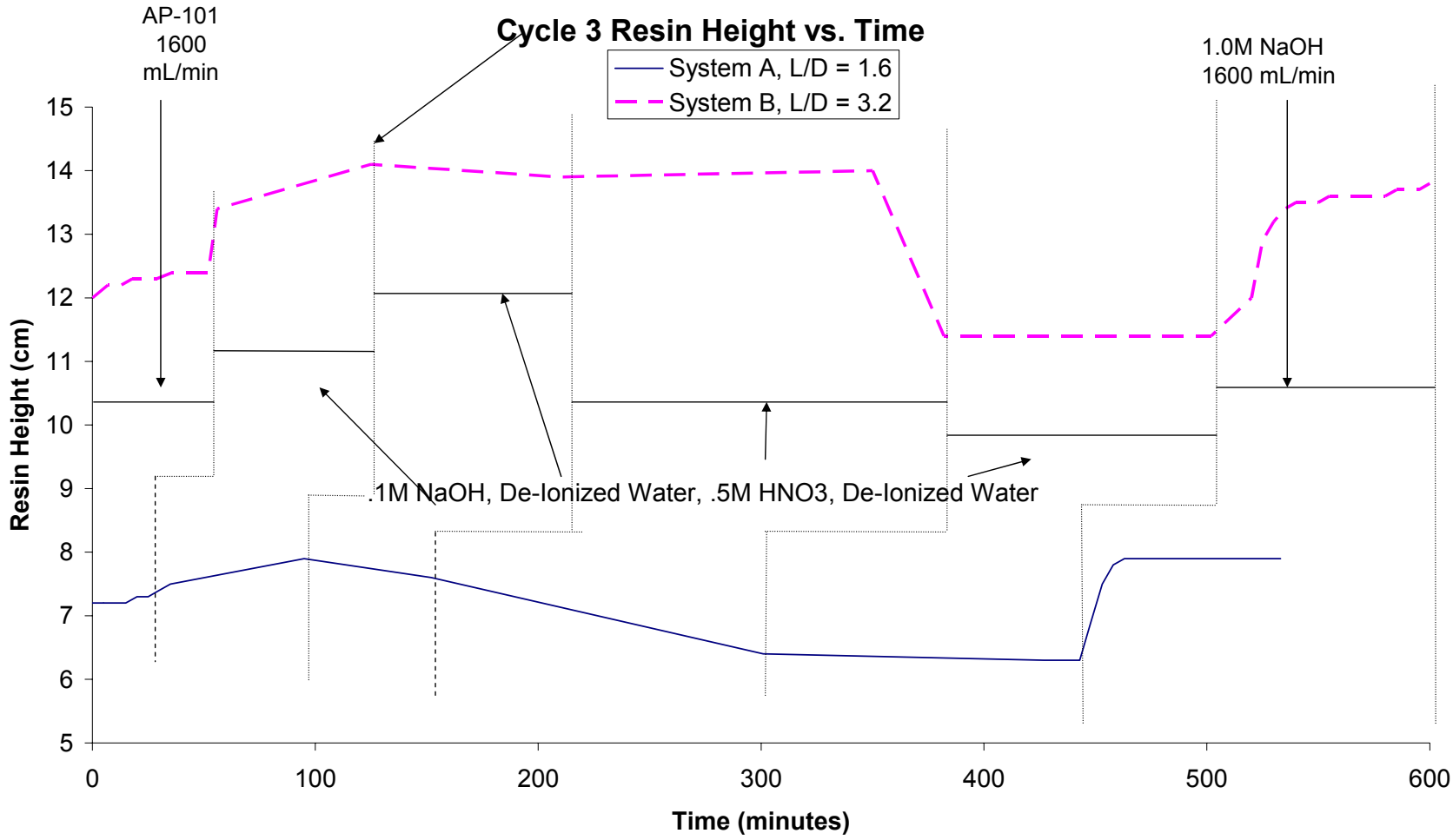

Figure D.10. Resin #3, Cycle #3, Resin Bed Height

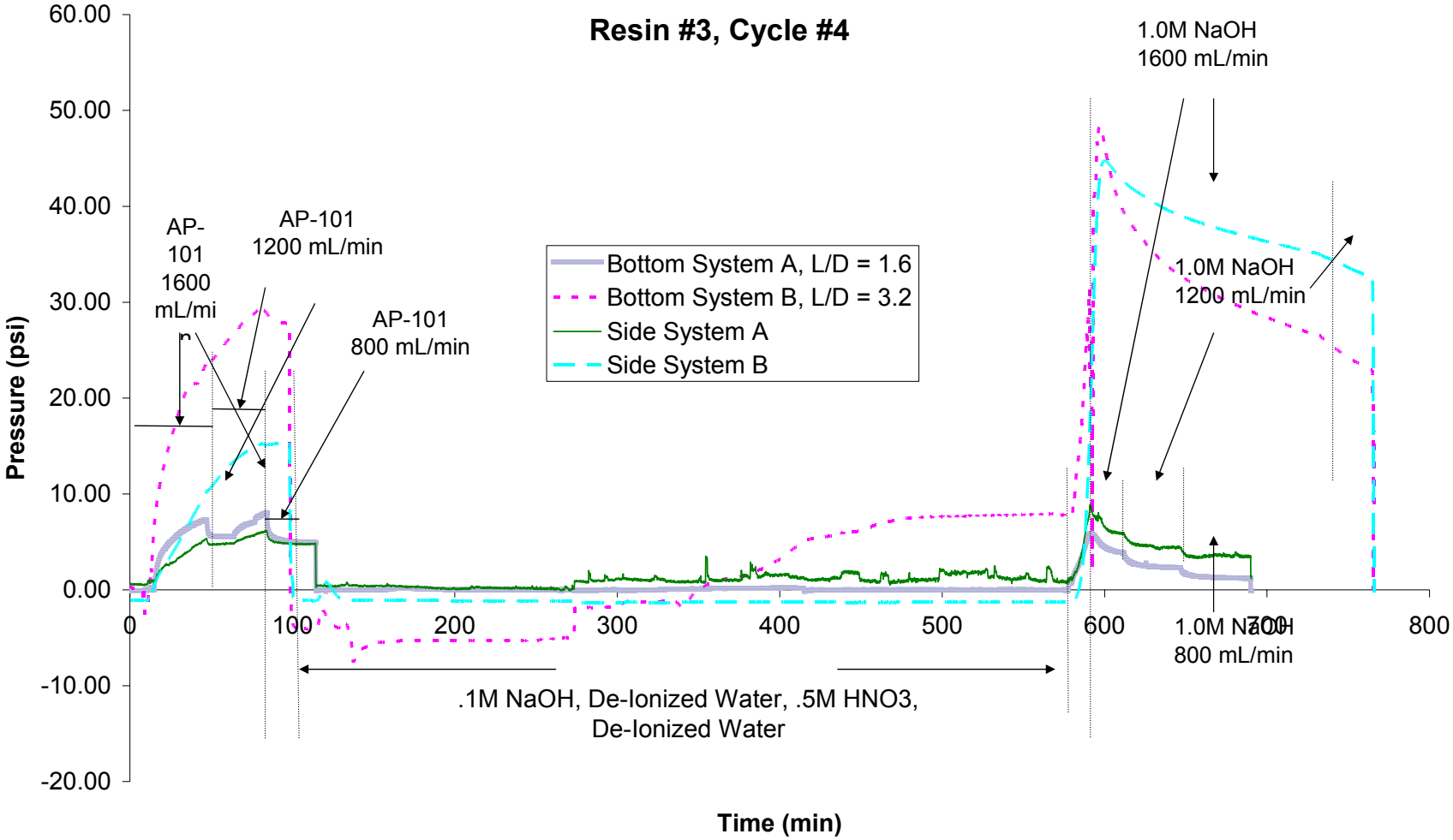

Figure D.11. Resin #3, Cycle 4, Load Cell Pressures

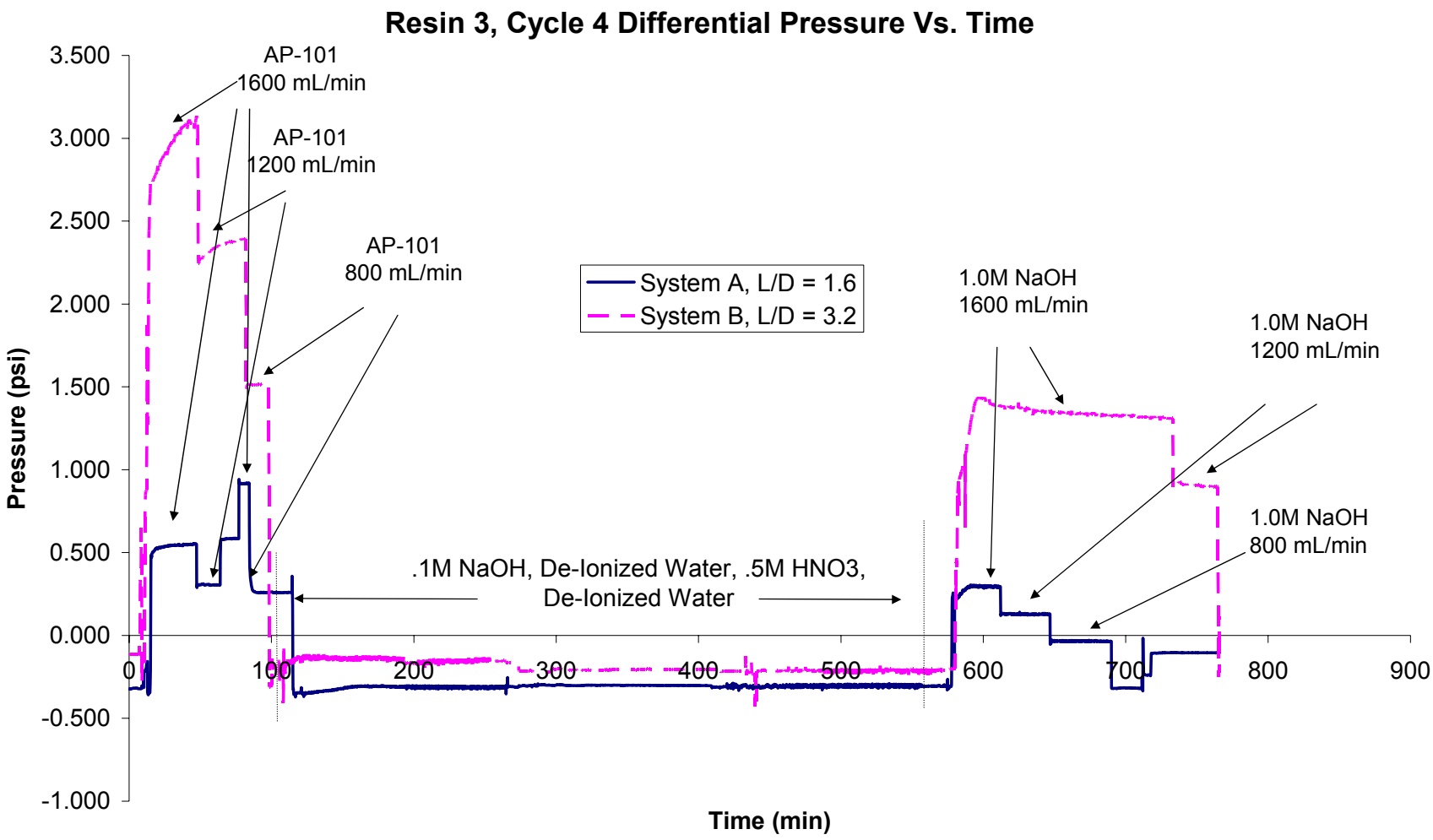

Figure D.12. Resin #3, Cycle 4, Liquid Differential Pressure

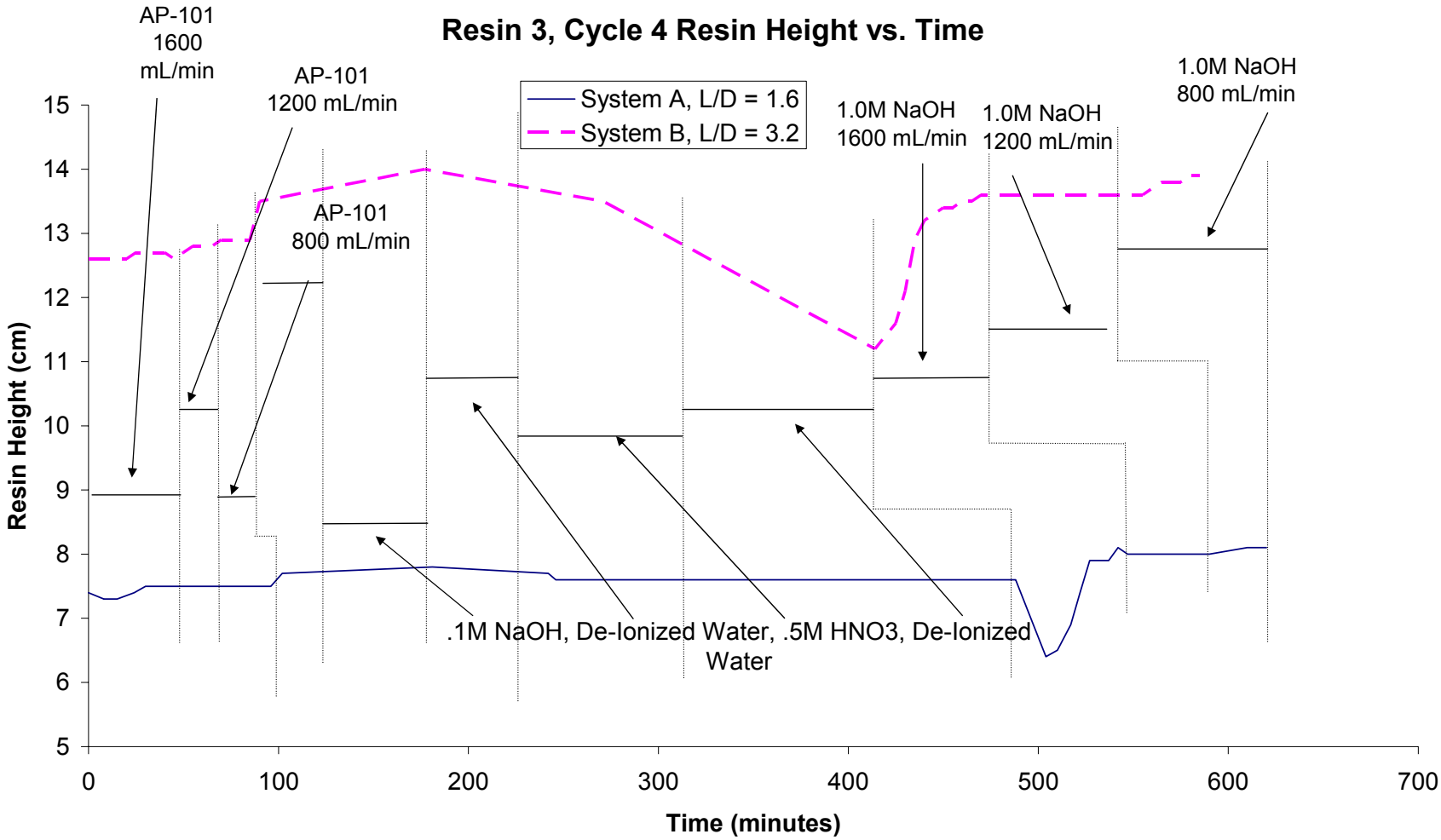

Figure D.13. Resin #3, Cycle 4, Resin Bed Height

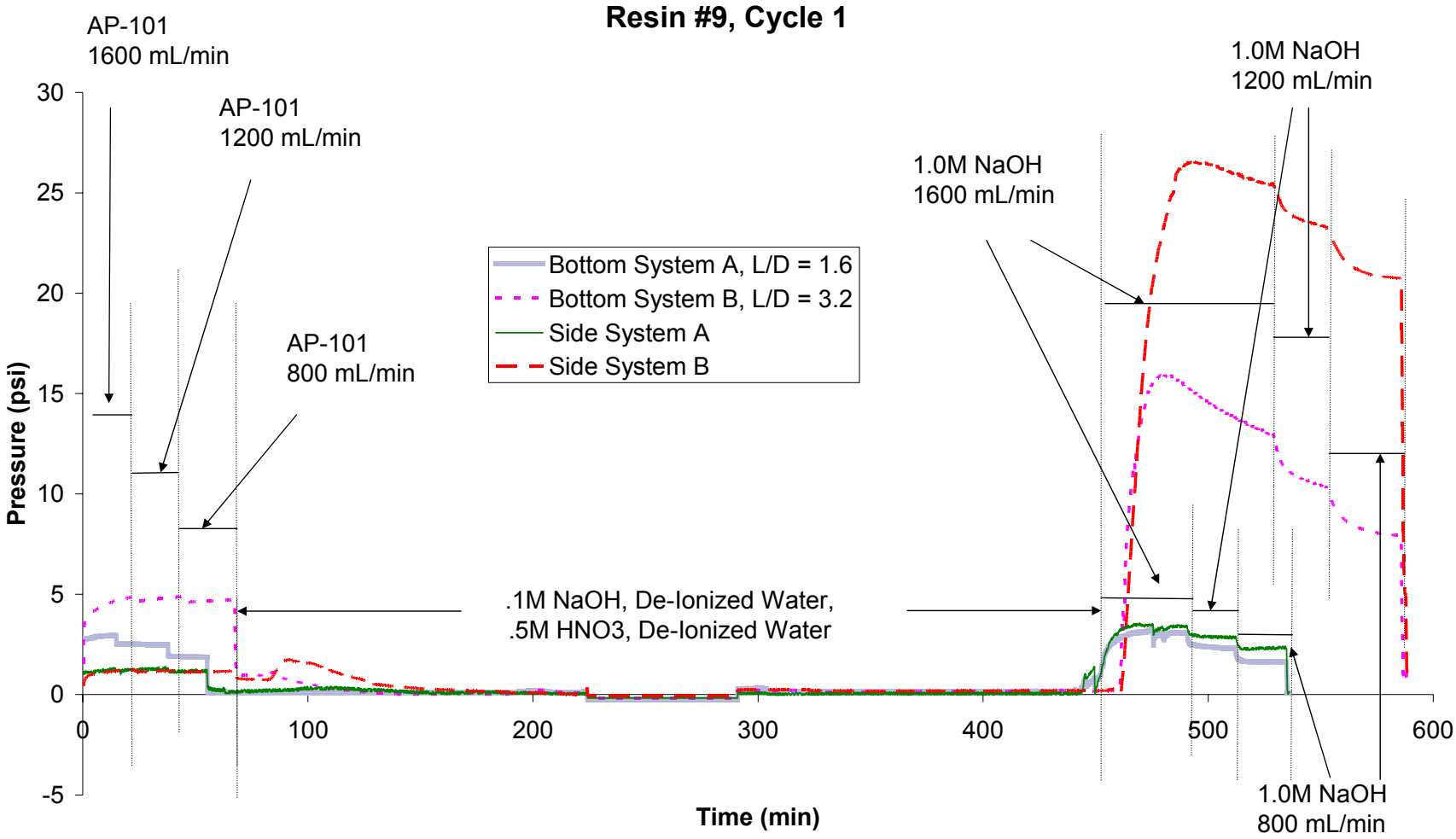

Figure D.14. Resin #9, Cycle 1, Load Cell Pressures

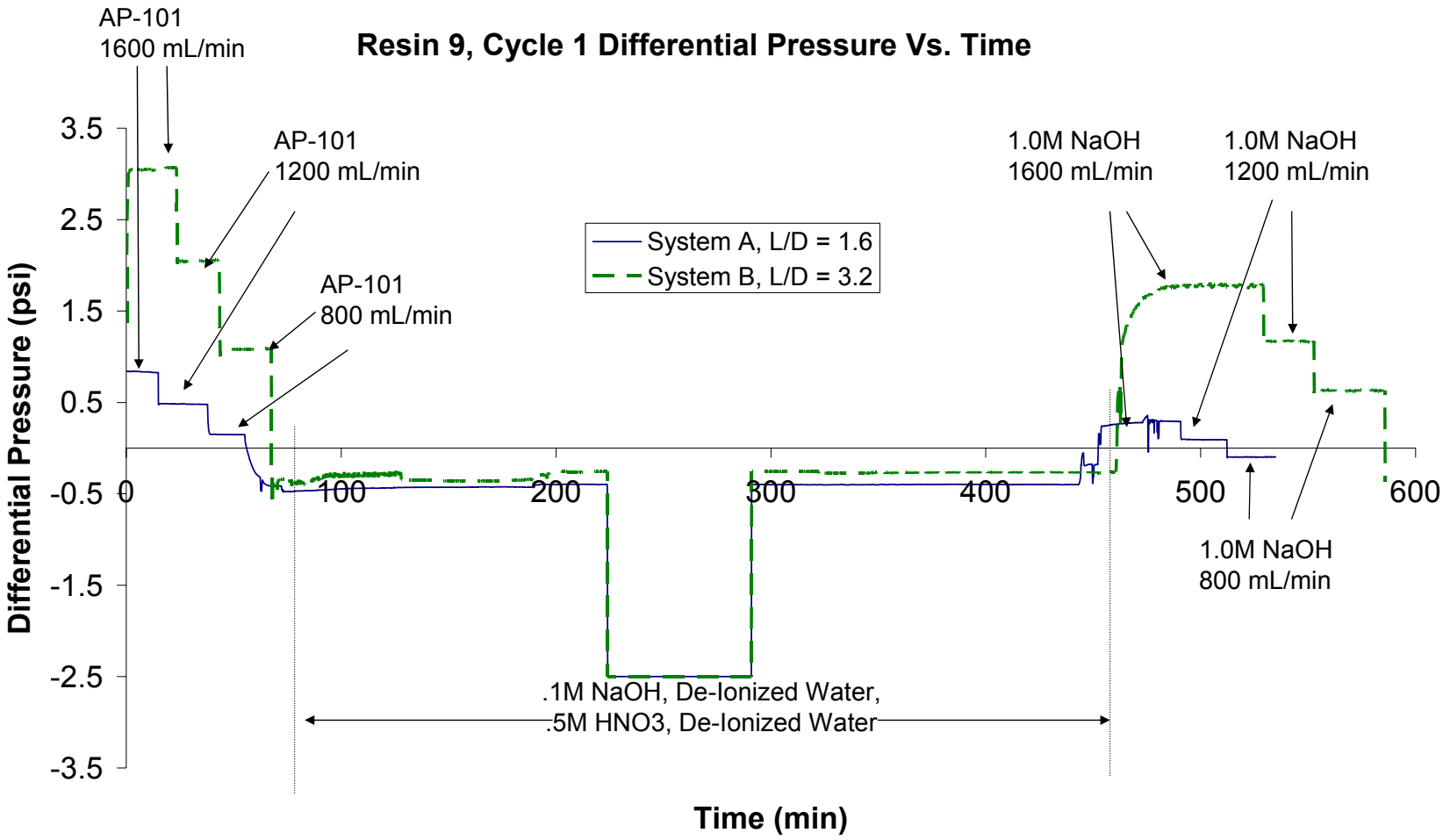

Figure D.15. Resin #9, Cycle 1, Liquid Differential Pressure

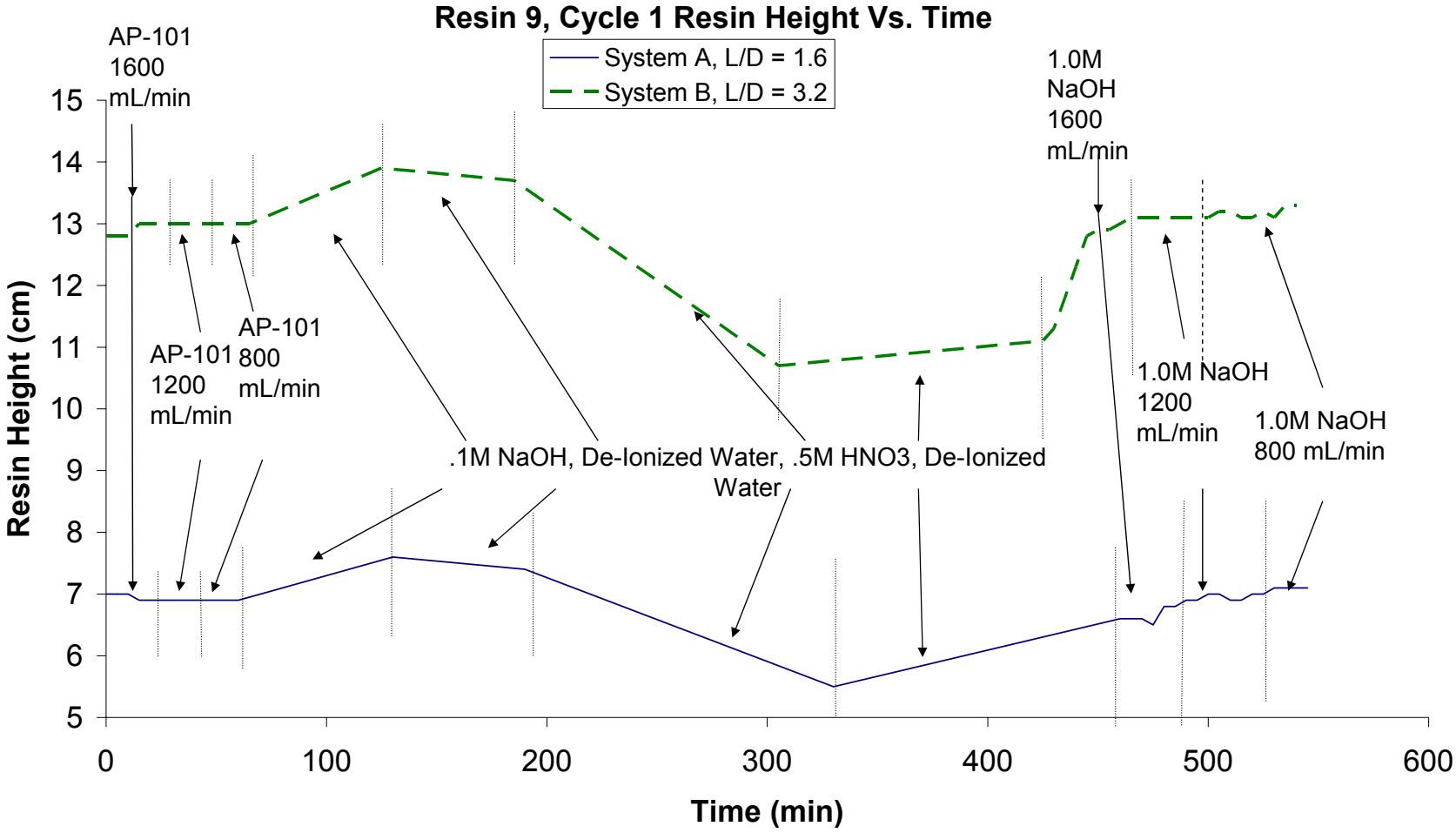

Figure D.16. Resin #9, Cycle 1, Resin Bed Height

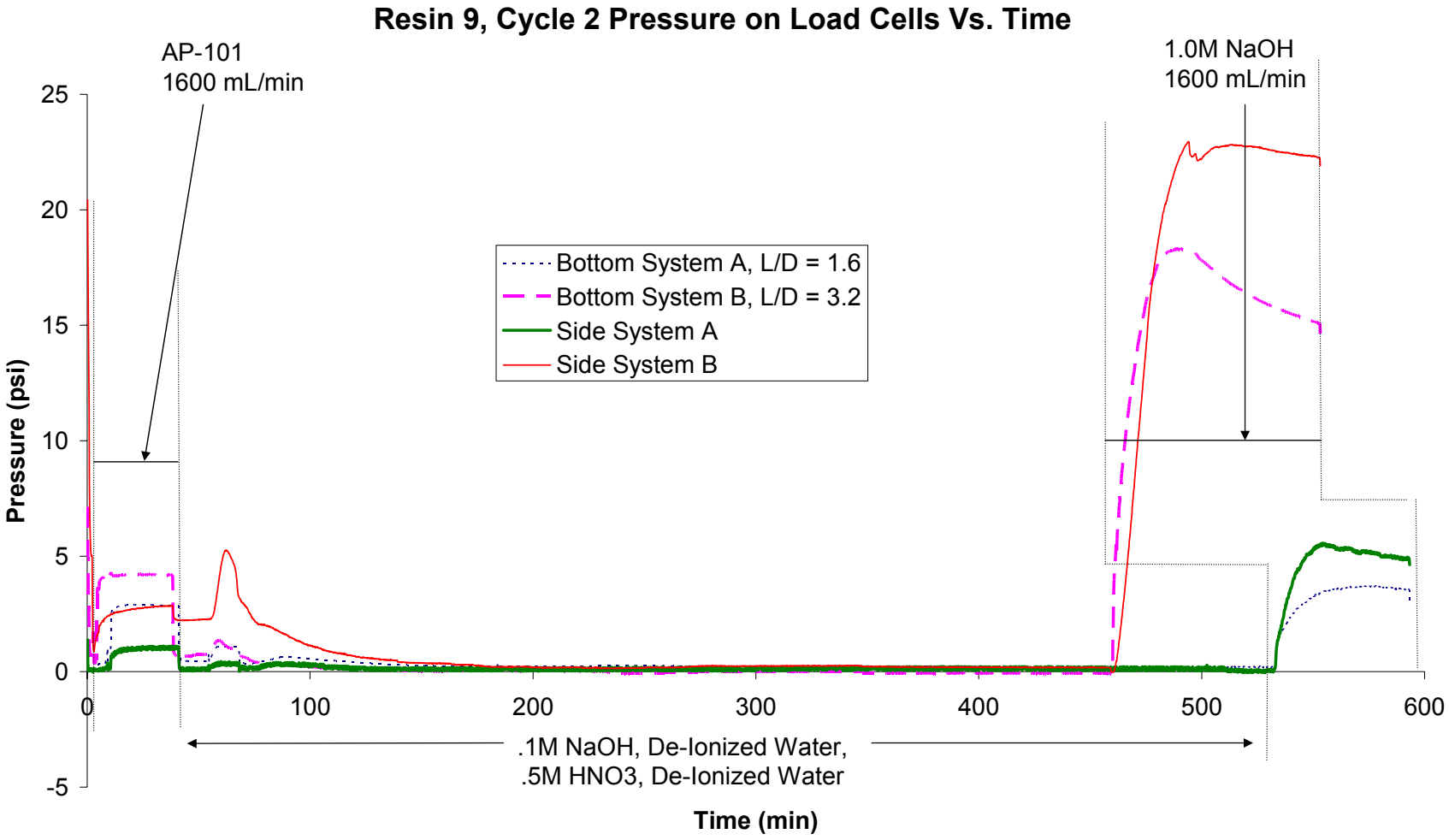

Figure D.17. Resin #9, Cycle 2, Load Cell Pressures

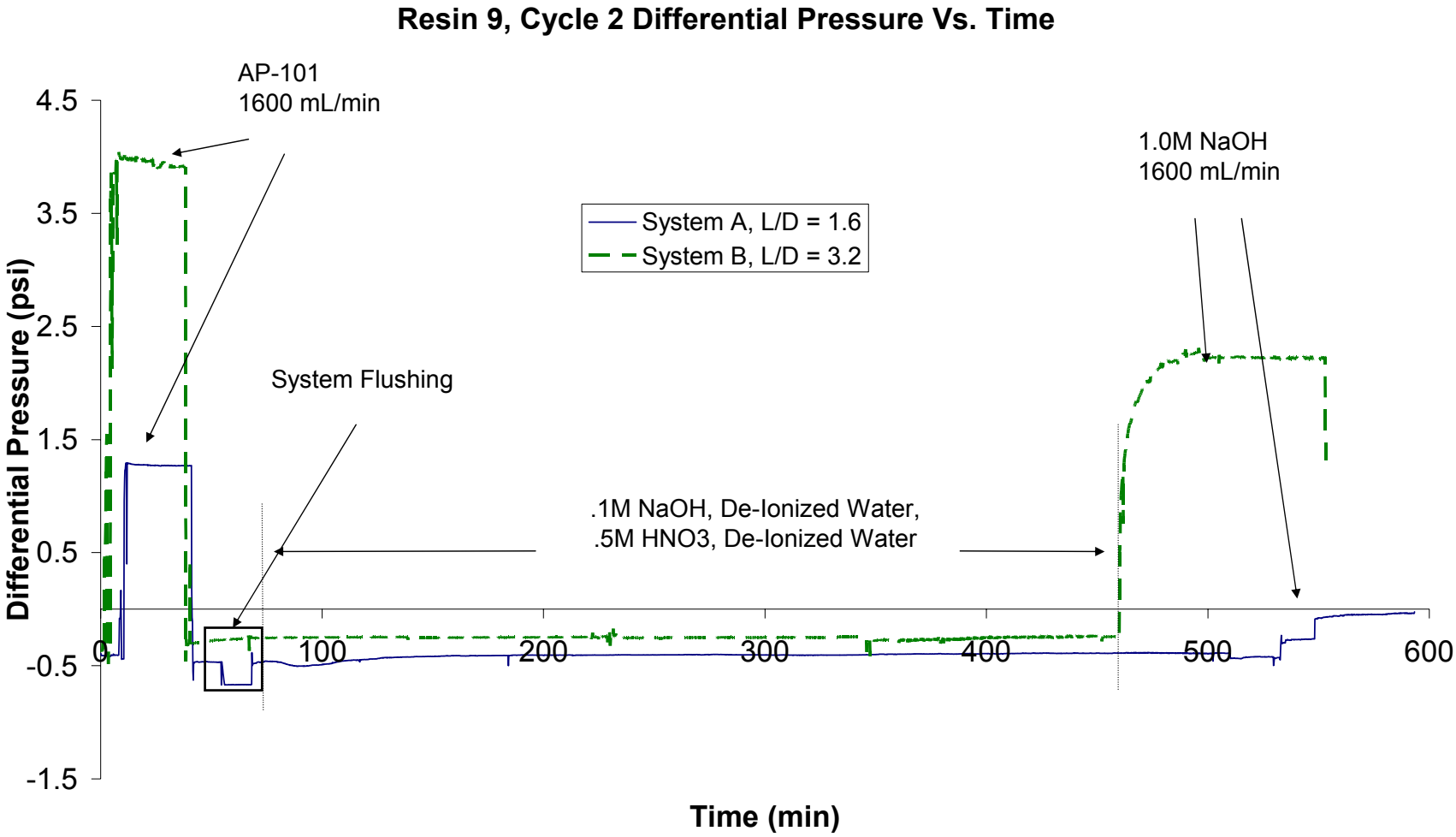

Figure D.18. Resin #9, Cycle 2, Liquid Differential Pressure

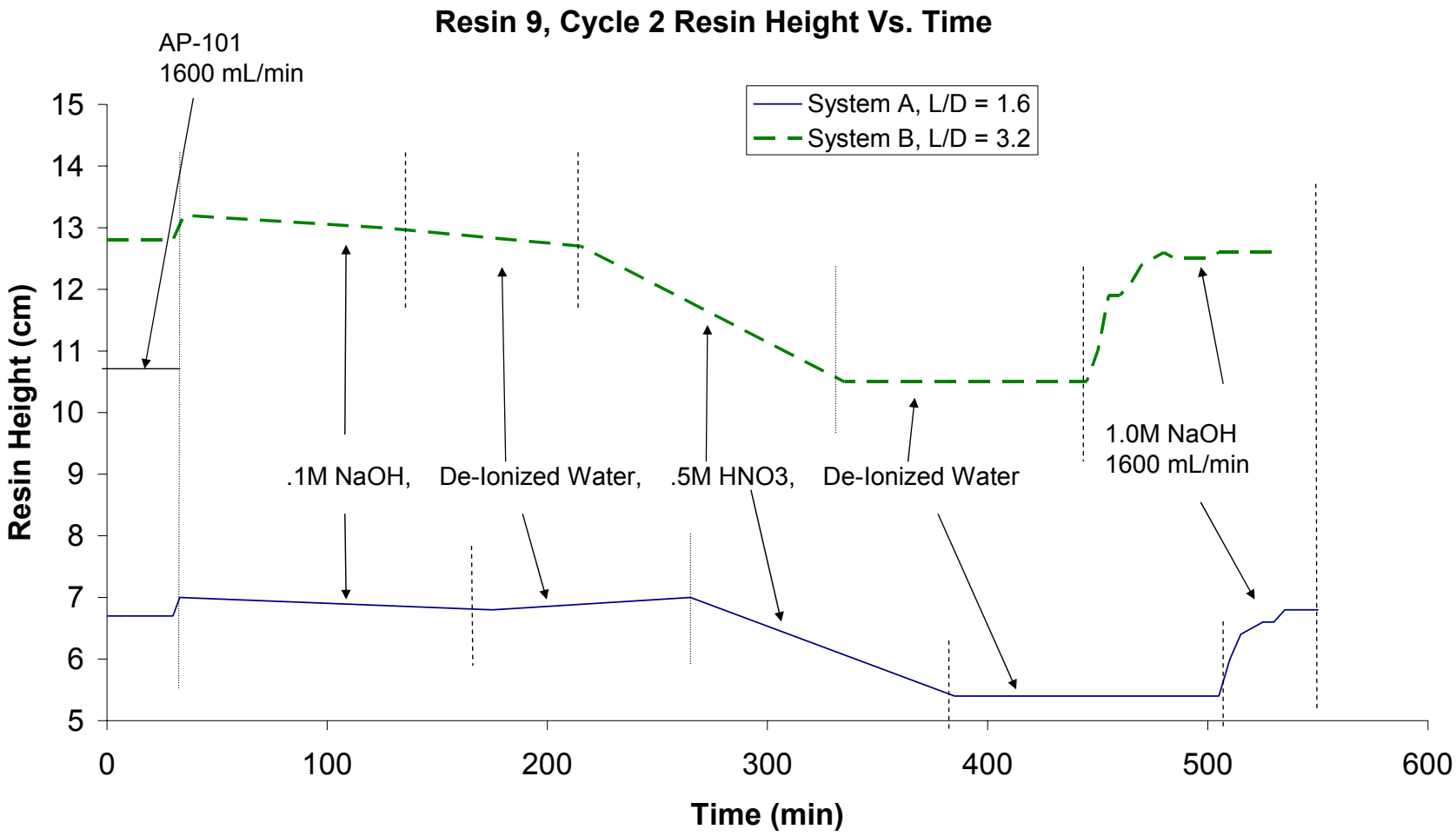

Figure D.19. Resin #9, Cycle 2, Resin Bed Height

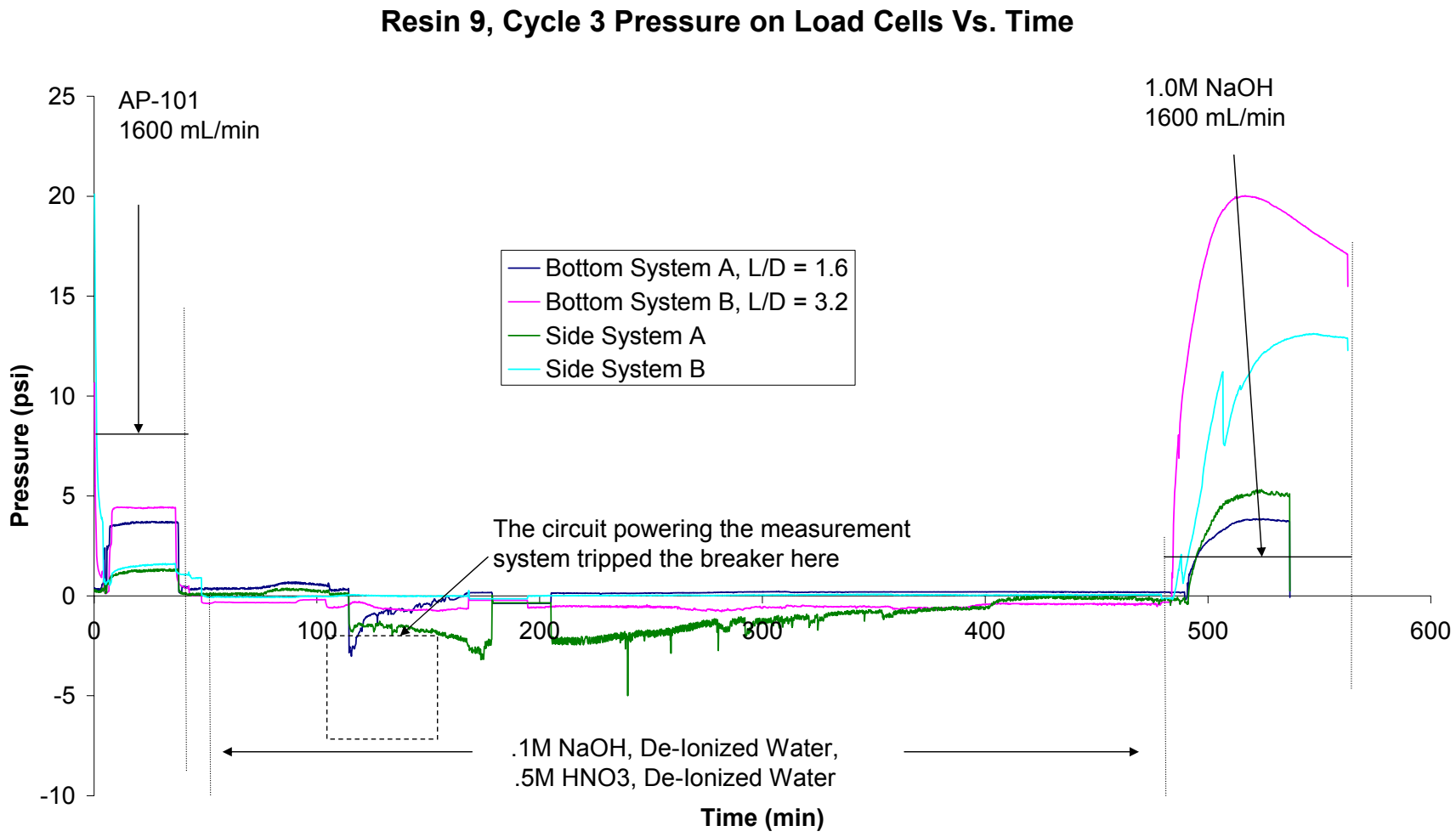

Figure D.20. Resin #9, Cycle 3, Load Cell Pressures

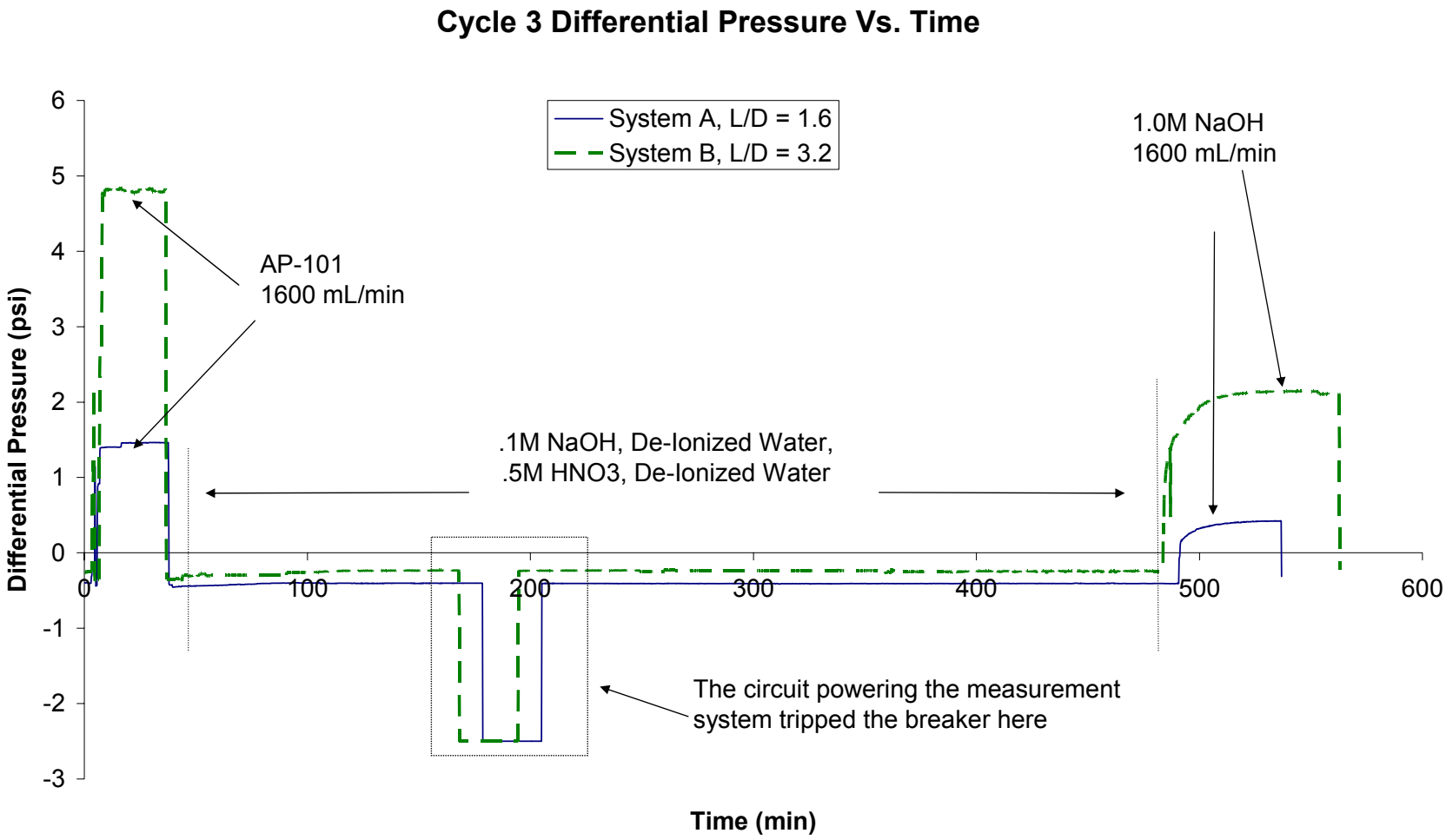

Figure D.21. Resin #9, Cycle 3, Liquid Differential Pressure

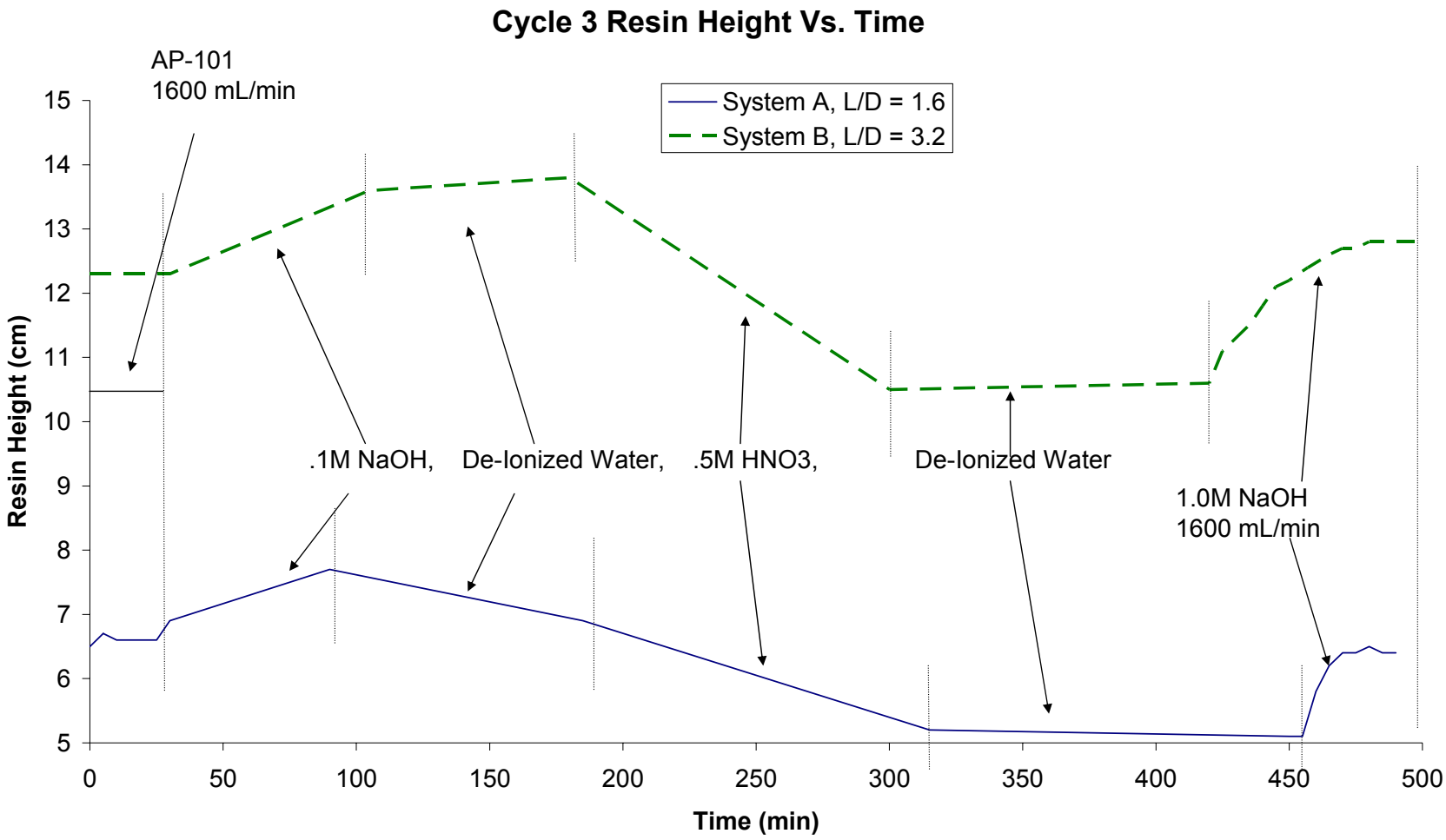

Figure D.22. Resin #9, Cycle 3, Resin Bed Height

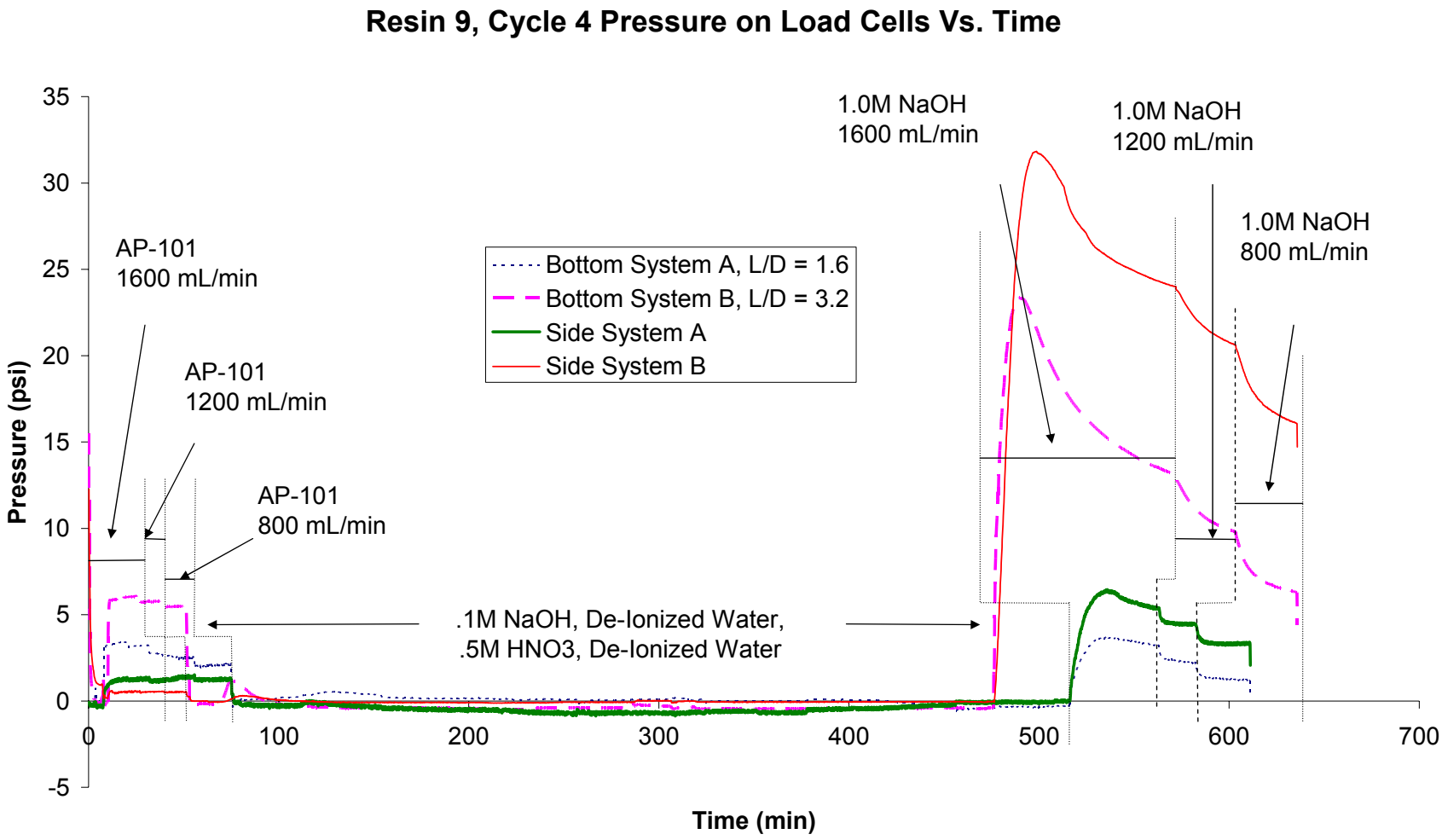

Figure D.23. Resin #9, Cycle 4, Load Cell Pressures

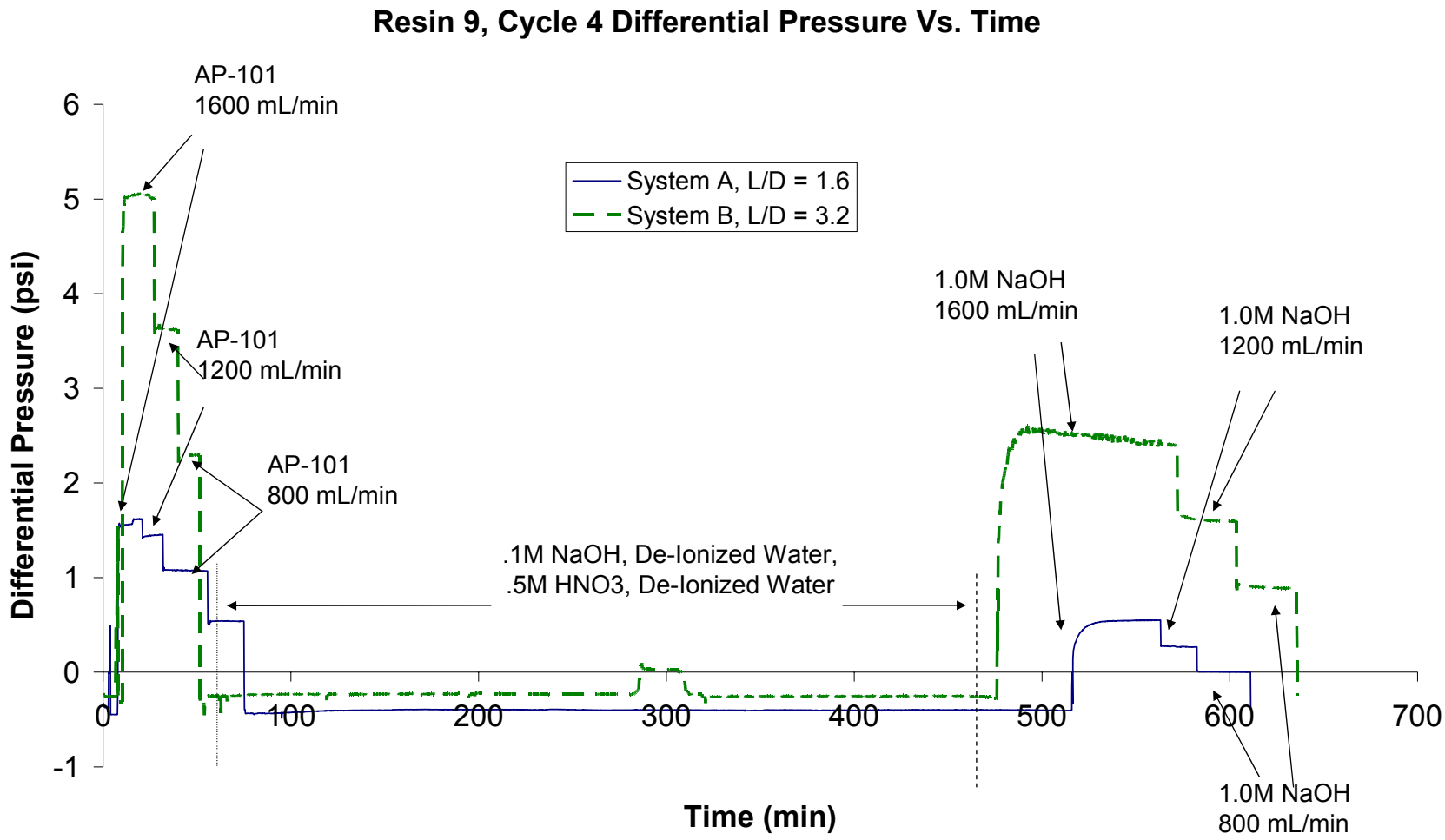

Figure D.24. Resin #9, Cycle 4, Liquid Differential Pressure

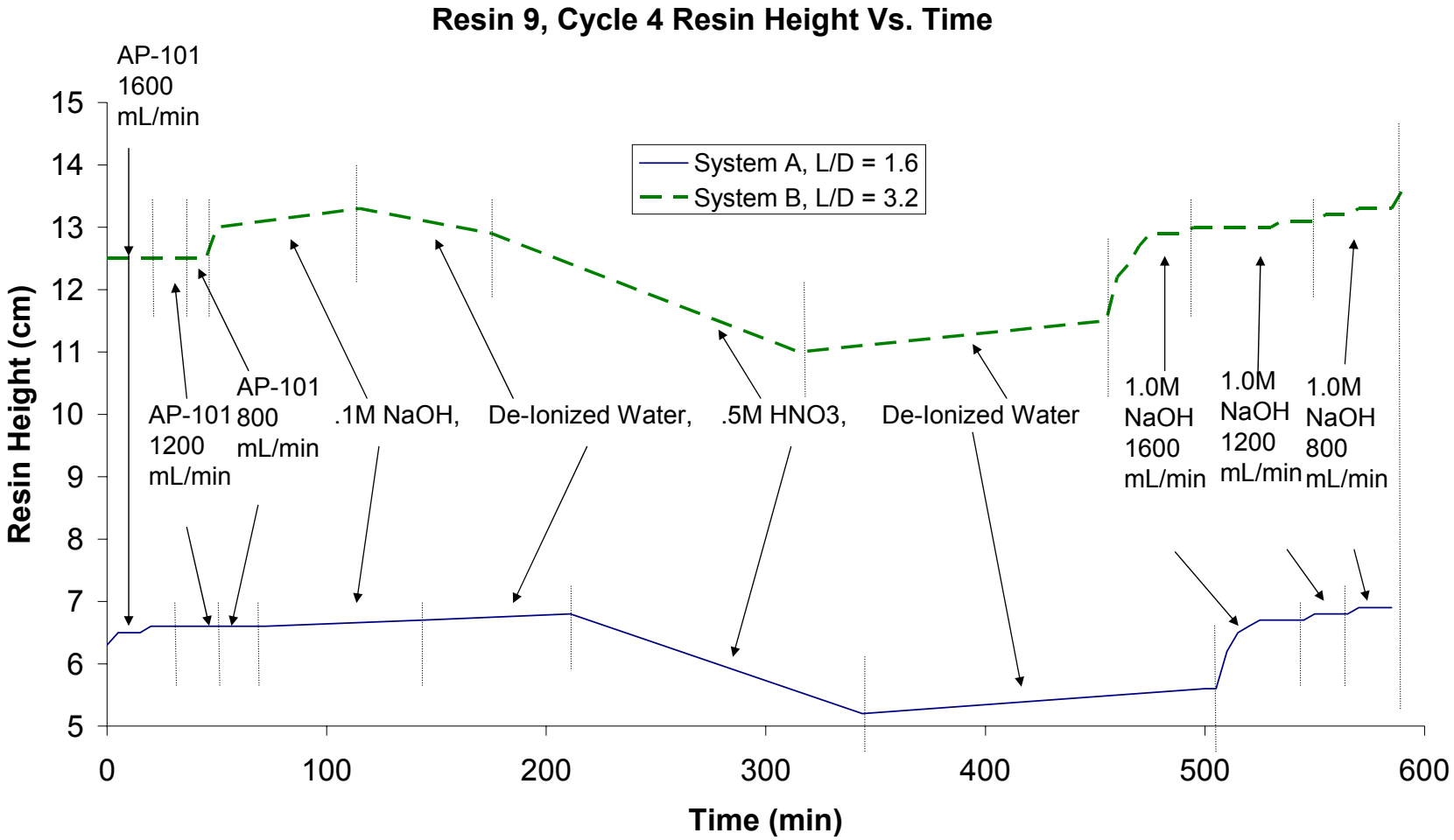

Figure D.25. Resin #9, Cycle 4, Resin Bed Height

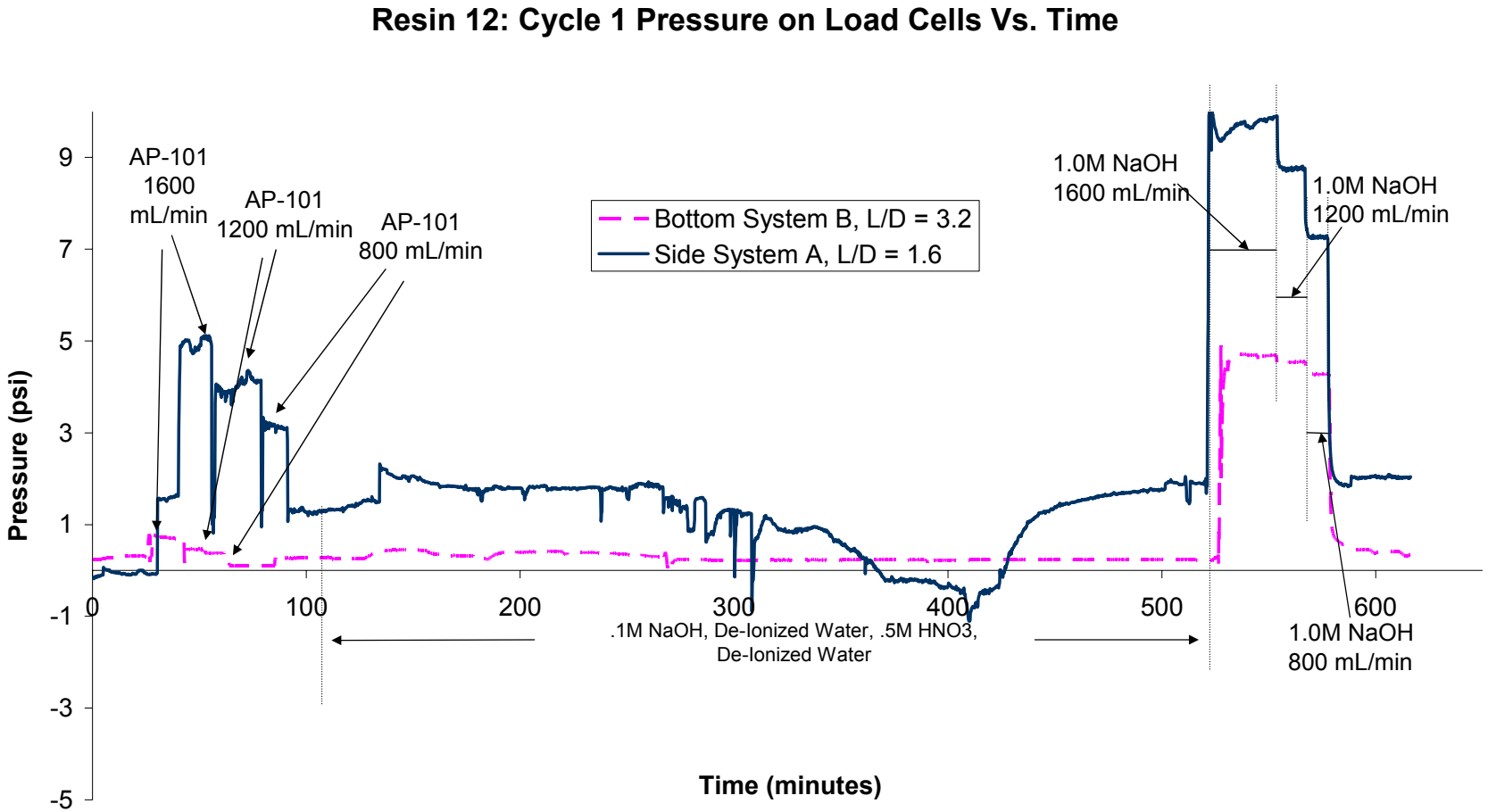

Figure D.26. Resin #12, Cycle 1, Load Cell Pressures

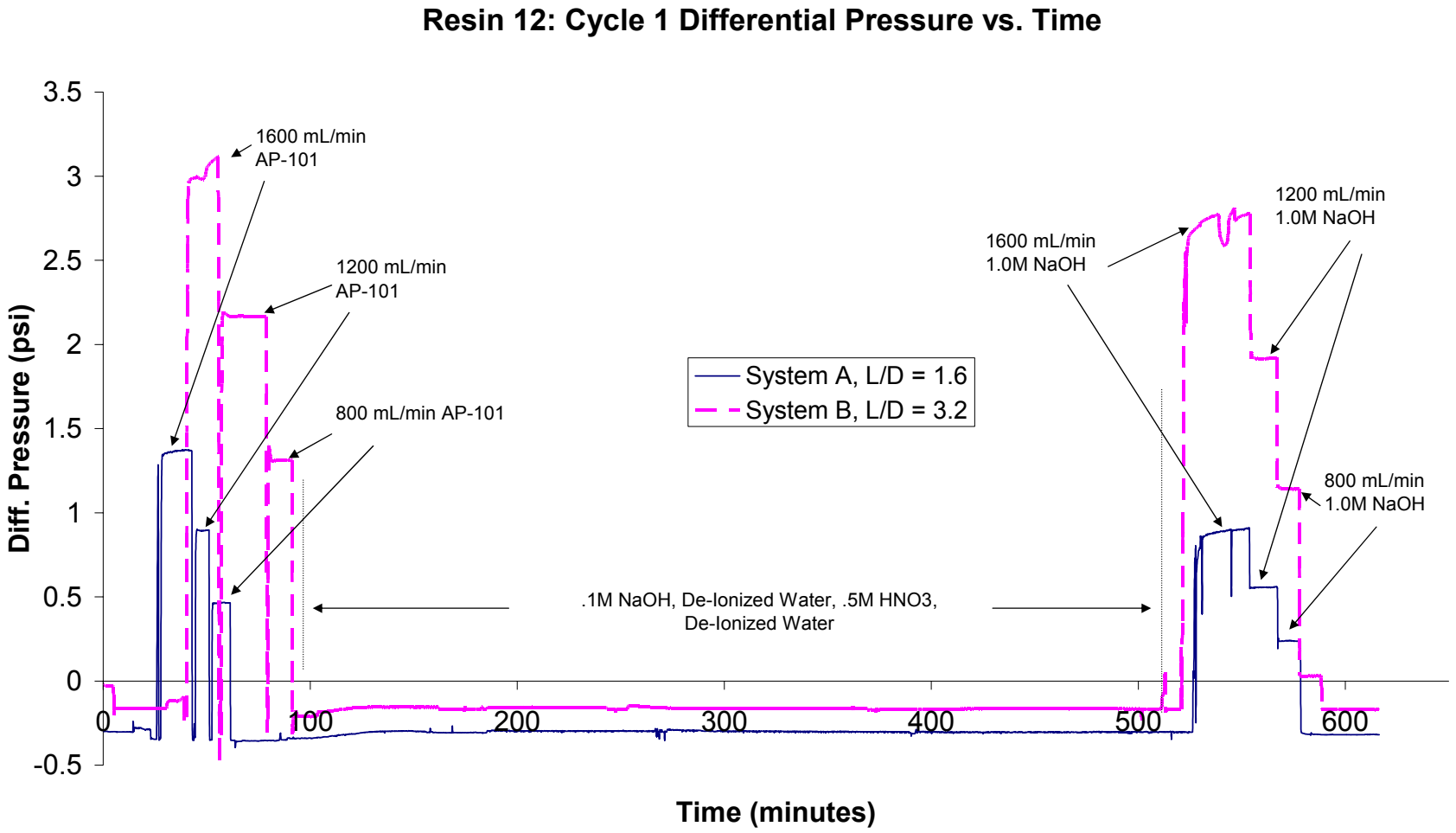

Figure D.27. Resin #12, Cycle 1, Differential Pressure

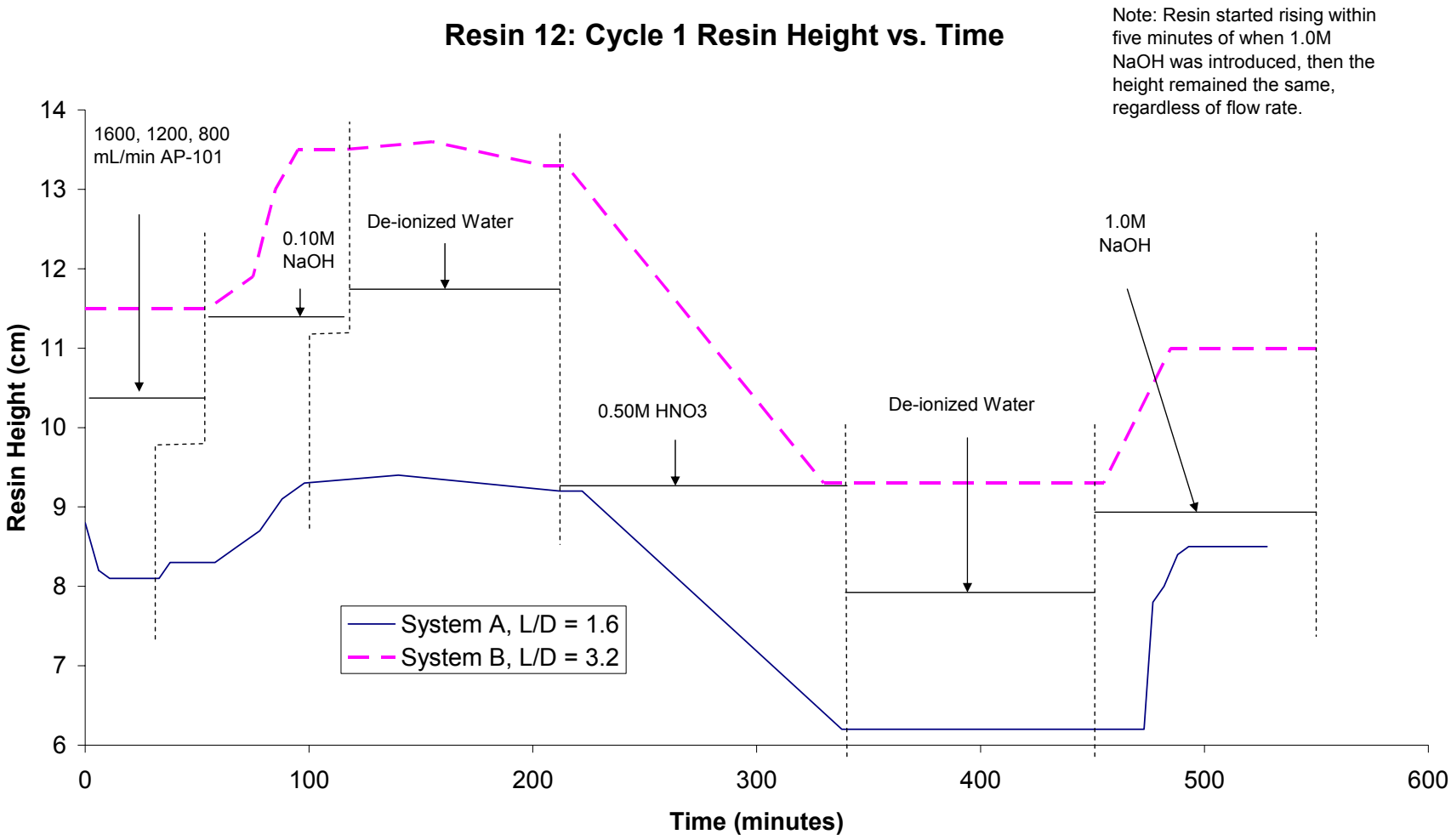

Figure D.28. Resin #12, Cycle 1, Resin Bed Height

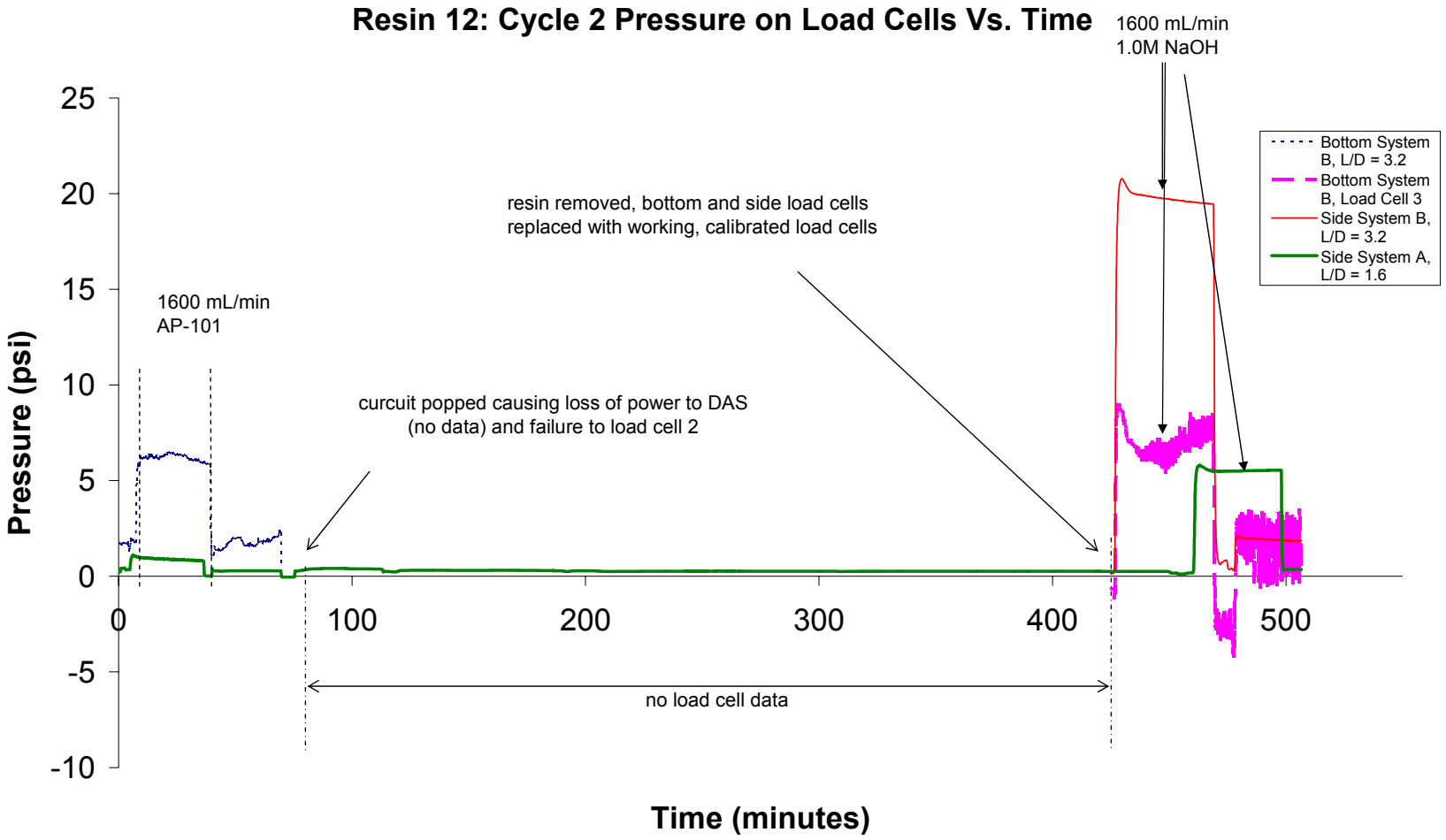

Figure D.29. Resin #12, Cycle 2, Load Cell Pressures

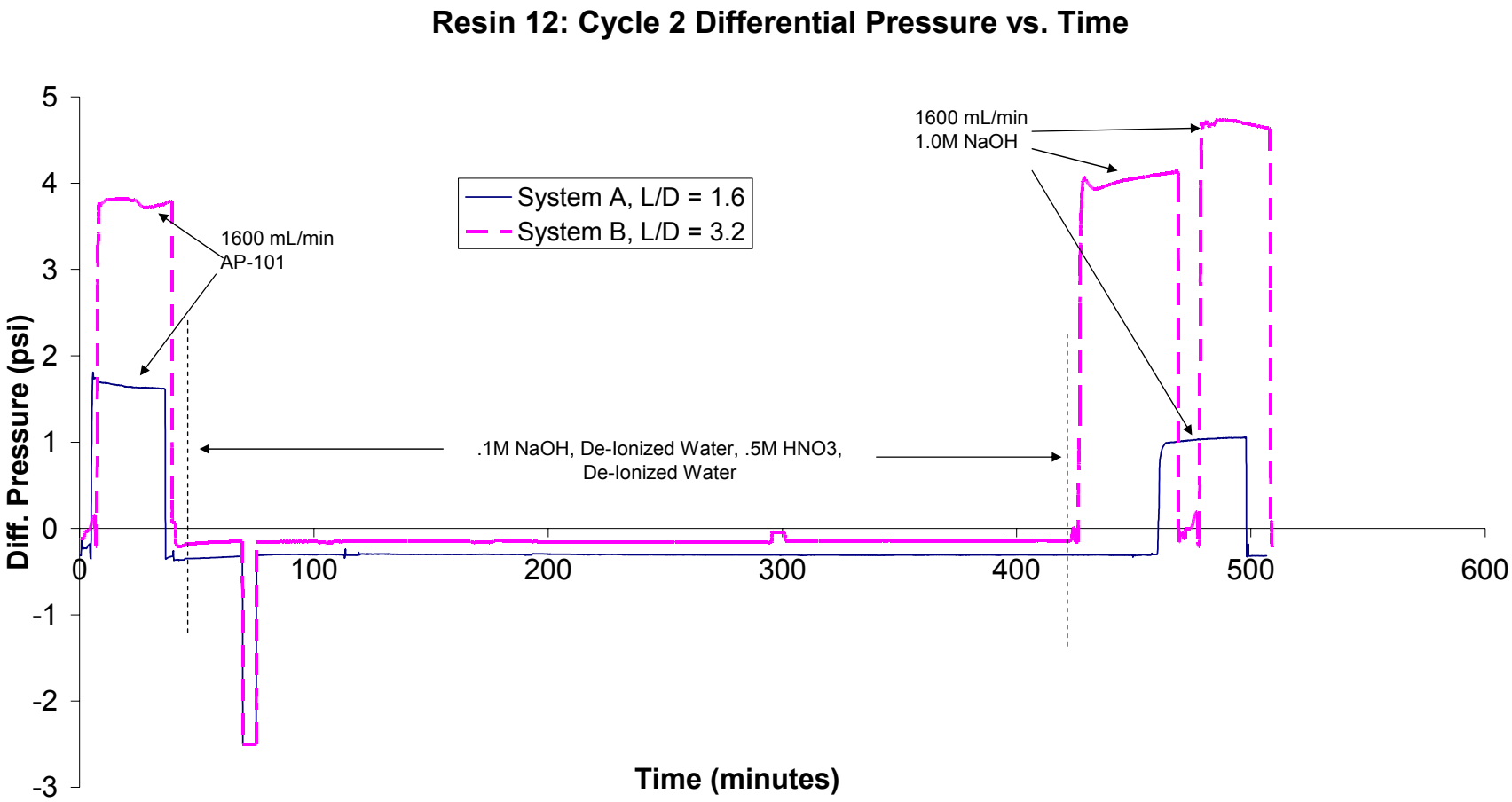

Figure D.30. Resin #12, Cycle 2, Liquid Differential Pressure

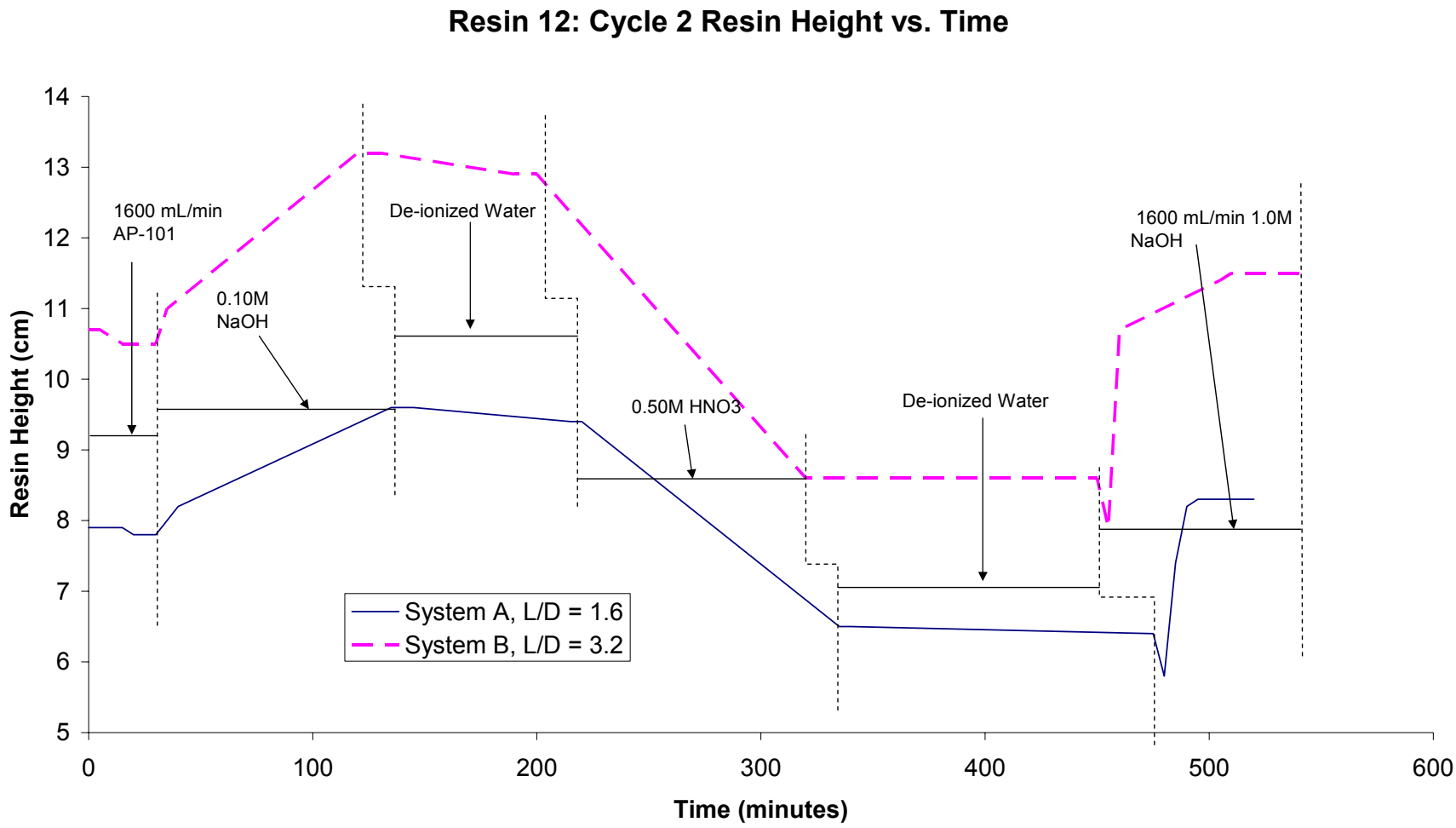

Figure D.31. Resin #12, Cycle 2, Resin Bed Height

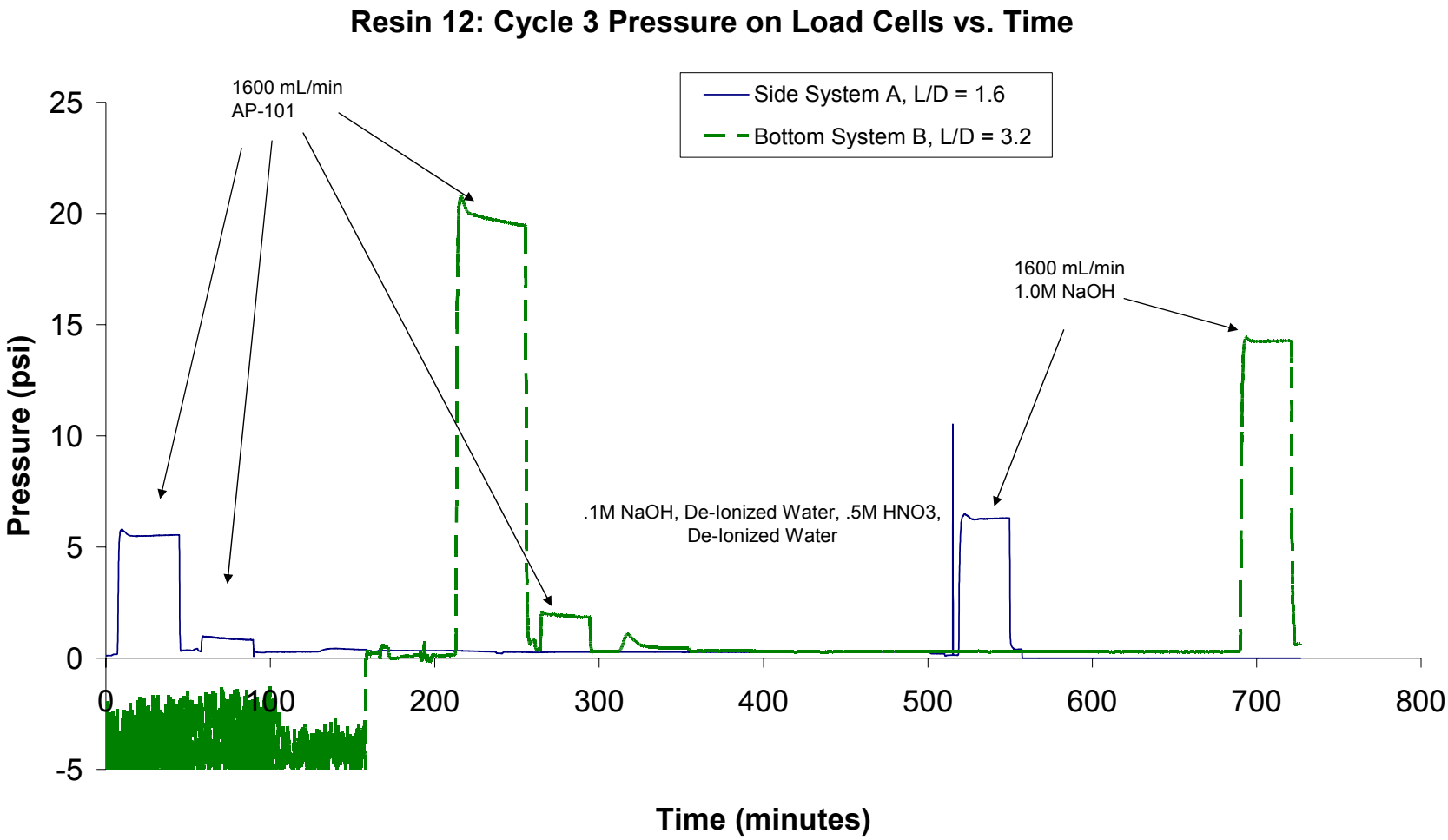

Figure D.32. Resin #12, Cycle 3, Load Cell Pressures

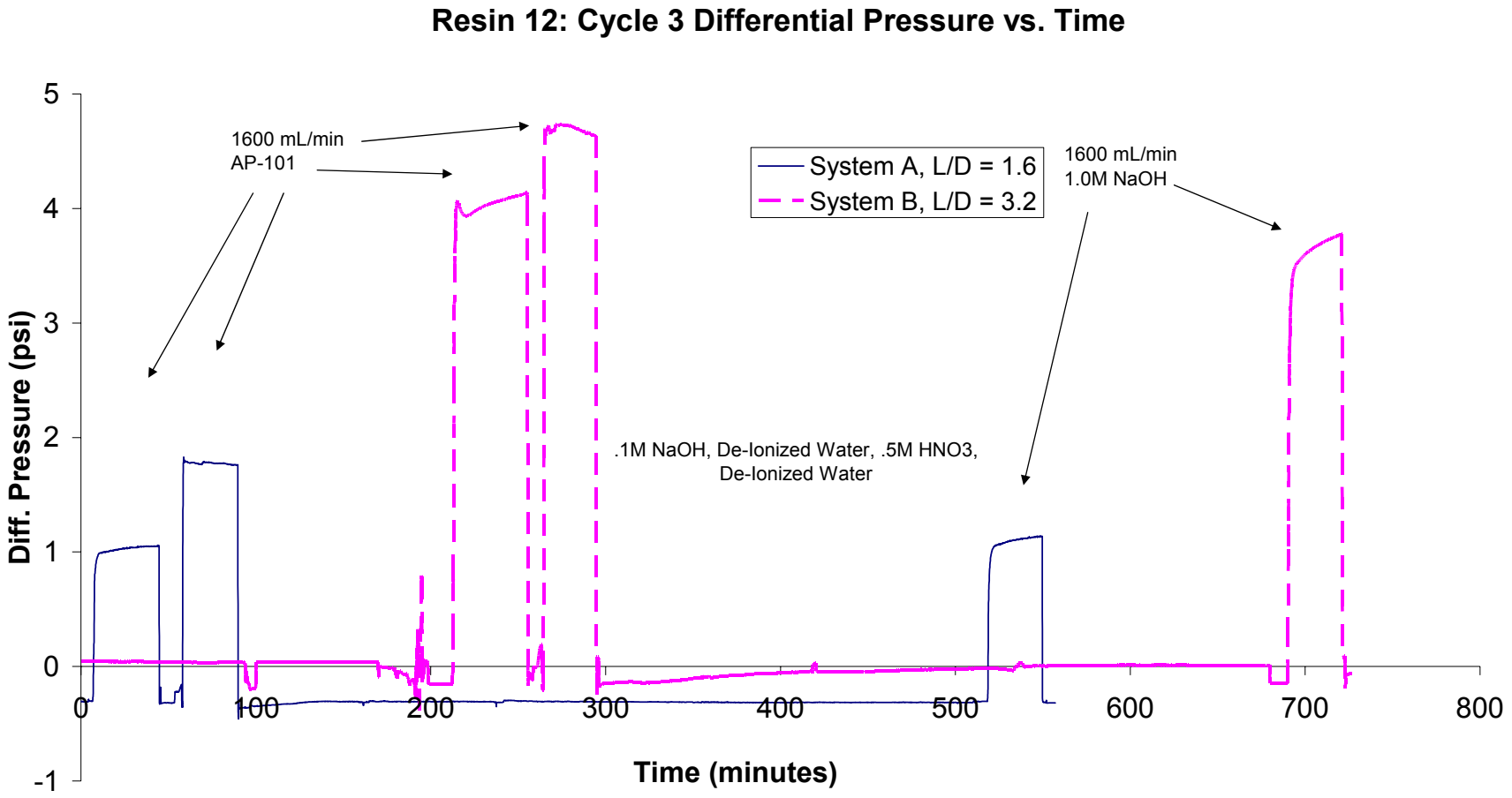

Figure D.33. Resin #12, Cycle 3, Liquid Differential Pressure

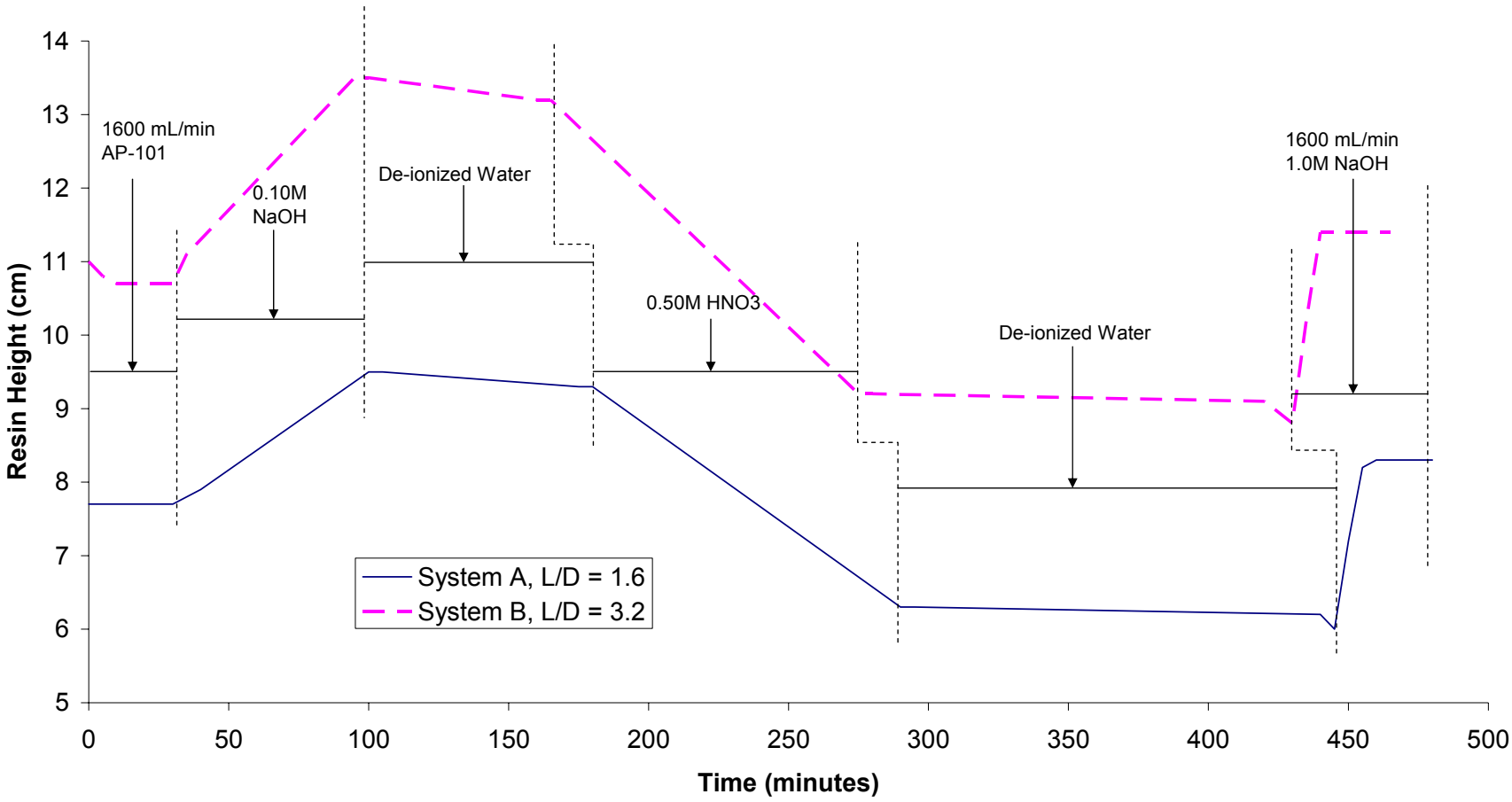

Figure D.34. Resin #12, Cycle 3, Resin Bed Height

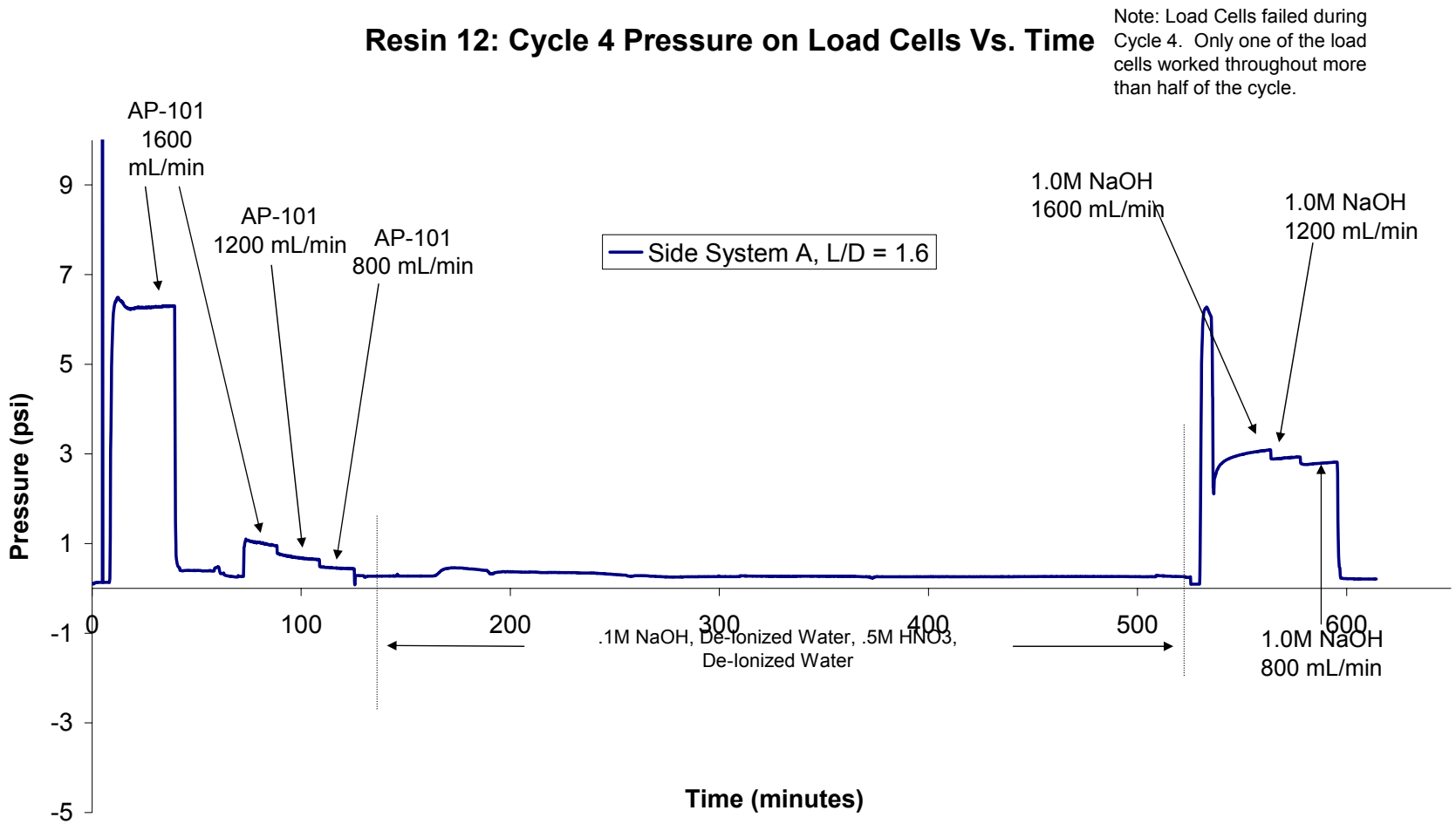

Figure D.35. Resin #12, Cycle 4, Load Cell Pressure

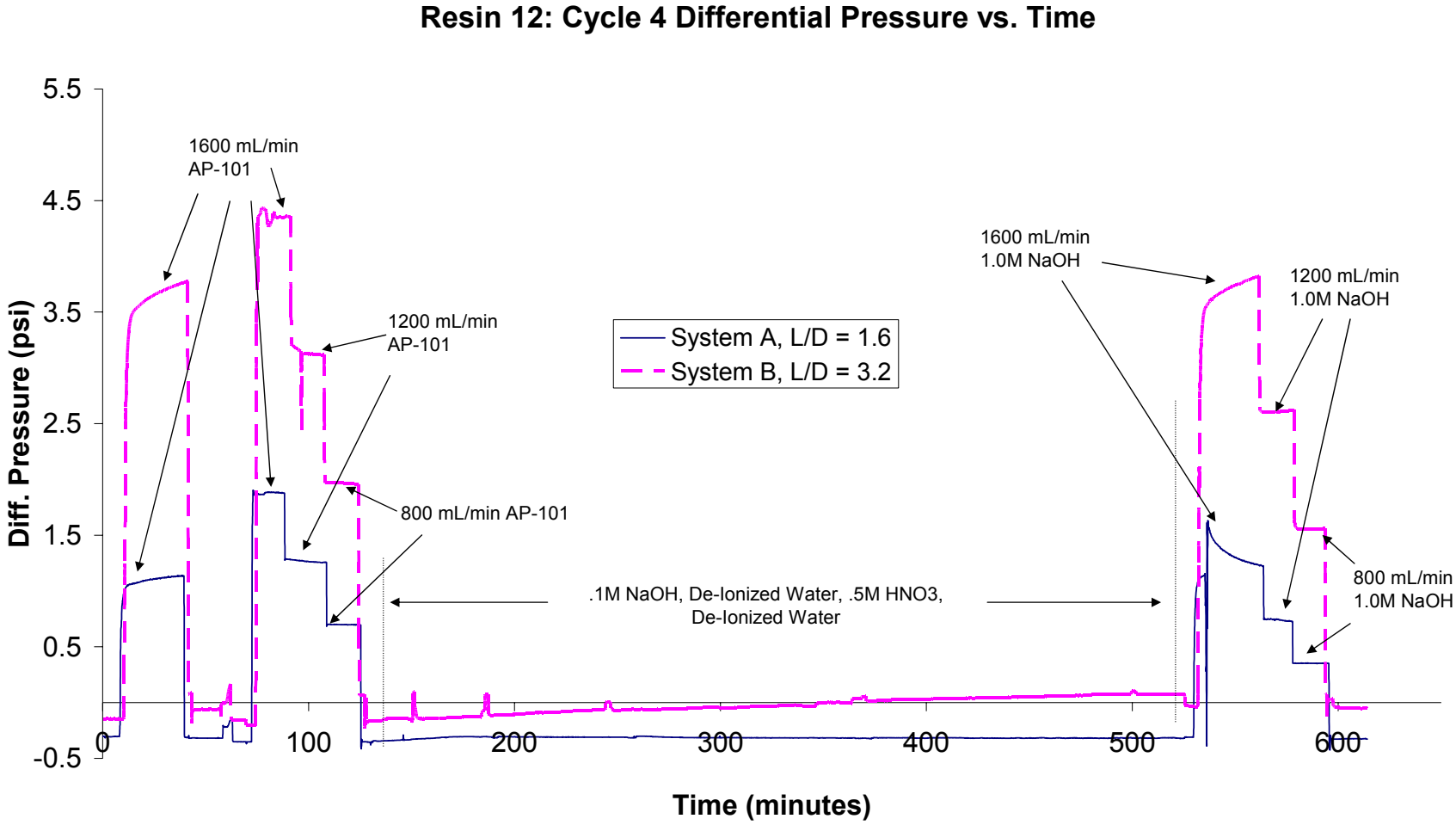

Figure D.36. Resin #12, Cycle 4, Liquid Differential Pressure

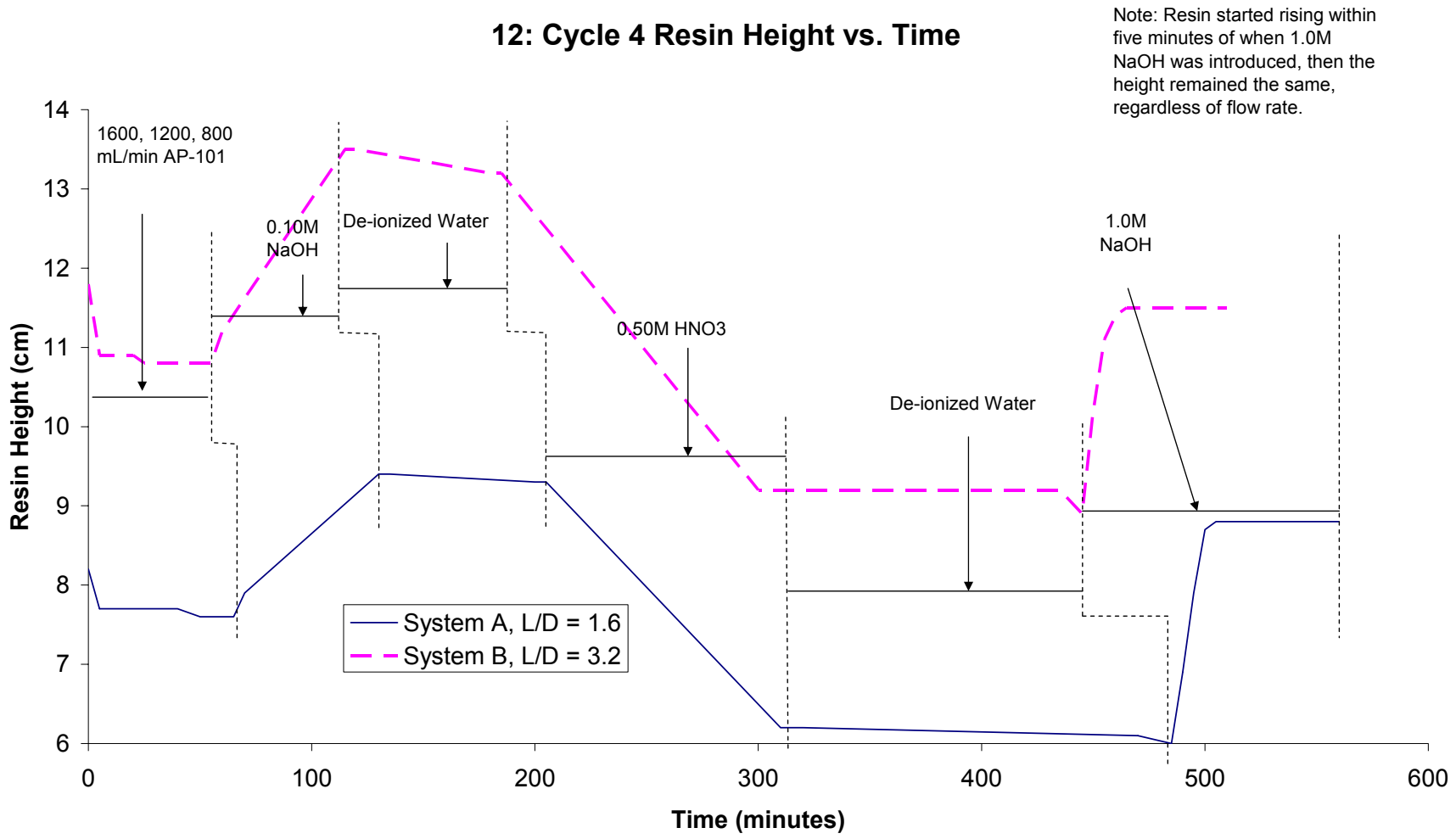

Figure D.37. Resin #12, Cycle 4, Resin Bed Height

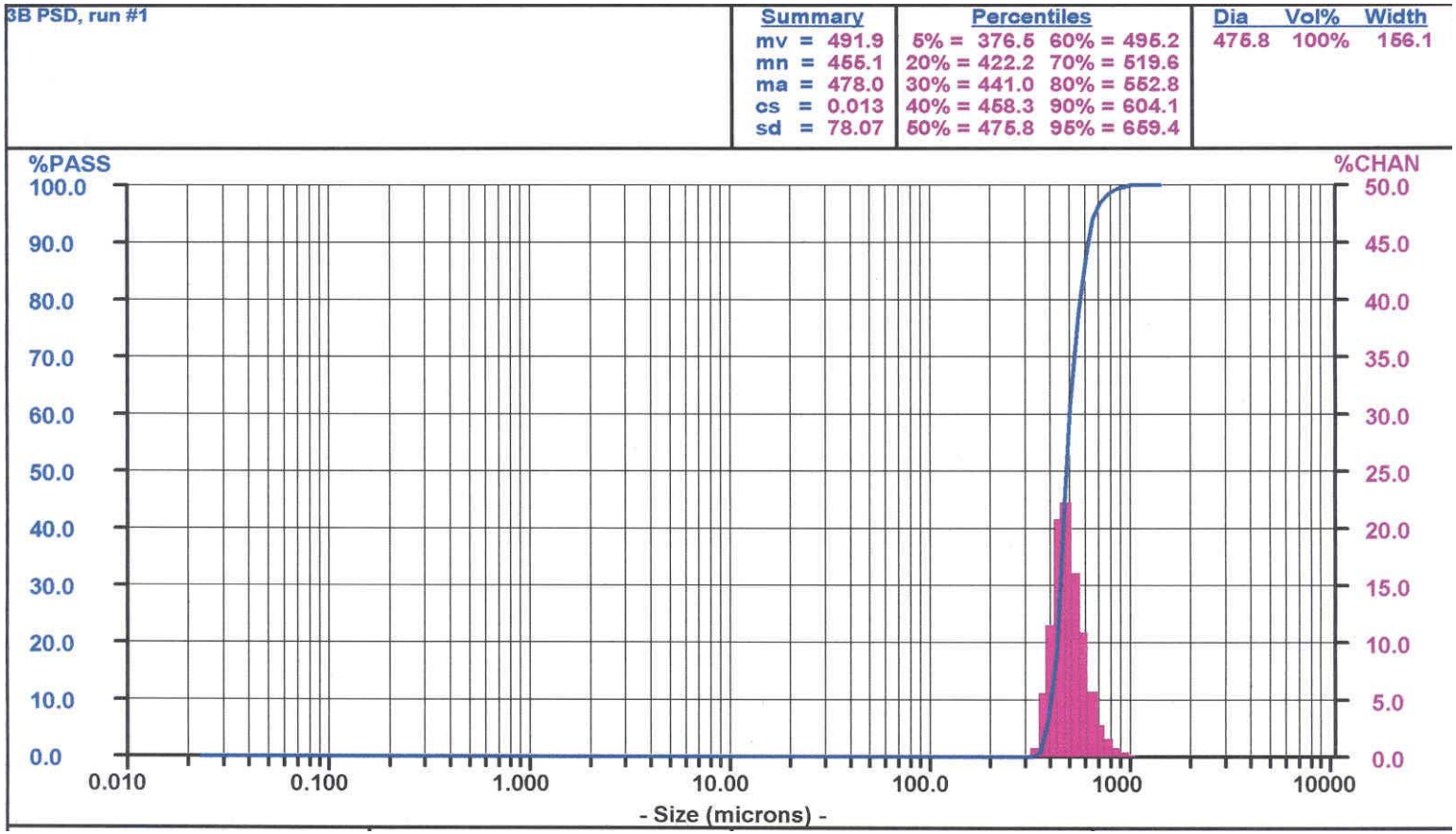

Figure D.38. Sample Particle Size Distribution Measurement for Resin #3, Column B
(Other PSD measurements are available in project records.)

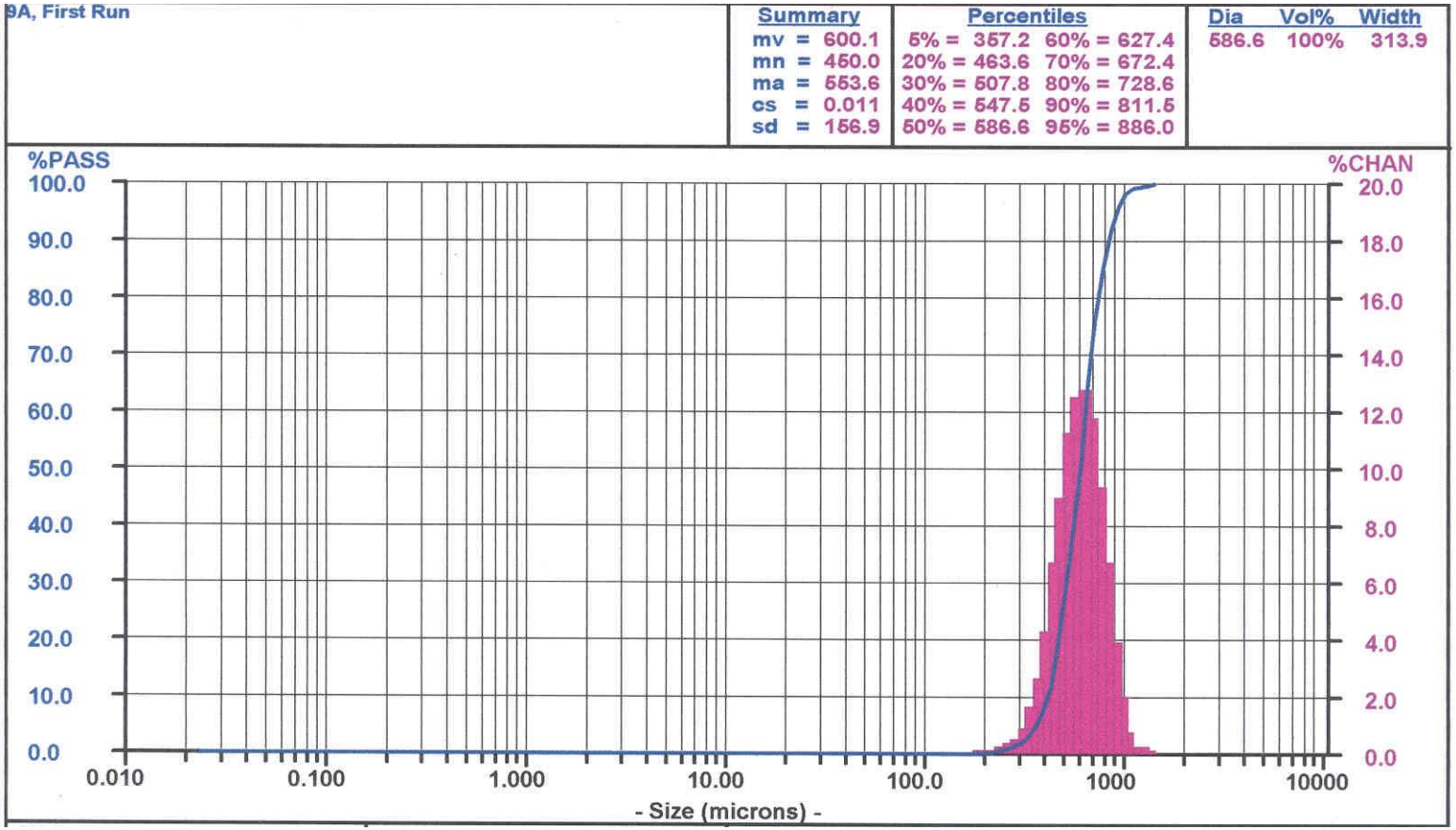

Figure D.39. Sample Particle-Size-Distribution Measurement for Resin #9, Column A
(Other PSD measurements are available in project records.)

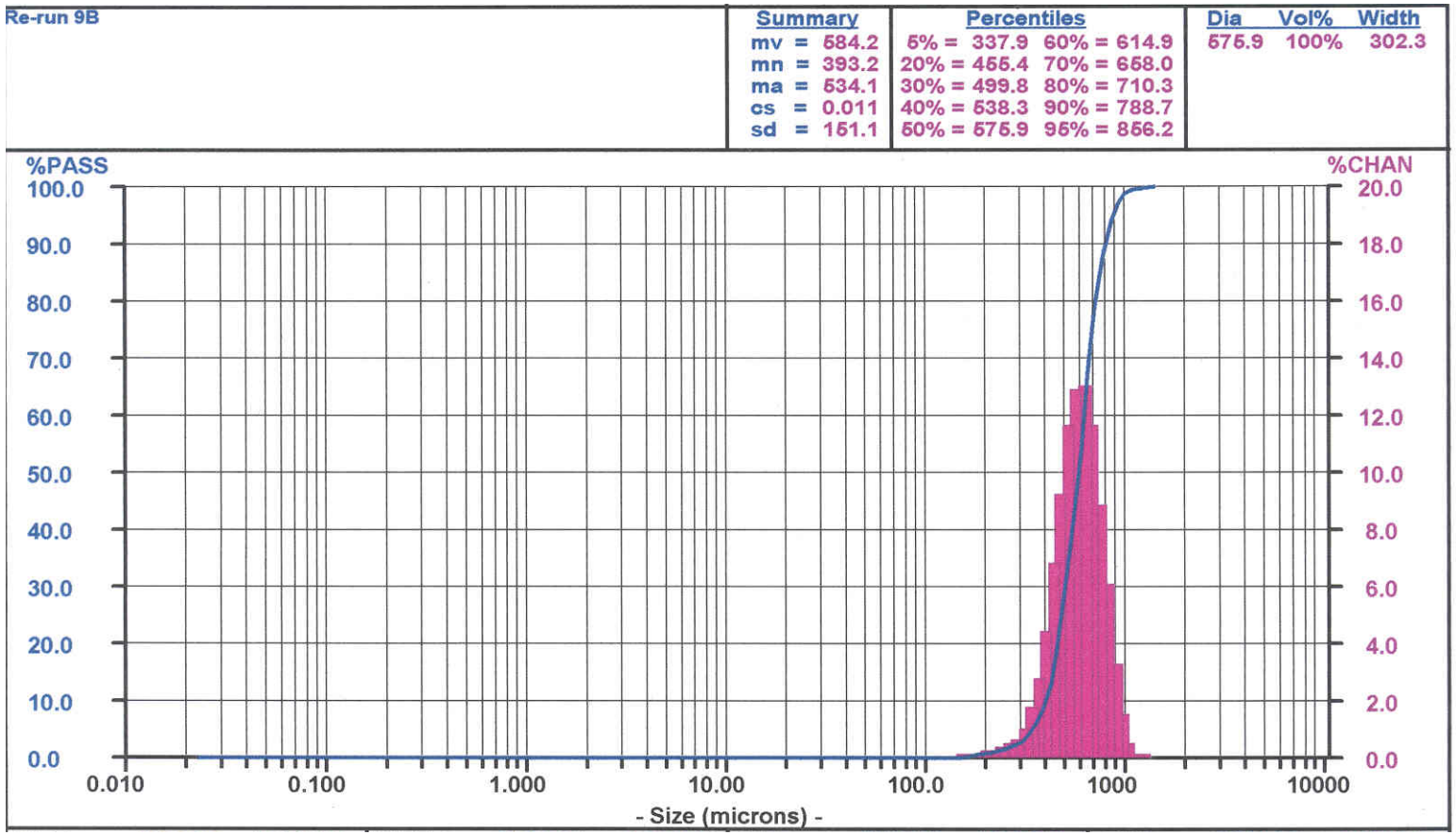

Figure D.40. Sample Particle-Size-Distribution Measurement for Resin #9, Column A
(Other PSD measurements are available in project records.)

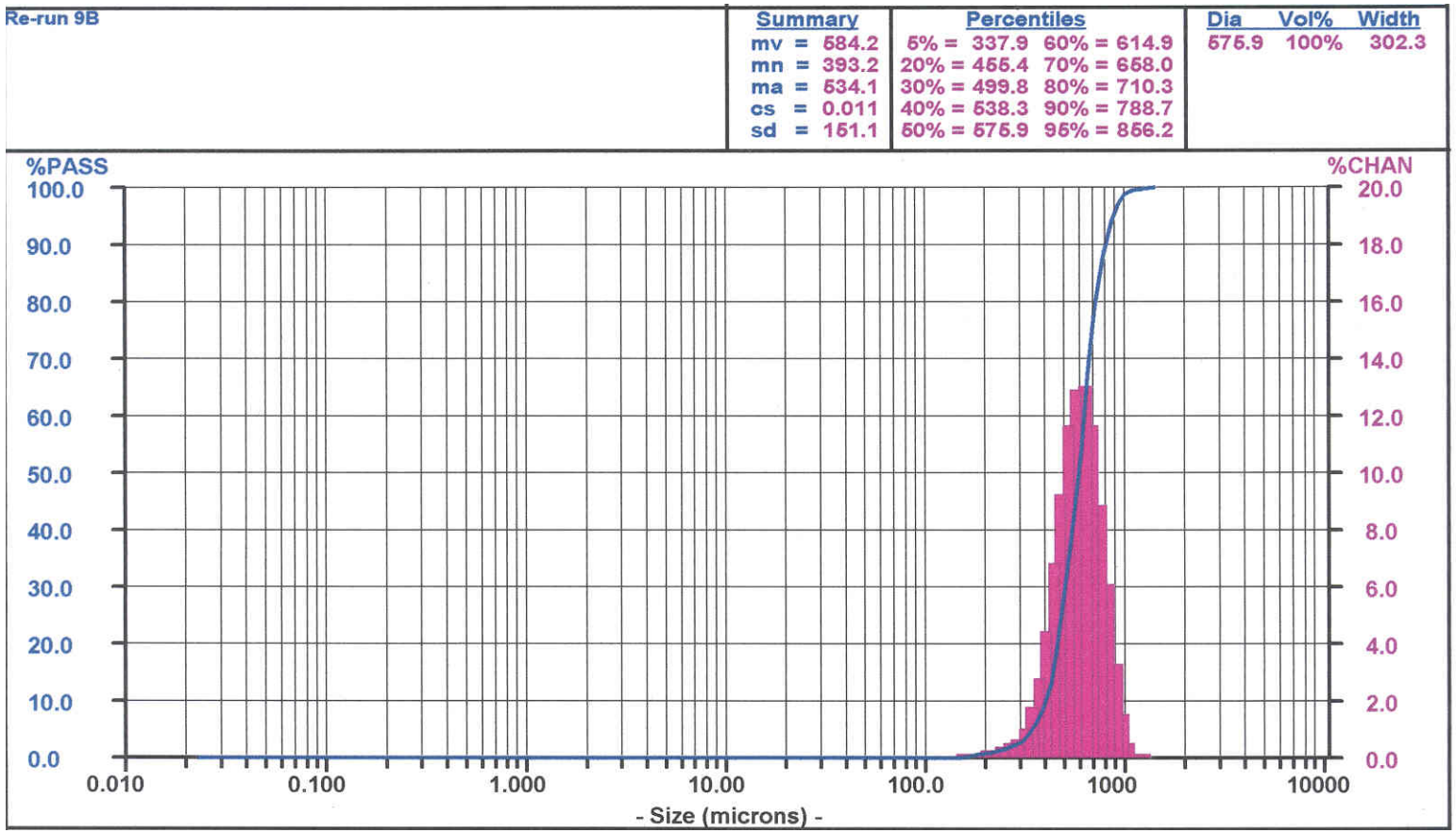

Figure D.41. Sample Particle-Size-Distribution Measurement for Resin #9, Column B
(Other PSD measurements are available in project records.)

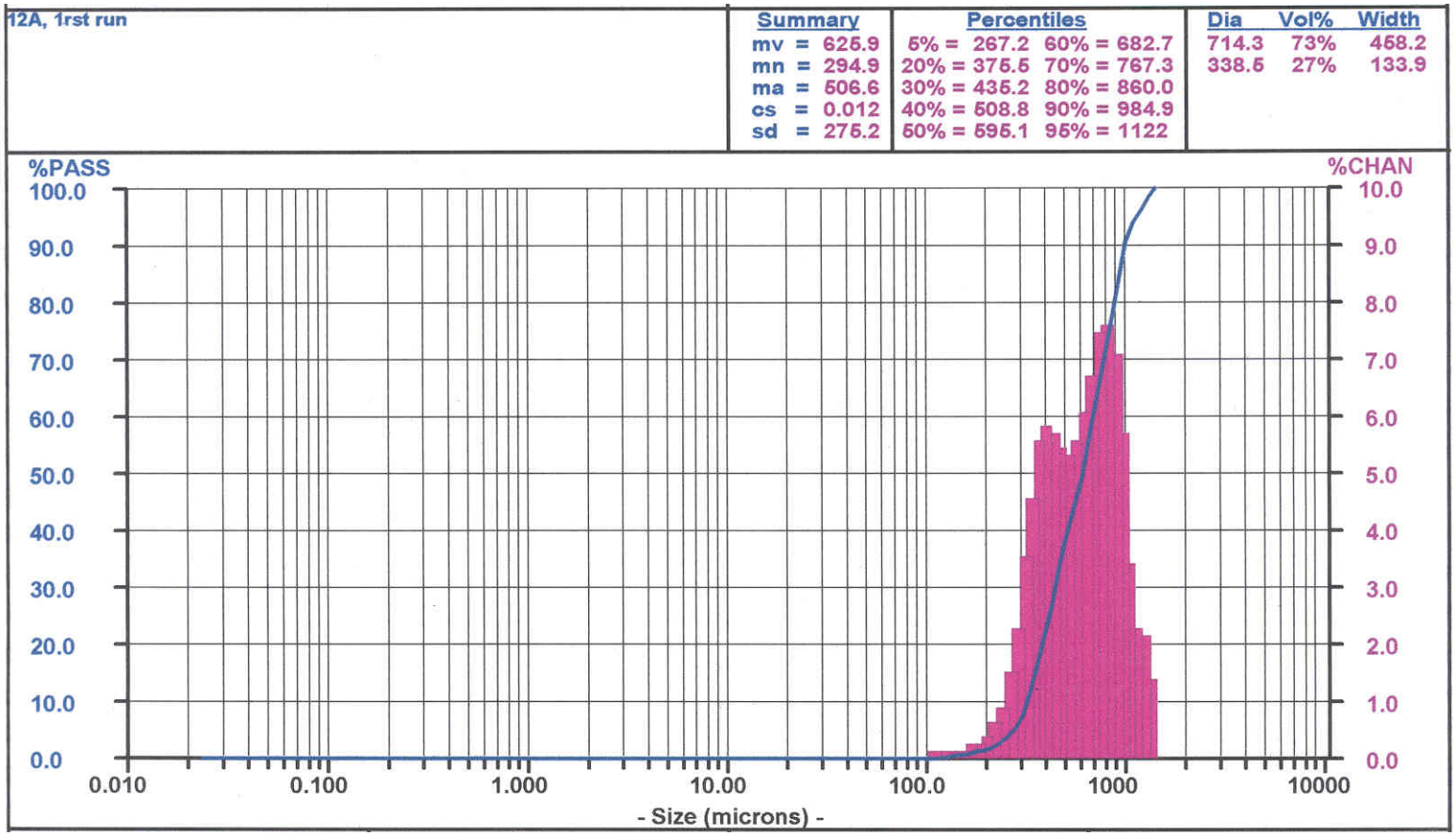

Figure D.42. Sample Particle-Size-Distribution Measurement for Resin #12, Column A
(Other PSD measurements are available in project records.)

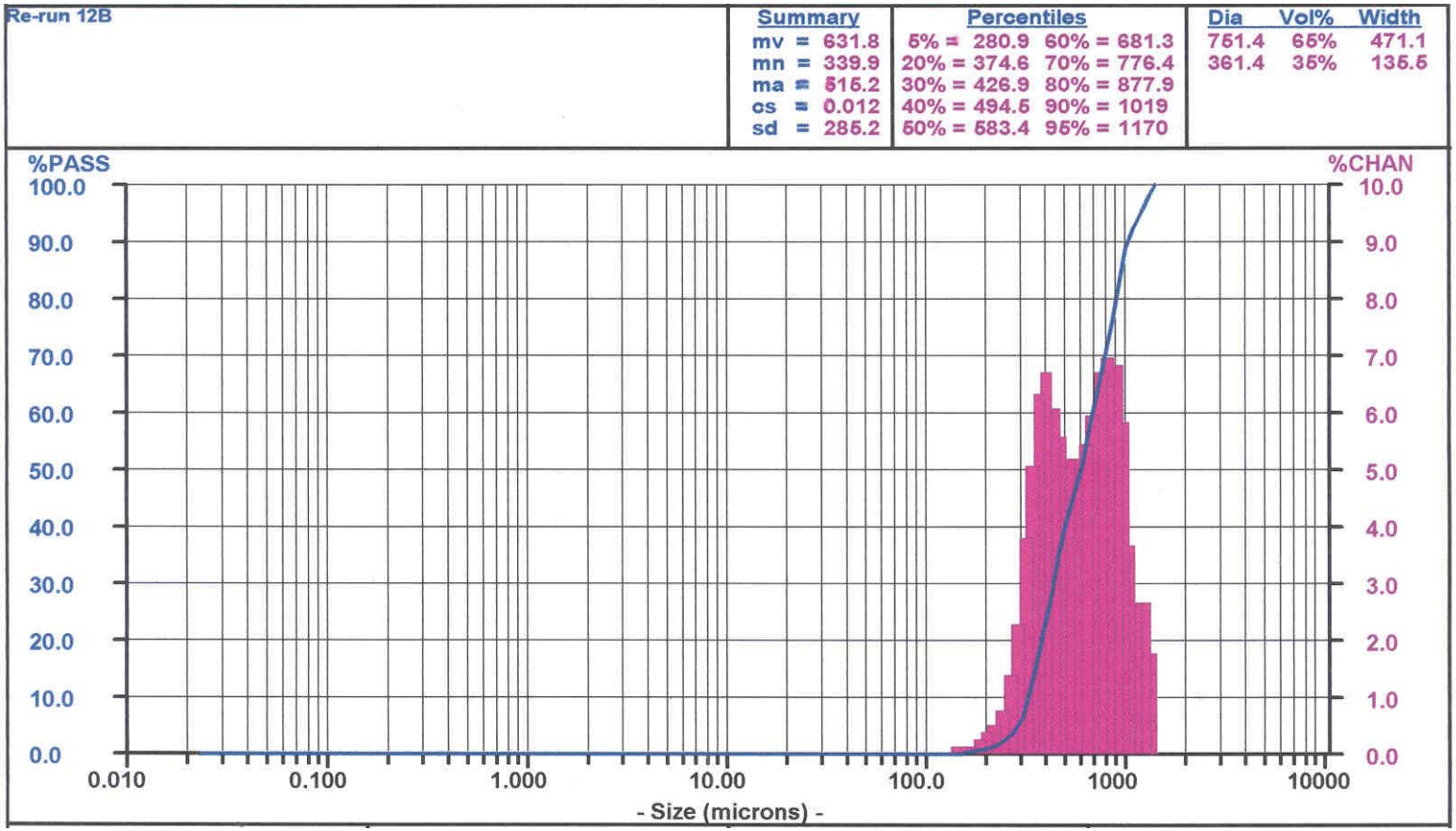

Figure D.43. Sample Particle-Size-Distribution Measurement for Resin #12, Column B
(Other PSD measurements are available in project records.)

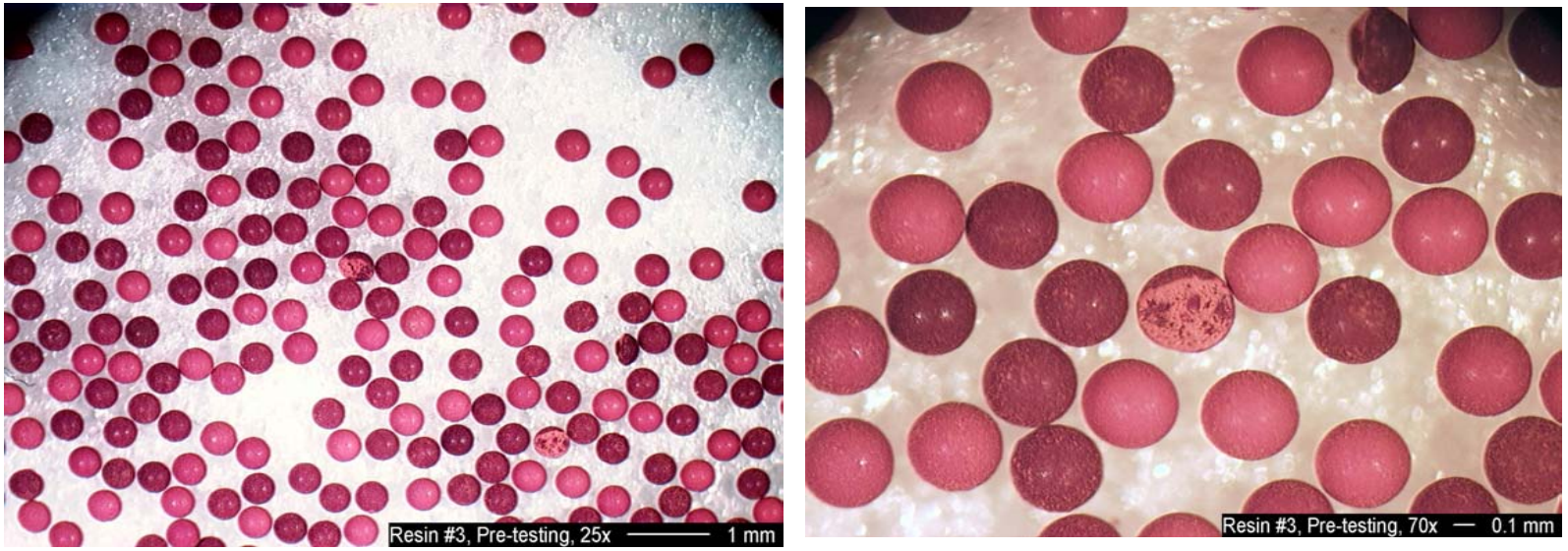

Figure D.44. Micrographs of Hydrogen Form of Resin #3 Before Testing (25× and 70×)

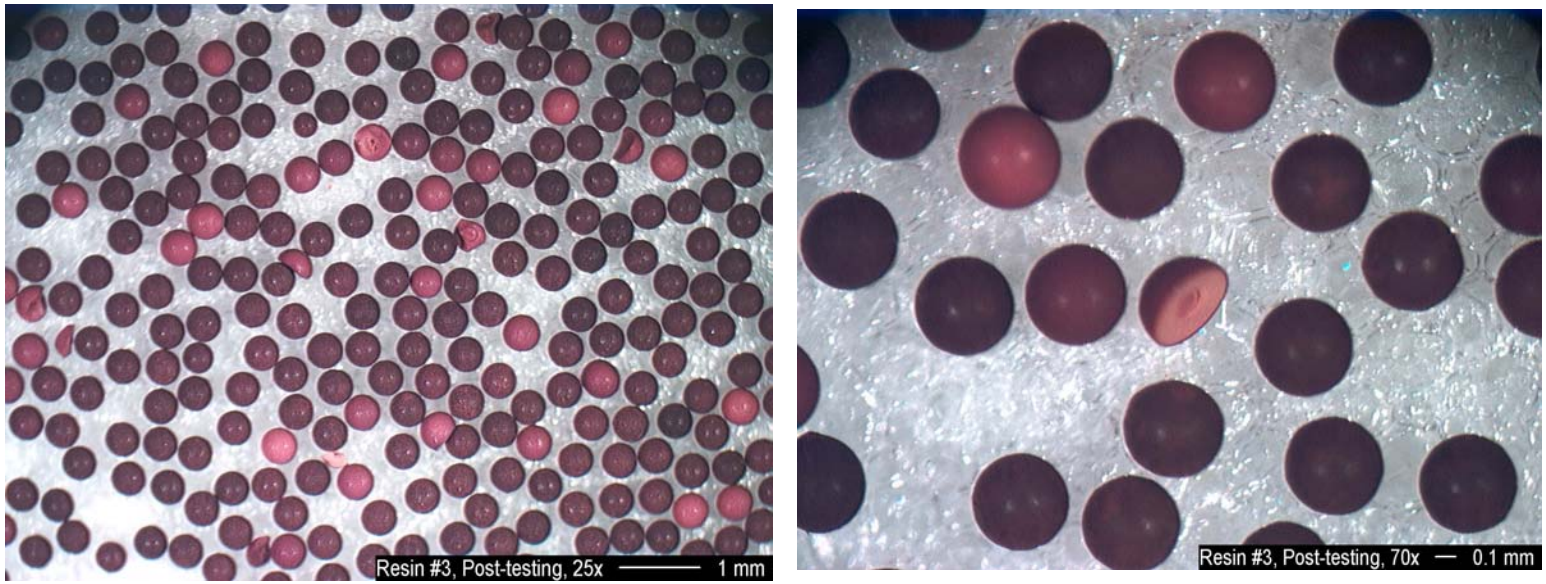

Figure D.45. Micrographs of Hydrogen Form of Resin #3 After Testing in Column A (25× and 70×)

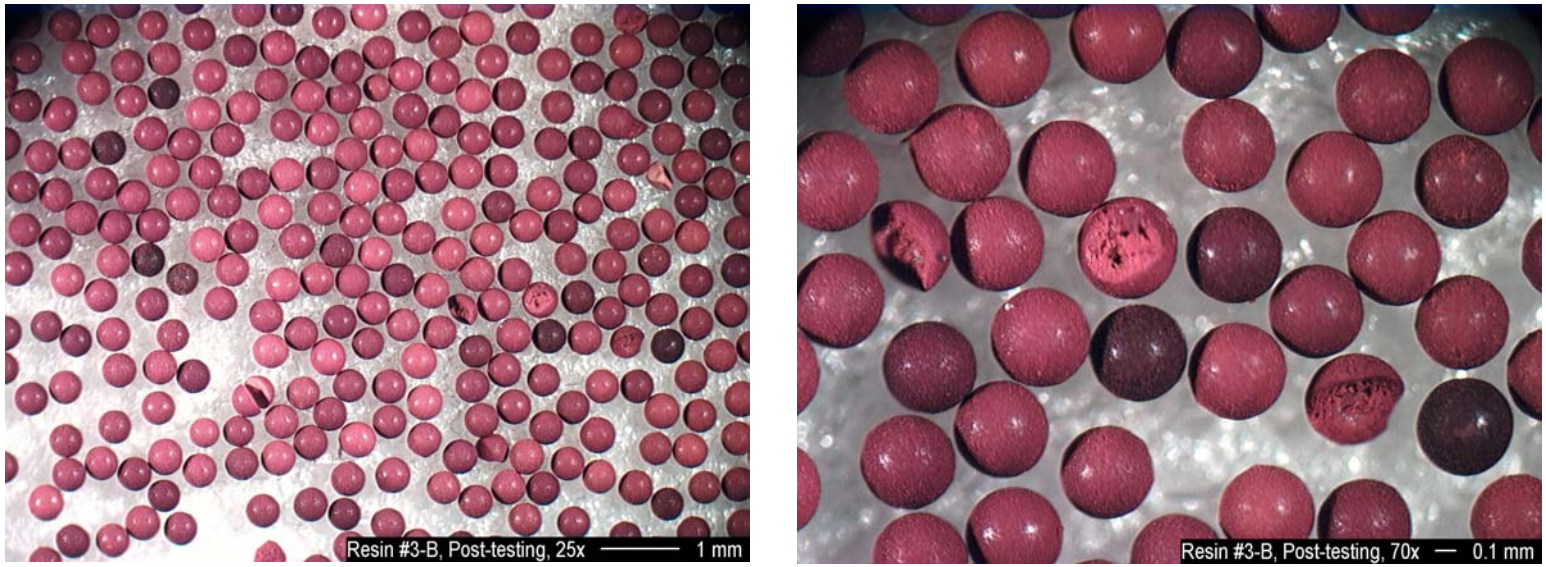

Figure D.46. Micrographs of Hydrogen Form of Resin #3 After Testing in Column B (25× and 70×)

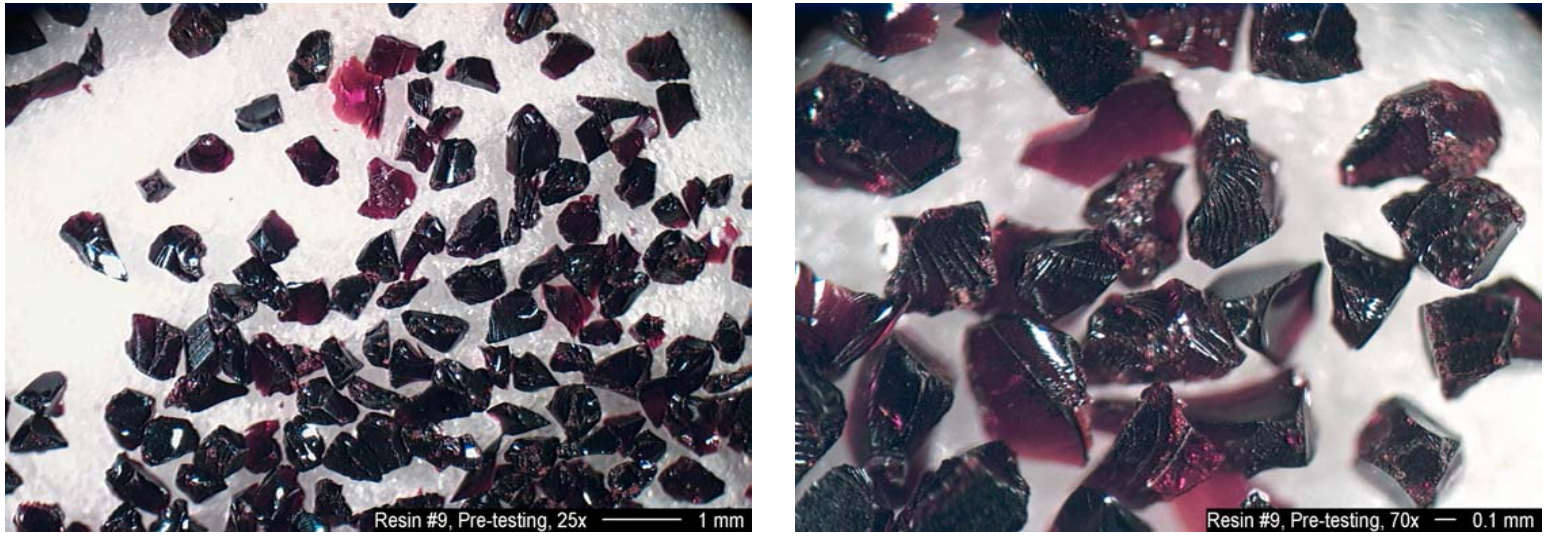

Figure D.47. Micrographs of Hydrogen Form of Resin #9 Before Testing

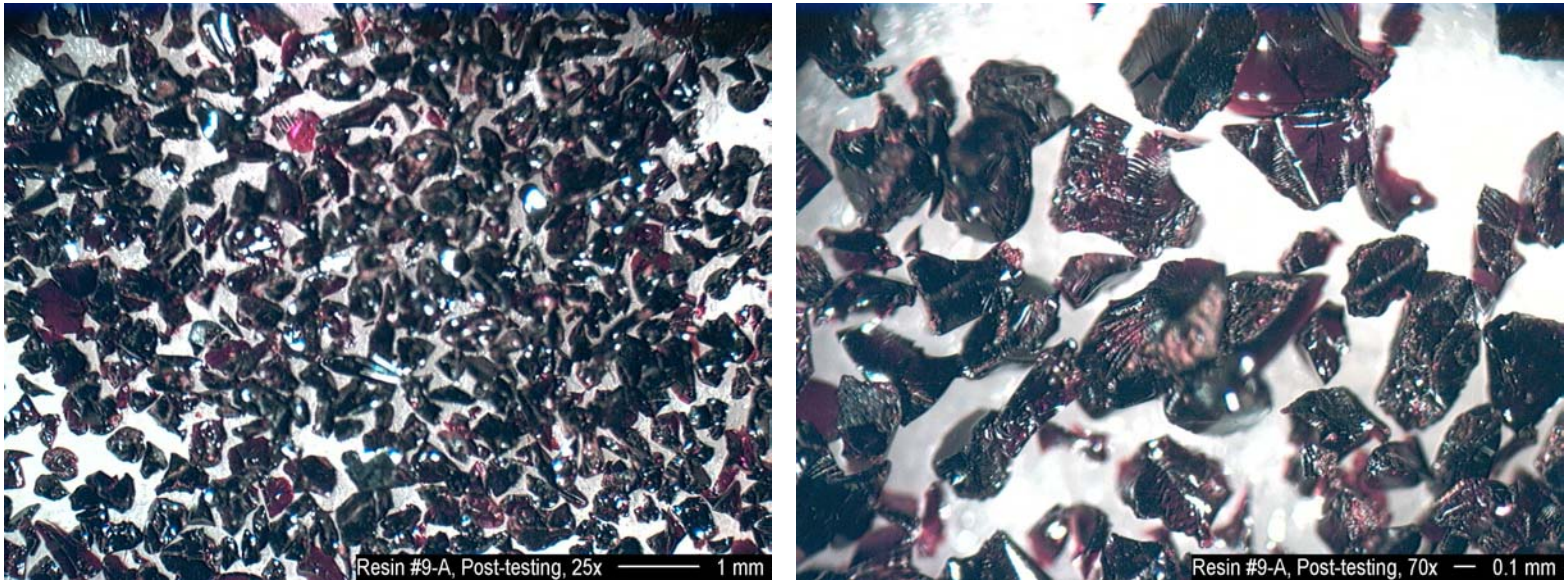

Figure D.48. Micrographs of Hydrogen Form of Resin #9 After Testing in Column A (25× and 70×)

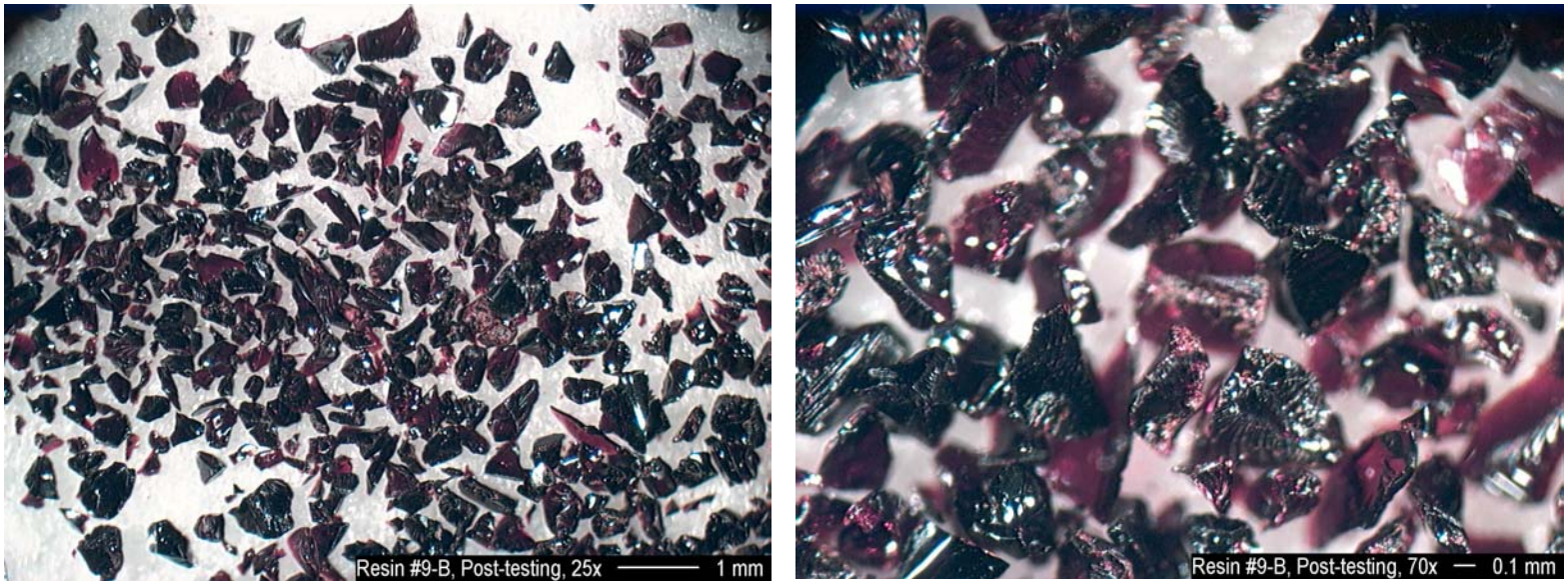

Figure D.49. Micrographs of Hydrogen Form of Resin #9 After Testing in Column B (25× and 70×)

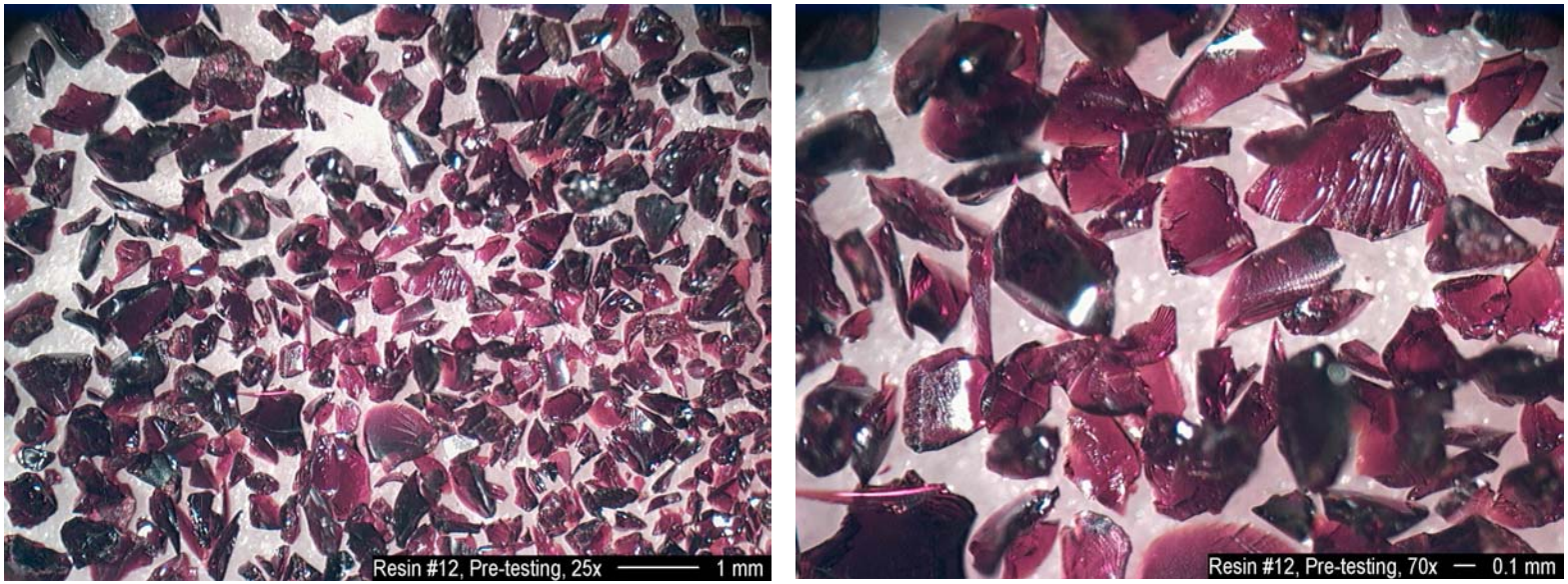

Figure D.50. Micrographs of Hydrogen Form of Resin #12 Before Testing (25× and 70×)

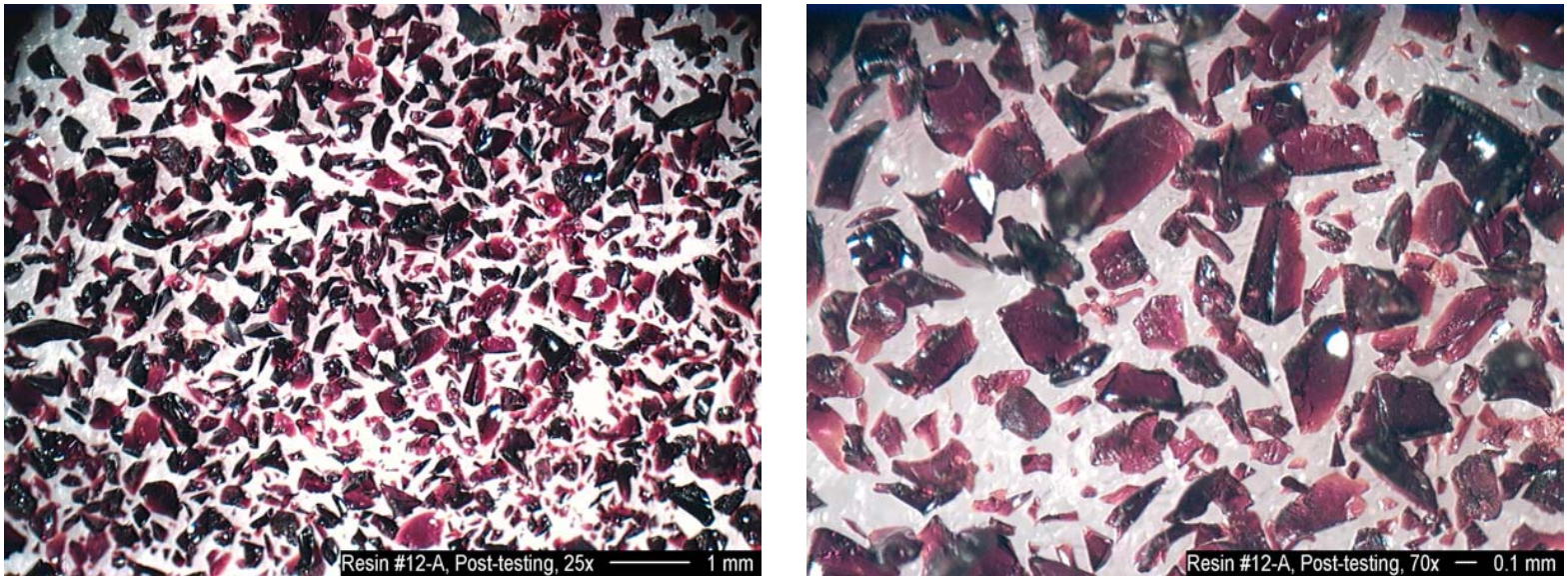

Figure D.51. Micrographs of Hydrogen Form of Resin #12 After Testing in Column A (25× and 70×)

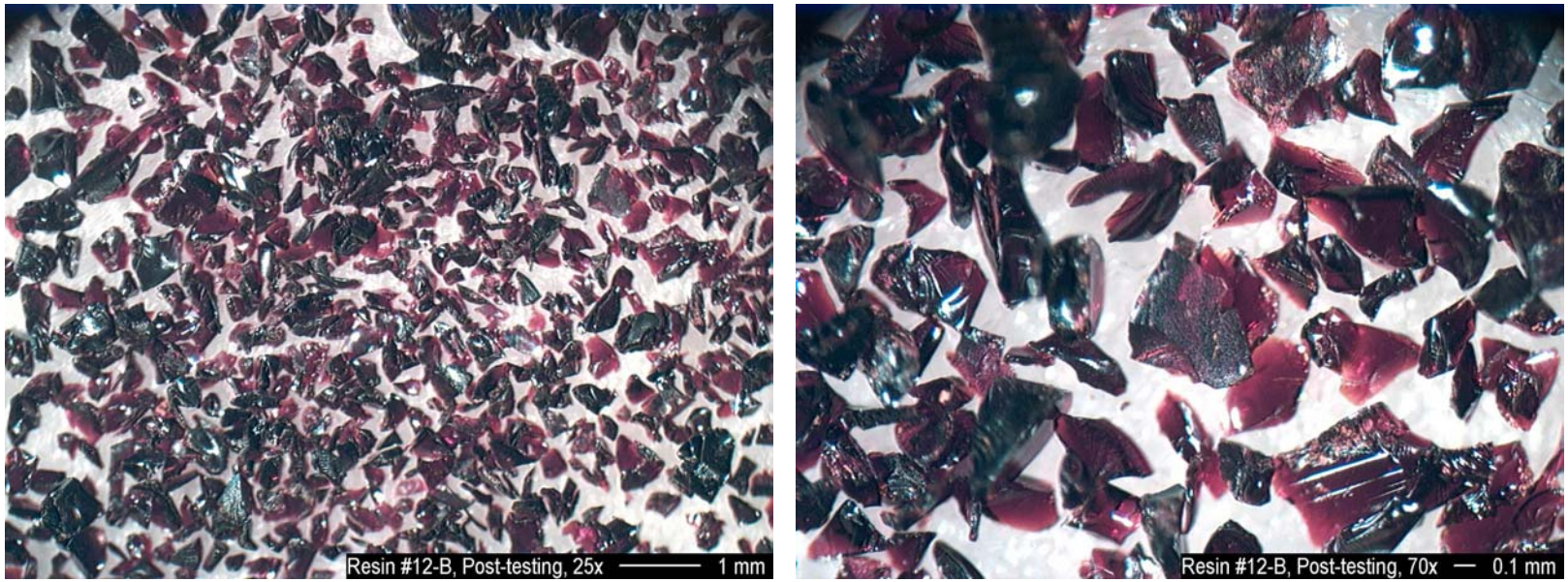

Figure D.52. Micrographs of Hydrogen Form of Resin #12 After Testing in Column B (25× and 70×)

Appendix E

Simulant Compositions

Appendix E: Simulant Compositions

Table E.1. Composition and Reagent Masses for 1-L of AP-101 Solution Simulant

Compound Name	Formula	Amount Added (g)
Add the following reagents, in the given order, to 200-mL water, mix and allow to dissolve completely.		
Sodium acetate	$NaCH_3CO_2$	2.029
Sodium oxalate	$Na_2C_2O_4$	2.385
Aluminum nitrate nonahydrate (60% solution)	$Al(NO_3)_3$-$9H_2O$	161.75
Barium nitrate	$Ba(NO_3)_2$	0.0005519
Beryllium oxide	BeO	0.003247
Cadmium nitrate tetrahydrate	$Cd(NO_3)_2$-$4H_2O$	0.004885
Calcium nitrate tetrahydrate	$Ca(NO_3)_2$-$4H_2O$	0.04036
Cesium nitrate	$CsNO_3$	0.008784 (1)
Rubidium nitrate	$RbNO_3$	0.006091
Copper nitrate trihydrate	$Cu(NO_3)_2$-$3H_2O$	0.005399
Iron nitrate nonahydrate	$Fe(NO_3)_3$-$9H_2O$	0.01606
Lead nitrate	$Pb(NO_3)_2$	0.02132
Lithium nitrate	$LiNO_3$	0.002982
Nickel nitrate hexahydrate	$Ni(NO_3)_2$-$6H_2O$	0.03488
Zinc nitrate hexahydrate	$Zn(NO_3)_2$-$6H_2O$	0.02266
Boric acid	H_3BO_3	0.08164
Molybdenum oxide	MoO_3	0.01930
Then add the following, with mixing, in the given order.		
Sodium chloride	NaCl	2.390
Sodium fluoride	NaF	0.1180
Sodium dihydrogen phosphate	NaH_2PO_4	1.492
Sodium sulfate	Na_2SO_4	5.298
Sodium nitrate	$NaNO_3$	60.00
Potassium nitrate	KNO_3	20.02
Sodium hydroxide (50% solution)	NaOH	238.4
Tungstic acid	H_2WO_4-H_2O	0.03200
Sodium meta-silicate	Na_2SiO_3-$9H_2O$	1.234
Sodium chromate	Na_2CrO_4	0.4735
Sodium formate	HCOONa	1.614
Sodium nitrite	$NaNO_2$	48.78
Sodium carbonate	Na_2CO_3	20.03
Potassium carbonate	K_2CO_3	35.52
Bring to a final 1-L volume and continue stirring several hours.		
Allow the solids to settle at least 24 h. Filter through a 0.45-µm nylon filter or equivalent. (1) The Cs will be added last such that a 10-L volume can be removed without added Cs.		

Table E.2. Composition and Reagent Masses for 1-L of AZ-102 Solution Simulant (5 M Na)

Species	Molarity	Formula Weight, g/mole	g for 1-L
Dissolve the following in 200 mL DI water and mix thoroughly.			
$Al(NO_3)_3$-$9H_2O$	5.02E-2	375.13	18.823
H_3BO_3	8.02E-4	61.83	0.04956
$Ca(NO_3)_2$-$4H_2O$	1.52E-3	236.16	0.3594
$CsNO_3$	3.80E-4	194.92	0.07412 (1)
K_2MoO_4	1.10E-3	238.14	0.2626
KNO_3	1.43E-1	101.1	14.503
$Sr(NO_3)_2$	4E-6	211.63	0.0008786
$NaCH_3COO$-$3H_2O$	2.03E-2	136.08	2.756
Disodium ethylene-diaminetetraacetate	1.38E-3	372.24	0.5149
n-Hydroxyethylethylene-diaminetriacetic acid	5.52E-4	278.26	0.1535
Iminodiacetic acid	3.22E-3	131.08	0.4218
Citric acid	4.10E-2	210.14	8.611
NaF	9.64E-2	41.99	4.050
Na_2SO_4	3.10E-1	142.04	44.095
Add the following slowly with good mixing.			
NaOH	5.34E-1	40.00	21.372
HCOONa	1.84E-1	68.01	12.510
Sodium glycolate	2.06E-1	98.03	20.176
Sodium oxalate	5.80E-2	134	7.777
Na_3PO_4-$12H_2O$	9.69E-3	380.12	3.685
Add nominally 300-mL DI water and mix thoroughly. Then add the following.			
Na_2CrO_4	2.67E-2	161.97	4.330
Na_2CO_3	8.76E-1	105.99	92.846
Mix the solution thoroughly and add the following and mix.			
$NaNO_3$	1.95E-1	84.99	16.602
$NaNO_2$	1.19E+0	69.00	82.086
Add water to 1-L final volume and density of 1.24 g/mL			
This AZ-102 simulant recipe was provided by SRTC on 1/31/03. It was amended to exclude Cs so that it can be added separately to specific concentrations needed. (1) The Cs will be added last such that a 20-L volume can be removed without added Cs.			

Distribution

No. of Copies

OFFSITE

4 Savannah River Technology Center

Larry Hamm
Savannah River Technology Center
Building 773-42A
Aiken, South Carolina 29808

Jim Marra
Savannah River Technology Center
Building 773-43A
Aiken, South Carolina 29808

Charles Nash
Savannah River Technology Center
Building 773-42A
Aiken, South Carolina 29808

Harold Sturm
Savannah River Technology Center
Building 773-A
Aiken, South Carolina 29808

No. of Copies

ONSITE

12 Battelle—Pacific Northwest Division

D. L. Blanchard	P7-22
S. K. Fiskum (3)	P7-22
D. E. Kurath	P7-28
R. L. Russell	K6-24
L. A. Snow	P7-22
J. J. Toth	P7-22
Project File (2)	P7-28
Information Release (2)	K1-06

4 Bechtel National, Inc.

J. F. Doyle	H4-02
R. A. Peterson	H4-02
M. R. Thorson	H4-02
I. Tsang	H4-02